# INFORMATION TO USERS

This manuscript has been reproduced from the microfilm master. UMI films the text directly from the original or copy submitted. Thus, some thesis and dissertation copies are in typewriter face, while others may be from any type of computer printer.

**The quality of this reproduction is dependent upon the quality of the copy submitted.** Broken or indistinct print, colored or poor quality illustrations and photographs, print bleedthrough, substandard margins, and improper alignment can adversely affect reproduction.

In the unlikely event that the author did not send UMI a complete manuscript and there are missing pages, these will be noted. Also, if unauthorized copyright material had to be removed, a note will indicate the deletion.

Oversize materials (e.g., maps, drawings, charts) are reproduced by sectioning the original, beginning at the upper left-hand corner and continuing from left to right in equal sections with small overlaps.

Photographs included in the original manuscript have been reproduced xerographically in this copy. Higher quality 6" x 9" black and white photographic prints are available for any photographs or illustrations appearing in this copy for an additional charge. Contact UMI directly to order.

Bell & Howell Information and Learning
300 North Zeeb Road, Ann Arbor, MI 48106-1346 USA

UMI®
800-521-0600

Université d'Ottawa · University of Ottawa

# PETROGENESIS OF THE LATE ARCHEAN LAC SIMARD INTRUSIVE COMPLEX, PONTIAC SUBPROVINCE, QUEBEC

by

© David M. Tarnocai

A thesis submitted to the School of Graduate Studies and Research in partial fulfillment of the requirements for the degree of M.Sc. in Earth Sciences

UNIVERSITY OF OTTAWA

OTTAWA, CANADA, 1997

## Abstract

The Archean Lac Simard Intrusive Complex (LSIC) represents an example of medium-K to shoshonitic and high-K transitional magmatism occurring in the Pontiac sedimentary terrane of the Superior Province. The complex formed from diverse magma batches ranging from weakly quartz saturated diorites to syenites and quartz monzodiorites to quartz monzonites and biotite-clinopyroxene bearing hornblendite magmas. The units of the LSIC are mutually intrusive and typically either display gradational or mingled contacts. All external contacts of the LSIC are variably sheared and intrusive contacts.

Granitoids of the LSIC are dominantly monzodioritic produced through fractional crystallization, primarily of amphibole, clinopyroxene, apatite, magnetite, titanite, and biotite, from a melt with shoshonitic affinities emplaced at shallow levels (~1 kbar.). Relatively oxidising primary conditions are evidenced by the mineral assemblage quartz + magnetite + titanite and a calculated $fO_2$ lies on this buffer at $\sim 10^{-13.7}$ at 800°C. Amphibole and clinopyroxene chemistry provide evidence for polybaric crystallization. Field relationships among units of the LSIC and mafic silicate chemistry suggest that the units of the complex were emplaced over a relatively short time interval from either a zoned magma chamber, or multiple cogenetic chambers at depth.

Shoshonitic samples of LSIC granitoids posses high $La/Yb_{CN}$, LREE, LILE/HFSE, $Mg^{\#}$, Cr and Nd indicative of a primary mantle melt with an arc-type trace element signature. Neodymium and Sr isotope compositions of primary mineral separates suggest that the LSIC rocks are similar Nd-Sr- isotopically to Abitibi Subprovince mantle derived rocks.

Hornblendites within the LSIC are comagmatic with the granitoids of the LSIC and form two compositional populations. One group of relatively uncontaminated hornblendites appears to have been generated by fractional crystallization whereas a second group of similar parentage records assimilation of up to approximately 40% of a Pontiac sedimentary rock component.

**Acknowledgements**

The author would like to thank Dr. Kéiko Hattori for her invaluable criticism, assistance, and advice during the course of writing and research. The author also gratefully acknowledges the assistance provided through funding by two Ontario Graduate Scholarships.

The computer support provided by J.-F. Tardif and B. Daneshfar, along with valuable assistance by H. DeGouffe and S. Thériault facilitated research and writing. Laboratory work benefited from assistance provided by J. Loop (ICP), R. Hartree (XRF), P. Jones (SEM-EDS, and electron microprobe), and G. Mrazek (Thin sections). Analytical work accomplished by Dr. K. Hattori (mass spectrometry) and the Geological Survey of Canada (X-ray fluorescence) laboratory were also greatly appreciated.

## Table of Contents

## List of Tables

## List of Figures

## List of Plates

# Chapter 1 Introduction

## 1.1 Introduction

Mildly alkaline to ultrapotassic monzodioritic to syenitic igneous rocks and alkalic volcanic rocks are present in many locations throughout the Superior Province, such as the Abitibi, Wabigoon, and Pontiac Subprovinces. These rocks are restricted to the late Archean and have crystallization ages of approximately 2680 Ma (Corfu et al, 1989; Othman et al, 1990; Mortensen, 1993). The chemical compositions of these rocks suggest that they are mantle derived and similar to alkaline rocks produced in the final stage of arc magmatism in Phanerozoic terranes (Morrison, 1980).

The Pontiac Subprovince is bounded by the Abitibi greenstone belt to the north and the Grenville front to the south (Figure. 1). Similar to many metasedimentary terranes, the Pontiac sedimentary rocks were intruded by S-type granites. Unlike many other metasedimentary terranes though, the Pontiac subprovince was intruded by numerous dioritic to syenitic intrusions at ~2680 Ma, forming dykes, sills, and composite bodies. The chemical, textural, mineralogical, and temporal similarities among these mildly alkaline to alkaline rocks suggest a common origin. These intrusions are contemporaneous with mineralogically and compositionally similar monzonitic-syenitic intrusions in greenstone belts of the Superior Province.

Mapping and sample collection was conducted during twenty-seven days of field work at the LSIC in 1992 and 1993. In excess of 250 grab samples were collected for chemical and petrographic analysis. The location of the samples that were utilised in this research is presented in Appendix 1. This research presents the first detailed documentation of the

# South-Eastern Superior Province

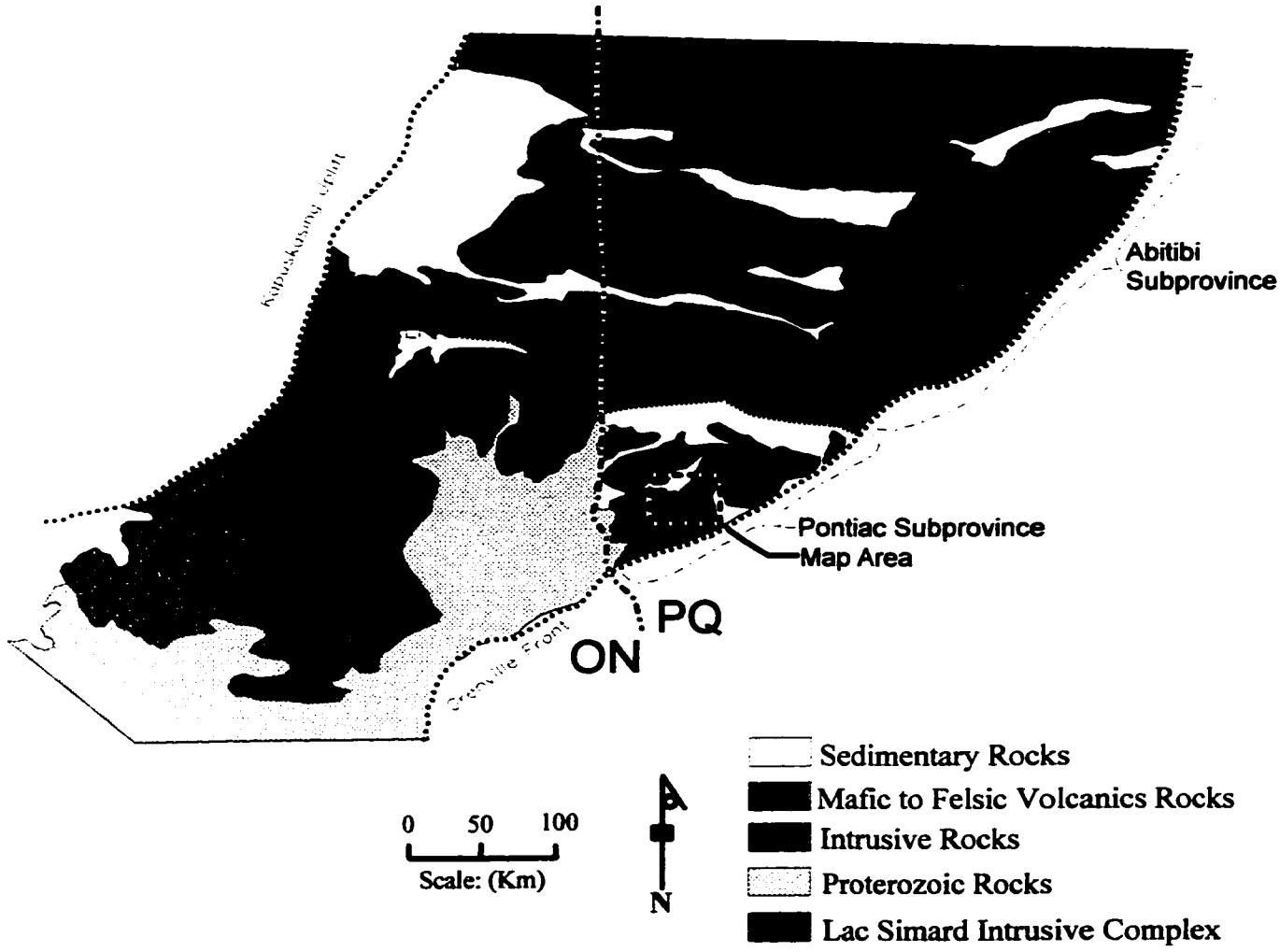


Figure 1. Location of the Pontaic Subprovince and Lac Simard Intrusive Complex with respect to the Abitibi Subprovince and Grenville Front.

mineralogy, chemical composition and isotopic data of the LSIC, one of largest diorite - monzonite intrusions in the Pontiac Subprovince, and evaluates the origin of the complex. The data obtained are also compared with those from other Archean alkaline rocks in greenstone belts.

## 1.2 Previous Work

The earliest published map of portions of what is now termed the LSIC is presented in a report by Denis (1937) although the monzodiorites of the LSIC were not identified and both the LSIC and Belleterre-Fugerville tonalites were mapped as granite. Chagnon (1968) mapped a portion of the LSIC, identifying the weakly quartz saturated nature of the rocks, and described the plutonic rocks in some detail. Later mapping by Rive (1975, 1986) provided greater insight on the spectrum of rock types present within the complex. Rive et al (1990) subdivided the granitoids of the Pontiac and Abitibi Subprovinces, following the IUGS classification scheme (Streckeisen, 1976), showing that complexes similar to the LSIC are found throughout the Pontiac Subprovince and Abitibi greenstone belt. Two U-Pb dates are available for the LSIC (Machado et al, 1991) and no direct structural studies related to the LSIC are available. Indirectly, a structural framework for the origin of the Lac Freschette complex (Miles, 1993) has been proposed which may be applicable to the LSIC, and a kinematic model outlining the origin of the Lac des Quinze complex suggests that the LSIC intruded into shear zones late in the Archean (Sawyer and Barnes, 1994).

The term "granitoid" (Streckeisen, 1976) refers to a granitic rock containing quartz as an essential mineral and plots between Q=20-60 on the modal QAP tetrahedron IUGS

tetrahedron. For this study, a looser description is used. A granitoid in this study applies to any of the medium to coarse grained rocks of the LSIC containing <90 modal % mafic minerals in order to simply describe the spectrum of slightly quartz saturated intrusive rocks of the LSIC.

Limited mineral exploration focused primarily on the ultramafic rocks within the complex has occurred in an effort to find Ni-Cu mineralization similar to the La Force occurrence. The La Force occurrence is situated south of the LSIC and contains an estimated 215,188 t of Ni-Cu sulphide mineralization grading 0.87 % Ni, 0.42 % Cu, (Avramtchev and Lebel-Drolet, 1981).

# Chapter 2 Regional Geology

## 2.1 Geology of the Pontiac Subprovince

The Pontiac Subprovince is a predominantly sedimentary rock dominated Subprovince bounded by the Abitibi Subprovince to the north, the Grenville front to the east and south, and Proterozoic sedimentary rocks to the west (Figure 1). The Pontiac sedimentary rocks comprise turbiditic wackes, pelites and minor conglomerates. The origin of the sedimentary rocks is a matter of much debate. The Pontiac sedimentary rocks have been interpreted to represent a fore-arc prism of material derived from the Abitibi (Dimroth et al, 1982) and an accreted sedimentary apron produced from the erosion of an old micro-continent (Feng and Kerrich, 1992). The latter interpretation is supported by the chemical discrepancies between Pontiac sedimentary rocks and Abitibi sedimentary rocks (Lacorne block) and the presence of old zircons and fine grained sedimentary rocks with old Nd model ages ($T_{CHUR}$) of up to 3100 Ma indicating different provenances (Feng et al, 1993). Feng et al (1993) suggest that the Pontiac may have been a sedimentary prism obliquely juxtaposed to the Abitibi which allowed for the sampling of both a proposed small exposed older continental material not recognized at present and the Abitibi Subprovince volcanic rocks. Mortensen and Card (1993) note that the U-Pb ages of zircons from the Pontiac sedimentary rocks is compatible with derivation from the Abitibi (or Belleterre volcanic rock) although an additional older source is required.

The Pontiac Subprovince hosts the Lac des Bois, Baby, and Belleterre greenstone belts which appear to have an allochthonous relationship to the sedimentary rocks (Sawyer and Barnes, 1993). These volcanic belts were previously thought to be related to magmatism in the Abitibi Subprovince. Recent U-Pb results indicate that these volcanic rocks crystallized

between approximatelly 2680 to 2689 Ma (Mortensen and Card, 1993), younger than Abitibi volcanic rocks dated at 2700 ± 5 Ma. The Lac des Bois and Belleterre volcanic belts are interpreted as arcs probably accreted to the Pontiac sediments (Mortensen and Card, 1993).

The Pontiac Subprovince was affected by north - south compression (Camire and Burg, 1993; Dimroth et al, 1983) probably resulting from northward directed subduction south of the Pontiac subprovince. The duration of this deformational event is inferred to be greater than ~26 Ma, lasting from ~2694 to <2668 Ma (Benn et al, 1994) during which time the Pontiac subprovince experienced plutonism by numerous distinct series of intrusions.

One suite of intrusive rocks is generally pre to early tectonic whereas two granitoid series are syn- to late-tectonic. The former suite comprises minor syn-volcanic gabbros (i.e. Laforce intrusion) and voluminous tonalitic to granodioritic plutons (i.e. Belleterre - Fugerville pluton, Lac Devlin pluton). The TTG (tonalite - trondhjemite - granodiorite) type intrusions are strongly foliated, homogenous in mineralogy, and spatially associated with the greenstone belts of the Pontiac Subprovince. The monzodiorite - monzonite - granodiorite - syenite (MMGS) series intrusions (Feng and Kerrich, 1992), such as Lac Freschette, Lac Remigny, Lac Simard, and Lac Soufflot intrusions, are considered syn- to late-tectonic (Rive et al, 1990) and intruded along shear zones at ~2680 in the Pontiac Subprovince (Sawyer and Barnes, 1993; Miles, 1993). These intrusions are metaluminous, weakly $SiO_2$ saturated, REE (rare earth element), LILE (large ion lithophile element), Mg, Cr enriched granitoids (Rive et al, 1990; This study) and considered I-Type as after Chappel and White (1974). The S-type garnet - muscovite granite series (GMG) series (Feng and Kerrich, 1992) plutons (i.e. Lac

Descelles monzogranite batholith) are the dominant granitoid in the Pontiac subprovince and forms thin sheet like masses (Benn et al, 1993).

## 2.2 Ages of Lithologies Present in the Pontiac Subprovince

The LSIC is inferred to have crystallized at ~2680 (U-Pb zircon = 2686 ± 4 Ma and titanite = 2675 ± 6 Ma; Machado et al, 1991). Intrusions lithologically similar to the LSIC in the Pontiac provide similar U-Pb (zircon and titanite) ages (Mortensen and Card, 1993). The Lac Freschette complex to the north of the LSIC yields a zircon derived U-Pb crystallization age of 2681.0 +1.9/-1.4 Ma (Mortensen and Card, 1993) and 2685 ± 8 Ma (Mortensen et al, 1988), Lac Remigny pluton yields zircon U-Pb ages between 2679.7 ± 0.8 Ma (Mortensen and Card, 1993), Tour de Belleterre crystallized at 2669 ± 3 Ma (Machado et al, 1991), and the Lac Maple intrusion at 2678 +3/- 2 Ma (Machado et al, 1991). Except for Tour de Belleterre, these inferred crystallization ages overlap between approximatelly 2676 Ma to 2683 Ma.

The LSIC intruded the Pontiac sedimentary rocks (<2683 ± 1 Ma; Mortensen and Card, 1993) to the north of the complex, Belleterre-Fugerville tonalite (2705 ± 3 Ma; Carignan et al, 1992) to the south and tholeiitic basalts of the Belleterre belt to the southeast (2690 ± 2 Ma; Mortensen and Card, 1993). The LSIC appears to have a sheared intrusive contact with the Lac des Quinze gneiss complex (2695 ± 1 Ma; U-Pb zircon, Mortensen and Card, 1993) to the west. The LSIC and all surrounding rocks have been intruded by fine grained to pegmatitic monzogranite dykes originating from voluminous granitic plutons of the Reservoir Descelles batholith to the north and east of the LSIC (Rive et al, 1990). Descelles

monzogranites have been dated at 2663-2668.5 Ma (Mortensen and Card, 1993) which represents the final major igneous activity in the Pontiac.

## 2.3 Metamorphism

The Pontiac sedimentary rocks, Belleterre - Lac des Bois volcanic rocks, and tonalitic rocks of the Pontiac Subprovince have undergone medium pressure Barrovian type metamorphism. There is a general increase in grade from upper greenschist facies conditions in the north of the subprovince to upper hornblendite facies metamorphism in the central Pontiac (Camire and Burg, 1993; Jolly, 1978). Sawyer and Barnes (1994) note that the metamorphic grade in the south of the subprovince is highly variable with greenschist to lower amphibolite facies conditions recorded in the Belleterre-Angliers greenstone belt and higher grade migmatitic sediments near the Proterozoic contact in the west. Mortensen and Card (1993) suggest that the southward increase in metamorphic grade may be the result of greater post metamorphic uplift in the south and thermal effects of widespread plutonism.

Metamorphic grade of Pontiac sedimentary rock samples close to the LSIC is biotite zone of the greenschist facies. Ultramafic volcanic rocks intercalated in the Pontiac sedimentary rocks east of the complex contain actinolite and biotite confirming greenschist facies conditions. Metamorphic grade of the Belleterre belt and Baby belt tholeiitic basalts is greenschist facies (Rive et al, 1990) with an increase to upper greenschist / lower amphibolite facies towards the LSIC as a result of contact metamorphism.

# Chapter 3 Geology of the Study Area

## 3.1 Geology of the LSIC

The LSIC is situated in the southern Pontiac subprovince and is bordered by the Descelles Granite and Pontiac sediments to the north and east, Lac des Quinze complex to the west, and Belleterre-Fugerville tonalites and Belleterre belt basaltic rocks in the south (Figure 2). Mapping during the course of this research (1992 - 1996) revealed that the units of the LSIC as presented by Rive (1986) differed from that observed in the field which prompted detailed mapping of the ~35 Km X 30 Km LSIC. Notable differences include separation of the southern from the northern complex, enlargement of the boundaries of the southern complex southward and westward and subdivision of the complexes by modal mineralogy. A sliver of Belleterre belt volcanic rock is noted to extend westward of Baie Klock of Lac Simard along the southern contact of the north complex, and the quartz rich granitoids to the south of this contact (Lac Devlin Pluton), included by Rive (1986) in the LSIC, were recognized to belong to the Belleterre Fugerville tonalites based upon mineralogy, texture, and chemistry. The Lac Devlin intrusion is a small dioritic to monzodioritic body located immediately north of the Belleterre belt volcanic rocks. The Lac Remigny and LSIC appear to represent a continuous intrusive complex that may be offset by a fault (mapped by Rive, 1986; Rive 1990) sinistrally. Due to time constraints, the westward extent of the LSIC was mapped to the boundary defined by Rive (1990) which terminates at Baie Gillies of Lac des Quinze.

The complex consists primarily of monzonites, monzodiorites / quartz monzodiorites, diorites, lesser monzonites, quartz monzonites, hornblende diorites, clinopyroxene bearing hornblendites, and volumetrically minor syenites/mela-syenites, alkali feldspar syenites and

# LEGEND

**Country Rock**

- Reservoir Descelles Granite
- Belleterre-Fugerville Tonalite
- Lac des Quinze Gniess/Tonalite
- Pontiac Meta-Sedimentary Rock
- Belleterre Belt Basalt
- Ultramafic Volcanic Rock
- Gabbro

**Lac Simard Intrusive Complex: Saccharoidal Units**

- Saccharoidal Monzonite
- Saccharoidal Monzodiorite
- Saccharoidal Syenite
- Saccharoidal Diorite

**Lac Simard Intrusive Complex: Non-Saccharoidal Units**

- Mela-Syenite
- Granodiorite
- Quartz-Monzodiorite
- Diorite
- Mela-Diorite
- Monzodiorite
- Mela-Monzodiorite
- Monzonite
- Mela-Monzonite
- Hornblendite

**Dyke Rock**

- ..... Mafic Dyke
- ------ Diabase Dyke

- $\dagger$ Foliation

**Figure 2.**

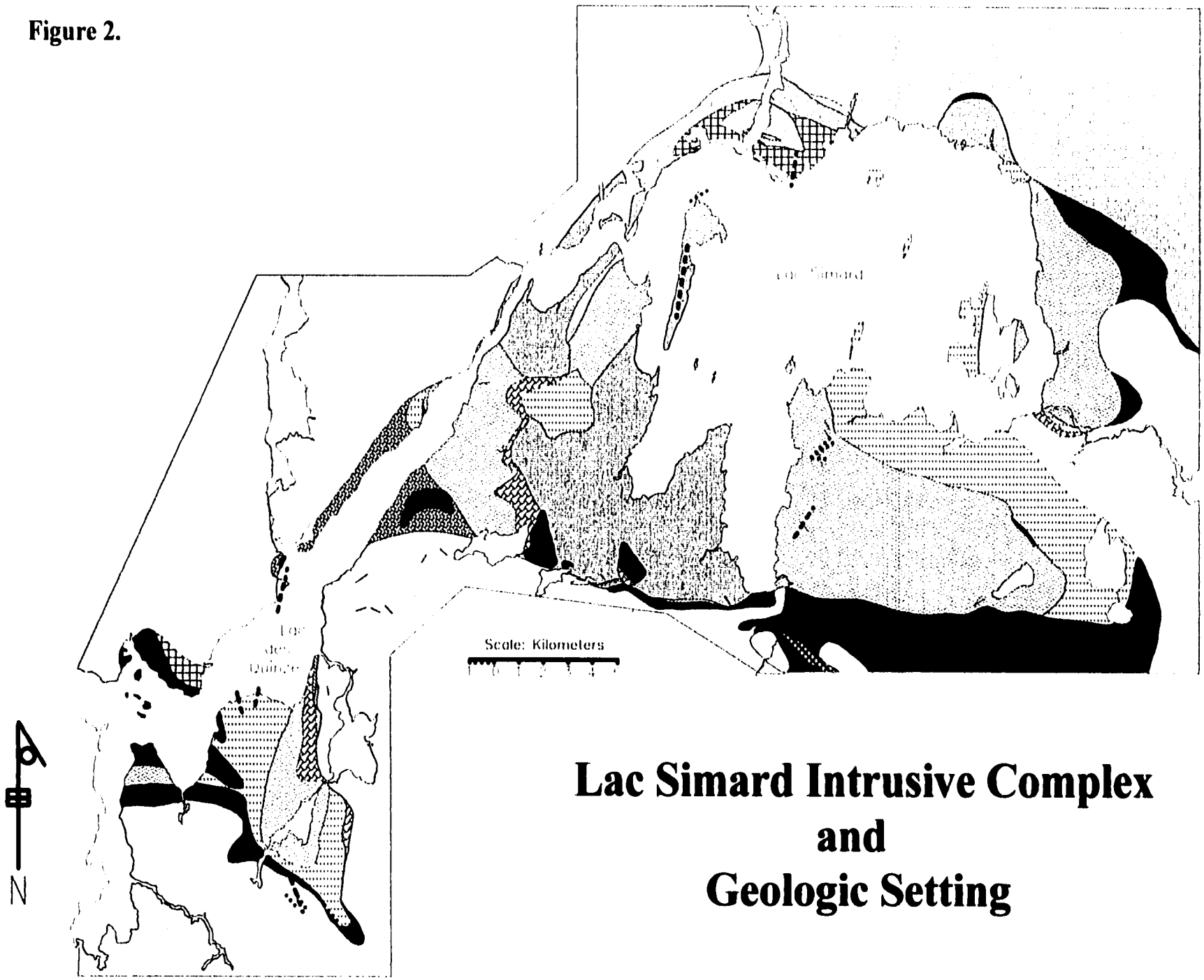


# Lac Simard Intrusive Complex and Geologic Setting

granodiorites. The LSIC has been subdivided into northern and southern complexes separated at surface by tonalitic rocks of the Belleterre - Fugerville pluton. The northern complex is an east-west elongate, south west tapering body that consists of diverse, multiple, contemporaneous intrusions of predominantly diorite, monzodiorite, quartz-monzodiorite, monzonite, and lesser syenite, and clinopyroxene-hornblendites (± biotite to phlogopite). Crudely north-south elongate plug-like to sigmoidal intrusions constitute the clinopyroxene bearing core rocks of the north complex. Clinopyroxene is absent in the peripheral, contact parallel, elongate intrusions partially enveloping the clinopyroxene bearing core intrusions along the north and west contacts. Clinopyroxene hornblendites have intruded as plugs near or at the contact of the LSIC and country rock and internal contacts in the southern half of the northern LSIC.

The southern complex is a smaller irregularly shaped, south tapered, roughly reversed rotated "L" shaped collage of differentiated diorite, quartz-monzodiorite to monzodiorites, and units of clinopyroxene mela-diorite, mela-monzonite, monzodiorite, and granodiorite. Granitoids of the LSIC are holocrystalline, hypidiomorphic to hypidiomorphic granular (saccharoidal textured units in the north complex) and fine to medium grained, with rare occurrences of pegmatitic phases and equigranular to feldspar porphrytic phases. Predominantly fine to medium massive grained clinopyroxene hornblendites intrude the complex as kilometer wide plugs. Textures, grain size and internal structures are highly variable within individual clinopyroxene-hornblendite intrusions and between the clinopyroxene-hornblendites. Rounded to attenuated actinolitic, melanocratic dioritic, and amphibolitic enclaves 0.5-5cm in length oriented parallel or subparallel to the foliation and

comprising 1-5 vol.% (locally 10-20 vol.%) are a common feature in a majority of the units of the LSIC.

Monzodiorites intrude Pontiac sedimentary rocks (Plate 1a), Belleterre belt volcanic rocks and Belleterre - Fugerville tonalites (Plate 1b). Fine grained, foliation concordant and discordant, monzodiorite dykes intrude the Belleterre-Fugerville tonalites and include angular xenoliths of tonalite for up to hundreds of meters from the LSIC - tonalite contact. Granodiorites, and tonalites of the Belleterre - Fugerville pluton, and LSIC monzodiorites intrude the Belleterre volcanic rocks as foliation parallel, 10-100cm wide dykes with the tonalitic granodiorite dykes being typically more highly folded and foliated than the thinner weakly to non-foliated monzodiorite dykes. Intrusion of the LSIC into the Pontiac sedimentary rocks to the north of the complex occurs as foliation parallel sills. Late dykes of fine grained and pegmatitic Reservoir Descelles granite, and later approximately north - south trending diabase intrude the LSIC. Numerous melanic mafic dykes are also present which are characteristically highly deformed relative to the granitoid host rocks.

The rock types present in the LSIC display both gradational and mutually intrusive contacts. Hornblendites appear to have intruded the diorite-monzodiorite-monzonite rocks, as they contain monzodiorite inclusions or blocks (Plate 2a), but are commonly intruded by the granitoids also. Hornblendites are mapped at or near to contacts between LSIC units or country rock-LSIC contacts in the north LSIC whereas those in the southern complex have intruded both at contacts and within major units of the complex. Hornblende diorites (± Bt), through monzodiorites and monzonites may show a gradational change with the coarse grained melanic gabbros exhibiting a cumulate texture (large hornblende grains in a feldspar

Plate 1a. Intrusive relationships between Pontiac sedimentary rocks and the LSIC. Pontiac sedimentary rock - LSIC intrusive relationships. Pontiac sedimentary rocks are intruded by LSIC granitoid sills and recrystallized at the LSIC - Pontiac sedimentary rock contacts.

Plate 1b. Intrusive relationships between the Belleterre - Fugerville tonalites and the LSIC. Undeformed dyke of LSIC granitoid (dark colored) with sharp contacts and intruding Belleterre - Fugerville tonalites (light colored rock at margins of photograph). The dyke contains xenoliths of tonalite (center of photograph) incorporated during intrusion.

a)

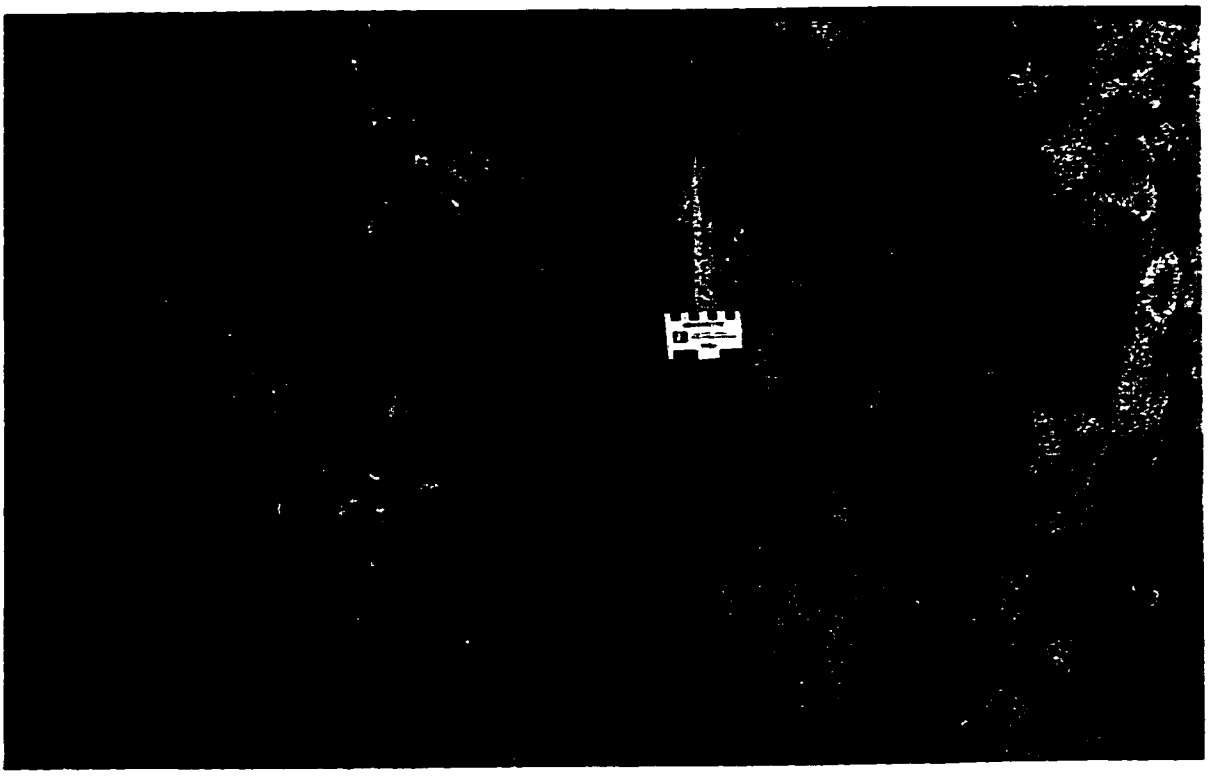

b)

Plate 2a. Large angular granitoid blocks included in a fine grained hornblendite unit. Xenocrysts of feldspar and angular granitoid blocks were stoped from adjacent units during hornblendite emplacement.

Plate 2b. Cumulate textured diorite with a high concentration mafic enclaves. Cumulate diorites contain large hornblende euhedra with interstitial plagioclase. A high mafic enclave density is usually associated with these rocks.

a)

b)

matrix and high actinolitic enclave density (Plate 2b)) but intrusion of monzodiorite into diorite also occurs resulting in a contact marked by large angular rafts or slices of diorite at the contact (Plate 3) and subround dioritic inclusions in monzodiorite farther into the monzodiorite from the contact. Gradations marked by varying proportions of mafic phases, commonly amphibole, are observed where melanic to relatively leucocratic variations of one rock type occur.

Contact mixing relationships and a non-gradational relationship between numerous units indicates that the LSIC is composed of a series of contemporaneous intrusions. Limited in situ fractionation of some units has occurred based upon gradational changes in lithology and mafic mineral concentrations.

Deformation is confined dominantly to the margins of the LSIC (Plate 4). Deformation within the core of the complex is confined to discrete zones as evidenced by a thin (30 cm) east contact parallel shear zone mapped in the central monzodiorite. Sheared mafic dykes crosscutting the LSIC granitoids also indicate that some degree of focused deformation was still ongoing late in the crystallization history of the LSIC. A very weak mineral alignment is present throughout the majority of the complex.

Plate 3. Contact mixing between dioritic and monzodioritic units of the LSIC. Oriented subround, elongate, diorite autoliths were incorporated into a coarser grained monzodiorite at their unit contacts during intrusion of monzodiorite into diorite.

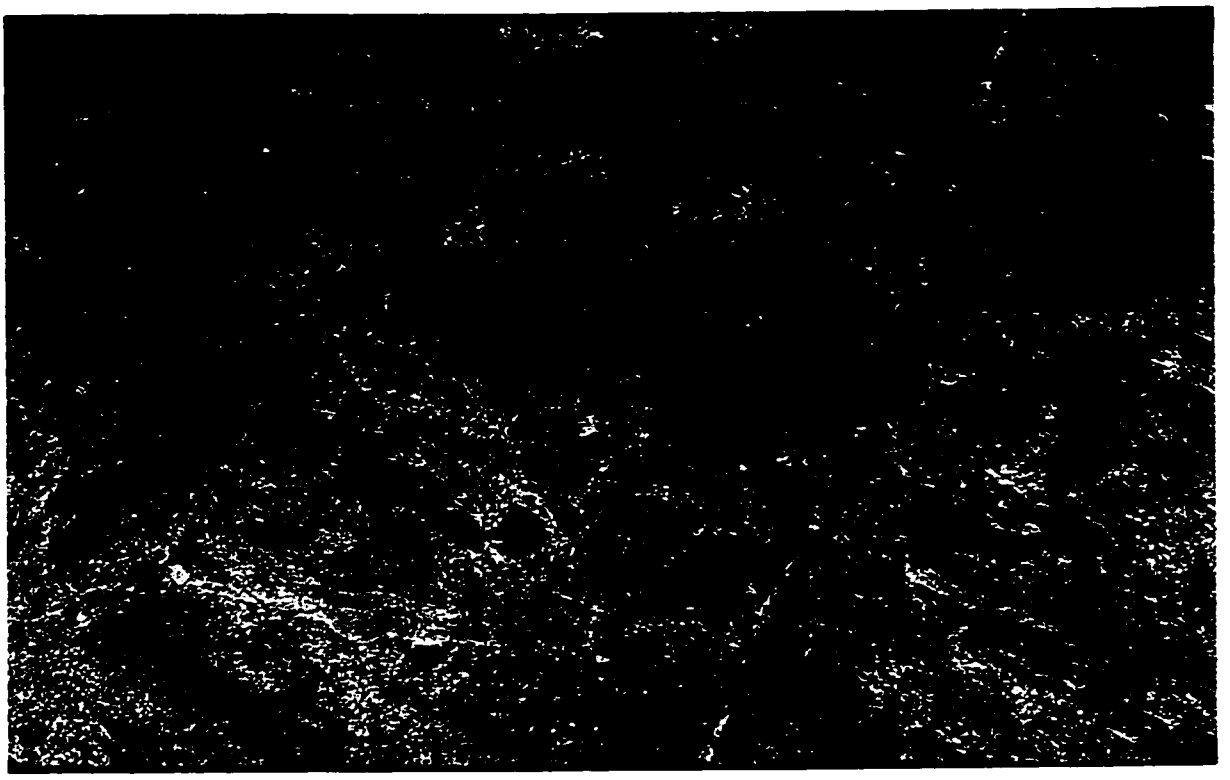

Plate 4. **Sheared granitoids at the western contact of the LSIC. Highly attenuated mafic enclaves are observed along the La Force shear zone at the sheared margin of the western contact of north complex of the LSIC with the Lac des Quinze complex. Enclaves may have been sheared while incompletely solidified leading, in part, to the banding observed in outcrop.**

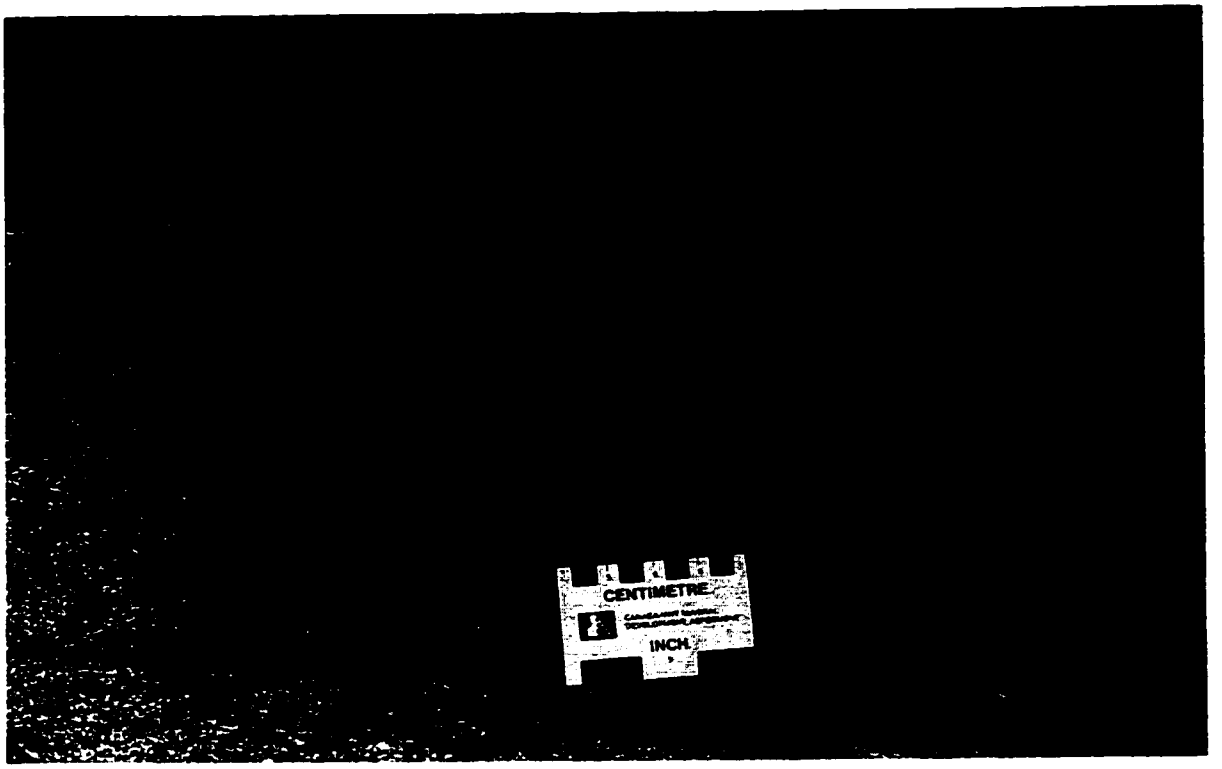
CENTIMETRE
INCH

## 3.2 Units of the North Complex

### 3.2.1 Non-Saccharoidal Clinopyroxene-Bearing Granitoid Units

Six main intrusive rock units have been mapped with the aid of thin sections and potassium staining (Appendix 2). Although lithologic heterogeneity exists within a given unit, the dominant lithologic units are defined below and presented in Figure 3.

**Eastern Monzodiorite**

In the eastern portion of the complex (Figure 3, 4), an inhomogeneous unit of monzodiorite, minor mela-monzodiorite, diorites and mela-diorite occurs. The diorites are the major rock type at the eastern contact of the LSIC. Thin units of mela-quartz-biotite diorite and quartz monzodiorite occur as lenses parallel to the southern contact of this unit with the Pontiac sedimentary rocks.

**Central Eastern Quartz Monzodiorite**

A sigmoidal, north-south elongate unit of relatively homogenous light pink quartz monzodiorite and minor monzodiorites occur adjacent to Pontiac sedimentary rock and the central monzodiorite (Figure 3, 4).

**Central Monzodiorite**

This monzodioritic unit (Figure 3, 4) forms a sigmoidal north-south oriented unit with minor diorites at the Central Western Monzonite contact, and large kilometer sized xenoliths

# Legend

**Units of the North Complex**
**Clinopyroxene Bearing Non-Saccharoidal Granitoid Units**

1. **Eastern Monzodiorite**
2. **Central Eastern Quartz Monzodiorite**
3. **Central Monzodiorite**
4. **Central Western Monzonite**
5. **Central Western Quartz Monzodiorite**

**Clinopyroxene Free Non-Saccharoidal Granitoid Units**

6. **North Monzonite**
7. **Western Mela-Monzodiorite and Western Monzodiorite**
8. **Western Hornblende Diorite**
9. **Western Mela-Syenite and Quartz Monzodiorite**

10. **Saccharoidal Units**

**Hornblendites**

11. **Central Western Hornblendite**
12. **South Eastern Hornblendite**
13. **Central Hornblendite**

**Units of The South Complex**
**Non-Saccharoidal Granitoid Units**

14. **North East Mela-Diorite**
15. **Eastern Mela-Diorite**
16. **South Western Diorite**
17. **Core Quartz Monzodiorite**
18. **Eastern Quartz Monzodiorite**
19. **Granodiorite**
20. **Core Monzodiorite**
21. **Western Monzodiorite**
22. **Mela-Monzonites - Mela-Syenites, Western Mela-Monzonites and Mela-Syenites**

**Hornblendite**

23. **Southern Hornblendite**
24. **North Central Hornblendite**
25. **Northern Hornblendite**
26. **Western Hornblendite**

Figure 3.

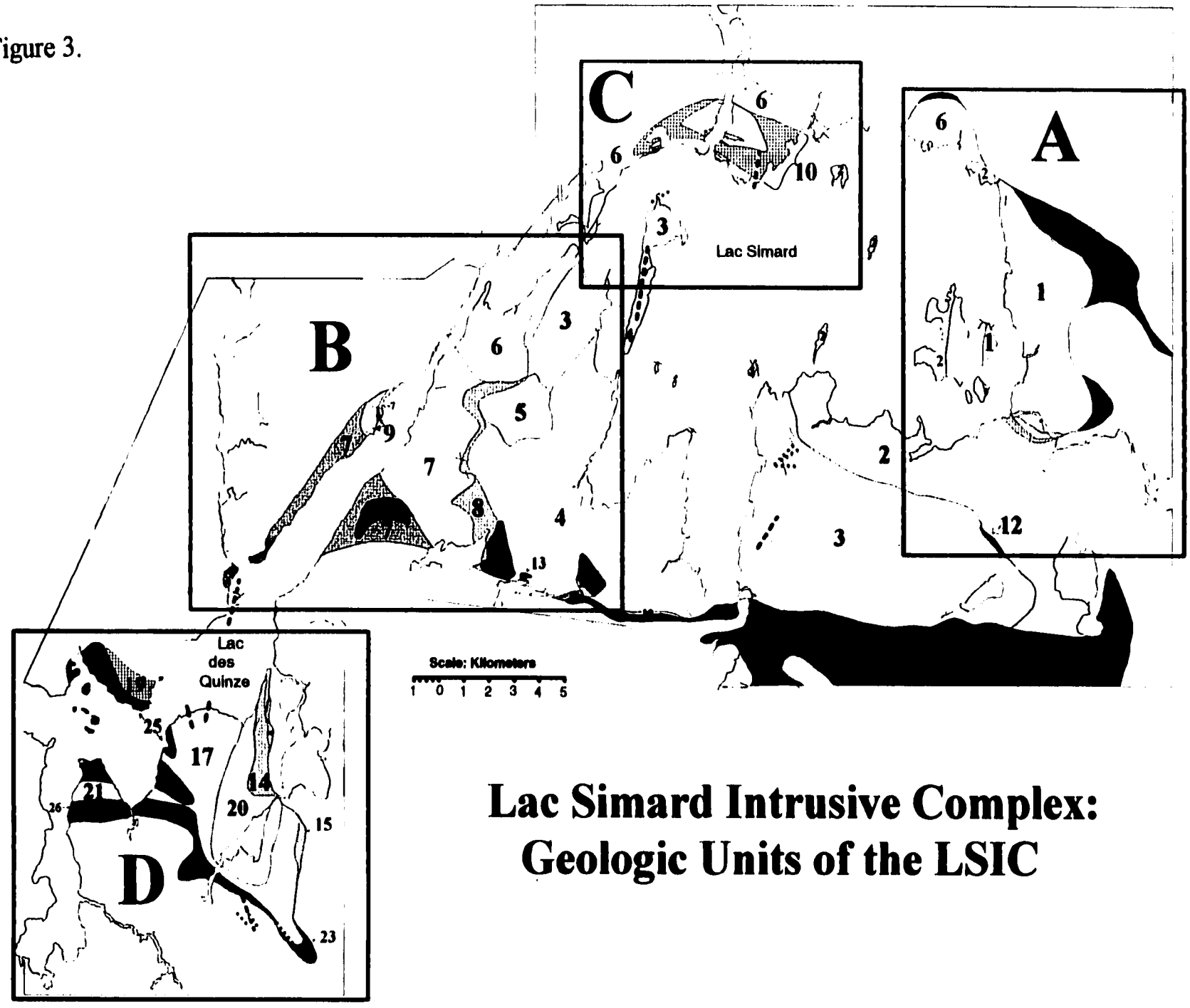


**Lac Simard Intrusive Complex: Geologic Units of the LSIC**

# Detail View A: Eastern LSIC

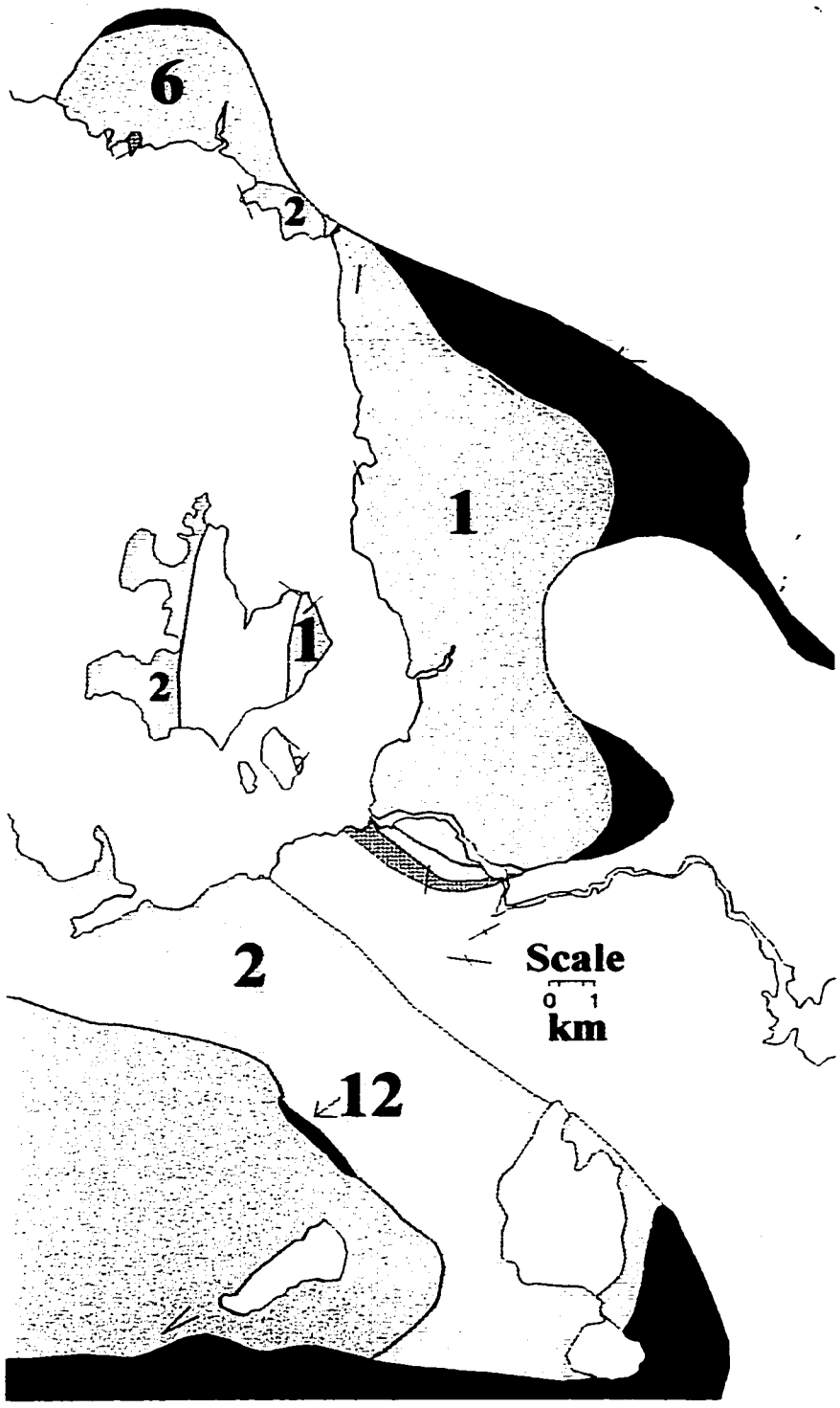


Figure 4. Detailed view of the eastern LSIC showing unit relationships not easily recognized at the scale of Figure 2. See text for description of units. Legend is the same as that for figure 3.

of Pontiac sedimentary rock at the north and north western contacts. A medium grained biotite - clinopyroxene hornblendite intrusion is also located at the contact between the central monzodiorite and central eastern quartz monzodiorite. Thin (<1 m), north-east and east west trending sheared melanic mafic dykes intrude the monzodiorites at the core of this unit. A thin undulatory shear zone (~1 m wide), and sheared mafic dykes indicate that localized deformation affected the complex late in its crystallization history.

**Central Western Monzonite**

This unit of predominantly light pink to salmon colored monzonite and lesser monzodiorite occurs in the south western quadrant of the clinopyroxene bearing core of the LSIC (Figure 3, 5). The southern margin of this unit is intruded by small clinopyroxene - hornblendite plugs and contains a thin zone of diorite and saccharoidal textured monzodiorite.

**Central Western Quartz Monzodiorite**

The central western quartz monzodiorite represents a small stock of highly magnetic, medium grained, light pink, feldspar porphrytic quartz monzodiorite.

### 3.2.2 Non-Saccharoidal Clinopyroxene-Free Granitoid Units

The clinopyroxene absent units have been divided into four main and two minor units.

Figure 5. Detailed view of the north - western LSIC showing unit relationships not easily recognized at the scale of Figure 2. See text for description of units. Legend is the same as that for Figure 3.

# Detail View B: North Western LSIC

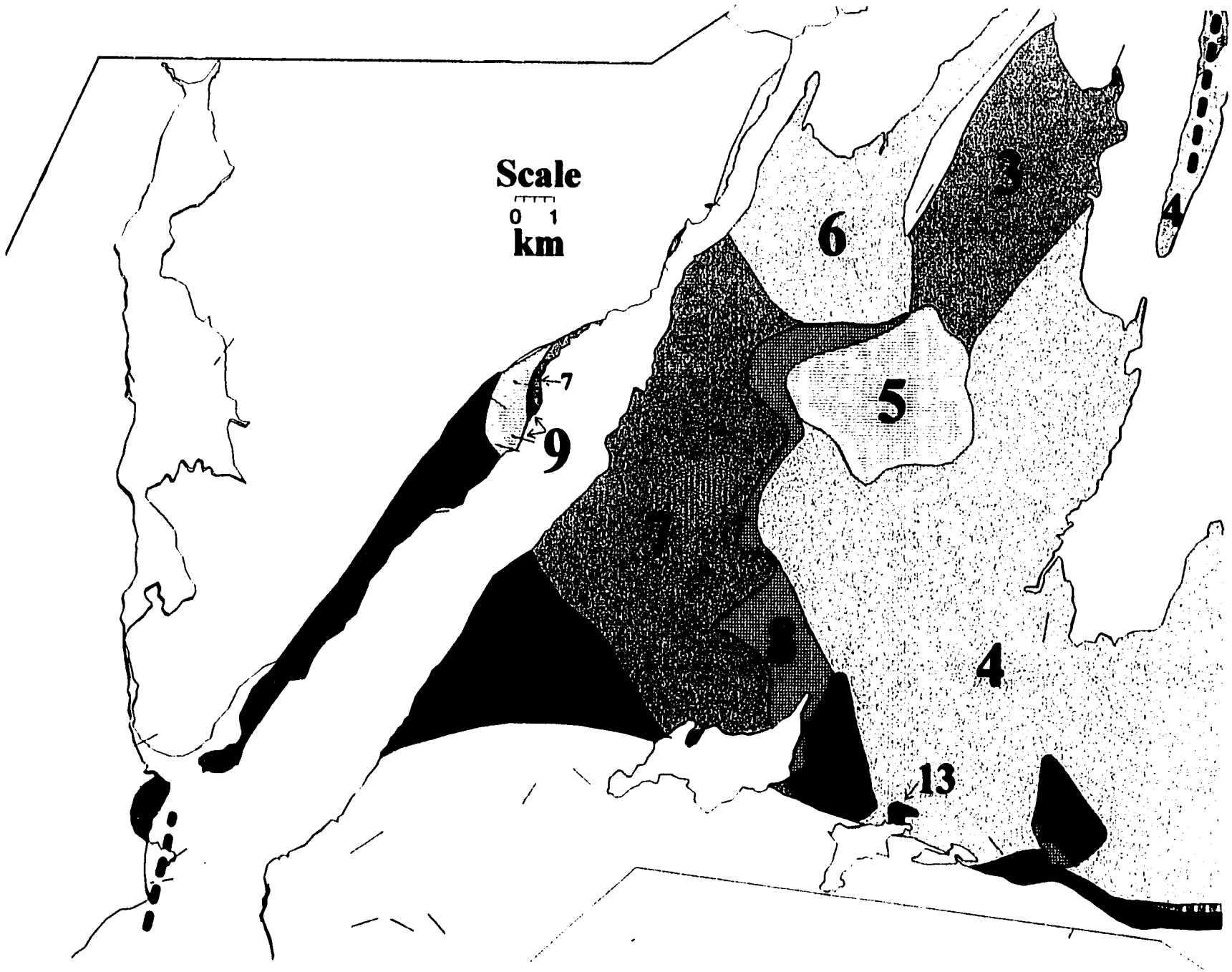

**North Monzonite**

A thin peripheral unit of variably K-feldspar porphrytic to equigranular medium grained monzonite wraps around the north and west of the complex (Figure 3, 5). Contacts with the Lac des Quinze gneisses and Pontiac sedimentary rocks are typically moderately to strongly foliated and enclaves are strongly attenuated (>5:1). A layered, melanic, hornblendite to hornblende porphyritic diorite with enclave rich horizons is located in the north eastern contact area of this unit.

**Western Mela-Monzodiorite and Western Monzodiorite**

Monzodiorites (Figure 3, 5) south of the north monzonite typically are more strongly K-feldspar porphrytic than the monzonites and may be either gradational or intrusive to the monzonites as no contact relations were observed. Towards the south of this unit, a sharp increase in the mafic mineral content, textural inhomogeneity due to amphibole wisps, mafic crystal clots and a higher mafic enclave density contrast strongly with the homogenous leucocratic western monzodiorite. The abrupt transition and incorporation of fine grained mela-monzodiorite as irregular layers, 2-10 cm thick, with sharp contacts, in the western monzodiorite indicate that these two units may represent synchronous intrusions with mixing along the contact.

**Western Hornblende (± Biotite) Diorite**

Fine to medium grained diorites outcrop along the western contact of the clinopyroxene bearing monzonites (central western monzonites) (Figure 3, 5). Some outcrops

are cumulate textured but not interpreted to represent cumulates of adjacent clinopyroxene bearing units. Cumulate diorites may have been derived from fractionation from this dioritic unit itself. Diorites contain feldspar phenocrysts and monzodiorite xenoliths which appear to be derived from nearby feldspar porphyritic monzodiorites (western monzodiorites) and indicate limited mixing occurred at the contact between these two contemporaneous units.

**Western Mela-Syenite and Quartz Monzodiorite**

These two minor units are located in the western margin of the northern LSIC (Figure 3, 5). The quartz monzodiorite is feldspar porphrytic and contains, in addition to elongate and ovoid mafic enclaves, amphibolitic wisps such as those found in the western mela-monzodiorite. The mela-syenite unit is a fine to medium grained equigranular hypidiomorphic amphibole and K-feldspar shore outcrop with a similar appearance as the western mela-monzodiorite. This mapped unit is small and may represent feldspar heterogeneity within the mela-monzodiorite and not a separate unit.

### 3.2.3 Saccharoidal Units

Foliated units of leucocratic clinopyroxene bearing saccharoidal textured monzonites, monzodiorites and syenites occur in the north of the complex as a roughly contact and foliation parallel elongate body with a zoned distribution of mapped lithologies (Figure 3, 6). A moderate to strong foliation, light color, equigranular saccharoidal texture, lack of large mafic enclaves, and the presence of large euhedral titanite and subhedral lathes of amphibole distinguish this group of units from other units of the LSIC. A small saccharoidal monzodioritic unit also outcrops along the southern contact of the LSIC (Figure 3).

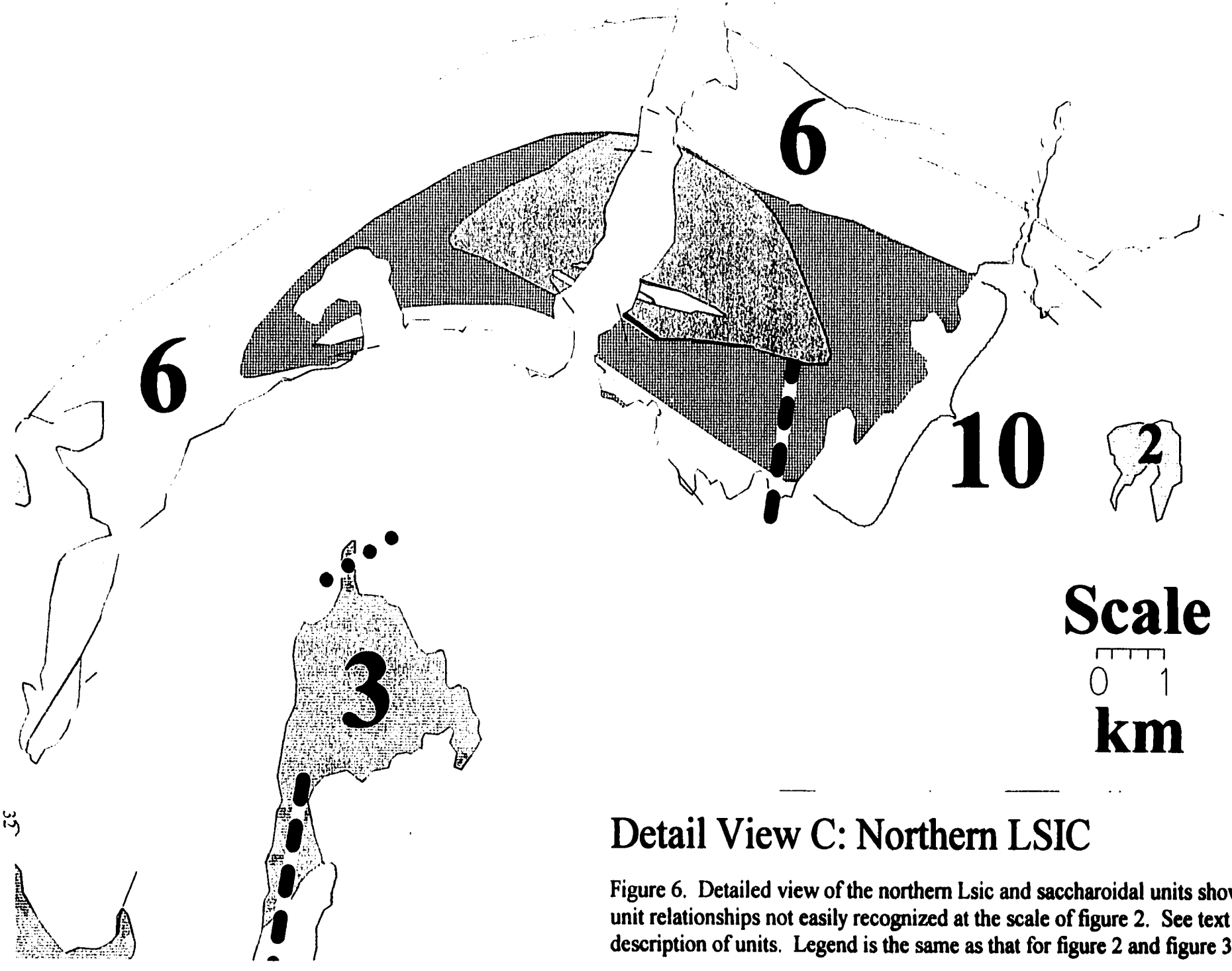


32

## Detail View C: Northern LSIC

Figure 6. Detailed view of the northern Lsic and saccharoidal units showing unit relationships not easily recognized at the scale of figure 2. See text for description of units. Legend is the same as that for figure 2 and figure 3.

### 3.2.4 Hornblendites

Clinopyroxene bearing hornblendites in the northern complex occur as two types; fine to medium grained dark green clinopyroxene-biotite-hornblendites, and epidote altered green black equigranular medium grained clinopyroxene hornblendites with rare biotite and exhibiting a strong aeromagnetic response.

#### Clinopyroxene-Biotite-Hornblendites

#### Central Western Hornblendite

A large unit of fine to medium grained allotriomorphic to granular dark green hornblendite intrudes at the inferred contact between the western monzodiorites and mela-diorite (Figure 3, 5). This plug is mineralogically distinct from the hornblendites intruding the central western monzonite by virtue of the presence of biotite/phlogopite and a lack of significant magnetite. This unit is massive and fractures with a blocky appearance along planes defined by biotite/phlogopite.

#### South Eastern Hornblendite

This dark green medium grained allotriomorphic clinopyroxene hornblendite with coarse subhedral biotite intrudes along the contact between the clinopyroxene bearing quartz-monzodiorites and monzodiorites (Figure 3, 4).

### Clinopyroxene- Hornblendites

#### Central Hornblendites

A cluster of three clinopyroxene hornblendites occurs at the southern contact of the north complex (Figure 3, 5). Hornblendites are relatively homogenous as black to green-black, equigranular, epidote altered, clinopyroxene - hornblendites which show complex intrusive relationships with the host monzonite. These hornblendites are commonly intruded by monzonites, and have very irregular contacts. Red, very fine grained leuco-syenite dykes approximately 30 cm wide are found in the most westerly of the three clinopyroxene-hornblendites in this unit.

## 3.3 Units of the South Complex

Unlike the northern complex, clinopyroxene bearing hornblendite units are minor in the southern complex and only two units of mela-dioritic were noted to contain clinopyroxene. Additionally, saccharoidal textured units were not observed. While the northern LSIC units are mapped as predominantly a collage of units, those in the eastern half of the southern LSIC are mapped with a zonal distribution (Figure 3, 7). Also, a small northern peripheral unit of granodiorite, a lithology not present in the northern complex, intrudes and brecciates adjacent units. Ultramafic intrusions compose a larger percentage of the southern complex, and are typically finer grained amygdaloidal and enclave rich relative to those in the northern complex.

# Detail View D: Southern Complex

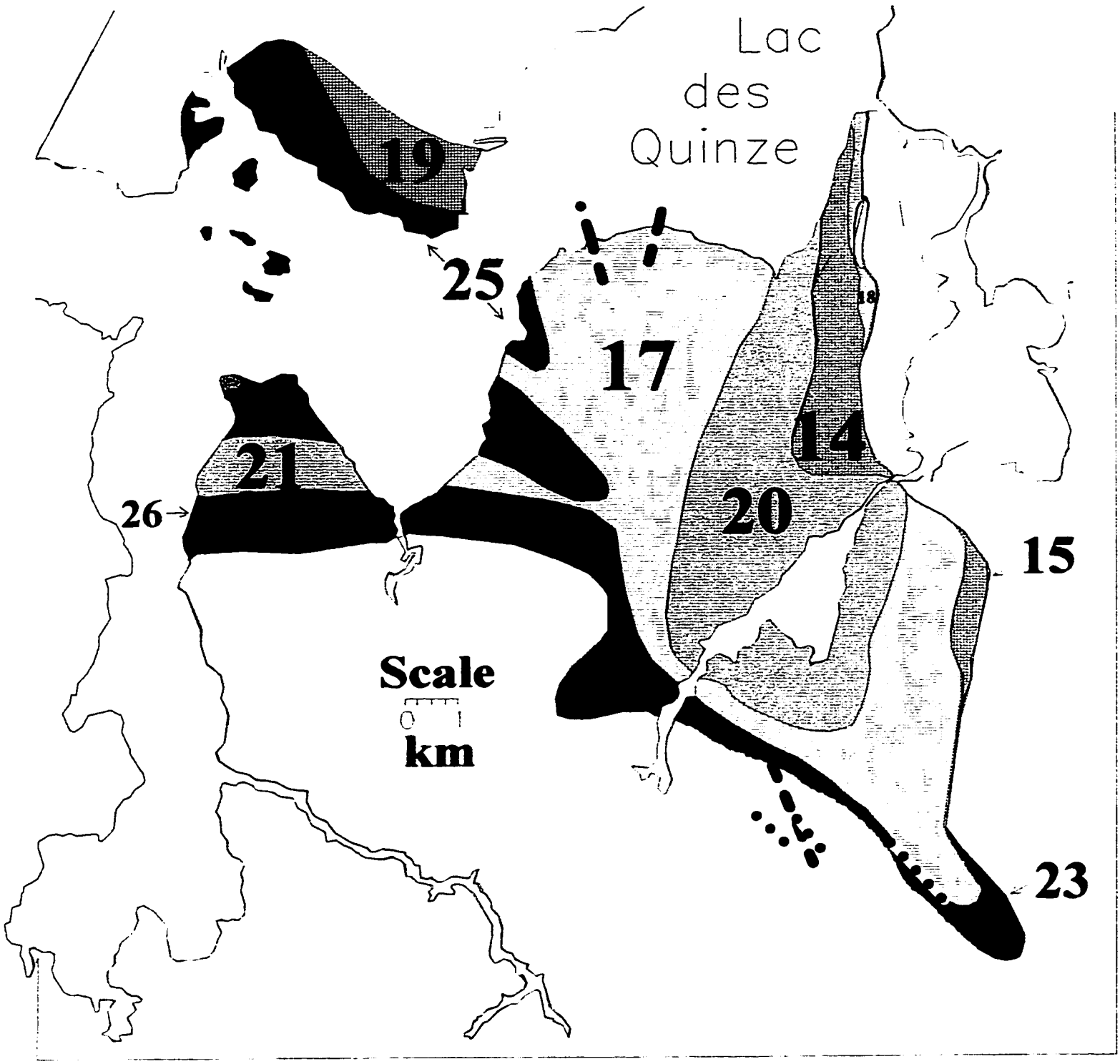


Figure 7. Detailed view of the southern complex of the LSIC showing unit relationships not easily recognized at the scale of Figure 2. See text for description of units. Legend is the same as that for figure 2 and figure 3.

### 3.3.1 Non-Saccharoidal Units

**North East Mela-Diorite**

Clinopyroxene bearing fine to medium grained equigranular to amphibole phenocrystic mela-diorites (Figure 3, 7) occur as an extensively brecciated unit (Plate 5a) with interstitial monzodiorite and granodiorite. Fragments of mela-diorite range from subround blocks to rounded elongate and rounded "bent" autoliths (Plate 5b) indicating that the intrusion of the granodiorites and monzodiorites was semi-contemporaneous with the earlier intrusion of the mela-diorite which was partially solidified. The degree of disruption of this unit appears to increase towards the north.

**Eastern Mela-Diorite**

This unit (Figure 3, 7) is equivalent to the north-east mela-diorite, to which it is probably related, but is not brecciated by later intrusions. Both of these mela-diorite units have intruded at the contact of the complex with the Belleterre-Fugerville tonalites.

**South Western Diorite**

The southwestern diorite (Figure 3, 7) ranges from diorite to very sporadic quartz diorite. At the contact to the quartz-monzodiorites, there is a border facies of mingled melanic diorite which is similar in appearance to the western mela-diorite. It grades into diorite with a lower mafic mineral concentration and a lack of mingling textures and to a homogenous hypidiomorphic grey-white to light pink quartz monzodiorite. A similar

Plate 5a. Intrusive brecciation of mela-diorite. Enclave rich mela-diorite in the southern complex of the LSIC are brecciated and infilled by intrusion of granodiorite.

Plate 5b. Mela-dioritic enclave in monzodiorite and granodiorite. Bent and fragmented autolithic enclave of melanic diorite indicates that the enclave may not have been completely solidified at the time of incorporation.

a)

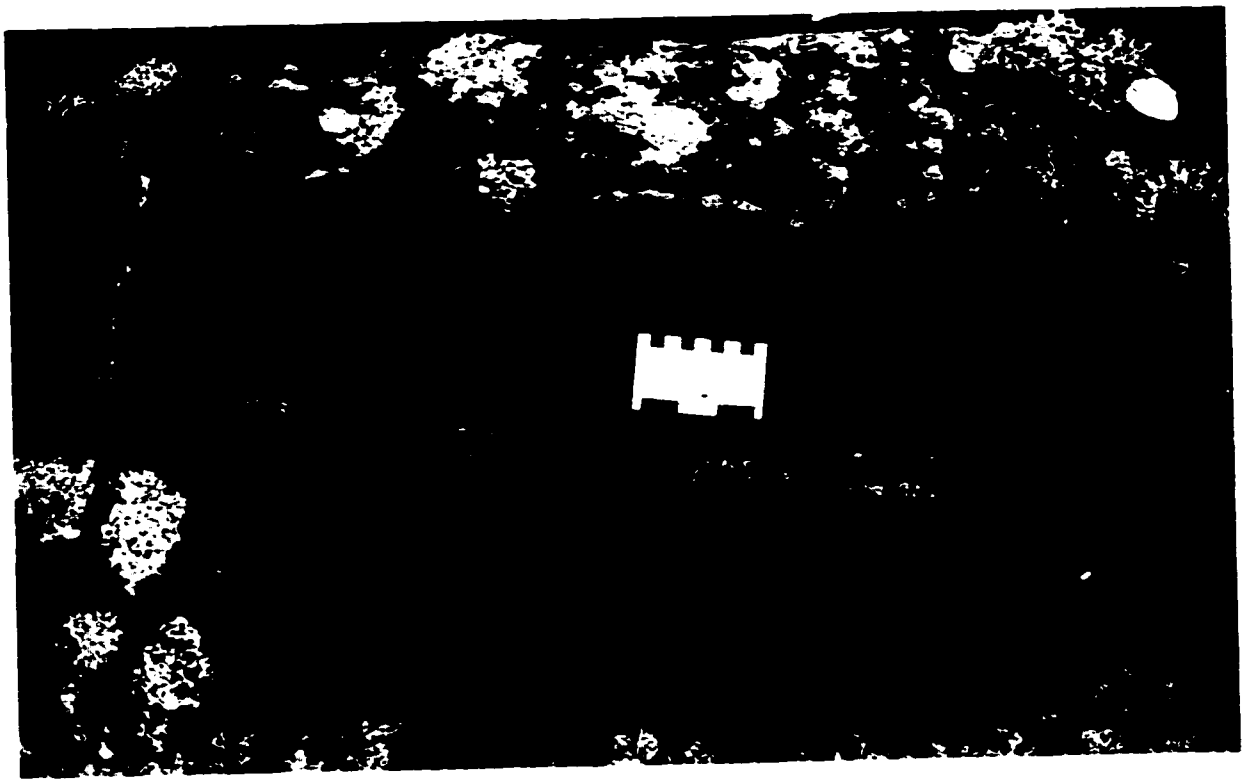

b)

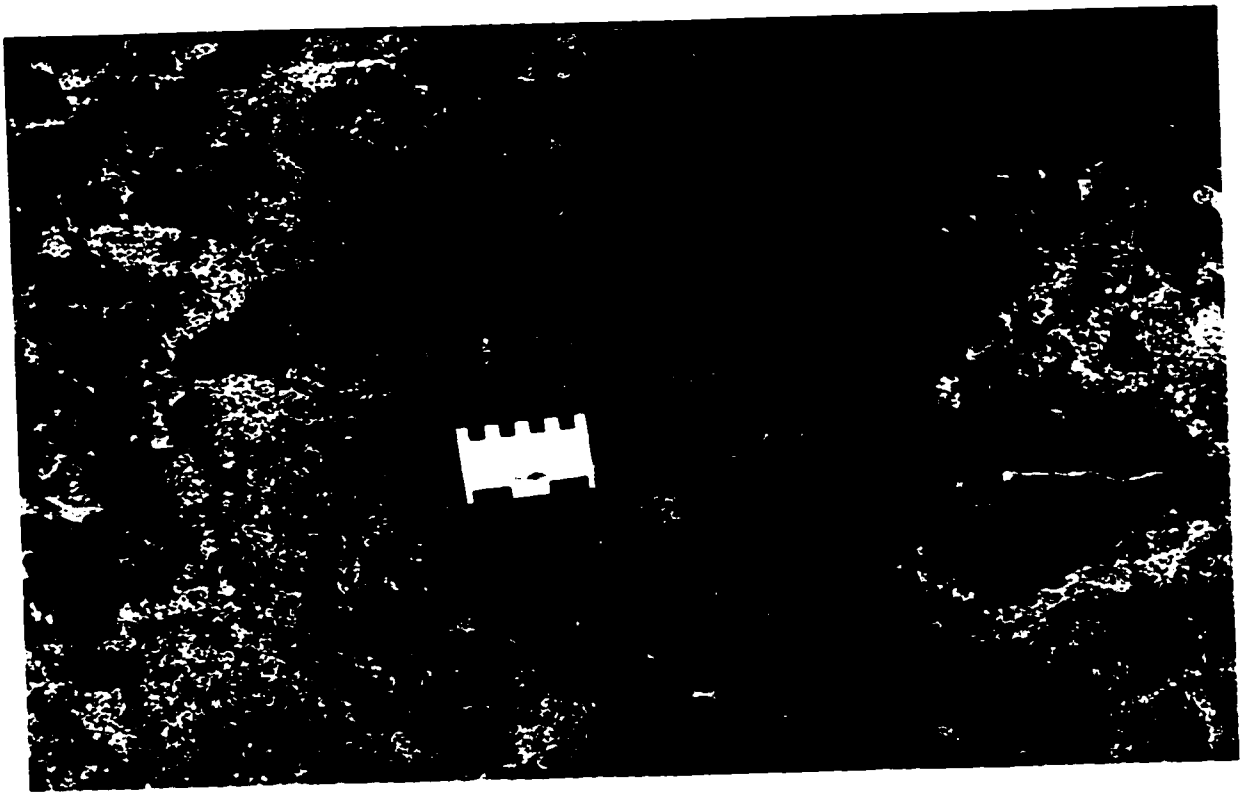

gradational change may exist between the monzodiorites and the quartz-monzodiorites but could not be ascertained in the field.

### Core Quartz Monzodiorite

As previously mentioned, field relationships suggest that this unit (Figure 3, 7) is possibly gradational from the south western diorite. All samples are medium grained, hypidiomorphic, equigranular to feldspar porphrytic and leucocratic with a weak fabric defined by alignment of amphibole, enclaves, and occasionally plagioclase lathes. A contact mixing relationship between the northern hornblendite and this unit is documented on an island in Lac des Quinze.

### Eastern Quartz Monzodiorite

A small outcrop of quartz monzodiorite (Figure 3, 7) was found on the east side of the north-eastern mela-diorite which is indistinguishable from the core quartz-monzodiorites. This may represent a small plug of related material or a large dyke cutting the mela-diorites.

### Northern Granodiorite

A northern peripheral unit of dark red colored medium grained granodiorite with sparse mafic enclaves is found in the north of this complex (Figure 3, 7). This unit was emplaced later than the northern hornblendite, melanic monzonites of the western portion of this complex, and the eastern mela-diorites, all of which this unit brecciates and fills resultant

interstices. A lack of mixing textures and intrusive brecciation of adjacent units may indicate that this unit was one of the last to be emplaced within the complex.

**Core Monzodiorite**

This unit is texturally and mineralogically similar to the core quartz-monzodiorites, but with a lower quartz content. No intrusive relationships with the quartz- monzodiorite were observed and it is possible that this represents a differentiation product of the south-western diorites. Brecciation of the adjacent north-east mela-diorite by this unit indicates the later emplacement of the monzodiorite.

**Western Monzodiorite**

Light salmon colored, fine to medium grained, equigranular monzodiorite is found as a discrete unit with indeterminate contact relations between adjacent hornblendite, mela-monzonite, and diorites (Figure 3, 7).

**Mela-Monzonites - Mela-Syenites Western Melanic Monzonites**

Fine to medium grained, dark colored, occasionally feldspar porphrytic monzonite to minor mela-syenite compose the western half of the southern LSIC (Figure 3, 7). Contacts in the north are brecciated with interstitial filling of granodiorite.

### 3.3.2 Hornblendites

In the southern complex, the most southern hornblendite (Figure 3, 7) is similar in hand sample to the green black clinopyroxene hornblendites of the northern complex. Three other hornblendites, although texturally variable, differ from those in the northern complex by virtue of very fine grain size, amygdular structures, abundant actinolitic enclaves, and the development of a glomerophyric texture composed of agglomerations of fine plagioclase and K-feldspar lathes in contact areas.

#### Southern Hornblendite

Contacts with adjacent units were not observed for this small unit of fine to medium grained hornblendite with minor biotite. This unit is located at the southern termination of the southern complex, and grades into a fine grained mela-biotitic diorite toward the north (Figure 3, 7).

#### North-Central Hornblendite

Fine grained hornblendites in the core of the complex (Figure 3, 7) display an oriented glomerophyric texture. Minor phlogopite/biotite is noticed and its concentration is inversely proportional to the feldspar concentration of the rock. Intrusion into adjacent quartz-monzodiorites and diorites has resulted in the incorporation of autolithic blocks of pink quartz-monzodiorite/monzodiorite and feldspar xenocrysts.

**Northern Hornblendite**

A variety of textures is noted in this intrusion. This biotite/phlogopitic hornblendite (Figure 3, 7) predominantly outcrops as a dark green black very fine grained homogenous intrusive rock with an oriented glomerophyric facies (Plate 6), abundant actinolite enclaves, feldspar xenocrysts, and small <0.5cm round felsic inclusions with a radiating texture and positive weathering cores. This fine grained material grades into a medium grained biotitic hornblendite to an actinolite biotite variant at the central quartz-monzodiorite contact. Dyking of the hornblendite by adjacent units and incorporation of fragments of adjacent units by the hornblendite indicate that intrusion of both units was semi- contemporaneous. A mixing relation is observed in the north of this unit as an incorporation of feldspar phenocrysts in the hornblendite and a decreasing hornblendite enclave density and mafic mineral content within the quartz-monzodiorite away from the contact.

**Western Hornblendite**

A fine grained actinolitic hornblendite intrudes at the southern contact with the Belleterre volcanic rocks in the western half of the complex (Figure 3, 7). Although similar in appearance to the basalts, the hornblendites are much more massive and do not exhibit the prominent cleavage developed in the basalts.

Plate 6. **Oriented glomerophyric facies in a fine grained hornblendite. This texture is produced during contact mingling of hornblendite with an adjacent granitoid leading to assimilation of felsic material in the hornblendite.**

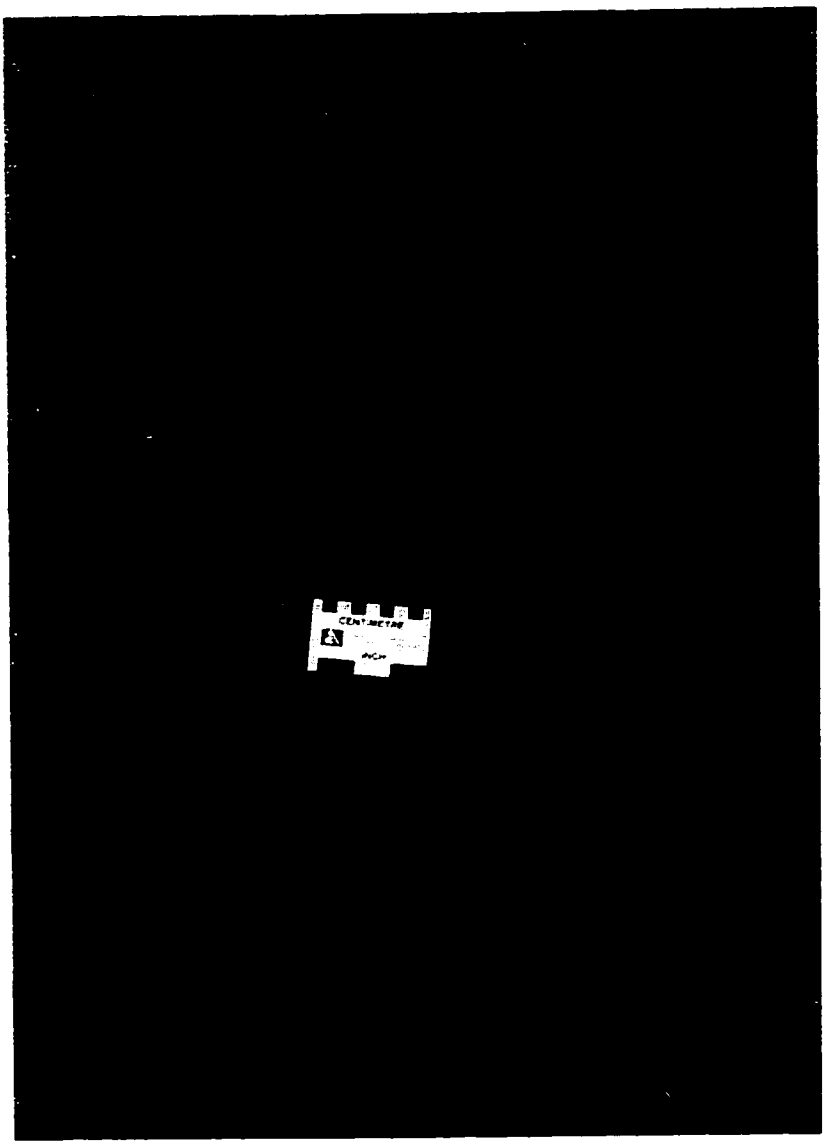

# Chapter 4 Enclaves

The ubiquitous occurrence of diverse types of enclaves is a notable feature of the LSIC. The rocks of the LSIC contrast strongly with the neighboring Belleterre-Fugerville tonalites and associated granodiorites by the occurrence of mafic enclaves in the LSIC.

## 4.1 Enclave Types

Terminology used to define enclave types follows that outlined by Didier and Barbarin (1990). Enclaves observed in the LSIC are of seven types: xenoliths of mafic volcanic rock, sedimentary rock, and tonalites, and autoliths of diorite, actinolite, monzodiorite, and hornblendite.

### 4.1.1 Sedimentary and Igneous Xenolithic Enclaves

Angular to subangular to xenoliths of Belleterre belt volcanic rocks (Plate 7a) and Belleterre-Fugerville tonalites are present within the LSIC in close proximity to contacts with these rocks. Dykes branching out from the LSIC intruding Belleterre belt volcanic rocks and Belleterre-Fugerville tonalites also contain xenoliths of these rocks. Rare large (~10 m) volcanic xenoliths are present near the northern and western LSIC margins far away from the basalt/LSIC contact. The shape of the xenoliths range from large (1-10 m) elongate slivers to small (3-10 cm) subround partially assimilated fragments. Large (>3m), strongly foliated sedimentary xenoliths were noted within the LSIC far away from the sediment rock/LSIC contacts. Sedimentary rock xenoliths at the LSIC/Pontiac sedimentary rock contact are typically subangular and foliated to skialithic at their margins or completely recrystallized.

Plate 7a. Xenolith of foliated basalt in LSIC granitoid. Volcanic rock xenoliths are angular and generally occur near the volcanic rock and LSIC contact.

Plate 7b. Form and texture of an actinolitic mafic enclave. Actinolitic enclave with radiating actinolitic outer zone and a negative weathering biotitic crust and rusty halo.

a)

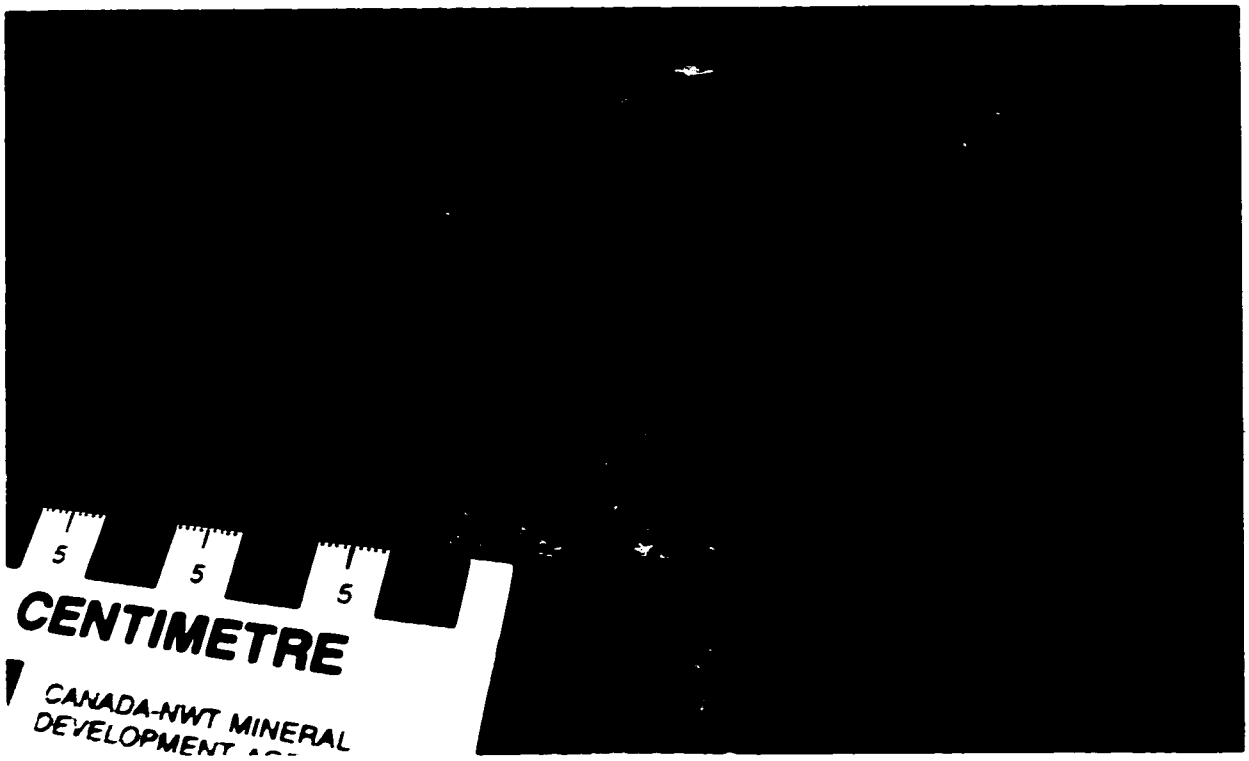
5
5
5
CENTIMETRE
CANADA-NWT MINERAL

b)

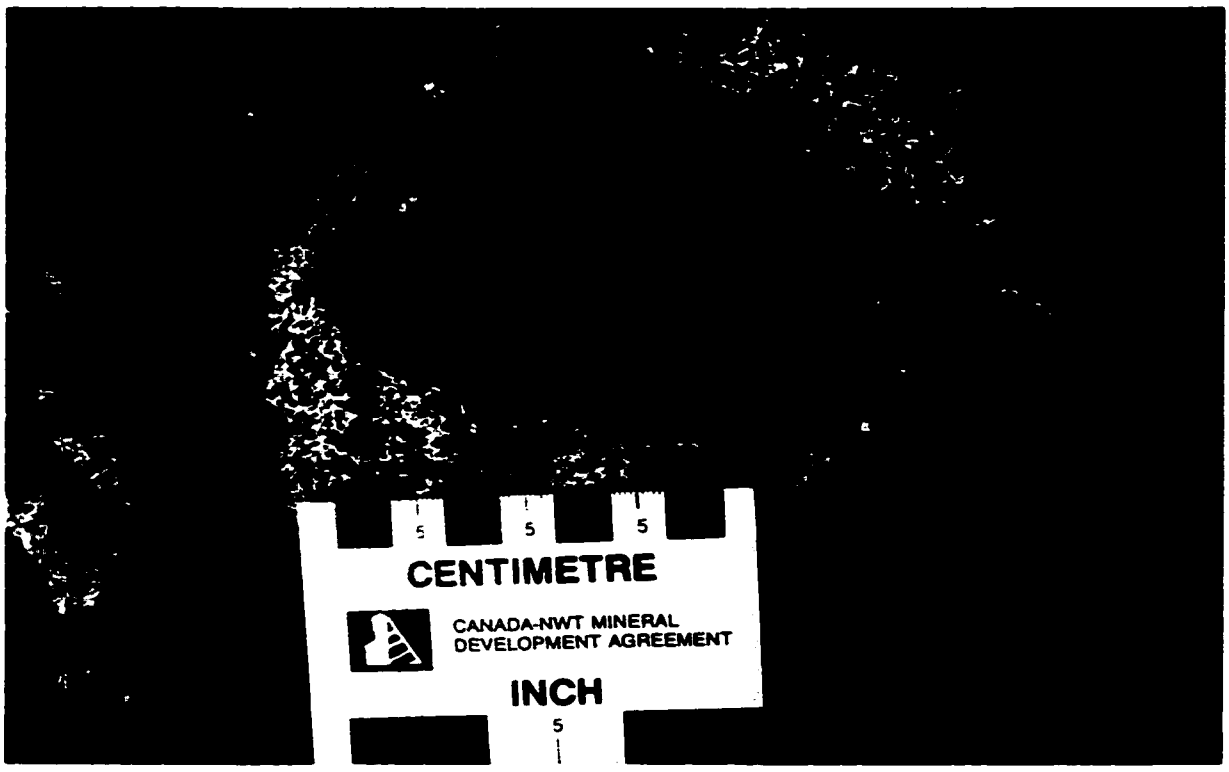
5
5
5
CENTIMETRE
CANADA-NWT MINERAL
DEVELOPMENT AGREEMENT
INCH
5

### 4.1.2 Autolithic Ovoid Mafic and Felsic Enclaves

A variety of mineralogically and texturally distinct autoliths are hosted within the LSIC. These enclave types are the most prevalent of the enclaves in the LSIC.

**Subtypes**

Two main groups of autolithic enclaves, mafic magmatic enclaves (MME) and felsic magmatic enclaves (FME), comprised of four main magmatic enclaves types have been recognized in the LSIC:

MME

1) Actinolite enclaves

2) Amphibolitic enclaves

3) Dioritic enclaves

FME

4) Monzodiorite enclaves

**Occurrence and Distribution of Enclaves**

The most prevalent enclave type is the amphibolitic enclaves (~55% of all enclaves), followed by the actinolitic enclaves (~30%), melanic dioritic enclaves (~14%), and monzodioritic enclaves (<1%). As a rule enclaves are more mafic than the host rock with the rare exception of some monzodioritic enclaves. Amphibolitic, actinolitic, and melanic dioritic enclaves are present in all rock types of the LSIC except for the saccharoidal monzonites which contain only rare small amphibole clots. The hornblendite units of the LSIC contain

rare spheroidal actinolitic structures which may have the same origin as the actinolitic enclaves. The monzodiorite enclaves are rare and found in only two locations.

Autolithic enclaves form approximately 0.5-5 vol.% the rocks of the LSIC. The concentration of these enclaves does not vary in a systematic manner within the complex. Monogenic swarms are found occasionally proximal to mafic dykes, or as linear arrays which may represent disrupted dykes. Very rare pod like polygenic swarms, up to 2 m in diameter, of crudely preferentially oriented FME and MME are also present. Large polygenic MME zones occur near the contact of the southern portion of the complex. Enclave types within these pods range from subangular hornblendites, leuco- and melano- equagranular microdiorites and cumulate melano-diorites to felsic enclaves of monzodiorite.

**Mafic Enclaves**

**Actinolitic Enclaves**

Ovoid, 2-8 cm in diameter actinolite enclaves display two dominant textures ranging from a felted (fine randomly oriented interlocking acicular grains) to a radiating texture of acicular medium green actinolite. The contact between the enclave and host rock is sharp. In some enclaves with radiating textures, a fine grained or biotitic margin is present and forms a thin negative weathering channel at the enclave/host interface on weathered surfaces (Plate 7b). A rusty halo in the host rock is also noted in this case. Actinolitic enclaves are composed of up to 95+ vol.% euhedral lathes and <1 vol.% magnetite. Light brown chlorite occurs as interstitial masses of equent euhedral lathes and as pseudomorphs of pyroxene. Approximately 20 % of the actinolitic enclaves contain phlogopite/biotite.

**Amphibolitic Enclaves**

Dark green amphibolitic enclaves range in size from 2-4 mm crystal clots (Plate 8a) to approximately 10 cm as subrounded to attenuated and ovoid rounded enclaves oriented subparallel to the host rock fabric. Contact with the host rock is sharp. Hornblende forms interlocking 0.2-0.6mm subhedra comprising >80 vol.% of the enclave. Subhedral aggregated and discrete magnetite is always present in concentrations from 10-25 vol.% and 0.2mm euhedral titanite occurs interstitially to hornblende and biotite ranges from 0-5 % in enclaves.

**Dioritic Enclaves**

Subround, 4 mm to 8 cm, melanic dioritic enclaves of equivalent mineralogy to the amphibolitic enclaves but with plagioclase being present up to 10 vol.%. Clinopyroxene concentrations within these enclaves are highly variably from 0-60 vol.%.

**Melanic Dioritic Mafic Magmatic Enclaves**

These enclaves are fine grained and subround and typically not concentrated in close proximity to a dioritic unit. The sporadic, but evenly distributed nature, form and grain size suggests they may represent quenched melt.

**Cognate Dioritic Xenoliths**

Some dioritic enclaves are hornblende porphrytic and subround to subangular with a grain size equivalent or greater than the host rock. This form of enclave is interpreted to represent cognate xenoliths of partially consolidated cumulate that was re-incorporated and

Plate 8a. Plane light photomicrograph of a magnetite rich hornblende crystal clot. These enclaves are interpreted to have originated from mingling of felsic and mafic LSIC melts. Width of view = 17 mm.

Plate 8b. Cognate dioritic cumulate xenolith in diorites. Textures indicate that these dioritic enclaves represent re-incorporated cumulate material.

a)

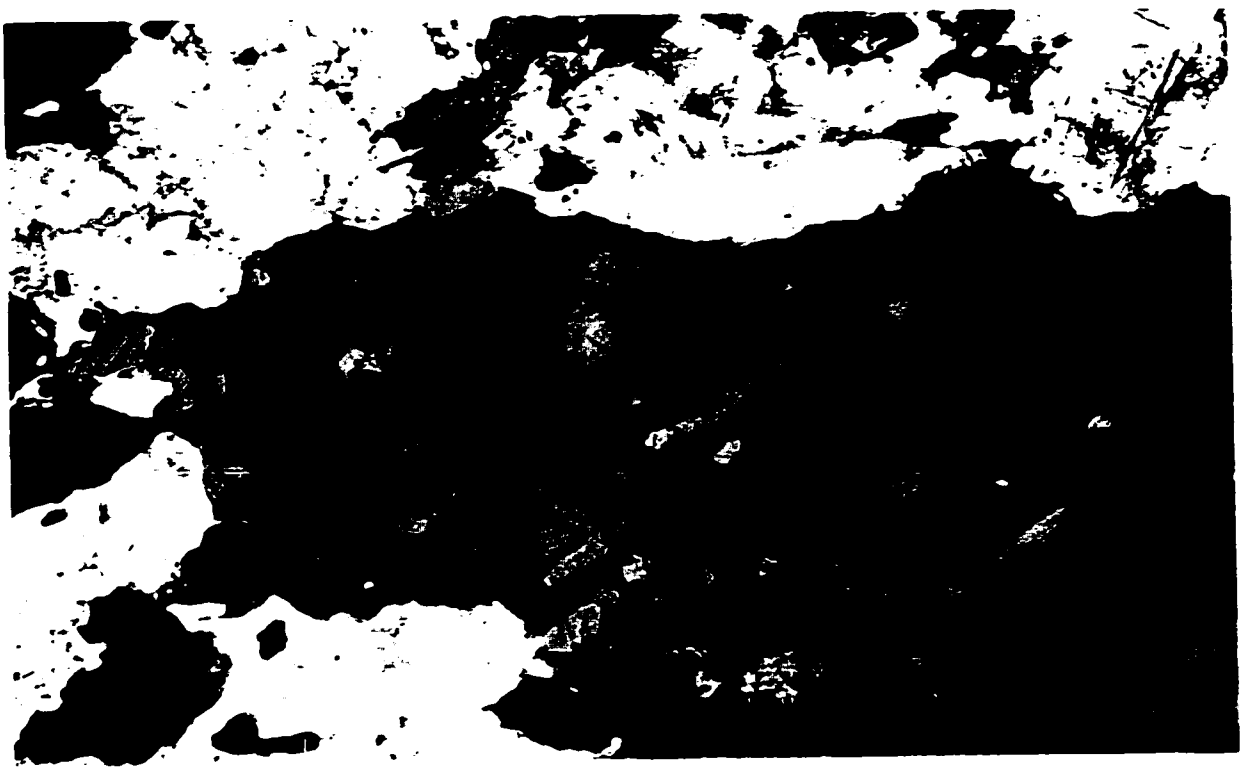

b)

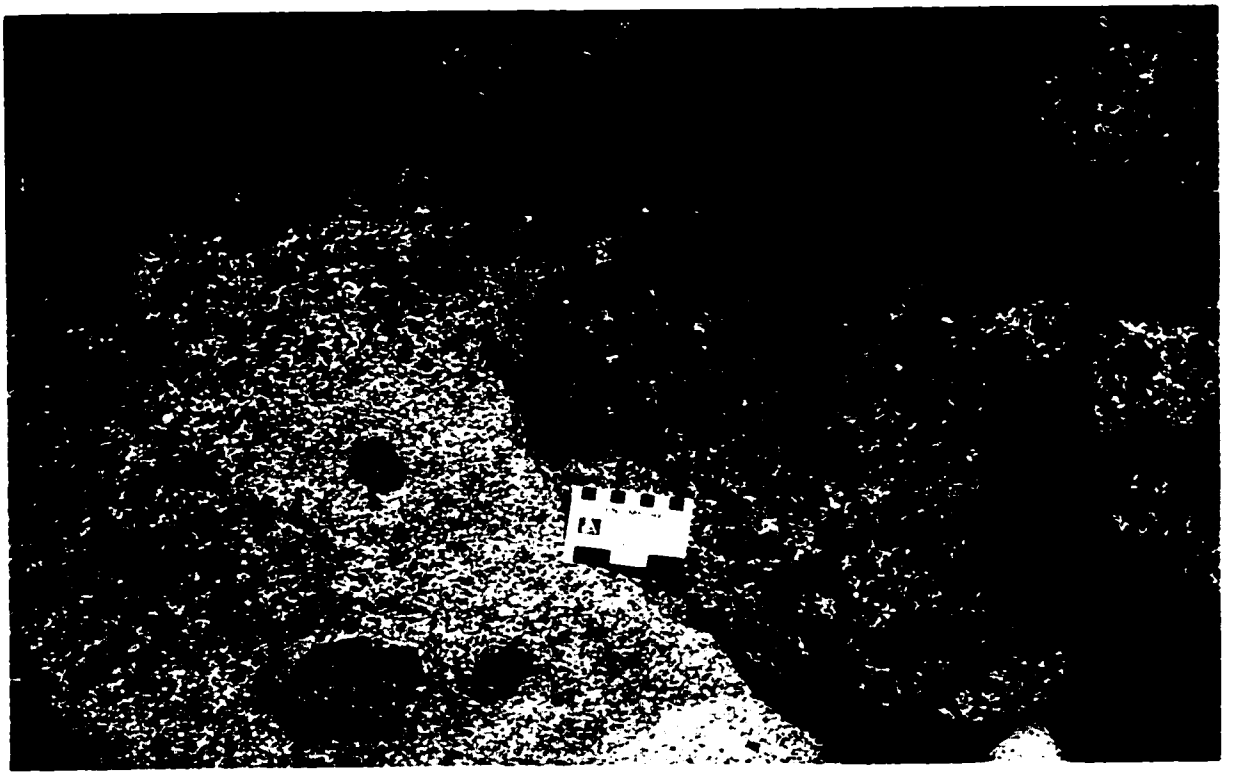

partially re-assimilated/fused in the liquid (Plate 8b). Dykeing or later magma pulses may have intruded earlier cumulate or crystallized units resulting in this enclave type.

### Felsic Magmatic Enclaves

### Monzodioritic Enclaves

Monzodioritic enclaves all occur as 5-15 cm elongate (>4:1) rounded, occasionally bent, or exhibiting a teardrop shaped inclusions (Plates 9a and 9b). These enclaves are more felsic than the rock in which they are hosted. The enclaves typically constitute >10 vol.% of the rock and are oriented subparallel to one another.

Plate 9a. Fused and partially assimilated felsic enclave. Note wispy tail extending from the felsic enclave in the center of photograph.

Plate 9b. Oriented felsic enclaves. The occurrence of felsic magmatic enclaves is rare in the LSIC. Incorporated cognate xenolithic fragments in contact areas of LSIC units are dominated by enclaves generally more mafic than the host rock in which they occur.

a)

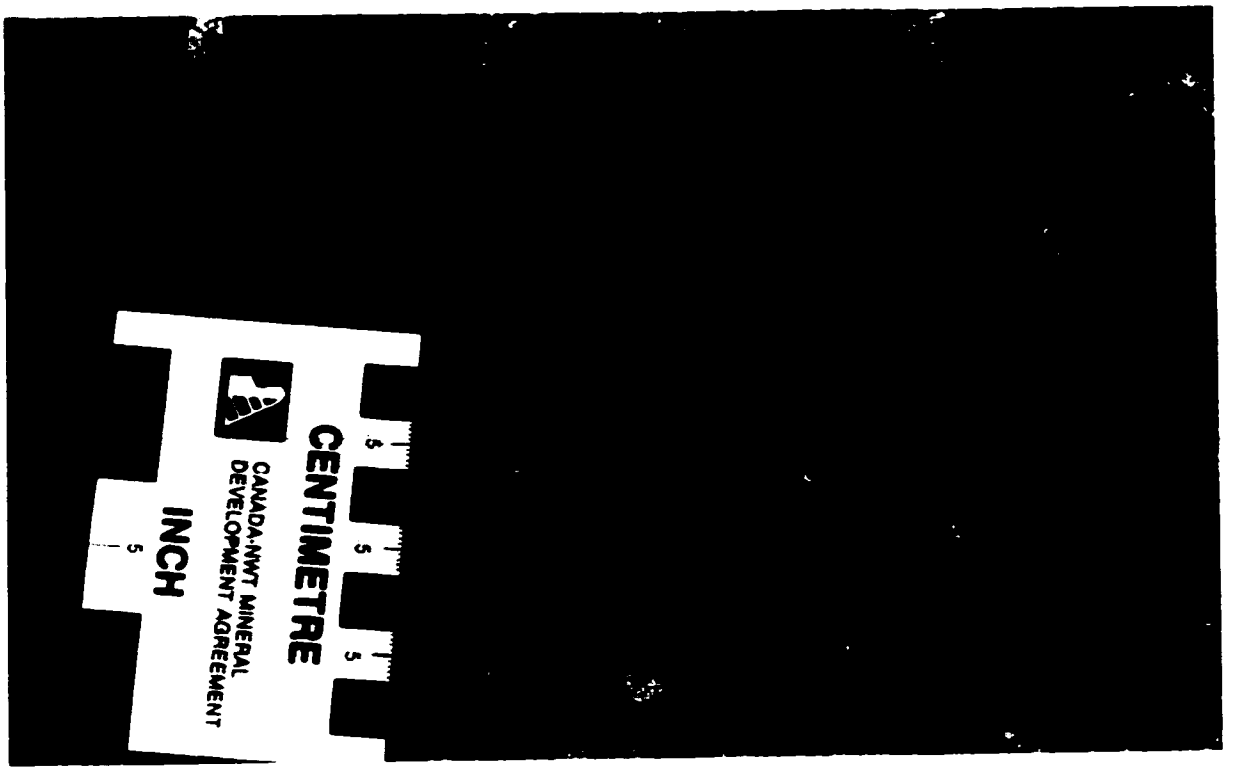
CENTIMETRE
INCH
CANADA-NWT MINERAL
DEVELOPMENT AGREEMENT

b)

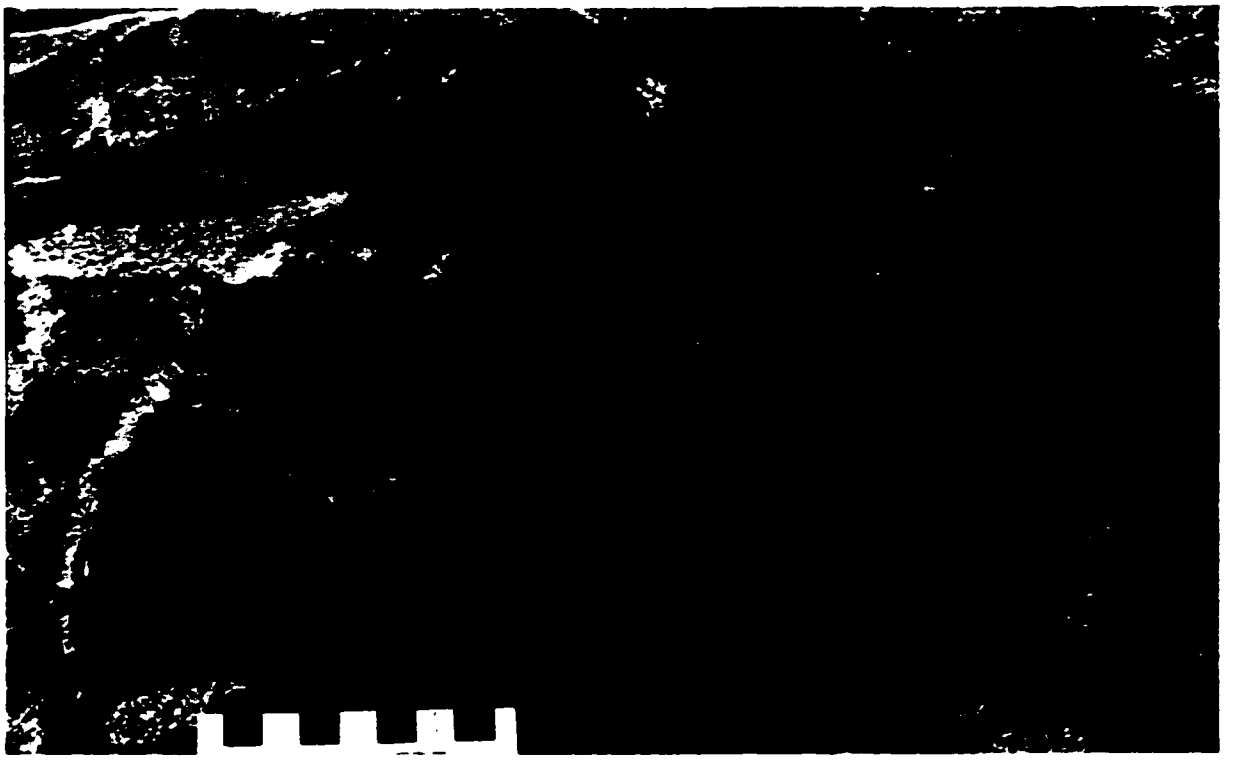

# Chapter 5 Petrography of the Complex

## 5.1 Saccharoidal Units

The saccharoidal rocks (Plate 10) have been classified and subdivided based upon modal mineralogy and the IUGS plutonic rock classification scheme (Streckeisen, 1976) into five main subgroups consisting of monzonites, monzodiorites, diorites, syenites, quartz monzodiorites and quartz diorites (Figure 8).

Mineralogy

*Clinopyroxene*, with inclusions of green pleochroic biotite, titanite and magnetite is present as altered grains. Least altered grains are subhedral rounded and appear corroded. Clinopyroxene occasionally occurs in aggregates of fine crystals which may represent mafic microgranular inclusions. Two generations of *amphibole* exist. The occasionally twinned subhedral amphiboles are primary igneous amphiboles whereas a later generation of uralite occurs after clinopyroxene. Amphibole is commonly heavily titanized. *Titanite* is present (<3 %) in all samples as subhedral to euhedral (to euhedral rounded) wedges with included magnetite. Alteration of titanite consists of an earthy brown amorphous mineral. *Oxides* are entirely comprised of magnetite with lamella and thin marginal discontinuous rims of hematite. The degree of hematization of magnetite appears to loosely correlate with the degree of sericitization/sausseritization of plagioclase. *Plagioclase* and *K-feldspar* occurs as albite and tartan twinned subhedral equent grains with simple grain boundaries to perthitic phenocrysts and grains with diffuse and sutured boundaries. Zoning in feldspar is not evident. *Quartz* is present as discrete grains exhibiting undulatory extinction and

Plate 10. **Photograph of a saccharoidal granitoid. Saccharoidal granitoids are characterized by granular feldspars, titanized hornblende, and low concentrations of mafic enclaves.**


.5
5
5
CENTIMETRE
CANADA-NWT MINERAL
DEVELOPMENT AGREEMENT
INCH
5

# IUGS Modal Classification: Units of the LSIC

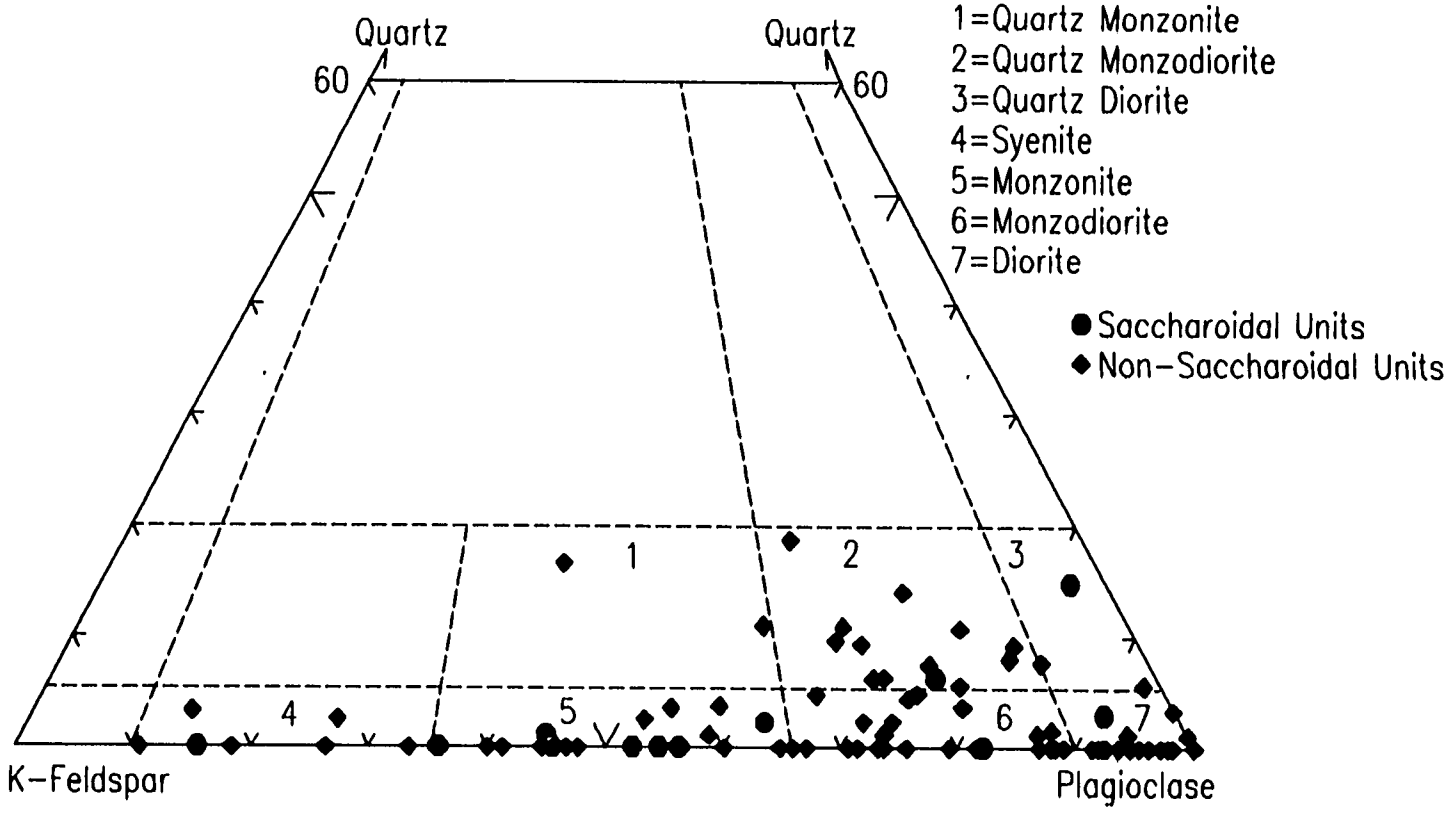


**Figure 8. Saccharoidal granitoids range from slightly quartz saturated diorites to syenites, and rarely, quartz monzodiorite. Non-saccharoidal granitoids range in composition from slightly quartz saturated diorites to syenites, and unlike the saccharoidal units, quartz monzodiorite and quartz monzonite are more prevalent.**

rarely, small rounded inclusions in amphibole. Epidote and chlorite occur as minor alteration products after biotite and amphibole and barite is noted occuring in association with biotite. A paragenetic sequence comprises 1) magnetite, 2) apatite+titanite, 3) Biotite/phlogopite + clinopyroxene, 4) amphibole, 5) plagioclase+K-feldspar 6) ± quartz, 7) alteration products of epidote, secondary titanite, chlorite, uralite, sericite, and hematite. Most samples have experienced strain, manifested as undulatory extinction in quartz and orientation of hornblende lathes.

## 5.2 Clinopyroxene Absent Non-Saccharoidal Granitoids

Samples (Plate 11a) range in composition from diorite, monzodiorite, monzonite, to quartz-monzodiorite, and syenite and are distinguished from other non-saccharoidal granitoids by the absence of clinopyroxene.

Mineralogy

*Amphibole* occurs as anhedral to twinned subhedral irregular/euhedral grains with inclusions of titanite, biotite, apatite, rare zircon, plagioclase and magnetite. Secondary quartz is found in some amphibole in a syenitic sample. Small subhedral grains of *magnetite* are included in amphibole and possess grain boundary lamella and mantles of *hematite* and titanite. *Pyrite* is found in the sheared syenites as rounded grains with mammillary mantles of hematite. *Biotite* occurs as green subhedral lathes associated and included in amphibole and altering to blue birefringent chlorite.

*Plagioclase* occurs as variably sericitized albite twinned subhedral grains which may contain inclusions of biotite. Grain boundaries are interlocking and diffuse for most plagioclase

Plate 11a. Typical non-saccharoidal granitoid. Non-saccharoidal granitoids are characterized by the presence of euhedral hornblende and an unaltered appearance.

Plate 11b. Crossed polar photomicrograph of a non-saccharoidal granitoid. Twinned euhedral hornblende and K-feldspar and plagioclase with embayed grain boundaries are common.

a)

b)

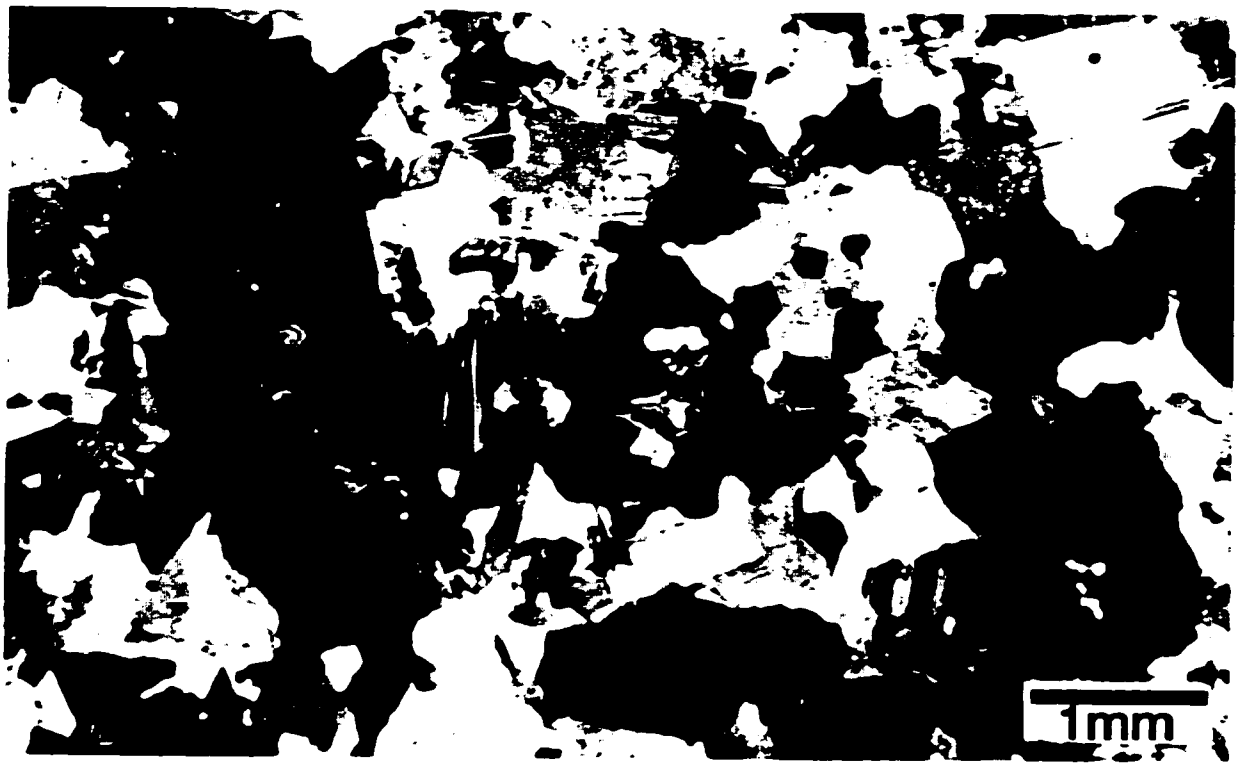

crystals but larger grains have irregular corroded grain boundaries. Smaller grains lack albite twins. Larger grains possess blebby replacements composed of tartan twinned K-feldspar and plagioclase grains have sericitized turbid zones and cores (Plate 11b). Weak strain is manifested as bent and pinched albite twins in plagioclase. Subhedral to anhedral tartan twinned *K-feldspar* may be weakly sericite altered and K-feldspar is interstitial to plagioclase and appears to have crystallised after plagioclase. Grain boundaries with plagioclase can be diffuse and sutured. K-feldspar within syenites are perthitic.

*Quartz* is found as rare subhedral to anhedral grains displaying undulatory extinction and limited secondary fluid inclusion trails. *Titanite* occurs as primary euhedral wedge shaped to fragmented, rarely twinned, grains associated with mafic minerals and commonly included within amphibole. Secondary titanite is subhedral to anhedral, and occurs as mantles on primary minerals. Rarely, titanite forms skeletal grains in altered samples. *Apatite* occurs as fine, early crystallising euhedra. *Allanite* and *zircon* comprise minor rare subhedral to euhedral phases.

*Chlorite* frequently contains cleavage parallel elongate inclusions of titanite and hematite and displays a red-purple-blue birefringence. *Epidote* forms anhedral yellow green pleochroic grains after amphibole and in some cases is included within amphibole. Epidote is occasionally associated with hematized magnetite and is also found as an alteration product of biotite. Alteration after titanite produces earthy brown leucoxene.

## 5.3 Clinopyroxene Bearing Non-Saccharoidal Granitoids

Divisions based upon modal mineralogy include monzodiorites, monzonites, diorites, quartz-monzonites, and quartz-monzodiorites.

Mineralogy

*Clinopyroxene* occurs in the majority of the samples as fractured, highly epidote altered and replaced by amphibole. Clinopyroxene is subhedral, occasionally twinned and contains inclusions of apatite and abundant magnetite grains and occasionally symplectic magnetite. *Amphibole* occurs as subhedral irregular occasionally twinned grains enclosing and mantling clinopyroxene (Plates 12a and 12b), and as discrete grains. Inclusions consist of magnetite, titanite, ± K-feldspar, ± biotite, and plagioclase with alteration products of epidote and rare carbonate.

*Plagioclase* is found as sericitized, untwinned and albite twinned, occasionally Carlsbad twinned, subhedral equent to lath-like grains. Some grains, typically the larger phenocrysts, posses tartan twinned blebby exsolutions or replacements (anti-perthite or deuteric perthites). Large phenocrysts are frequently zoned with turbid, sericitized cores (as in Plate 11b). Patchy extinction in large grains, undulatory extinction and discontinuous albite twins (inversions) record brittle deformation. Plagioclase grains that are twin free in altered samples may be the product of albitization and/or recrystallization. Plagioclase infrequently contains inclusions of magnetite, titanite and apatite and is rarely included within amphibole. *K-feldspar* occurs as subhedral to anhedral embayed interstitial (to plagioclase), occasionally perthitic grains with complex grain boundaries and rare sericite alteration. Crystallization of K-feldspar appears after plagioclase based upon grain boundary relations. *Quartz* is a relatively minor component as subhedral irregular grains with undulatory extinction and occasional two phase fluid inclusions.

*Titanite* and *apatite* occurs as subhedral to euhedral inclusions in amphibole and clinopyroxene. Frequently twinned euhedral titanite contains a high proportion of magnetite inclusions and is usually associated with amphibole and pyroxene. Anhedral titanite associated with

Plate 12a. Hornblende - Clinopyroxene crystallization relationships. Plane light photomicrograph of clinopyroxene enclosed in hornblende. Hornblende aggregate clot enclave at right of photo. Width of photograph = 8 mm.

Plate 12b. Crossed polar photomicrograph of plate 12a. Photomicrograph shows continuous twin plane in hornblende mantle on clinopyroxene. Width of photograph = 8 mm.

a)

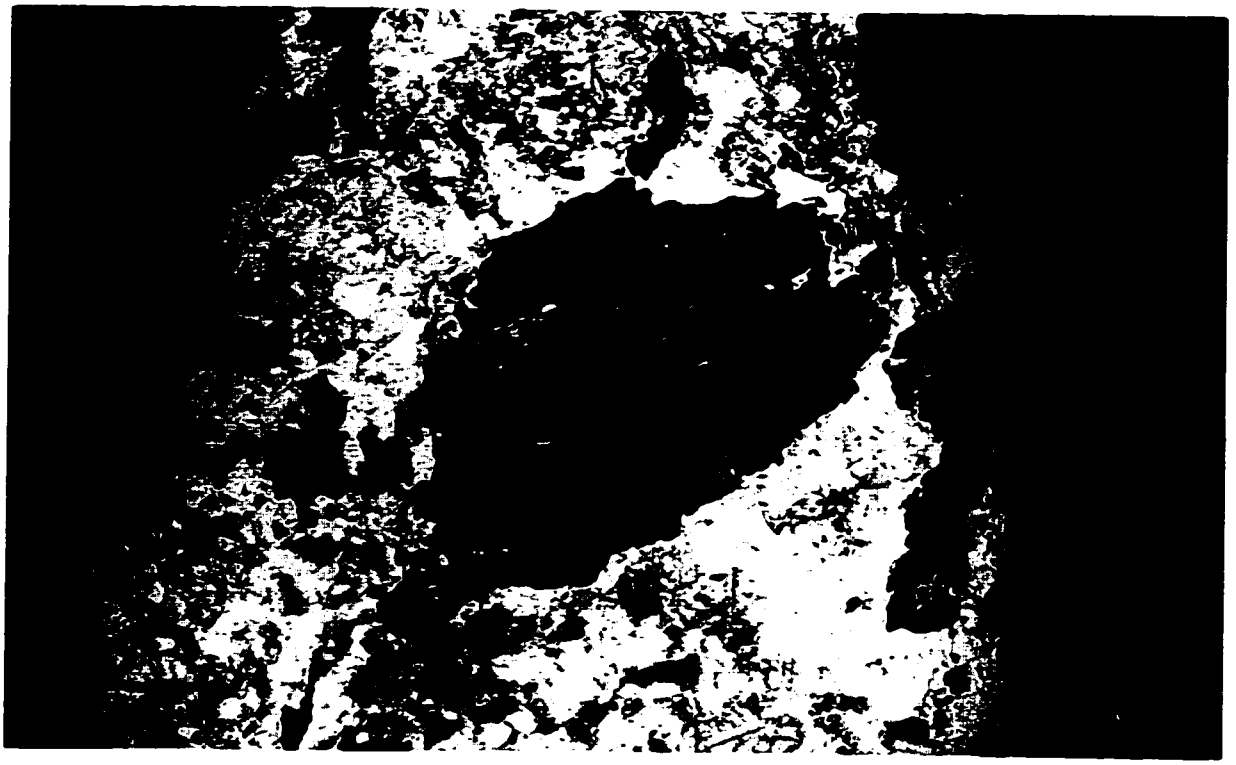

b)

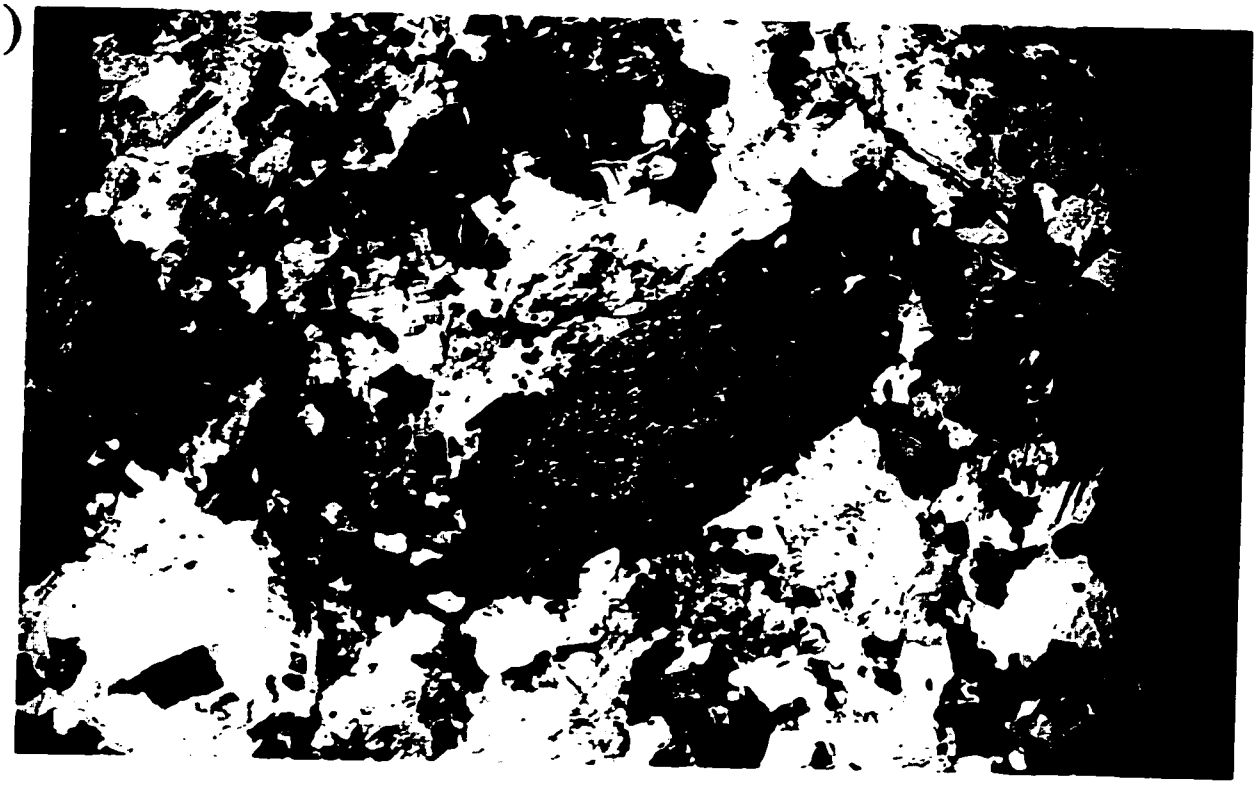

amphibole and clinopyroxene may represent alteration products of amphibole and clinopyroxene. Mafic phases generally occur in clotty or concentrated in patches. Apatite, in one case, is included in magnetite.

*Magnetite* occurs as subhedral irregular grains with variable amounts of *hematite* lamella and margins or patches and magnetite included within titanite also posses lamella. *Pyrite* occurs in very rare cases as exceedingly small rounded grains. *Biotite* is present as subhedral sagenitic brown-green pleochroic lathe like grains with cleavage parallel alteration patches of chlorite. Grain boundaries are occasionally titanized in very fine discontinuous rims. *Biotite* is included in amphibole, and contains inclusions of titanite, magnetite, and apatite. *zircon* and *allanite* are present as small very rare rounded grains in two samples. Alteration consists of sericite after feldspar, epidote after amphibole, titanite after clinopyroxene, biotite and amphibole, and chlorite after biotite and amphibole.

## 5.4 Hornblendites and Biotite Hornblendites

The hornblendites (Plate 13) contain a subordinate volume of clinopyroxene mantled by amphibole. These rocks vary from very fine to medium grained homogenous and massive holocrystalline hornblendite to biotitic hornblendite in which clinopyroxene has been altered to actinolite and epidote.

Plate 13. Outcrop photograph of a biotite - clinopyroxene hornblendite. This shows the typical appearance hornblendite units in the northern complex of the LSIC.

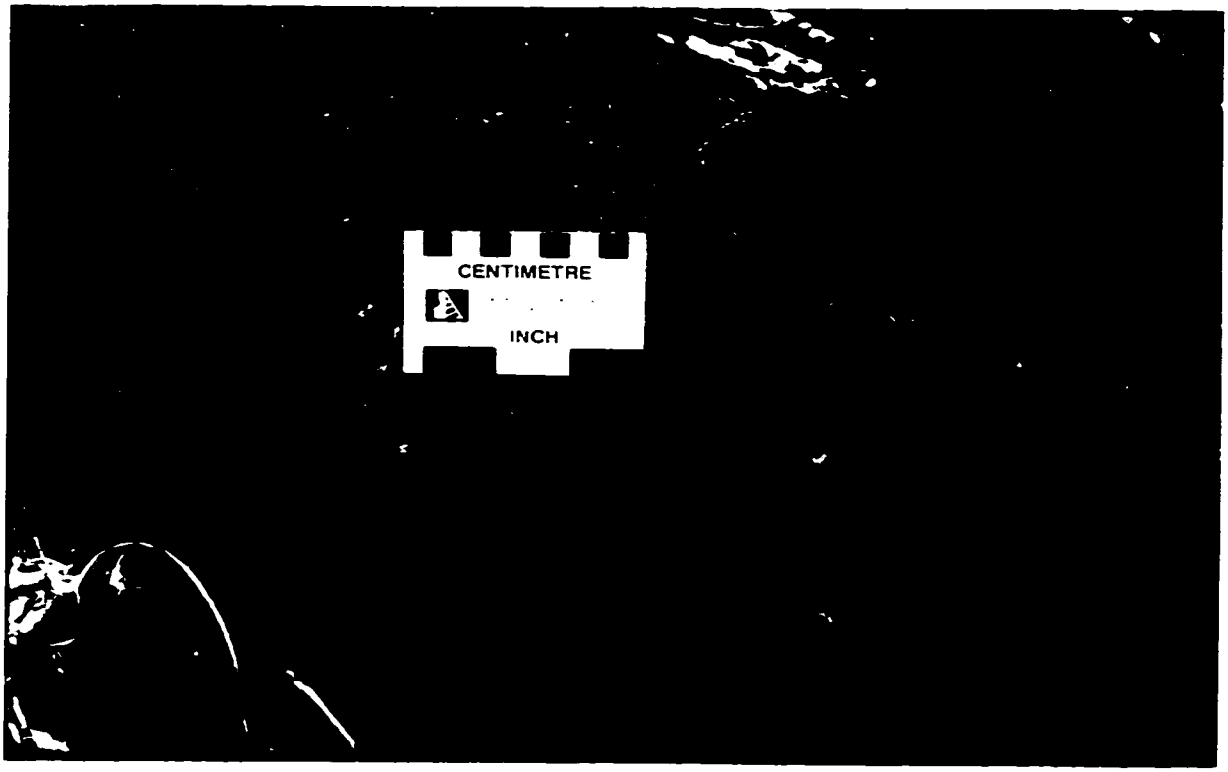
CENTIMETRE
INCH

Mineralogy

*Amphibole* occurs as yellow to light green pleochroic subhedral to euhedral, zoned, interlocking, and interfering grains with frequent clinopyroxene cores. Amphibole also occurs as a fine grained groundmass constituent. There may be two generations of amphibole with the euhedral amphibole, occasionally twinned grains representing primary grains and the groundmass and subhedral irregular grains being secondary in origin. *Clinopyroxene* occurs as pale green cores in single amphibole grains or is mantled by amphibole grains (Plate 14a). A sagenitic texture is developed in rare cases in some altered clinopyroxenes. Clinopyroxene is subhedral to corroded (Plate 14b) with irregular grain boundaries and exhibits non-synchronous extinction in some sections suggestive of limited zoning. Grains range from being inclusion free to magnetite inclusion bearing.

*Biotite* occurs as green and brown coloured subhedral lathes with corroded or irregular grain boundaries and contains inclusions of titanite and apatite. *Titanite* is found included within amphibole and as occasionally twinned subhedral rounded to irregular grains with high concentrations of included magnetite. Secondary titanite occurs as anhedral masses and titanized mantles around some amphibole grains. *Plagioclase* occurs as small sericitized subhedra with occasional albite twins and sutured and diffuse grain boundaries. Alteration and deformation is evident as seicitization and sausseritization of plagioclase and discontinuous twin lamella. One altered sample contains trace *K-feldspar*. *Magnetite* occurs as small anhedral, ameboid to rounded grains. Early crystallising *Apatite* is present as small rounded euhedra in variable percentages as inclusions in amphibole. Some apatites were observed to contain small (~2 μm) monazite inclusions and what appears to be K-amphibole inclusions are also noted.

Plate 14a. Hornblende - clinopyroxene relationships in hornblendites. Crossed polar photomicrograph of clinopyroxene grain in hornblendite mantled by hornblende crystals.

Plate 14b. Plane light photomicrograph of corroded clinopyroxene grain. Clinopyroxene is mantled by primary amphibole which contains abundant apatite inclusions. Clinopyroxene is partially replaced by amphibole and contains inclusions of magnetite.

a)

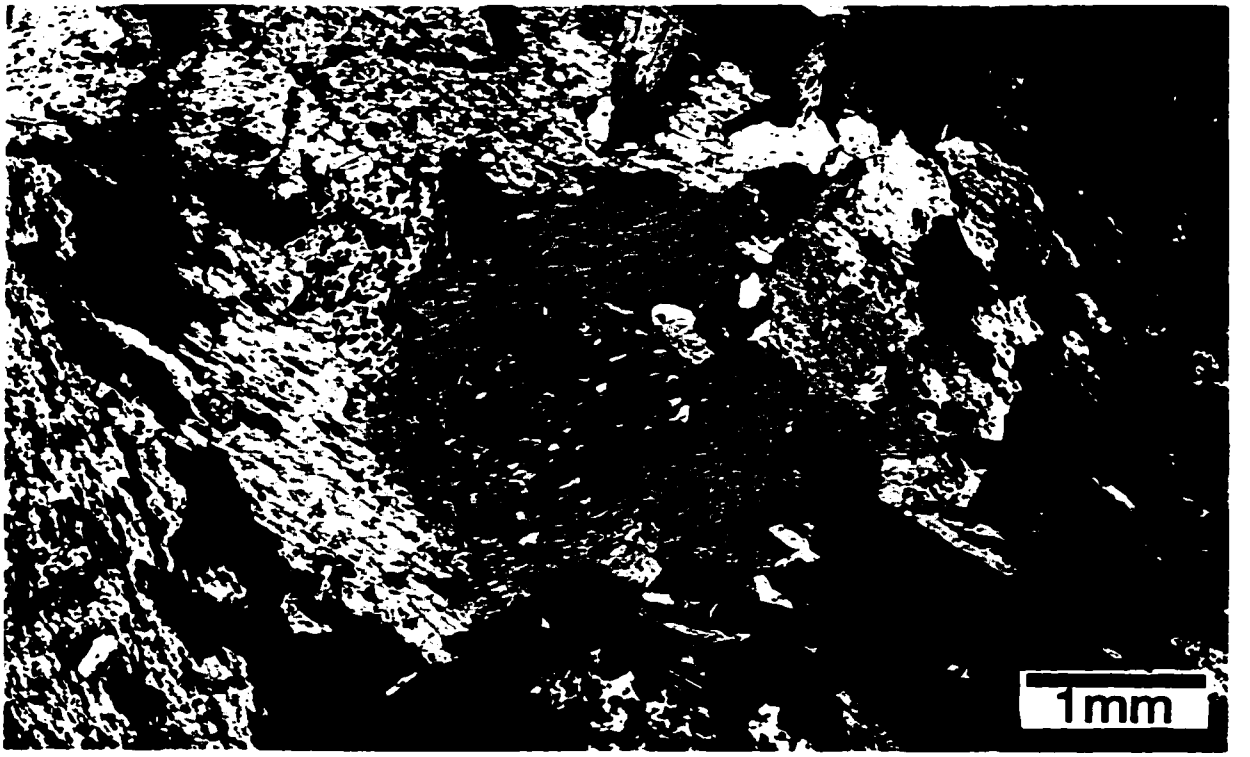


b)

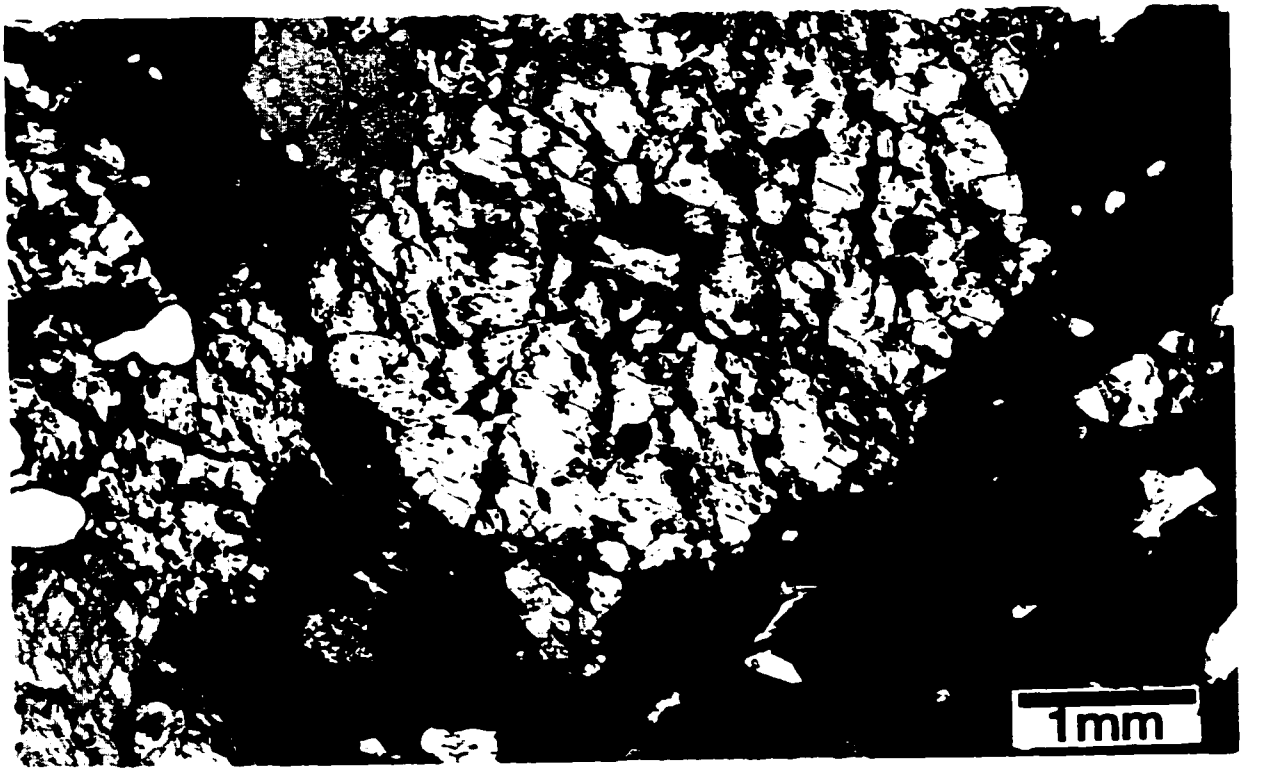

Alteration products include epidote and chlorite (± biotite) after amphibole, hematization of amphibole, uralite and carbonate after clinopyroxene, epidote after biotite, hematization of magnetite, development of sagenitic textures in biotite and clinopyroxene, and sericite/sausserite after plagioclase.

## Chapter 6 Geochemistry of the Complex

### 6.1 Non-Saccharoidal Granitoids

Compositional data for the intrusive rocks of the LSIC are presented in Appendix 3. Granitoids are shoshonitic to transitional medium- K calc-alkaline (Figure. 9) and metaluminous with molar $Al_2O_3/(CaO+Na_2O+K_2O)$ of ~1 - 1.6 and $Al_2O_3/Na_2O+K_2O$ = ~1.5 - 2.0. They define alkali-lime coefficients (Peacock, 1931) of ~54-58, indicating a alkalic-calcic to calc-alkalic association, a molar K/Na range of 0.2-0.84 (avg.=0.39), and plot along the alkaline - sub-alkaline divide of Irvine and Baragar (1971) (Figure 10).

The granitoids are characterised by decreasing $Fe_2O_3^T$, $TiO_2$, MnO, MgO, CaO, and $P_2O_5$, and increasing $Na_2O$ with increasing $SiO_2$ in a range from 50 to 67 wt.% (Figs. 11a, 11b, 11c). Magnesium numbers ($Mg^{\#}$ = $MgO/(FeO^T+MgO)$) are high for rocks with such elevated $SiO_2$ and range from $Mg^{\#}$ 27-60. Granitoids may be either olivine or quartz normative.

Granitoids contain high LILE abundances with Ba, Rb, and Sr up to 2500 ppm, 100 ppm, 1850 ppm, respectively. Compatible element abundances are also high with variable Ni (10-125 ppm) and Cr (75-425ppm). Total contents of REE decrease from 192 to 31 ppm with increasing $SiO_2$. Chondrite-normalized (normalizations after Taylor and McClennan, 1985) REE patterns (Figure. 12a) are steeply sloped ($(La/Yb)_{CN}$ = 7-30; avg.=19) with flatter HREE profiles ($(Gd/Yb)_{CN}$=1.8-5.6; avg.=3.0, $(Dy/Yb)_{CN}$=1.41-1.95). The magnitude of the Eu anomaly ($Eu/Eu^*=Eu_{CN}/(Sm_{CN}*Gd_{CN})^{0.5}$) is variable from 0.47-1.08. The high field strength elements (HFSE) display variable anomalies on extended element plots (Figure 12b) with $Nb/Nb^*$ ($=Nb_{CN}/(Ba_{CN}*La_{CN})^{0.5}$) ranging between 0.04-0.2, and $Ti/Ti^*$ ($=Ti_{CN}/(Sm_{CN}*Y_{CN})^{0.5}$)

# Potassium vs. Silica Variation for the Non-Saccharoidal Granitoids

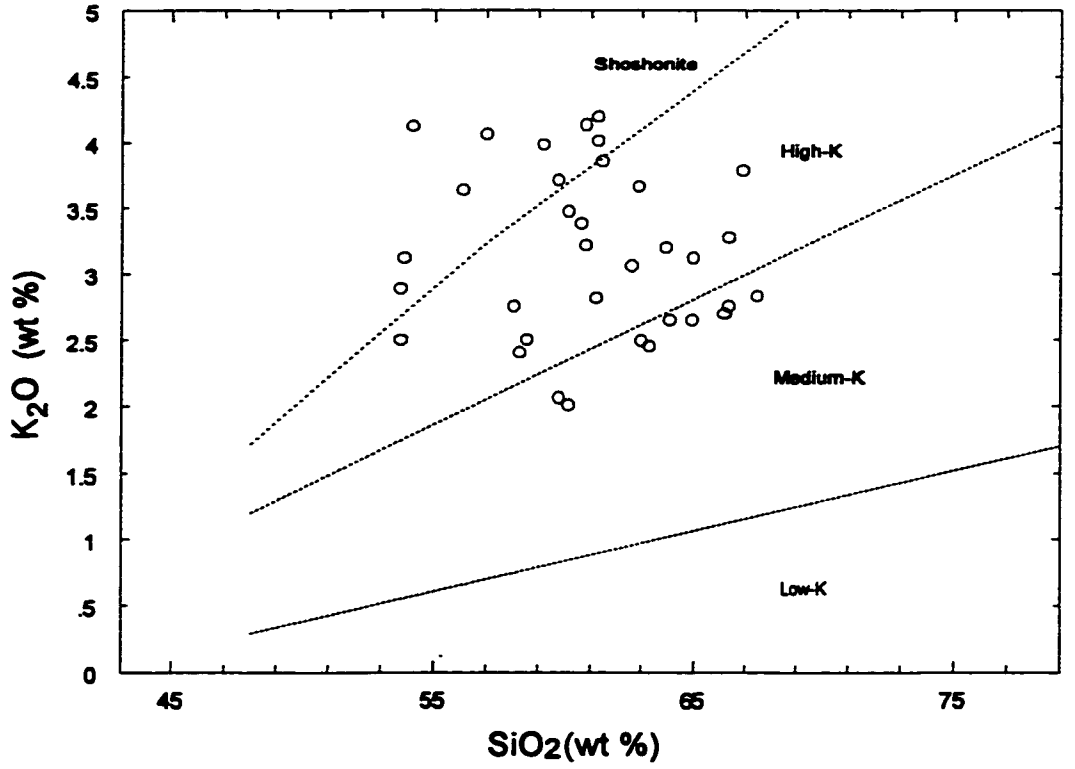


Figure 9. The LSIC non-saccharoidal granitoids are shoshonitic to medium-K calc-alkaline in terms of $K_2O$ and $SiO_2$. Magmatic series classification of LSIC non-saccharoidal granitoids after Le Maitre (1989). Shoshonitic division line after Innocenti et al (1982).

# $Na_2O + K_2O$ vs. $SiO_2$ Composition of LSIC Non-Saccharoidal Granitoids

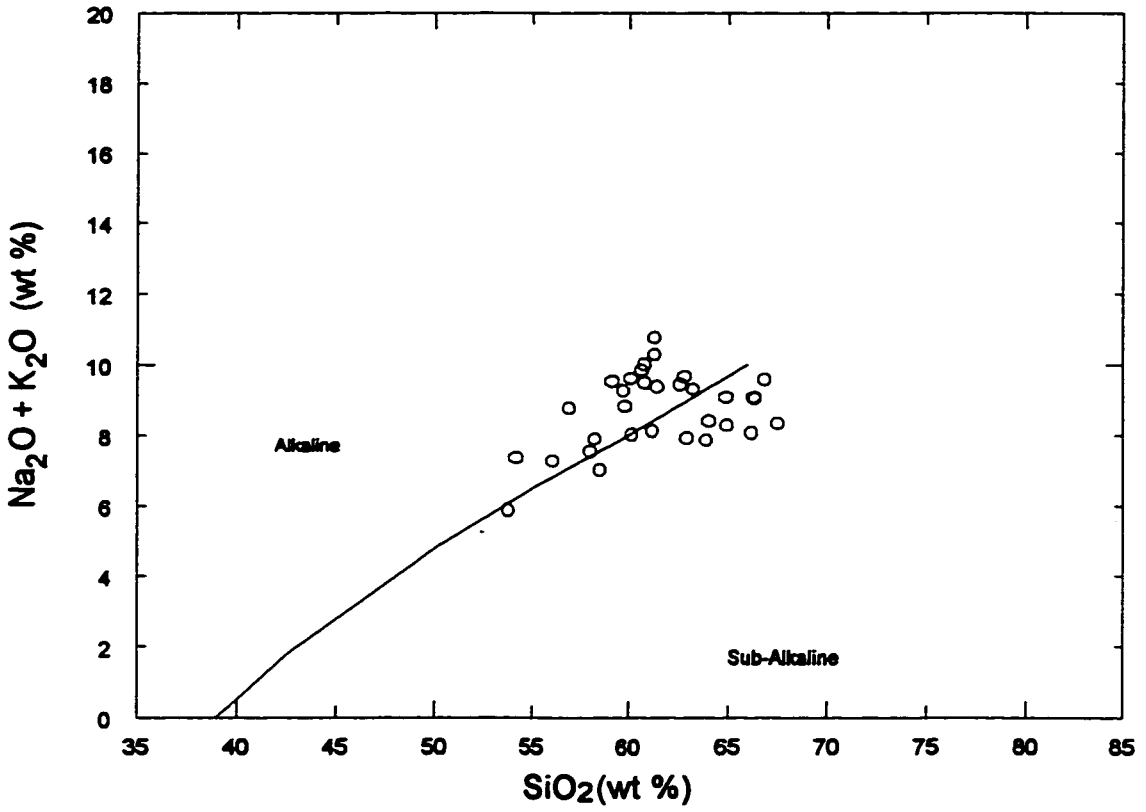


Figure 10. Non-saccharoidal granitoids compositions fall along the sub-alkaline to alkaline divide of Irvine and Baragar (1971).

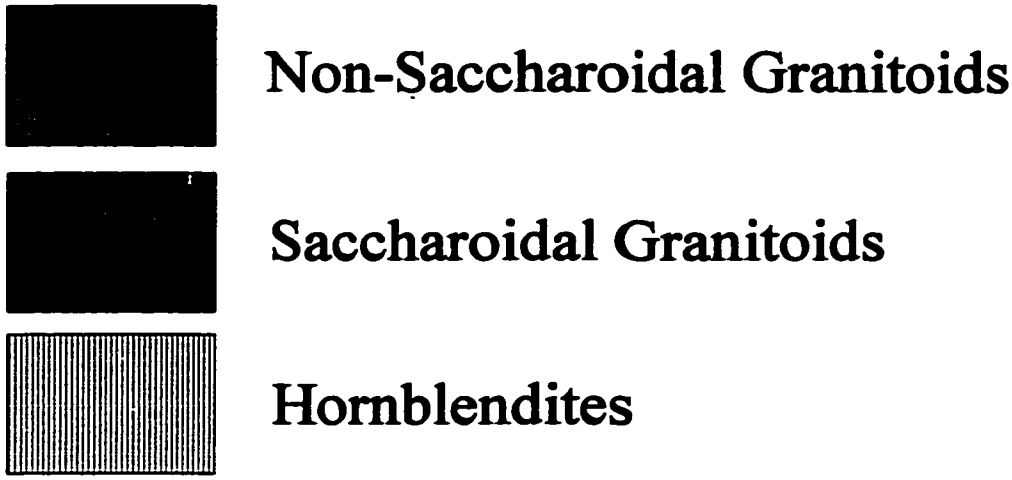


Figure 11. **Selected Harker Diagrams. Granitoids and hornblendites form a continuous array suggesting a cogenetic relationship for all major units of the LSIC.**

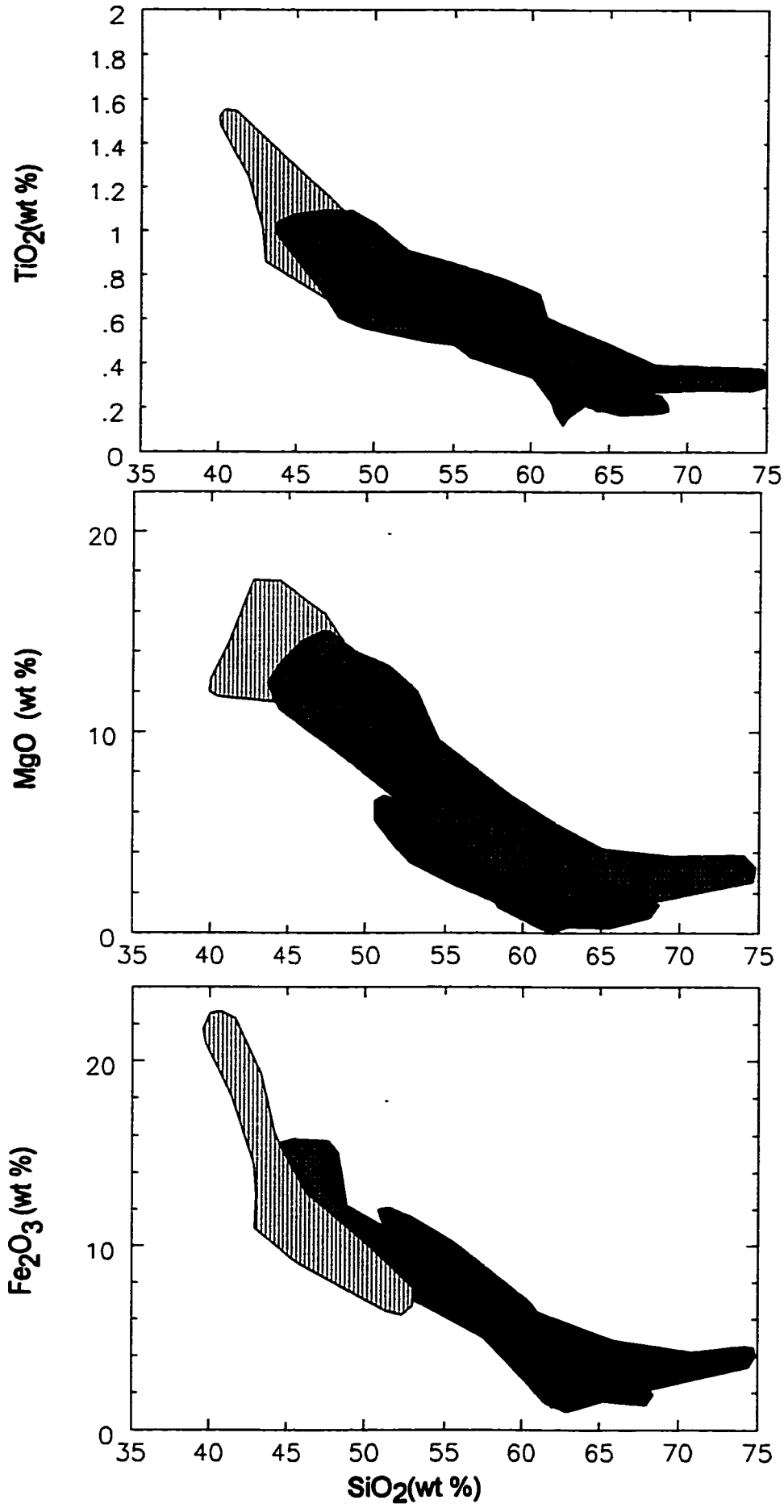
TiO2(wt %)
2
1.8
1.6
1.4
1.2
1
.8
.6
.4
.2
0
35 40 45 50 55 60 65 70 75
MgO (wt %)
20
10
0
35 40 45 50 55 60 65 70 75
Fe2O3 (wt %)
20
10
0
35 40 45 50 55 60 65 70 75
SiO2(wt %)

Figure 12a. Chondrite normalized REE abundances of non-saccharoidal granitoids. All samples (n=9) are REE fractionated with $La/Yb_{CN}$=7-30 and posses weakly sloped HREE ($Gd/Yb_{CN}$ ) averaging ~2.95. A weak and variable Eu anomaly is present averaging $Eu/Eu^*$=0.86. Chondrite normalization values are after Taylor and McClennan (1985).

Figure 12b. Chondrite normalized extended element plot of the non-saccharoidal granitoids. Samples (n=9) are charactrerised by high Ba, a positive $Sr/Sr^*$ anomaly, and negative Nb and Ti anomalies. Chondrite normalization values are after Taylor and McClennan (1985).

# Non - Saccharoidal Granitoids

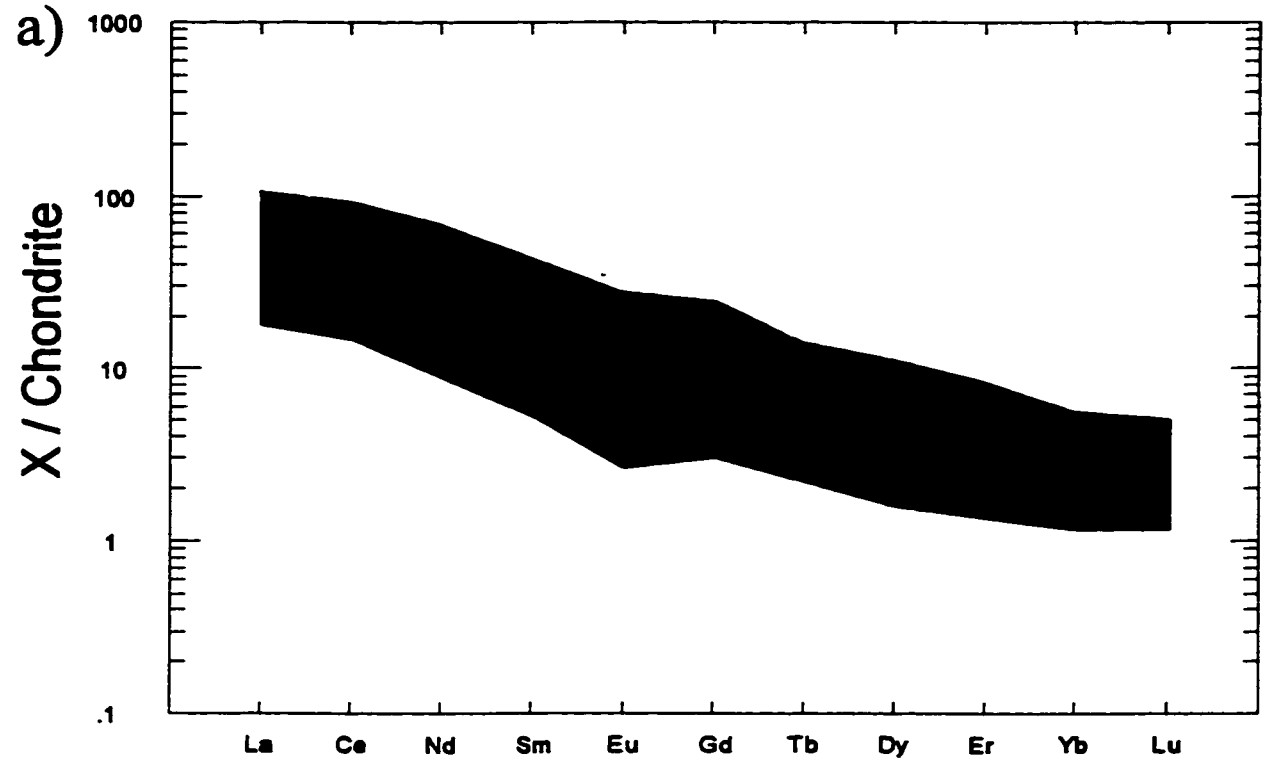


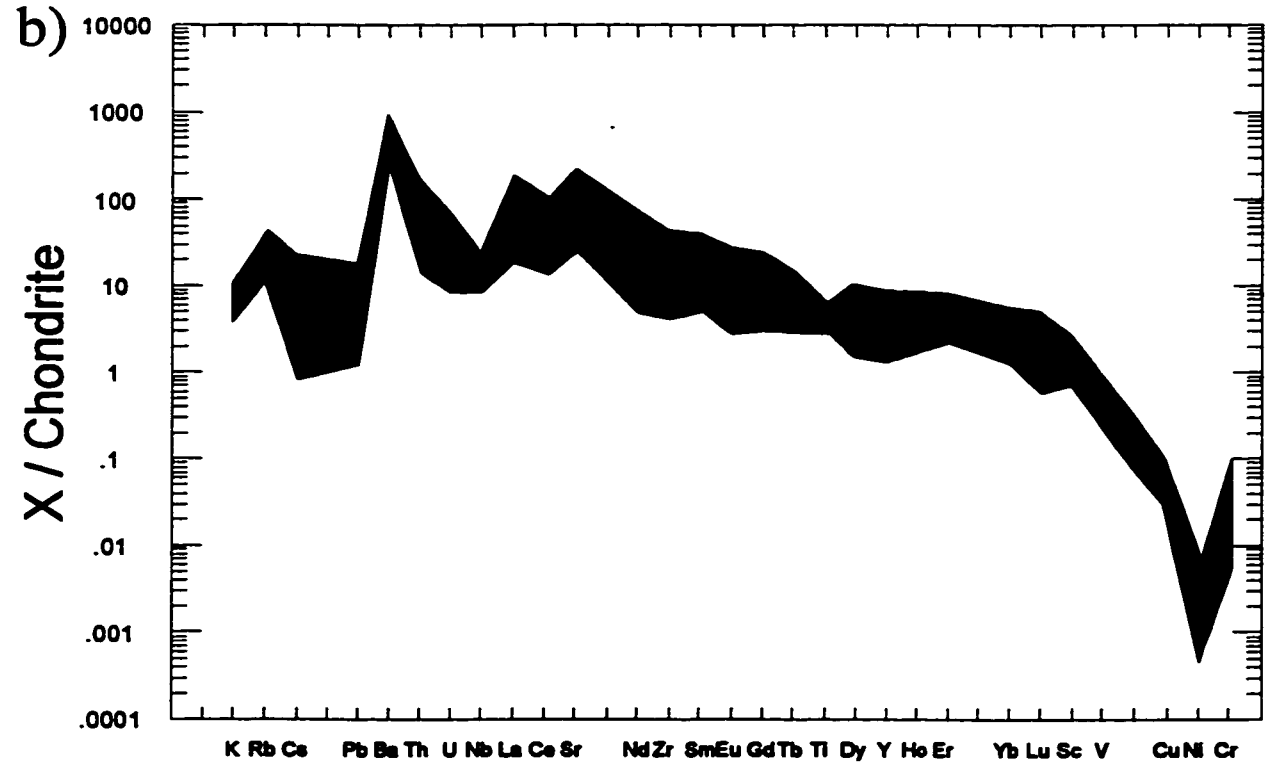

between 0.28-1.94 (avg.=0.56), all displaying generally negative anomalies, whereas Zr/Zr* (=$Zr_{CN}/(Nd_{CN}*Sm_{CN})^{0.5}$) is on average positive (avg.=1.21). Strontium and Ba concentrations are high and variable, from 300-2600 ppm (avg. ~1100 ppm) and 777-3503 ppm (avg.~1500 ppm), respectively. A positive Sr/Sr* [=$Sr_{CN}/(Ce_{CN}*Nd_{CN})^{0.5}$] anomaly between 0.64-7.92 averaging 2.87 is also noted. On a plot of $K_2O$ vs. $SiO_2$, some samples plot in the field of shoshonites. These samples display some of the highest Mg#, Cr, and Ni of the non-saccharoidal granitoids and may represent the original melt composition for the granitoids.

### 6.1.1 Characteristics of the LSIC Shoshonitic Series

The LSIC shoshonitic series granitoids (n=10) are characterised by $SiO_2$=53.93-61.44 wt.%, high $K_2O/Na_2O$=0.7-1.3 (molar K/Na = 0.44-0.84), $K_2O+Na_2O$=6.6-10.7 wt.%, $Mg^{\#}$=0.44-0.60, LREE (La=14-38 ppm), La/Nb=4.0-9.6, steep $La/Yb_{CN}$=15-28 with sloped HREE ($(Gd/Dy)_{CN}$=2.39-3.76) (Figure 13a), low Ti/Ti* (0.82-0.28), Nb/Nb* (0.8-0.04) and high Sr/Sr* (1.00-4.85) (Figure 13b) and variable Eu/Eu* (0.72-1.07). Total REE is high, from 65 to 193 ppm and averaging 140 ppm. The magnitude of the Zr anomaly varies but is generally negative as all but two samples posses Zr/Zr* >0.86. Samples are near silica saturated and can be either quartz or olivine normative, contain no normative feldspathoids and have a D.I. (differentiation index defined by Thornton and Tuttle, 1960) between ~49-79. These geochemical features are typical for shoshonitic magmas found in modern orogenic environments (Morrison, 1980; Lin et al, 1989).

Figure 13a. Chondrite normalized REE abundances for non-saccharoidal shoshonitic series granitoids. All samples (n=8) are fractionated with $La/Yb_{CN}$=15-23 and weakly sloped HREE $Gd/Yb_{CN}$=2.39-3.76. The magnitude of the Eu anomaly ranges from 0.72-1.07 although only two samples exceed 0.95 suggesting that the shoshonites posses a minor negative Eu anomaly (average = 0.89). Chondrite normalization values are after Taylor and McClennan (1985).

Figure 13b. Chondrite normalized extended element plot for non-saccharoidal shoshonitic series granitoids. All samples (n=10) are characterised by high LILE, especially Ba, and positive Sr anomalies ($Sr/Sr^*$=1.00-4.85) at high Cr and $Mg^\#$. Negative HFSE anomalies such as $Ti/Ti^*$=0.82-0.28, $Nb/Nb^*$=0.04-0.09 and $Zr/Zr^*$ <0.86, except for two samples, coupled with the high LILE is typical of arc-type rocks. Chondrite normalization values were obtained from Taylor and McClennan (1985).

# Shoshonite Series: Non-Saccharoidal Granitoids

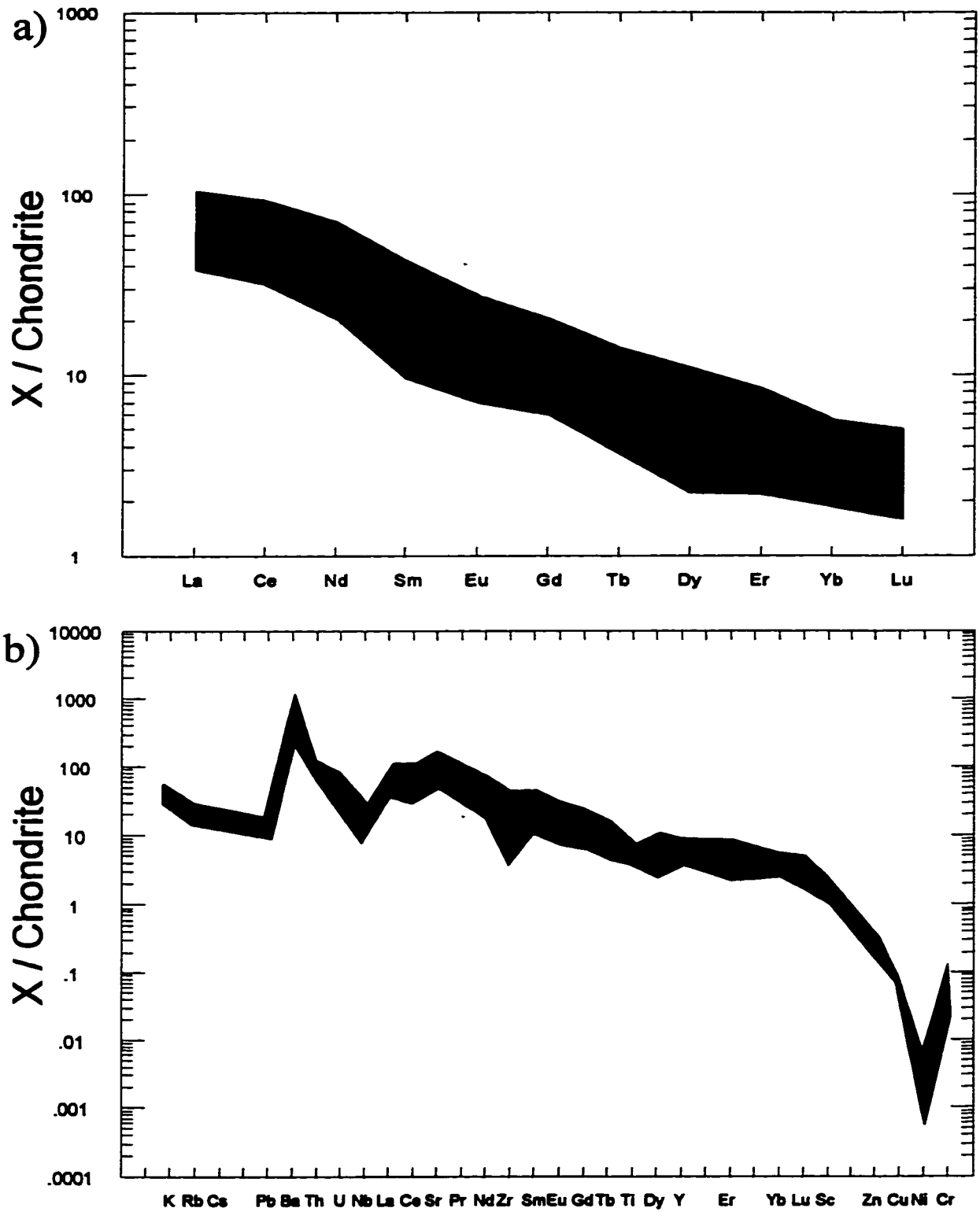

The sample 930616-1 represents the most primitive sample of all granitoids as it contains high MgO (7.48 wt.%), $Mg^{\#}$ =0.60, Cr (409 ppm) and Ni (101 ppm). This sample is a massive, medium grained, hornblende-rich, shoshonitic monzodiorite with 54.17% $SiO_2$ and relatively potassic with molar K/Na of 0.84 and $K_2O/Na_2O$ = 1.28. Total REE is high (192 ppm) and the REE pattern is steeply sloped from 106 times chondrite for La, with $La/Yb_{CN}$=23.07 and moderately sloped HREE ($Gd/Yb_{CN}$ = 3.7) and lacks an Eu anomaly (Eu/Eu*=0.98). The HFSE are low compared to low field strength elements of similar ionic radii (Zr/Zr*=0.39, Nb/Nb*=0.04; Ti/Ti*=0.39).

## 6.2 Saccharoidal Granitoids

The saccharoidal granitoids range in $SiO_2$ from 51.54-67.75 wt.% which is similar to the range of $SiO_2$ found for the non-saccharoidal granitoids although on average, saccharoidal samples are higher in $SiO_2$ (avg.=59.67). Saccharoidal granitoids are lower in $Mg^{\#}$ (34-69, avg.=46), P, Cr, K/Rb, and Ba than non-saccharoidal granitoids. Saccharoidal granitoids exhibit slightly higher $K_2O$ (up to 6.24 wt. %), Sc, Ni, Y, Th, and U abundances than non-saccharoidal granitoids. These rocks posses negative HFSE anomalies (Figure 14a) with Nb/Nb* = 0.07-0.51 (avg.=0.21), Ti/Ti* = 0.3-0.61 (avg.=0.42), and variable Zr/Zr* (0.38-1.43) and high LILE with Ba <1677 ppm, Rb<176 ppm, Sr<2663 ppm, and $K_2O$ <6.24 wt.% consistent with an arc trace element signature.

The REE's are variably enriched with La between 19 and 132 times chondrite (normalizations after Taylor and McClennan, 1985), averaging 70 times chondrite. Normalized REE profiles are fractionated ($La/Yb_{CN}$=6.29-28.05, avg.=15.6), with weakly

Figure 14a. Chondrite normalized extended element plot for the saccharoidal granitoids. Samples (n=9) are compositionally similar to non-saccharoidal samples and are characterised by high Ba, a positive Sr/Sr* anomaly, and negative HFSE anomalies such as Nb/Nb*=0.07-0.51 and Ti/Ti*=0.3-0.61. Normalizations after Taylor and McClennan (1985).

Figure 14b. Chondrite normalized REE abundances for the saccharoidal granitoids. All samples (n=9) are high in total REE (48-225 ppm) and are REE fractionated with $La/Yb_{CN}$=6-28 and posses weakly sloped HREE ($Gd/Yb_{CN}$) averaging ~2.6. A weak and variable Eu anomaly is present averaging Eu/Eu*=0.93. Normalizations after Taylor and McClennan (1985).

# Saccharoidal Granitoids

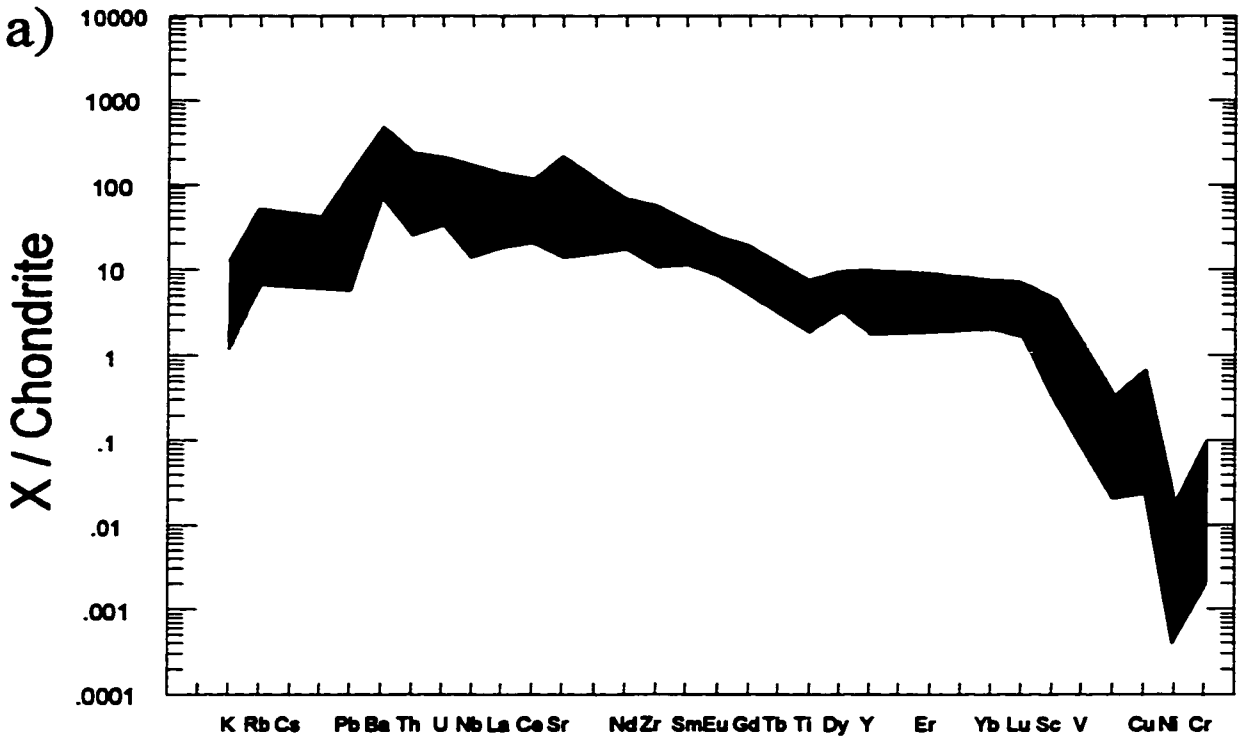


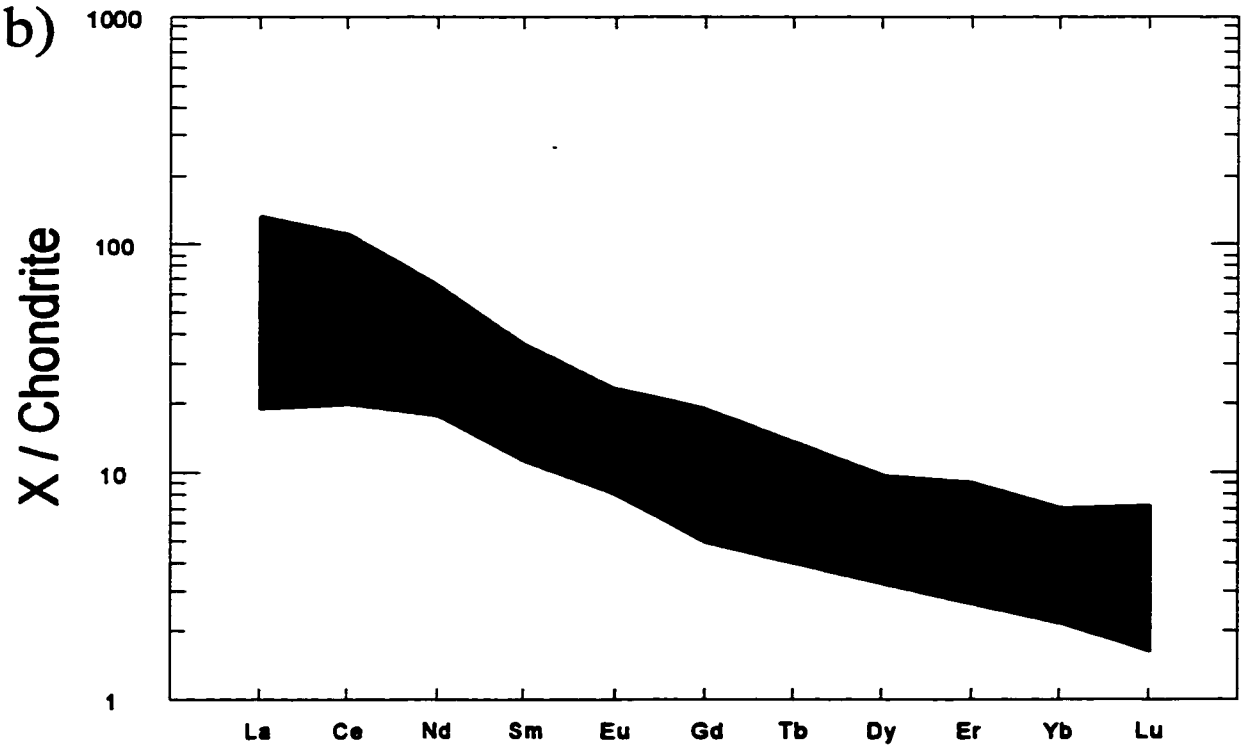

sloped HREE ($Gd/Yb_{CN}$=1.22-4.1, avg.=2.6), and generally weak negative Eu anomalies (Eu/Eu*=0.77-1.11, avg.=0.93) (Figure 14b).

## 6.3 Hornblendites

Hornblendites are characterized by low $Al_2O_3$ (5-12 wt.%), low to moderate $SiO_2$ (40-52 wt.%), moderate to high CaO (7-15 wt.%), and highly variable $Na_2O$ (0.6-3.1 wt.%). The rocks are mildly alkaline with $K_2O$ up to 3 wt.% and four samples are potassic, with molar ratios of K/Na of 1 to 1.54. All samples are silica undersaturated and contain normative feldspathoids except 930616-6.

The LILE are high and variable (200-800 ppm Sr, 15- 100 ppm Rb, 180-1500 ppm Ba, 65-140 ppm total REE), as is MgO (12.15 - 19.34 wt.%), Cr (450-1300 ppm) and Ni (80-600). Low Zr/Zr* (0.16-0.51), Nb/Nb* (0.1-0.2) (Figure 15a) are also evident and Ti/Ti* is variable between 0.36-1.55. Chondrite-normalized REE profiles (Figure 15b) show variable degrees of enrichment in LREE ($La/Yb_{CN}$=7-26) and HREE ($Gd/Yb_{CN}$=2.5-5; Fig. 8) with weak Eu anomaly (average Eu/Eu*=0.74, n=8). Hornblendites have less than chondritic ratios of $Al_2O_3/TiO_2$ and $CaO/TiO_2$.

## 6.4 Mafic Dykes

The mafic dykes range between 45.62 and 55.68 wt.% $SiO_2$ and are typically HFSE depleted with Zr/Zr*, Nb/Nb*, and Ti/Ti* averaging 0.48, 0.08, and 0.71 respectively. The LILE are high with Ba up to 1939 ppm (avg. 849 ppm), Rb less than 151 ppm (avg. 63 ppm),

Figure 15a. Chondrite normalized extended element plot for the hornblendite units. Hornblendites (n = 12) are characterised by elevated LILE at high transition element abundances and negative Zr ($Zr/Zr^*$ = 0.16-0.15) and Nb ($Nb/Nb^*$=0.1-0.2) anomalies. Normalizations after Taylor and McClennan (1985).

Figure 15b. Chondrite normalized REE abundances for the hornblendite units. Samples (n = 8) are variably fractionated with $La/Yb_{CN}$ = 7-26 and $Gd/Yb_{CN}$=2.5-5. A weak negative Eu anomaly is also present averaging 0.74. Normalizations after Taylor and McClennan (1985).

# Hornblendites

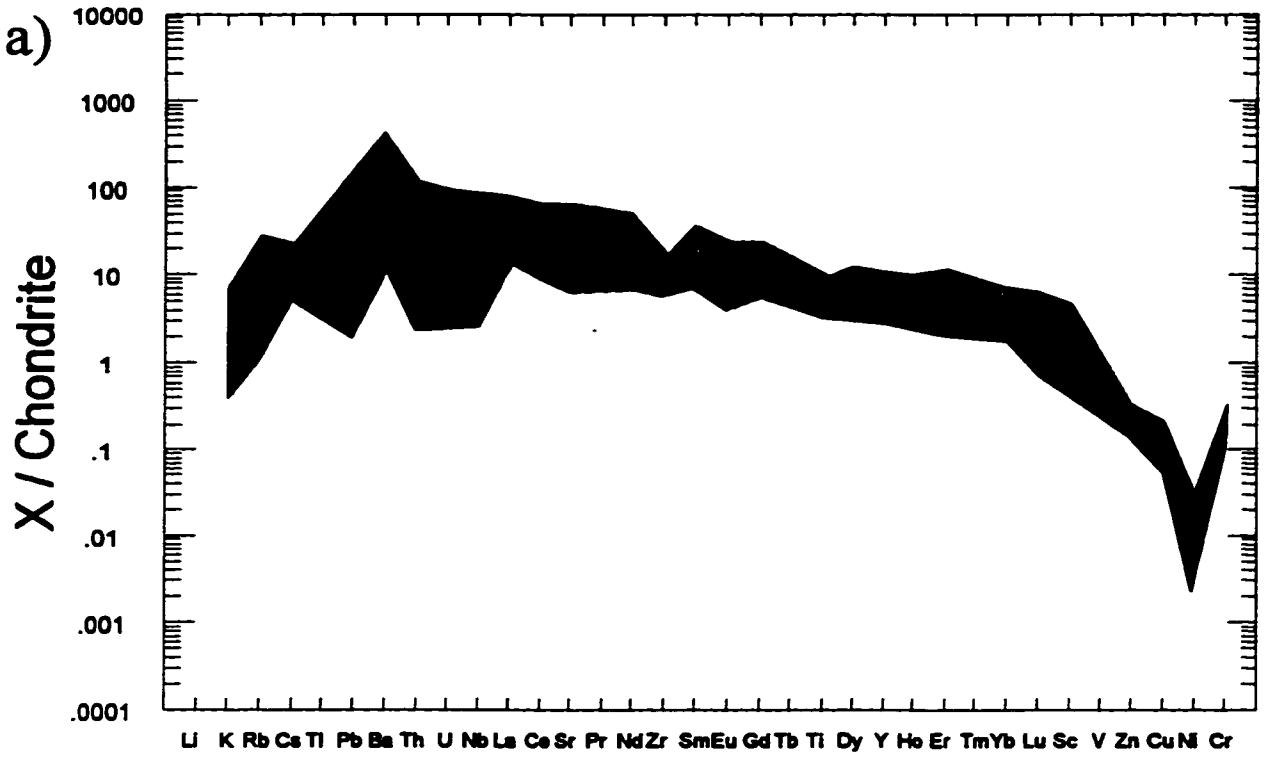


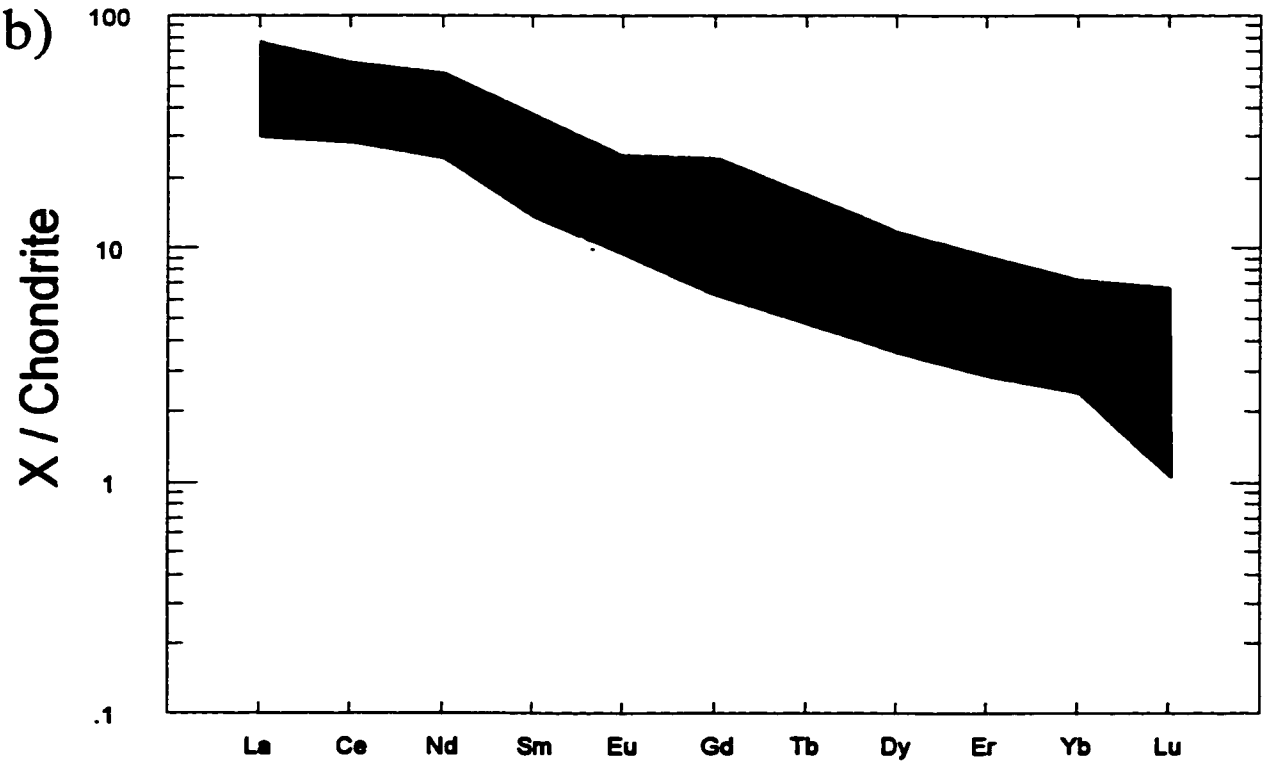

and Sr up to 1342 ppm (avg. 728 ppm) in consideration of the high $Mg^{\#}$ (58-73) and Cr (292-1190 ppm, avg.=681 ppm) of these rocks.

Total REE are high (avg. 132 ppm), with up to 194 times chondrite enrichment in La (avg. 76 ppm) in the eight samples analyzed. Rare earth element profiles are highly fractionated with $La/Yb_{CN}$ up to 30 and HREE are weakly sloped and averaging $Gd/Yb_{CN}$ = 3.2. The magnitude of the Eu anomaly varies between $Eu/Eu^{*}$=0.53-1.02 (avg.=0.85).

Although the mafic dykes share many chemical similarities with the LSIC hornblendites, notable differences exist, indicating that they are not directly related to any of the mafic intrusions exposed at surface in the LSIC. The dyke samples have higher D.I., are not corundum and feldspathoid normative, and are quartz normative unlike the hornblendites. Additionally, $Al_2O_3$, $SiO_2$, Sr, Zr and REE are typically higher than hornblendite concentrations whereas MgO, $Fe_2O_3$, Ni, and K/Na are lower in the mafic dykes. Mafic dykes are similar in terms of $CaO/TiO_2$, $CaO/Al_2O_3$ and $Al_2O_3/TiO_2$ to lamprophyres from the Pontiac Subprovince (Camire et al, 1993).

## 6.5 Mafic Enclaves

A total of six actinolitic enclave compositions were obtained and found to exhibit unusual chemistry for igneous rocks. All enclaves are quartz normative with a D.I. of 7-24 (avg.=12), moderate $SiO_2$ (49.62-54.66 wt.%, avg.=52.45 wt.%), high MgO (14.93-20.01 wt.%, avg.= 18.05 wt.%), $Mg^{\#}$ (69-81, avg.=76), Cr (343-1053 ppm, avg.=916 ppm), and Ni (30-526 ppm, avg.=193). The LILE concentrations are low with Ba ~528 ppm, Rb ~54 ppm, and Sr ~92 ppm and very low $Al_2O_3$ (2.36-7.91 wt.%, avg. 3.85 wt.%) and low Zr (1-19 ppm,

avg.=5 ppm). The molar K/Na of the enclaves is variable between 0.22-2.07 (avg.=0.8) indicating some are ultrapotassic although total alkalis are low. A significant modal percentage of biotite is present in samples with elevated $K_2O$.

On an extended element plot, enclaves are characterized by negative Ti ($Ti/Ti^*$=0.23-0.51, avg.=0.38) Zr ($Zr/Zr^*$=0.02-0.51, avg.=0.13), Sr ($Sr/Sr^*$=0.41-1.85, avg.=0.75) and Eu ($Eu/Eu^*$=0.46-0.94, avg.=0.70) anomalies. Rare earth element profiles define fractionated arrays with $La/Yb_{CN}$=1.03-43.8 (avg.=11.61) that are not subparallel and show up to $100X_{CN}$ LREE enrichment and weakly sloped HREE ($Gd/Yb_{CN}$=1.38-4.76, avg.=2.9).

Enclave chemistry is atypical of common regional mafic rock compositions such as Abitibi and Pontiac Subprovince komatiite, LSIC hornblendite and lamprophyre. Enclaves are distinguished from LSIC hornblendites and mafic dykes by lower D.I., K/Rb, $K_2O+Na_2O$, $Al_2O_3$, $Na_2O$, $TiO_2$, Zr, and total REE and higher $Al_2O_3/TiO_2$ (~43) and $Mg^{\#}$. The higher K/Na and $Sr/Sr^*$ and lower $Ti/Ti^*$ and $Zr/Zr^*$ of the actinolitic enclaves differentiate them from the LSIC hornblendites and mafic dykes. One mafic enclave from the Lac Freschette Complex was analyzed for major and trace element composition and found to be both mineralogically and chemically similar to enclaves from the LSIC. This suggests mafic enclaves in the LSIC may share a comparable origin as those from other similar complexes within the Pontiac Subprovince.

# Chapter 7 Mineral Chemistry

## 7.1 Amphibole

Mineral analysis was conducted on euhedra interpreted as primary grains in the granitoids except for actinolites from enclaves. Calcic hornblende comprises the dominant ferro-magnesian silicate in the spectrum of rocks in the LSIC. Compositions of hornblendes classified after Hawthorne (1983) (Appendix 4) range from magnesian hornblende to actinolite for phenocrysts with Na+K <0.5 p.f.u., and edenite and silicic edenites at Na+K >0.5 p.f.u. (Figure 16). Compositional variation is large within a single section and no consistent core-to-rim variations were noted. On a plot of $Si_{p.f.u}$ vs. $Mg^{\#}_{p.f.u}$, three separate lines of evolution are identified (Figure 17). The data array containing the bulk of the granitoid data contains two slightly divergent lines of evolution whereas the clinopyroxene hornblendites form a sub-parallel array at higher $Mg^{\#}$. Since the compositions of primary hornblende reflect liquid compositions and are the product of various charge balancing crystal substitutions, the subparallel arrays indicate that the amphiboles within the clinopyroxene hornblendite equilibrated with a liquid of higher Na+K and $Mg^{\#}$ than the bulk of the granitoids. The two slightly divergent data arrays within the bulk of the granitoid data may indicate compositionally variable initial liquids and either slightly differing degrees of the various operative substitutions or different AFC or magma mixing histories.

The range in amphibole compositions can be attributed to coupled substitutions involving $Al^{IV}$ for cations in the C and A sites, and simple substitutions of C site cations. Hornblende compositions plotted in terms of $(Na+K)_A$ vs. $Al^{IV}$ define a trend with a slope indicative of hastingsite and pargasite control. With this axis formulation, hastingsite and

# Composition of LSIC Amphiboles

## LEGEND

Actinolitic Enclaves

Non - Saccharoidal Granitoids

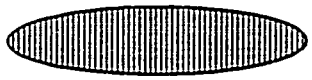

Saccharoidal Granitoids

Hornblendite

| Field | Sample |
|---|---|
| 1. | 921018-6 |
| 2. | 921014-9 |
| 3. | 921012-7 |
| 4. | 921010-4 |
| 5. | 921018-8 |
| 6. | 921012-9 |
| 7. | 930623-5 |
| 8. | 930620-3 |
| 9. | 921014-3 |
| 10. | 930819-3 |
| 11. | 921013-9 |
| 12. | 921011-16x |
| 13. | 921012-9 |

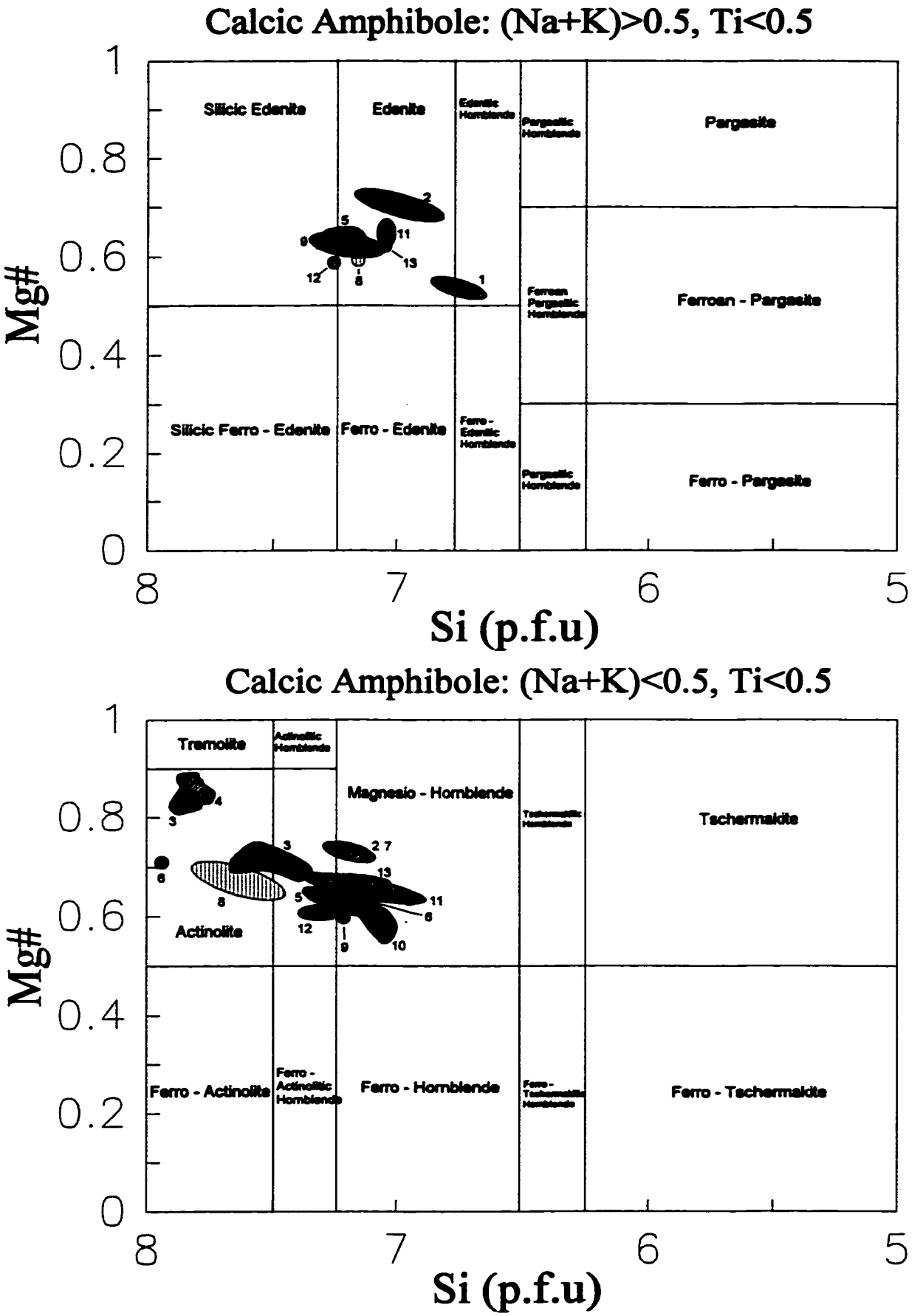


Figure 16. Classification of LSIC amphiboles after Hawthorne (1983). See legend on opposite page for key to notation and field fills.

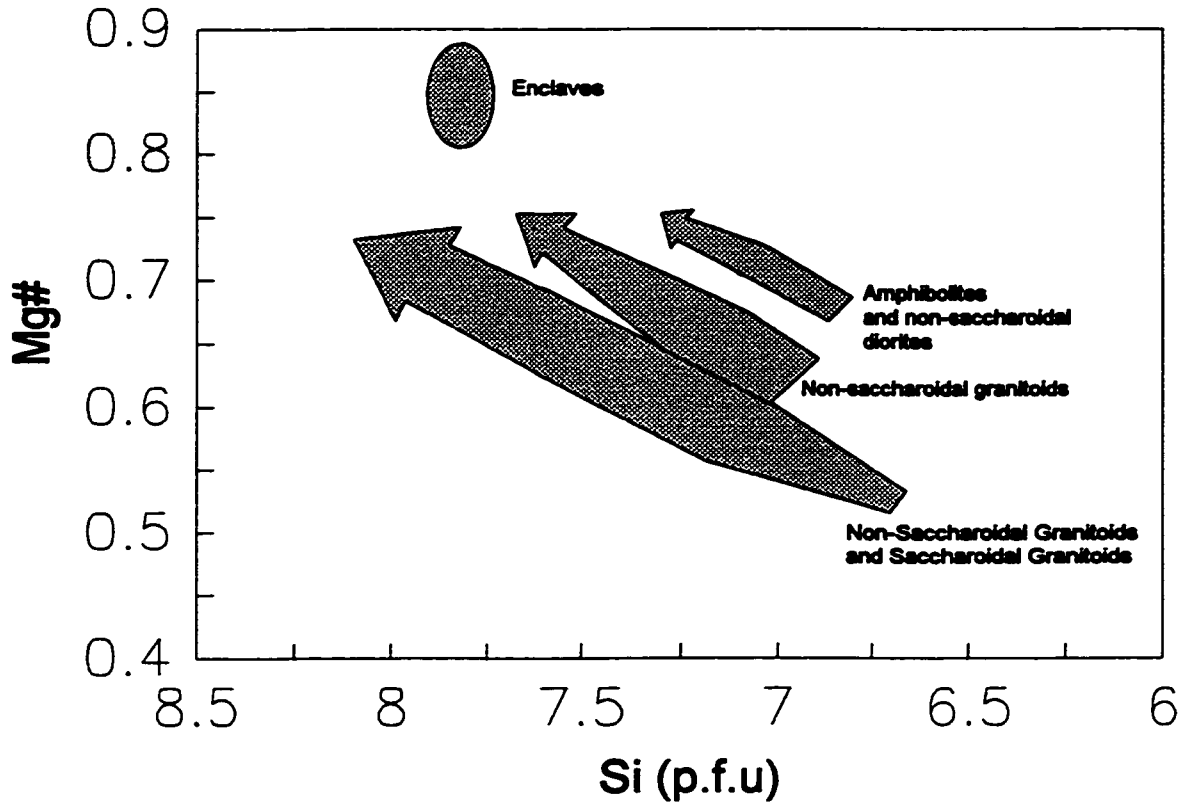


Figure 17. Si vs. Mg/(Mg+total Fe) for LSIC Hornblendes. Three separate trends are identified and inferred to represent hornblende crystallization from liquids of slightly differing initial composition.

pargasite substitution represents an ideal combination of both edenite and total tschermakite substitutions and the slope of the regression line suggests tschermakite substitution dominates over edenite substitution. Plots of 2Ti, $Fe^{3+}_C$, and $Al^{VI}$ vs. $Al^{IV}$ can be utilized to test the relative importance of the various tschermakitic substitutions. Correlations are poor, but slopes of regression lines outline the dominance of Fe-tschermakite substitution over Al-tschermakite substitution, and the lesser importance of Ti-tschermakite substitution. It is inferred that the weak correlation between $Fe^{3+}$ and $Na_B$ implies riebeckite substitution controls Na in the B site and richterite and glaucophane substitutions are insignificant. The well correlated (r=0.96) relationship for amphiboles in terms of $Al^{IV}$ vs. $Fe^{3+}+2Ti+Al^{VI}+(Na+K)_A$ defines a slope of 0.98 indicating that combined edenite, Ti-tschermakite, Al-tschermakite, and Fe-tschermakite substitutions account for the bulk of the compositional variability in the LSIC hornblendes (Figure 18). This set of coupled substitutions is commonly observed in most igneous hornblendes (Helz, 1982). Strong positive correlations between $Na_B$ vs. Ti and negative correlations between $Na_B$ vs. $Al^{VI}$ and Ti vs. $Al^{VI}$ suggest that a $Ca_B+Al^{VI} = Ti+Na_B$ coupled substitution proposed by Czamanske and Wones (1973) and observed by Vyhnal et al (1991) in calc-alkaline granitoids might also be operative. A strong inverse correlation between $Fe^{2+}$+Mn and Mg is the result of simple substitution in the C site. Simple substitutions in the A site are not apparent.

## 7.2 Clinopyroxene

Clinopyroxenes compositions (Appendix 4) fall within the field of quadrilateral pyroxenes in Q (Wo+En+Fs) vs. Jd (2Na) space (Morimoto, 1989) (Figure 19) and therefore

# Dominant Coupled Substitutions in LSIC Hornblendes

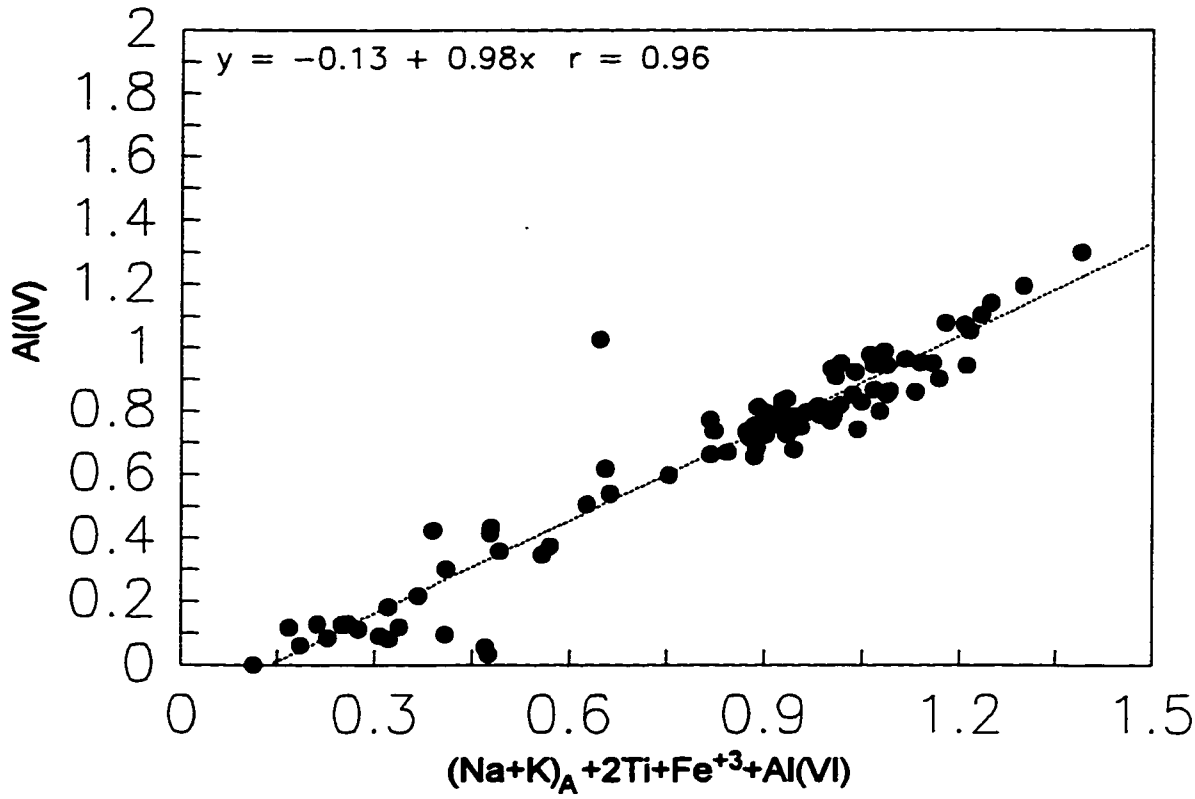


**Figure 18. Plot illustrating the combined effects of edenite and Ti, Fe, and Al tschermakite coupled substitutions. The hornblende data form an array with r=0.98 and a slope of 0.98 (equation given in upper left corner of diagram) indicating that the compositional variation exhibited by the LSIC hornblendes results from the combined effects of these substitutions.**

# Classification of Clinopyroxene Compositions I

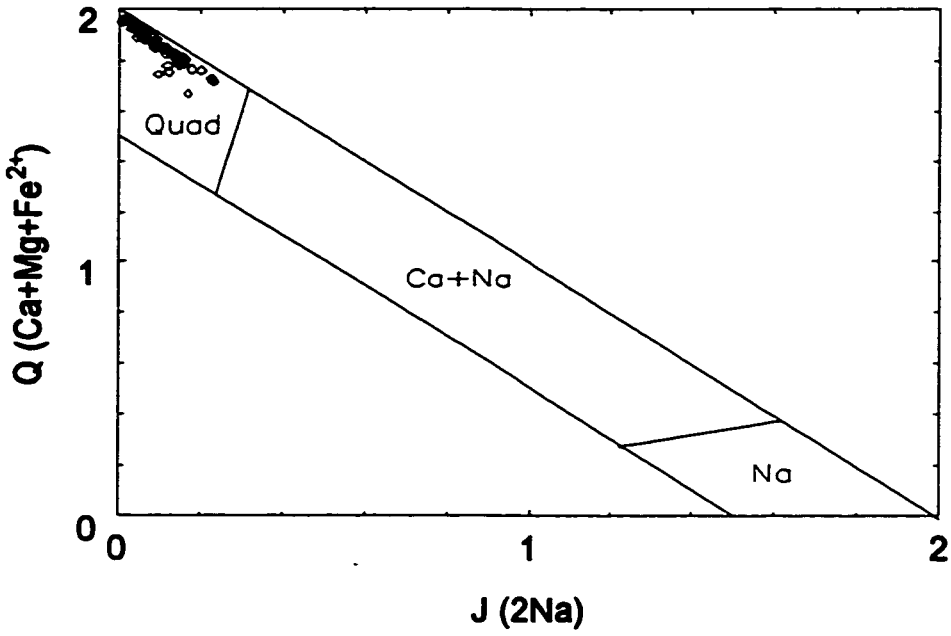


Figure 19. All LSIC clinopyroxenes plot within the quadrilateral compositional space of Morimoto (1988) and have been classified in terms of the Ca-Fe-Mg ternary (Morimoto, 1988).

have been classified in terms of the Wo - En - Fs quadrilateral (Figure 20). Phenocrysts are all calcic and range from diopside to salite with minor endiopside and augite. Magnesium numbers ($Mg^{\#}$ = molar ratios of $Mg/Mg+Fe^{2+}$) range from 0.78 to 0.95 in the clinopyroxene hornblendites to 0.76 - 0.91 in the non-saccharoidal granitoids. Saccharoidal granitoids contain phenocrysts which range in $Mg^{\#}$ from 0.69 to 0.74 with significantly higher $Na_2O$ compared to pyroxene from granitoids and hornblendites.

A general increase in the XWo (mole % wollastonite component) with decreasing XEn (mole % enstatite component) and host rock $SiO_2$, negative relationships between XEn and XFs+Mn (mole % clinoferrosilite + Mn), $Na_{p.f.u}$ and XEn, and positive relationship between $Cr_{p.f.u}$ and XEn is observed. These relationships indicate that clinopyroxene compositions record crystallization in evolving liquid compositions. The range in clinopyroxene chemistry can be resolved as predominantly a combination of calcium tschermakite ($Al^{IV}$ - $Al^{VI}$), calc-titan pyroxene ($Al^{IV}$ - Ti), aegerine (Na - $Fe^{3+VI}$) coupled substitutions. The major $Fe^{2+}$ - Mg simple substitution in pyroxene leads to the observed diopside ($CaMgSi_2O_6$) - hedenbergite $CaFe^{2+}Si_2O_6$) trend. A highly correlated Na - $Fe^{3+VI}$ data array with a regression equation slope near 1 and intersection at the origin indicates that the Na and $Fe^{3+}$ distribution between the pyroxenes can be accounted for predominantly by the aegerine coupled substitution. Combined esseneite ($Fe^{3+}$), fassiate (Cr), calcium tschermakite ($Al^{VI}$), and $CaTiAl_2O_6$ (2Ti) versus $Al^{IV}$ yield a regression equation with a slope of 0.97, intersection of 0.04, and a correlation coefficient of 0.78 indicating that the bulk of $Al^{IV}$ can be accounted for by these combined substitutions.

# Classification of Clinopyroxene Compositions II

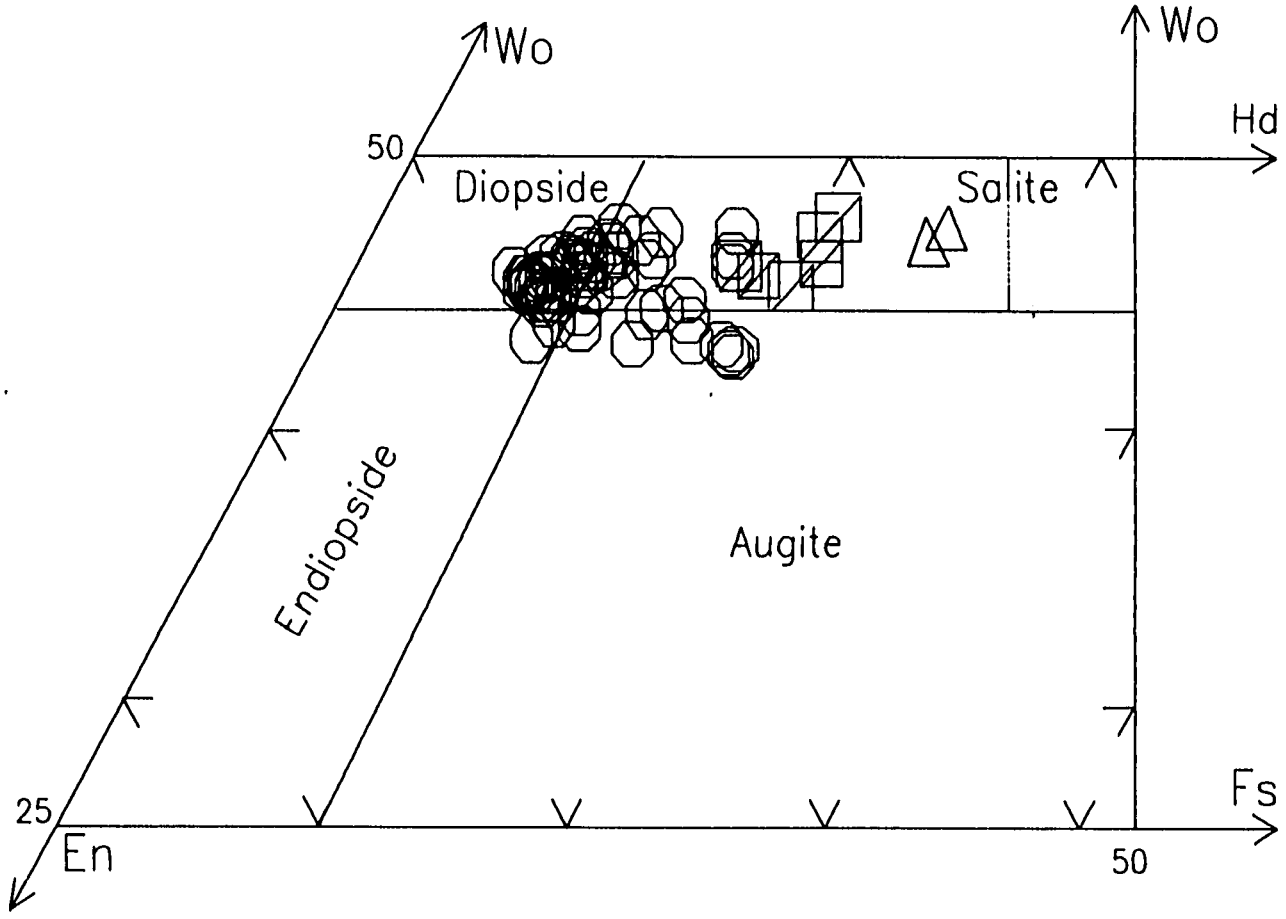


**Figure 20. Portion of the Ca-Fe-Mg ternary (Morimoto, 1988). circles = hornblendites and granitoids, squares and triangles = granitoids.**

## 7.3 Magnetite

Magnetites (Appendix 4) from granitoids and hornblendites represent nearly pure endmember magnetite with $X_{magnetite}$(X=mole percent) = 90.03-99.42. Minor fractions of other endmembers are present such as $X_{chromite}$ = 0.0-7.86, $X_{hercynite}$ = 0.0-1.36, $X_{Vmagnetite}$ = 0.23-0.69, $X_{jacobsite}$ = 0.0-0.59. The majority of magnetites contain no ulvospinel component although one sample possesses $X_{ulvospinel}$ = 0.55. Location of probe spots were carefully scrutinized by SEM backscattered images for inclusions or impurities. The Si in the analysis has been allocated to the $^{+}3$ site of magnetite, and Ca to the $^{+}2$ site according to Deer et al (1962a). The presence of Si, and Ca in magnetite is not uncommon (Westendorp et al, 1991) and has been attributed to magnetite crystallizing in the presence of a $Cl^{-}$ rich fluid (Shcheka et al, 1977).

Magnetite is common in modern calc-alkaline rocks and generally contains $X_{ulvospinel}$ between 10-75 (Ewart, 1982) and the low Ti concentration of the LSIC magnetites relative to magnetites in modern calc-alkaline rocks is probably due to a number of factors. Low Ti in magnetite is most likely the result of subsolidus re-equilibration. Subsolidus re-equilibration of magnetite occurs rapidly in even volcanic rocks (Hattori, 1993). Mantles of titanite on magnetite were noted in some instances in the LSIC indicating Ti removal had occurred. Grains with visible titanization were avoided in the analysis. Recrystallized magnetites from the Murdock Creek Intrusion (Rowins, 1990) contain higher Ti, and lower Mn and Cr on average compared to LSIC magnetites and the low Ti of the LSIC magnetites is inferred to be the product of re-equilibration.

## 7.4 Titanite

Titanite analysis (Appendix 4) were obtained for a monzodiorite, quartz - monzodiorite, and a saccharoidal syenite. Non-saccharoidal granitoids contain nearly pure $CaTiSiO_5$ with minor Al substituting for Si, and Cr and V substituting for Ti. Variations in titanite composition are a function of the compositions of the host rock. An increase in $Si_{titanite}$ occurs with increasing host rock $SiO_2$ , and a decrease in $Fe_{titanite}$ and $Cr_{titanite}$ with decreasing host rock $Fe_2O_3$ and Cr. Titanite from saccharoidal syenites is lower in Ti, and higher in Si reflecting higher $SiO_2$ and $TiO_2$ of the host rock. Systematic core and rim variations are noted in two titanite samples from a saccharoidal syenite such as exchanges of (Fe + Mg + Ti) for (Al + V).

## 7.5 Feldspars

Feldspar analysis was obtained from an absorokititic monzonite and a high K quartz monzodiorite. Compositions are relatively homogenous with K-feldspar varying from $XOr_{94}$ to $XOr_{98}$ and plagioclase from $XAb_{98}$ $XAn_{01}$ to $XAb_{80}$ $Xan_{15}$. Plagioclase is typically $An_{30-80}$ in modern high K calc-alkaline and shoshonitic rocks (Ewart, 1982) and $An_{25-35}$ in Archean calc-alkaline examples (Condie, 1982). The near endmember compositions of the LSIC feldspars imply equilibration temperatures for mineral pairs at temperatures from ~400°C to less than 350°C between 1-7 kbar. (Barth, 1968; Brown and Parsons, 1981) respectively. Clearly this does not represent magmatic temperatures and suggest subsolidus equilibration during either protracted cooling or metamorphism.

## 7.6 Barite, Epidote, Allanite

Epidotes (Appendix 4) from a saccharoidal monzonite are relatively homogenous in composition with $(Fe^{2+}_{0.223-0.106}\ Mn_{0.029-0.033}\ Ca_{3.860-3.898})(Al_{3.849-4.033}\ Fe^{3+}_{1.926-1.849})(Si_{6.113-6.037})O_{24} \cdot OH$ (Appendix 4). Barite $(Ba_{1.014}Ca_{0.01}Sr_{0.012})\ S_{0.988}\ O_4$, partially mantled by biotite, occurs in an altered non-saccharoidal quartz-monzodiorite. A single allanite from a monzodiorite has a composition of $(Ca_{1.609}\ Mg_{2.894}\ Mn_{0.052})(Al_{2.454}\ Fe^{3+}_{1.822}\ Ti_{0.187}\ La_{0.278}\ Ce_{0.478}\ Nd_{0.069}\ Th_{0.032})\ Si_{6.622}\ O_{24} \cdot OH$.

## 7.7 Biotite - Phlogopite

Biotite analysis is heavily biased towards samples from clinopyroxene hornblendites with only one analysis from a non-saccharoidal diorite (Appendix 4). Biotites have been classified in terms of $Al^{TOT}$ vs. Fe/Fe+Mg on a per formula unit basis with analysis calculated to 22 oxygens (Figure 21). The majority of samples are classified as biotites with a subordinate number of phlogopites present in the clinopyroxene hornblendites. The annite component of biotite generally increases with decreasing $Al^{TOT}$. In a differentiated rock series, $Al^{TOT}$ in biotite commonly declines as a result of increasing $aSiO_2$ (Czamanske and Wones, 1973) and Al preferentially entering other six-fold coordinated silicate mineral sites at lower temperatures (Thompson, 1947). The late appearance of feldspars in the LSIC paragenesis undoubtedly influenced the $Al^{IV}$ incorporation into biotite. The $Fe^{3+}/Fe^{2+}+Fe^{3+}$ ratio of LSIC biotites decreases with increasing biotite evolution, as monitored by $Al^{TOT}$ and Si contents of biotites, which indicates a reducing trend of evolution. This is also supported by the weak

# Biotite Compositions Plotted in Terms of Total Al and Fe/(Fe+Mg)

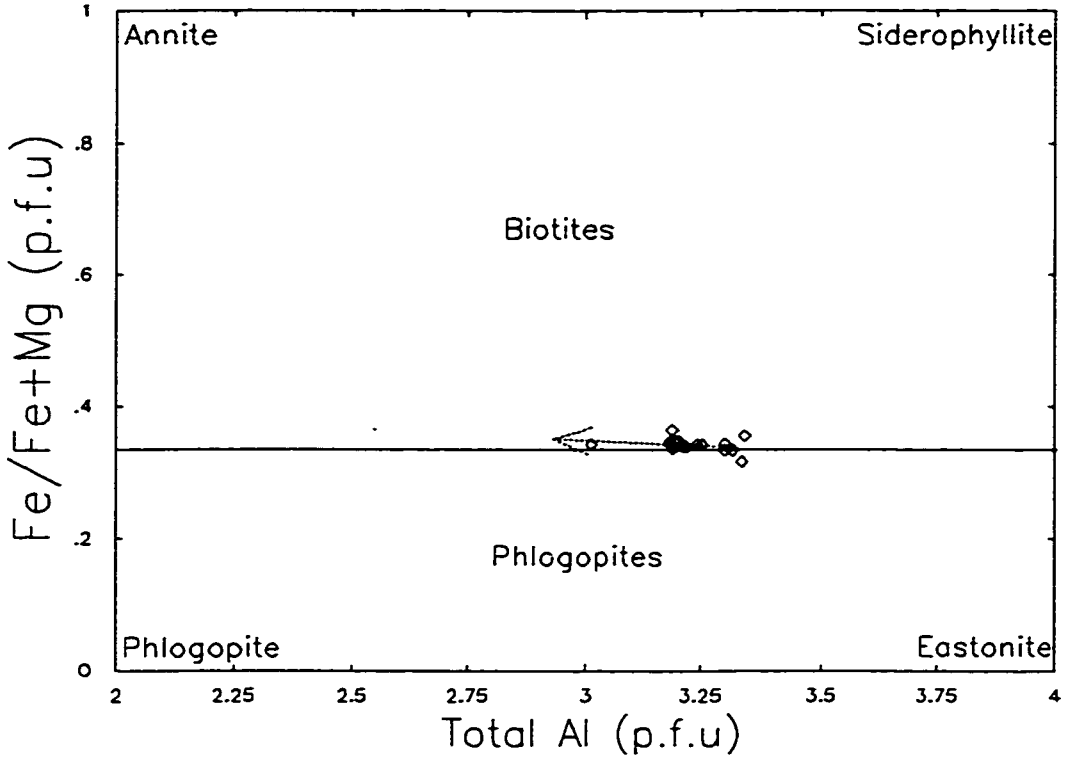


**Figure 21. Mica compositions plotted in terms of the phlogopite - Eastonite - Siderophyllite - Annite quadrilateral. Mica compositions are dominantly biotitic and appear to increase slightly in Fe/Fe+Mg with decreasing Al. Arrow indicates direction of host rock evolution. Phlogopite - Biotite division line after Deer et al (1962b).**

Fe/Mg+Fe enrichment trend developed in the LSIC biotites generally regarded as the product of crystallization under increasingly reducing conditions (Nash and Wilkinson, 1970).

The compositional variation of biotites can be expressed as the possible product of two sets of simple exchanges and 4 coupled exchanges any of which may be operative to varying degrees. Common simple exchanges in biotite are:

$Fe^{2+}$ - Mg

K - Na

The four primary coupled substitutions (Dymek, 1983) are:

$Al^{VI} + Al^{IV}$ - Mg +Si (Al Tschermakite)

$2Al^{VI} + VAC^{VI}$ - 3Mg (Dioctahedral)

Mg + Ti - $2Al^{VI}$ (Ti Spinel)

$VAC^{X} + Si - K + Al^{IV}$ (Talc)

where $VAC^{X}$ and $VAC^{VI}$ refers to a vacancy in the interlayer and octahedral sites respectively.

Other exchanges represent linear combinations of these four major coupled substitutions. The majority of the analysis was derived from clinopyroxene hornblendite hosted biotites. The lack of data obtained for more evolved rocks in the LSIC does not permit determination of substitution mechanisms beyond that of the hornblendite units.

### 7.7.1 Biotite from Clinopyroxene Hornblendites

A significant correlation of -0.86 occurs between $Fe^{2+}$ and Mg suggesting simple exchanges of these elements within the M site. The slope of the regression line is steeper than would by expected for balancing of Mg with $Fe^{2+}$ and another substitution must be involved

account for the high $Fe^{2+}$ relative to Mg. A well correlated (r = -0.79) inverse relationship exists for Ti - $Al^{VI}$ and a positive relationship with r = 0.66 for $Fe^{2+}$ - Ti, the only positive $R^{2+VI}$ - Ti relationship observed, attests to a spinel type substitution of $2Al^{VI}$ - $Fe^{2+}$ +Ti and might account for the $Fe^{2+}$ excess noted to occur in the case of simple $Fe^{2+}$ - Mg exchange. The linear relationship (r = -0.66) between $Fe^{2+}$ and $Al^{VI}$ is further evidence of this Fe spinel exchange. Both $Fe^{2+}$ and Ti generally increase with biotite evolution based upon $Mg^{\#}$ and Si which indicates the direction of the exchange mechanisms. An inverse correlation between Ti and $Al^{IV}$ suggests that neither Ti-tschermakite type or $Al^{VI}$+Si-Ti+$Al^{IV}$ exchanges are operational. Positive correlations between $Al^{IV}$-$Al^{VI}$ and $Al^{IV}$-$Fe^{3+}$ indicate the operation of Al and ferri tschermakite exchanges except that an excess of $Al^{IV}$ cannot be balanced by these reactions alone. An $Al^{VI}$ reducing exchange, such as the Fe spinel type exchange discussed above, or another $Al^{IV}$ enriching exchange must have been active. Positive relationships for K-Mn and K-$Fe^{2+}$, negative relationships for K-$Fe^{3+}$ imply an exchange in the style of K+$R^{2+VI}$ - $VAC^{X}$+$R^{3+VI}$ (Dymek, 1983), might have occurred where $R^{2+VI}$ is $Fe^{2+}$ with the possible involvement of Mn, and $R^{3+VI}$ is $Fe^{3+}$. This would be expected to decrease A-site vacancies with biotite evolution since K increases with biotite evolution and a high correlation of 0.78 is observed for K - A site charge implying that this exchange has occurred. A positive relationship is observed for K-Na indicative of simple substitution in the A site although K is in excess of that required to balance the exchange as would be expected if the latter coupled K assisted vacancy reducing substitution was operative. No evidence exists for Cr - $R^{3+VI}$ and talc exchanges.

In summary, the major simple and coupled substitutions responsible in the clinopyroxene hornblendite hosted biotites are:

$Mg - Fe^{2+}$

$Na - K$

$Fe^{3+} + VAC^{X} - K+Fe^{2+}$ with the possible involvement of Mn with $Fe^{2+}$

$2Al^{VI} - Fe^{2+} + Ti$

$Si+Mg - Al^{VI} + Al^{IV}$

$Si+Mg - Al^{IV} + Fe^{3+}$

## 7.8 Equilibrium Between Fe-Mg Minerals

### 7.8.1 Clinopyroxene - Hornblende

Under equilibrium, for a specific set of P-T conditions, element partitioning between mineral pairs should be constant regardless of bulk rock composition (Cooper, 1972). The Fe-Mg exchange between clinopyroxene and hornblende has been determined based upon the relation:

$$K_{D\ Mg/Fe^{2+}}^{Cpx-Hbl} = [(X_{Mg}/X_{Fe2+})^{Cpx}/(X_{Mg}/X_{Fe2+})^{Hbl}]$$

where $X = Mg^{\#} = (Mg/(Fe^{2+}+Mg)$ (Kretz and Jen, 1978) on a p.f.u. basis. The $K_D^{Fe-Mg}$ ranges from 2.13 - 4.08 (n=5) in the clinopyroxene hornblendites. This range in $K_D$ is typical to slightly higher than that found in ultramafic, gabbroic, and volcanic rocks (Onuki, 1965; Ghandi, 1970) and synthetic clinopyroxene - hornblende pairs crystallized between 820-1100°C (Helz, 1973). Clinopyroxene - hornblende mineral pairs from a monzonite (sample 921018-8) yield $K_D^{Fe-Mg}$ between 1.97 - 2.28 (n = 4), still within the range of igneous rock $K_D^{Fe-Mg}$ of 1.7 to ~3.2 (Kretz and Jen, 1978) whereas a clinopyroxene - hornblende pair from a saccharoidal monzonite possess

a $K_D$ of 1.28, significantly lower than that obtained from other sections and slightly lower than the minimum value of 1.3 derived from some igneous gabbroic rocks (Ghandi, 1970).

The wide variation in apparent $K_D$ may indicate equilibration at a range of T-P conditions, mineral compositional effects, principally by an increase in $Al^{IV}$ which tends to increase $Fe^{2+}$ relative Mg in amphibole, increasing the clinopyroxene - hornblende $K_D$ (Sen, 1973; Kretz and Jen, 1978), or disequilibrium. High $K_D$s' for mineral pairs are obtained from least evolved samples in which hornblendes are relatively high in $Al^{IV}$, hence higher $K_D^{Cpx\text{-}Hbl}$, than hornblendes from more evolved samples. From a plot of $K_{DCpx\text{-}Hbl}$ vs. hornblende $Al^{IV}$, a positive linear relationship is observed for 921014-9 pairs suggesting $Al^{IV}$ in hornblende may exhibit a very large control on $K_D$. Although the $K_D$ are within the range of igneous values, hornblende in these rocks typically crystallized later than clinopyroxene which exhibits reaction relationships with amphibole. Mineral relationships suggest disequilibrium is a more likely explanation for the scatter in $K_D$ and a mineral compositional control on $K_D$ is of lesser importance. Disequilibrium between clinopyroxene and amphibole is indicated by rounded or corroded cores of clinopyroxene in hornblende euhedra with the cores partially replaced by amphibole. On a plot of hornblenede $Mg/Fe^{2+}$ against clinopyroxene $Mg/Fe^{2+}$, the 921018-8 samples form a cluster suggesting that pyroxene and amphibole represent near equilibrium compositions. The $K_D$ determined for the saccharoidal monzonite hornblende - pyroxene pair is lower than that expected for metamorphic pairs crystallized at ~700°C (Kretz and Jen, 1978).

### 7.8.2 Biotite - Hornblende

The exchange of Mg and $Fe^{2+}$ between biotite and hornblende has been determined based upon the relation:

$$K_{D\ Mg/Fe^{2+}}^{Hbl-Bio} = [(X_{Mg}/X_{Fe2+})^{Bio}/(X_{Mg}/X_{Fe2+})^{Hbl}]$$

where X equals the cation on a p.f.u. basis. Coexisting biotite and hornblende from a diorite sample (930623-5) yield $K_D$ = 0.72 (n=1) which is within the range of 0.69 - 0.93 commonly obtained from mineral pairs from igneous rocks (Speer, 1987) and likely represent equilibrium pairs. Biotite - hornblende pairs from a clinopyroxene hornblendite produce $K_D$ values significantly higher than those commonly observed in igneous rocks, ranging from 1.06 - 1.99. Speer (1987) notes that high $K_D$ values may be obtained for mineral pairs if biotite represents a replacement product of hornblende. Biotite from clinopyroxene hornblendites is commonly ragged, has patchy interference colours and is occasionally sagenitic suggesting that the high $K_D$ may be the product of the oxidative alteration of biotite increasing the $Fe^{3+}/Fe^{2+}$ and $Mg/Fe^{2+}$ ratios of biotite. Lack of alteration in the diorite sample and inclusion of biotite in hornblende in the non-saccharoidal diorite sample suggest that the $K_D$ of 0.72 is probably an equilibrium igneous value.

### 7.8.3 Clinopyroxene - Biotite

The large range in $K_D$ (~1.6 - 2.7) observed for biotite - clinopyroxene pairs from the clinopyroxene hornblendites represents disequilibrium. This disequilibrium may be the result of both alteration of biotite and the late crystallization of biotite relative to clinopyroxene. A $K_D$ of 1.5 for a saccharoidal monzonite pair is observed.

It appears from the $Mg/Fe^{2+}$ partitioning between mafic minerals in the LSIC that mafic mineral compositions in the hornblendites are in disequilibrium, whereas equilibrium $K_D$ values between hornblende and clinopyroxene is observed in the non-saccharoidal granitoids. Although the $K_D$ values obtained for the non-saccharoidal granitoids are within the range observed in magmatic rocks, the common occurence of amphibole mantling and replacing clinopyroxene suggests disequilibrium. The $K_D$s' noted in the saccharoidal granitoid mineral pairs likely reflect alteration effects by conditions less than magmatic temperatures as suggested by the low $K_{D\ Hbl-Cpx}$ less than high temperature metamorphic $K_{D\ Cpx-Hbl}$ of 1.7 (Kretz 1978) but higher than that for low temperature metamorphic clinopyroxene - actinolite pairs ($K_D$~1) (Muller, 1962).

## 7.9 Nd - Sr Isotopic Compositions of Mineral Separates

The Nd and Sr isotopic compositions of mineral separates from the LSIC are given in Table 1 with procedure in Appendix 5. Neodymium isotopic composition of primary minerals yield $\varepsilon Nd_T$ (T=2.68 Ga) = +2.1 - +2.9 for titanite (n=4), $\varepsilon Nd_T$ = +1.4 and +3.9 for hornblende (n=2), $\varepsilon Nd_T$ = +3.3 for apatite (n=1), and $\varepsilon Nd_T$ = +3.7 for allanite (n=1). Secondary minerals are highly variable in $\varepsilon Nd_T$ (T=2.68 Ga) with actinolite (n=2) from mafic enclaves yielding -2.3 and +4.2, and epidote (n=1) from a hornblendite yields +6.8 while an epidote (n=1) from a non-sacharoidal diorite yields +9.1.

An estimate of the isotopic composition of the Archean Abitibi mantle inferred from clinopyroxenes obtained from Abitibi mafic and ultramafic rocks indicates $\varepsilon Nd_T$ = +2.2 - +2.8 at ~2.7Ga (Machado et al, 1986), from Kamiskotia gabbroic complex and associated volcanic rocks range $\varepsilon Nd_T$ = +2.2 - +2.6 (Barrie and Shirey, 1991), $\varepsilon Nd_T$ = +0.9-+2.3 from Abitibi

Table 1. Neodymium and Sm Concentration and Nd Isotopic Composition of LSIC Minerals

| Sample | Mineral | Sample Weight (mg) | Nd (ppm) | Sm (ppm) | $^{143}Nd/^{144}Nd$ Measured | $^{147}Sm/^{144}Nd$ | $^{143}Nd/^{144}Nd$ 2680 Ma | εNd Present Day | εNd† 2680 Ma |
|---|---|---|---|---|---|---|---|---|---|
| Primary Minerals | | | | | | | | | |
| 921015-14 | Hornblende | 26.69 | 37.01 | 7.75 | 0.511467 | 0.12648 | 0.509231 | -22.8 | 1.4 |
| 921010-5 | Titanite | 0.25 | 2345.4 | 409.10 | 0.511169 | 0.10541 | 0.509305 | -28.6 | 2.9 |
| 921018-8 | Allanite | 0.40 | 7505.2 | 468.16 | 0.510012 | 0.03769 | 0.509346 | -51.2 | 3.7 |
| 921011-17 | Titanite | 1.03 | 4063.6 | 797.57 | 0.511387 | 0.11862 | 0.509290 | -24.4 | 2.6 |
| 921014-3 | Titanite | 0.34 | 3143.3 | 551.14 | 0.511142 | 0.10596 | 0.509268 | -29.2 | 2.1 |
| 930623-05 | Apatite | 5.30 | 757.5 | 133.89 | 0.511217 | 0.10681 | 0.509328 | -27.7 | 3.3 |
| 930623-05 | Hornblende | 20.90 | 40.67 | 9.97 | 0.511976 | 0.14811 | 0.509358 | -12.9 | 3.9 |
| 921018-7 | Titanite | 1.11 | 3031.5 | 515.04 | 0.511084 | 0.10267 | 0.509269 | -29.6 | 2.1 |
| Secondary Minerals | | | | | | | | | |
| 921018-8 | Epidote | 3.80 | 38.75 | 6.42 | 0.511392 | 0.10007 | 0.509622 | -24.3 | 9.1 |
| 930619-11a | Actinolite | 22.67 | 8.51 | 2.52 | 0.512204 | 0.17873 | 0.509044 | -8.5 | -2.3 |
| 921010-4 | Actinolite | 20.30 | 8.00 | 2.54 | 0.512572 | 0.19120 | 0.509371 | 2.2 | 4.2 |
| 921014-9 | Epidote | 4.40 | 29.59 | 5.30 | 0.511421 | 0.10828 | 0.509506 | -23.7 | 6.8 |

† Present day CHUR values used in the calculation of εNd are: $^{143}Nd/^{144}Nd = 0.512638$ and $^{147}Sm/^{144}Nd = 0.1967$

Subprovince shoshonitic lamprophyre clinopyroxene separates (Hattori et al, 1996), and from komatiite whole rock analysis, $\varepsilon Nd_T$ ~+1.0 to ~+4.0 (Zindler, 1982; Dupre et al, 1984; Cattell et al, 1984; Lahaye et al, 1995). The values obtained for the LSIC fall within the depleted mantle spread of data (Figure 22) indicating an extraction of magma from mantle similar in Nd isotopic composition to that which gave rise to the mafics and ultramafic rocks of the Abitibi belt.

Strontium isotopic compositions for LSIC titanite (n=4) range from $^{87}Sr/^{86}Sr_I$ = 0.70080 to 0.70138 and for apatite (n=1), $^{87}Sr/^{86}Sr_I$ = 0.701696 (Table 2). These ratios are similar to Abitibi mafic and ultramafic igneous rocks with ratios of 0.70105 ± 6 (Machado et al, 1986) and the $^{87}Sr/^{86}Sr_I$ = 0.7008 - 0.7016 determined from clinopyroxene separates from Abitibi shoshonitic lamprophyres and syenitic stocks (Hattori et al, 1996) (Figure 22).

## $\varepsilon Nd_T$ vs. $^{87}Sr/^{86}Sr_I$ Correlation Diagram for LSIC Mineral Separates

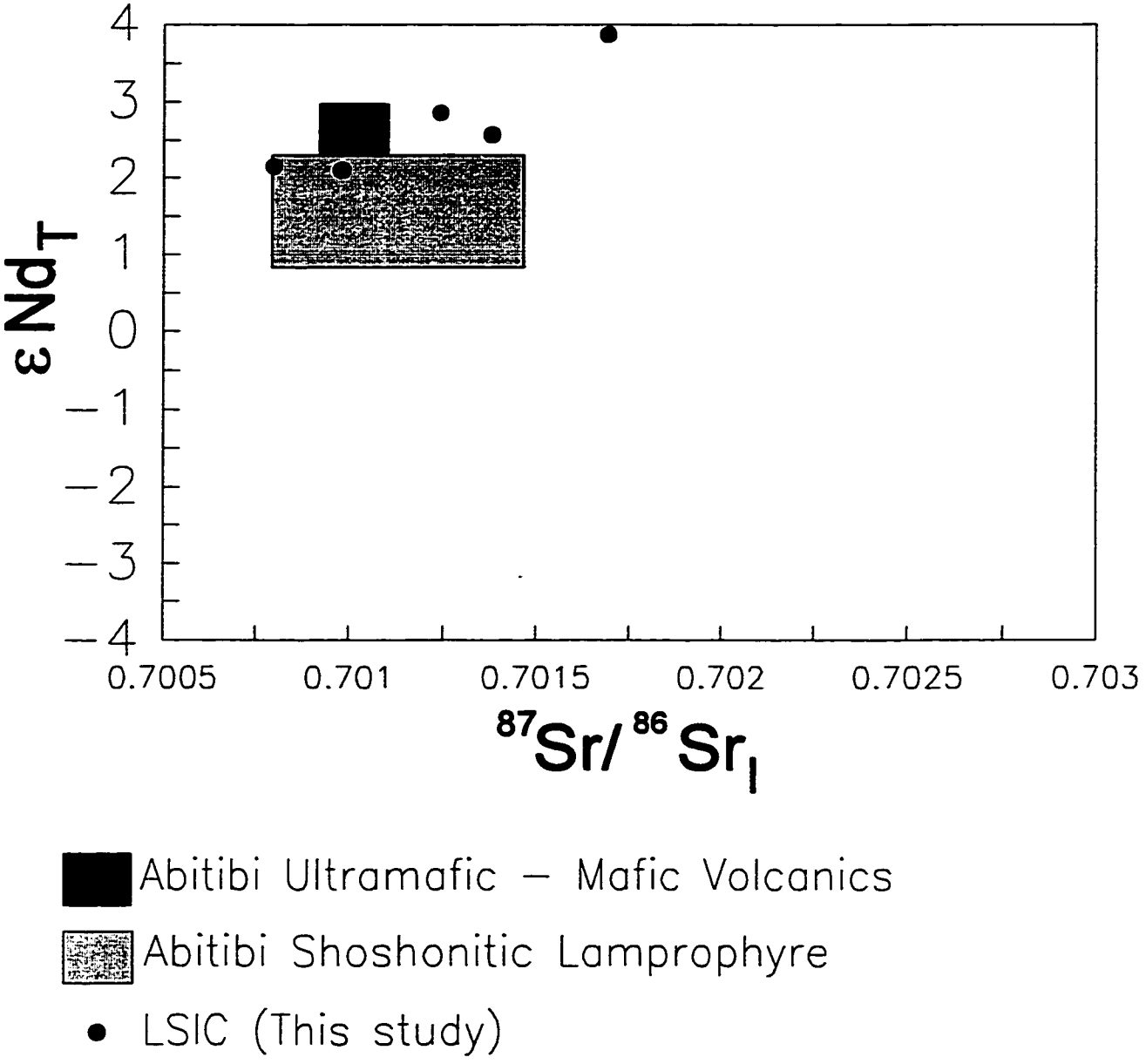


**Figure 22. $\varepsilon Nd_T$ values of primary mineral separates from the LSIC are within the range of εNd observed for mineral separates from Abitibi mafic, ultramafic (Machado et al, 1986) and alkaline rocks (Hattori et al, 1996). Initial $^{87}Sr/^{86}Sr$ of LSIC samples is in the same general range as that observed in Abitibi mafic and alkaline rocks.**

Table 2. Strontium and Rb Concentration and Sr Isotopic Composition of LSIC Minerals

| Sample | Mineral | Rb (ppm) | Sr (ppm) | $^{87}Sr/^{86}Sr$ measured | $^{87}Rb/^{86}Sr$ | $^{87}Sr/^{86}Sr$ 2680 Ma |
|---|---|---|---|---|---|---|
| 921010-5 | Titanite | 2.05 | 246.5 | 0.70216 | 0.0240 | 0.701228 |
| 921011-17 | Titanite | 2.18 | 385.8 | 0.70201 | 0.0164 | 0.701379 |
| 921014-3 | Titanite | 3.80 | 277.6 | 0.70289 | 0.0493 | 0.700977 |
| 921018-7 | Titanite | 1.82 | 206.4 | 0.70179 | 0.0255 | 0.700801 |
| 930623-5 | Apatite | | | 0.701696 | | 0.701696* |

* The present day $^{87}Sr/^{86}Sr$ value is assumed to represent the initial $^{87}Sr/^{86}Sr$ ratio of the apatite sample due to the high Sr/Rb ratio of apatites.

# Chapter 8 Petrogenesis

## 8.1 Granitoids

### 8.1.1 Source of the Initial Granitoid Melt

The initial melt for LSIC granitoids may have originated by partial melting of i) Pontiac sedimentary rocks, ii) Belleterre belt volcanic rocks, iii) Belleterre-Fugerville tonalite, iv) melting of pre-existing shoshonitic rocks or v) mantle.

(i) It has been noted that the Pontiac sedimentary rocks display chemical compositions similar to Timmiskaming type alkalic rocks (high Ni, Cr, MgO, $SiO_2$, LREE/HREE, LILE and negligible Eu anomalies) (Ujike, 1984) and should be considered as a possible source for the LSIC granitoids. The metaluminous composition of LSIC granitoids precludes Pontiac sedimentary rocks as their source since Pontiac sedimentary rocks are high in $SiO_2$ and $Al_2O_3$ (Lajoie and Ludden, 1984; Rocheleau and Dimroth, 1985; Feng et al, 1993) and are peraluminous with an average molar $Al_2O_3/(CaO+Na_2O+K_2O)$ of ~ 1.2 (data from Feng et al, 1993). Melts derived from Pontiac sedimentary rocks would also likely be peraluminous. Partial melting of sedimentary rock leaving a residual aluminous phase and producing a metaluminous melt is unlikely. The aluminous phase would likely be plagioclase feldspar at the crustal pressures that are recorded for peak metamorphism in the Pontiac sedimentary rocks (4.1-7.2 kbar; Ghassemi, 1996) and the melt would be depleted in CaO, Eu, and Sr. The LSIC granitoids are higher in CaO and Sr, and similar in $Al_2O_3$ to the Pontiac sedimentary rocks and unlikely to be derived from a sedimentary rock source.

Furthermore, the high $\varepsilon Nd_T$ values for the granitoids are not consistent with the derivation of the magma from the Pontiac sedimentary rocks, which have the values ranging from +0.96 to -3.87 at 2.68 Ga (Feng et al, 1993).

(ii) Melting of tholeiitic volcanic rocks could not have given rise to the LSIC melt since the most primitive LSIC rocks contain higher Cr, Ni than the Belleterre belt volcanic rocks. The mafic LSIC rocks cannot represent residues from melting basalt due to higher LREE and LILE in the LSIC and residues are unlikely to be intermediate in composition. Granitoids derived from direct partial melting of basalt generally are tonalitic to granodioritic (Arth and Hanson, 1975; Rapp et al, 1991).

(iii) Derivation of the LSIC melt from tonalite melting is also unlikely due to lower $SiO_2$ and higher Cr, Ni, MgO, Sr, and Ba concentrations in the monzodiorite than tonalites.

(iv) It has been argued that the derivation of high-K calc-alkaline rocks requires melting of a compositionally similar precursor (Roberts and Clemens, 1993). Smith (1994) suggested that the alkalic monzonites, such as those occurring in the Superior Province, are derived from melts of a hydrated alkali basalt precursor. This implies that alkaline rocks would have to be formed before the melting event that produced the LSIC melts. Shoshonitic and ultrapotassic igneous activity in the Superior Province is contemporaneous with the intrusion of the LSIC. The Otto Stock (2680 ± 1 Ma; Corfu et al, 1989), Garrison Stock (2678 ± 2 Ma; Corfu et al, 1989), Clericy

Pluton (2682 ± 3; Mortensen, 1993), lamprophyre dykes (Bristol Twp., 2687 ± 3 Ma, Barrie, 1990; southern Abitibi Subprovince, 2674 ± 2 Ma, Wyman and Kerrich, 1993) Lac Freschette and Lac Remigny possess crystallization ages that are coincident with the LSIC. Earlier high LILE sources are not recognised in the southern Superior Province therefore a compositionally similar precursor is lacking. It is therefore concluded that the initial melt for granitoids formed by partial melting of the mantle material.

(v) High Cr concentrations and $Mg^{\#}$ in the initial shoshonitic sample are indicative of a mantle origin. This interpretation is also supported by high $\varepsilon Nd_T$. Compositions of primary basaltic magmas range in MgO and Ni concentration from 11-13% (Hart and Davis, 1978) and 235-390 ppm respectively (Sato, 1977). It is possible to produce primary magmas with MgO less than 11%, Ni <100 ppm and greater than 50% $SiO_2$ through hydrous melting of mantle peridotite (Hart and Davis, 1978). The initial shoshonitic LSIC melt is weakly quartz normative (<5%), which suggests they represent hydrous partial melt products of mantle peridotite (Green, 1976). Equilibrium olivine compositions calculated from an initial shoshonitic sample $FeO^T/MgO$ ratio of 0.84 and a mantle olivine $FeO^T/MgO$ D of 0.3 ± 0.03 (Roeder and Emslie, 1970) indicate equilibration with an olivine composition of $Fo_{84}$ - $Fo_{87}$ or $Mg^{\#}$ 86-89. Peridotite olivines range from $Mg^{\#}$=86 to 94 (Hess, 1989) although compositions between $Mg^{\#}$ ~88 - 91 are usually observed. These data suggest that the initial shoshonite sample probably best represents a primary mantle derived magma that has experienced negligible olivine removal. The majority of the non-saccharoidal

granitoids with compositions below 58 wt.% $SiO_2$ are shoshonitic (Figure 23) indicating that the initial melts for the LSIC granitoids were probably shoshonitic in composition, not calc-alkaline.

The mantle source was undoubtedly metasomatised as is evident by the high LILE/HFSE ratios and $La/Yb_{CN}$ in conjunction with high $\varepsilon Nd_T$. The moderate HREE slope may suggest that derivation of the shoshonitic granitoid melt involved a source with residual garnet. High LILE/HFSE, high LREE/HREE, negative HFSE anomalies, low Ce/Pb (à la Chauvel et al, 1995) suggest the source was similar to an arc-type mantle source and inconsistent with OIB and MORB type sources. Low Nb/Nb*, Y/Zr, and $TiO_2/Al_2O_3$ (à la Muller et al, 1992) confirm that the source was dissimilar from OIB. High $Ce/P_2O_5$ vs. $Zr/TiO_2$, characteristic of shoshonitic rocks occuring in modern continental arcs (Muller et al, 1992), suggest that the environment of emplacement may have been a continental arc.

### 8.1.2 Estimate of Depth of Initial Granitoid Melt Derivation

The pressure of derivation of the various phases of LSIC has been investigated with the aid of the $Al_2O_3$ vs. $CaO/Al_2O_3$ peridotite melt compositional pressure dependency relationship of Herzberg (1995). The $Al_2O_3$ and $CaO/Al_2O_3$ of a mantle melt is a function of pressure dependent stability of garnet relative to other peridotite minerals since this mineral controls Al at pressures higher than ~20 kbar. (2 GPa). Pressure increases the stability of garnet resulting in mantle melts that decline in $Al_2O_3$ concentration with increasing pressure (Herzberg, 1995). Herzberg (1995) has used the pressure dependent melting behavior of garnet in relation to other peridotite minerals to produce a pressure - composition diagram

# Relationship Between Non-Saccharoidal Shoshonitic and Calc-Alkaline Granitoids

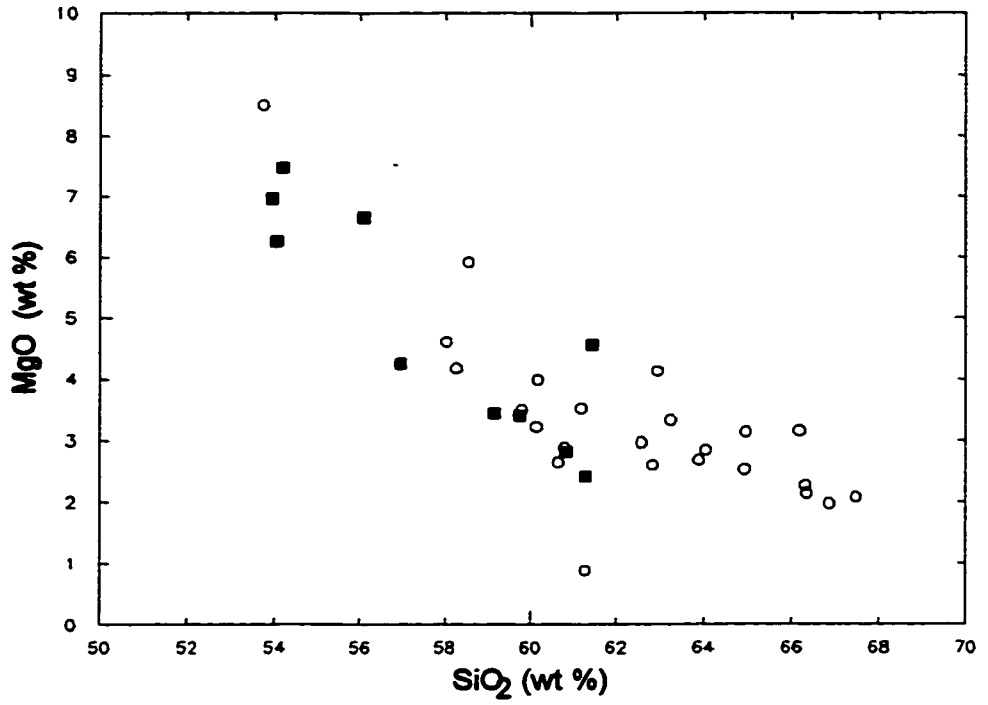


■ Shoshonitic Series Non-Saccharoidal Granitoids
○ Medium to High-K Calc-Alkaline Non-Saccharoidal Granitoids

**Figure 23. Granitoid samples with less than 58 wt.% silica and high in MgO dominantly display shoshonitic affinities. This suggests that primary melts for the granitoids were probably shoshonitic in composition.**

based upon the melting behavior of garnet peridotite. At pressures of ~2-4 GPa, partial melts will be high in $Al_2O_3$ and low in $CaO/Al_2O_3$ reflecting the higher stability of clinopyroxene relative to garnet. At pressures greater than 4 GPa, garnet is stable relative to clinopyroxene therefore partial melts are lower in $Al_2O_3$ and $CaO/Al_2O_3$. The peridotite solidus is marked for the pressure at which the $Al_2O_3$ content and $CaO/Al_2O_3$ coincides with that obtained from peridotite melting experiments at various pressures (see Herzberg (1995), and references therein). Peridotite solidus and liquidus positions are based upon anhydrous melting conditions. It is probable that the melting conditions which formed the LSIC granitoids was hydrous which should depress the liquidus. Pressures therefore may represent maximums since the peridotite melt field should shift to lower $Al_2O_3$, although the absolute effects are unknown. The $Al_2O_3$ and $CaO/Al_2O_3$ concentrations of the granitoids are plotted in relation to the peridotite solidus - liquidus field in order to estimate their primary nature and pressure of derivation.

The granitoid data lie to the left of the peridotite melt field in terms of $Al_2O_3$ and $CaO/Al_2O_3$ (Figure 24) indicating that LSIC granitoids are not truly representative of primary mantle melts (unless the source had possessed low $CaO/Al_2O_3$) and have probably experienced a prior history of fractionation. The least evolved LSIC granitoids plot on the critical plane on an R1-R2 diagram. Peridotite compositions essentially plot on the critical plane of silica saturation (De La Roche, 1980), therefore fractionated melts derived from peridotite lying on the critical plane are likely produced by removal of minerals which plot on the critical plane. This suggests that the most likely earliest fractionating minerals were olivine, clinopyroxene, or hornblende. Hornblende is discounted since the initial water concentrations were not high

# Estimation of the Depth of the Mantle Source for the Initial Granitoid Melts

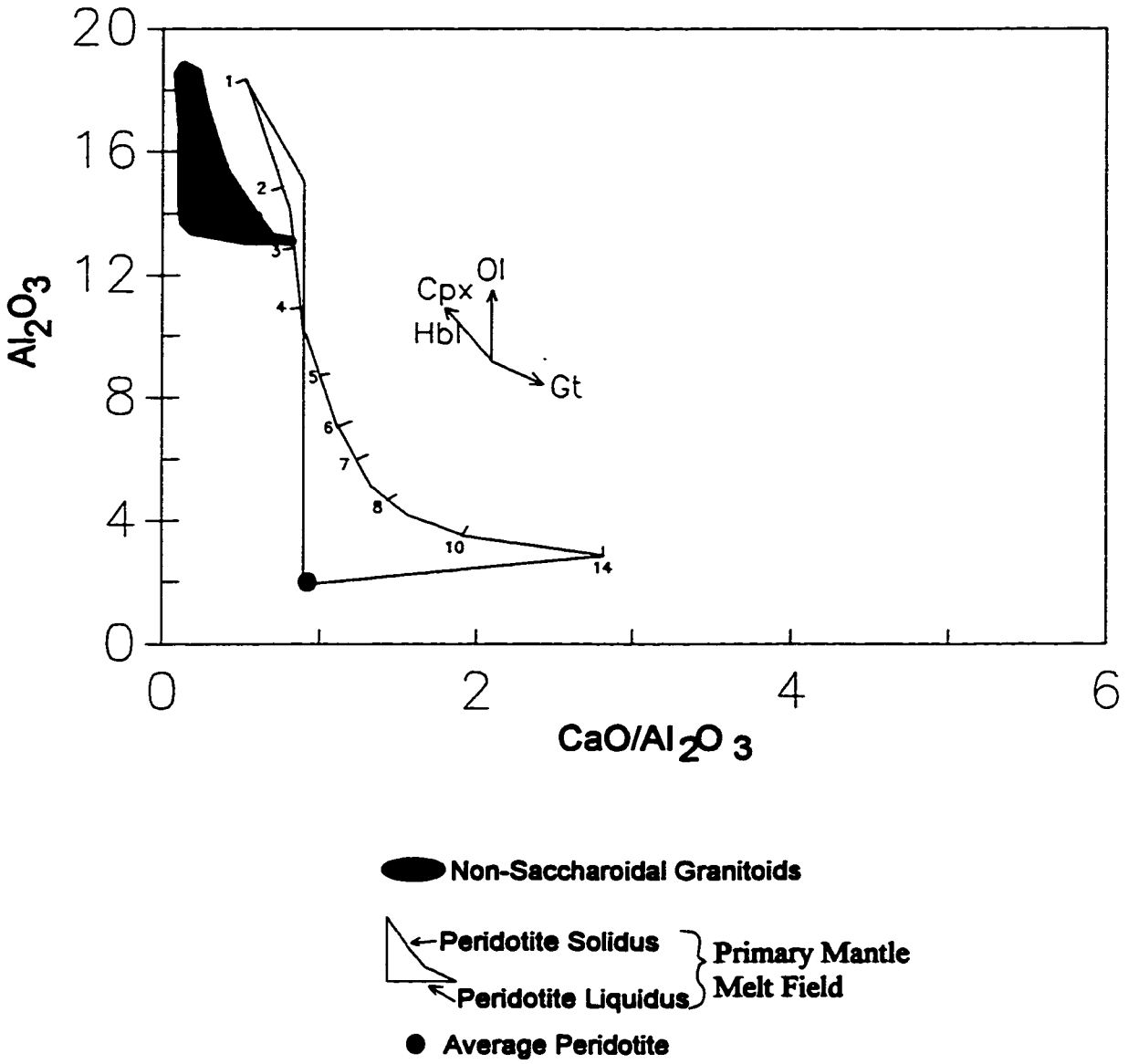


Figure 24. Non-saccharoidal granitoids of the LSIC compared to the pressure dependent peridotite melt field of Herzberg (1995). Fractionation vectors are approximate and represent the evolutionary direction of the liquid by removal of the specified mineral phase. The peridotite solidus is marked off in gigapascals for the pressure at which a primary mantle melt with the specified CaO and $Al_2O_3$ exists.

enough to stabilize this mineral. The low Ni contents of the granitoids indicate they may have suffered an early episode of olivine fractionation, although no samples contain olivine and the low Ni may only reflect low proportions of olivine entering the initial granitoid melt. Additionally, olivine removal results in near vertical evolution of the liquid on a plot of this type since olivine does not appreciably partition CaO or $Al_2O_3$ and removal increases the concentration of $Al_2O_3$ in the liquid. Granitoid samples cannot be displaced from the peridotite melt field by olivine fractionation alone since vertical evolution would not intersect the mantle melt field. The early crystallization of clinopyroxene is well documented in the LSIC and removal of this mineral likely has resulted in the low $CaO/Al_2O_3$ relative to $Al_2O_3$ in these samples. The granitoids form a trend which can be projected back to a source pressure of derivation for the initial melt of approximately 3 GPa. This is consistent with $La/Yb_{CN}$ indicating that the granitoids were derived from a source in which garnet remained in the residue.

The proportion of octahedrally coordinated Al in clinopyroxene increases with increasing pressure (Aoki and Kushiro, 1968; Aoki and Shiba, 1973) and Ti/Al tends to decrease with increasing pressure (Cundari and Ferguson, 1982). Low $Ti/Al^{tot}_{p.f.u}$ (0.1-0.3) and high $Al^{VI}/Al^{IV}$ ratios recorded in the pyroxenes are indicative of a high pressure origin. The $Ti/Al^{tot}$ ratios indicate pressures in the range of 20-30+ kbar., equivalent to the depth estimate from whole rock $CaO/Al_2O_3$ and $Al_2O_3$ relations but should be treated with caution since determination of this coarse barometer is based upon experiments utilizing $SiO_2$ undersaturated samples (Lloyd, 1981) and increased $aSiO_2$ has been shown to lead to a

reduction in Al and Ti in pyroxene (Alok et al, 1973), a condition which may be valid for the LSIC pyroxene crystallization conditions.

This method of Herzberg (1995) for source pressure estimation was tested with the shoshonitic volcanic rock data of Brooks et al (1982) as a check of consistency of the applicability of the model to other similar alkaline rocks. The data of Brooks et al (1982) was chosen since they found $^{87}Sr/^{86}Sr_I$ (0.700395 - 0.701994) and $Tb/Yb_{CN}$ (~1) suggesting derivation from a garnet free mantle source with negligible crustal involvement. Their data define an array originating on a projection of the peridotite solidus at <1 GPa and trending towards low $Al_2O_3$ and low $CaO/Al_2O_3$. This pressure estimate is lower than the stability of garnet and in accord with HREE observations. Plotting of the mafic samples of the shoshonite series on a projection of the peridotite solidus is consistent with $^{87}Sr/^{86}Sr_I$ results suggesting a mantle origin. The trend of the data away from the mantle melt field is opposite that observed for the LSIC granitoids. In the Oxford Lake samples, $Al_2O_3$ and $CaO/Al_2O_3$ decrease with increasing $SiO_2$, indicative of fractionation of an aluminous mineral. In the LSIC, $CaO/Al_2O_3$ decreases, but $Al_2O_3$ increases and remains nearly constant at $SiO_2$ concentrations above ~55%. At Oxford Lake, this variation is a product of plagioclase fractionation, possibly combined with biotite fractionation, since these minerals contain low $CaO/Al_2O_3$ and high $Al_2O_3$. Brooks et al (1982) propose that the lack of an Eu anomaly in the volcanic rocks indicate plagioclase did not fractionate, although, this is more likely a function of high $fO_2$. In view of these results, it is felt the $Al_2O_3$ - $CaO/Al_2O_3$ - pressure discrimination diagram of Herzberg (1995) is applicable to the LSIC granitoids and predicts the approximate depth at which derivation of the initial melts from the mantle source may have occurred.

### 8.1.3 Identification of Processes Controlling Granitoid Diversity

**Interpretation of Isotope Data**

The range of isotopic compositions obtained from mineral separates, and analytical uncertainties in the determination of Nd and Sr isotopic compositions of mineral separates do not allow for petrogenetic interpretations based upon linearity as expressed on plots of $\varepsilon Nd_T$ - $^{87}Sr/^{86}Sr_I$.

**Process Identification**

There are four main processes which may be invoked to explain the compositional variability expressed in the LSIC, i) partial melting, ii) fractional crystallization, iii) mixing, or iv) AFC.

i) Partial Melting: Due to analytical uncertainties and the narrow range in $\varepsilon Nd_T$ observed, it is not possible using mineral isotopic compositions alone to asses whether variable degrees of partial melting produced the range of rock compositions present in the LSIC. Different degrees of partial melting would produce melts with highly variable concentrations of incompatible elements and lesser variability in compatible element concentrations. Large variations in Cr and Ni in granitoids discount partial melting as being the cause of compositional variability at the LSIC unless the granitoids resulted from small percentages of partial melting.

ii) Fractional Crystallization: On a plot of $\varepsilon Nd_{T(mineral)}$ vs. $1/Nd_{(rock)}$, fractional crystallization will lead to data distributions that are parallel to the Nd concentration

axis (Figure 25). Analytical uncertainties do not allow for interpretaion based upon $\varepsilon Nd_T$ variability of the mineral separates. Variability in Nd concentration may be attributable to a number of processes.

iii) Mixing: Sample relationships based upon isotopic compositions cannot be used to infer possible mixing relationships. Other lines of evidence are required. Potential crustal contaminants (Compositions in Table 3) and their calculated mixing curves are plotted in relation to an initial LSIC non-saccharoidal granitoid sample to test simple mixing in terms of Cr - Sr - Zr (Figure 26). The trace element data distributions cannot be accounted for by simple mixing plausable crustal sources. A multicationic R1-R2 plot (De La Roche et al, 1980), which has been derived from a major element binary transposition of the normative tetrahedron of Yoder and Tilley (1962) has been utilized to interpret petrogenetic processes by a number of researchers (Leterrier and Maury, 1978; Pagel and Leterrier, 1980; Batchelor and Bowden, 1985; Leterrier, 1985) and can be used to test the relationship of the granitoid samples to possible contaminants.

On a plot of this type, mixing produces purely linear relationships between endmembers. The non-saccharoidal samples define a trend of $SiO_2$ enrichment accompanied by evolution away from the plane of critical silica saturation towards the Pontiac sedimentary rock field (Ujike, 1984; Feng et al, 1993), Belleterre - Fugerville tonalite, and Lac des Quinze gneiss samples (Figure 27). Variation in whole rock chemistry cannot be ascribed to contamination with Belleterre volcanic rocks since granitoids are displaced away from the volcanic rock. Simple mixing is not evident on

# εNd - 1/Nd Correlation Diagram for LSIC Mineral Separates

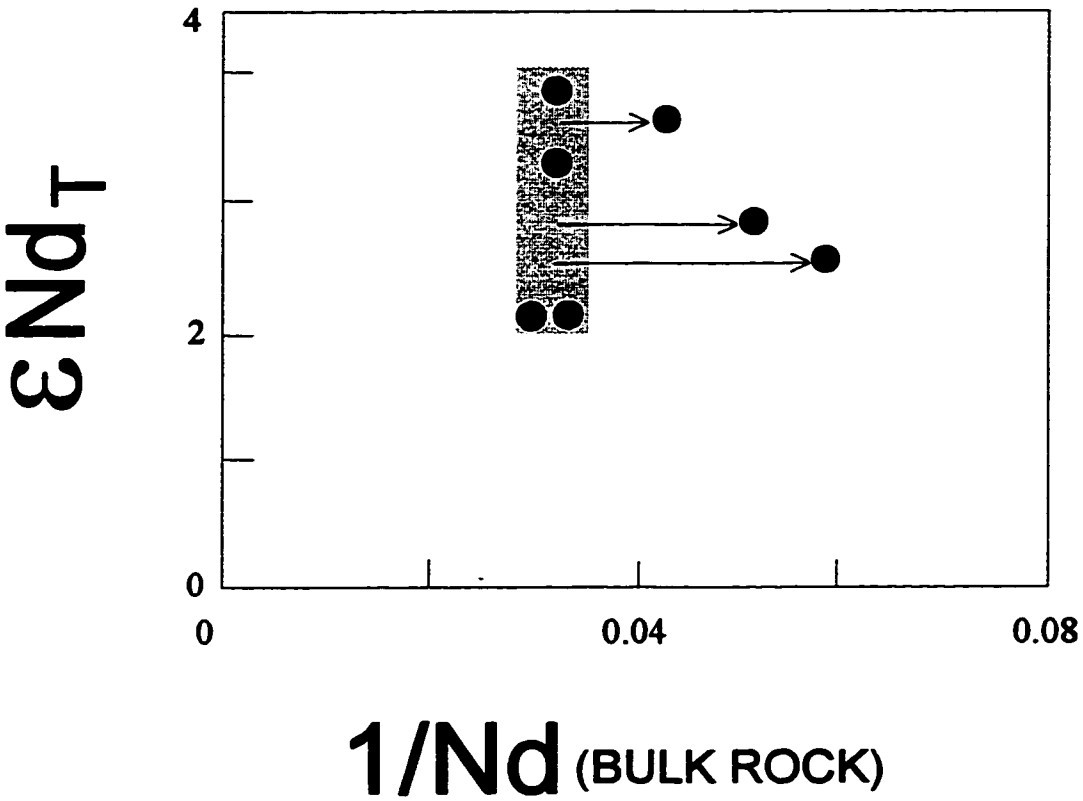


Interpreted Mantle source field

→ Interpreted Fractional crystallization vector

● LSIC Mineral Separate

**Figure 25. Variation in 1/Nd that may have occured if the data represents the product of fractional crystallization of melts which possessed initial Nd concentrations between 25-50 ppm.**

Table 3. Simple Mixing Endmember Compositions

| | Endmember | | | | |
|---|---|---|---|---|---|
| Element (ppm) | Lac des Quinze Gneiss[a] | Belleterre - Fugerville Tonalites[b] | Pontiac Meta-Sediment[c] | Belleterre Belt Basalt[d] | Average Archean Upper Crust[e] |
| Cr | 23 | 17 | 203 | 218 | 140 |
| Sr | 379 | 598 | 413 | 253 | 300 |
| Zr | 119 | 127 | 147 | 48 | 100 |

Data Sources:

a) Lac des Quinze gneiss (Feng et al, 1993; Sawyer and Barnes, 1994).

b) Belleterre - Fugerville tonalites (Feng et al, 1993; Sawyer and Barnes, 1994; This Study).

c) Pontiac sedimentary rocks (Ujike, 1984; Feng et al, 1993).

d) Belleterre belt basaltic rock (This Study).

e) Average Archean Upper Crust (Taylor and McClennan, 1985).

# Sr-Cr-Zr Simple Mixing Model

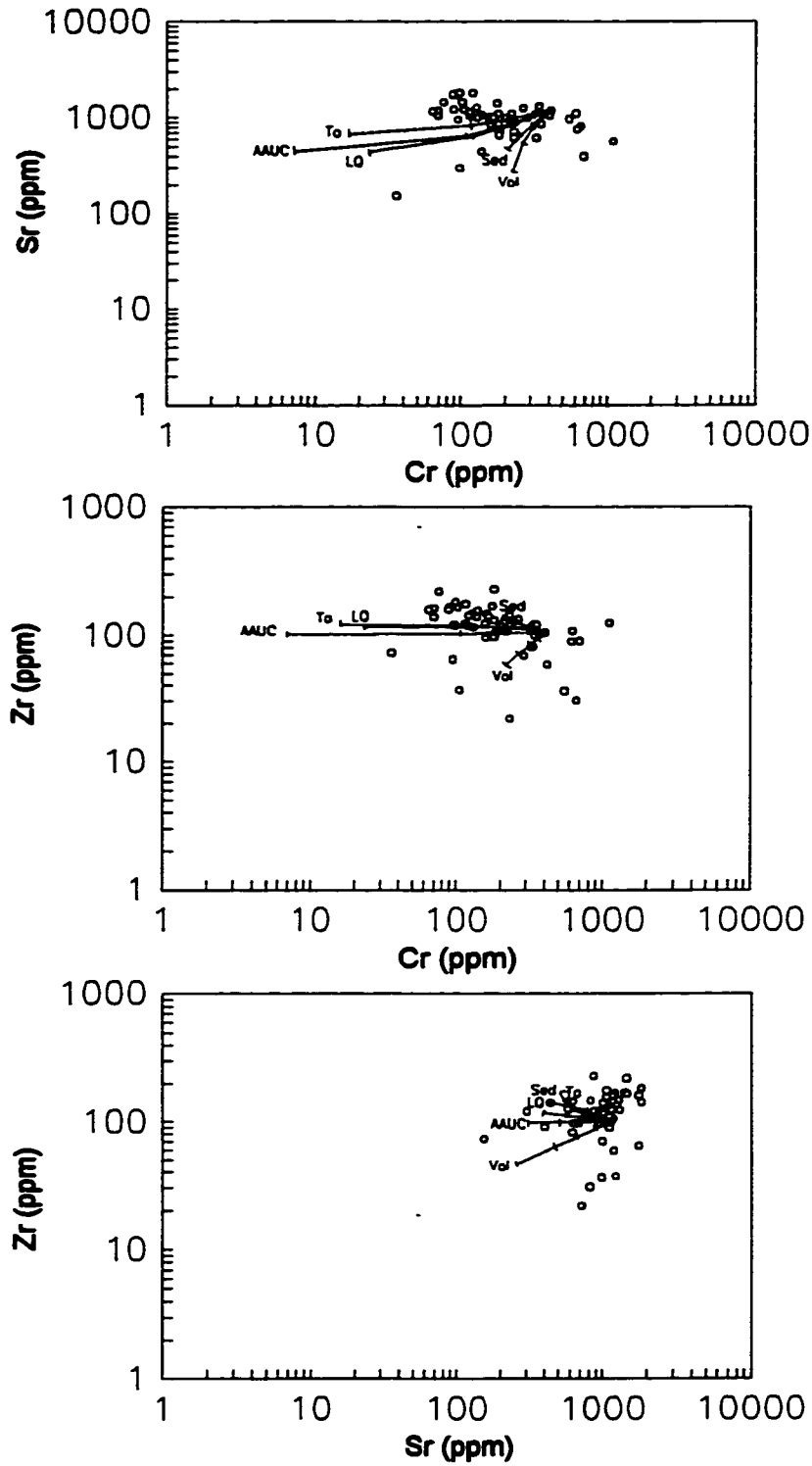


Figure 26. Mixing curves ticked at 25% intervals originating at shoshonite sample 930616-1. Belleterre belt rocks (Vol), Pontiac sedimentary rock (Sed), Lac des Quinze gneiss (LQ), Belleterre - Fugerville tonalite (To), and average Archean upper crust (AAUC) compositions are included in Table 3. Mixing between these crustal endmembers cannot explain the compositional variability of the non-saccharoidal granitoids.

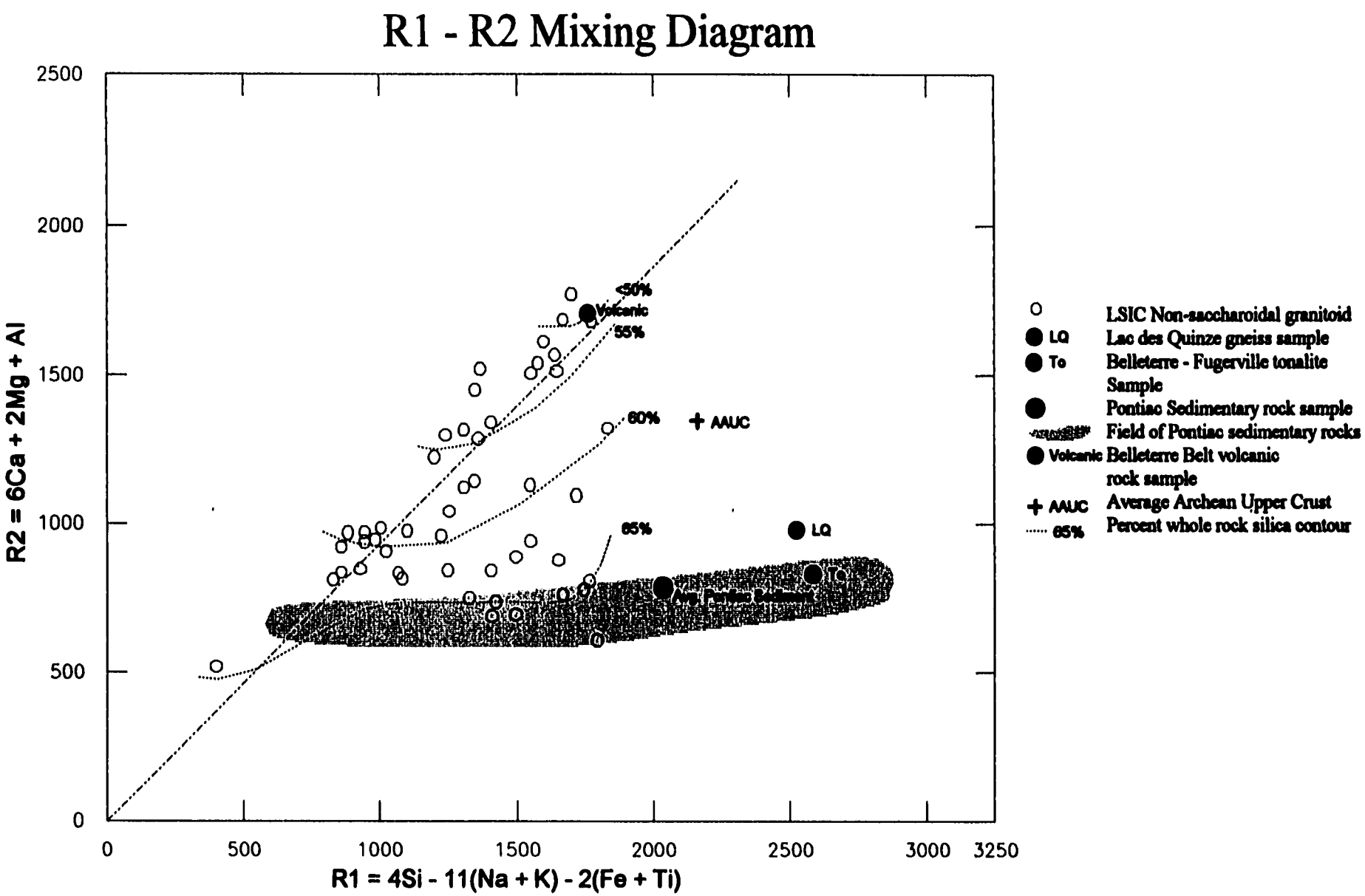


Figure 27. Possible crustal contaminants are included in this diagram. Variation in LSIC sample composition is incompatable with a simple mixing process, which would produce a linear data distribution unless the contaminant was heterogenous in composition. Pontiac metasedimentary rocks exhibit a wide compositional range and may represent plausable contaminants.

a plot of this type for the LSIC samples. A lack of readily apparent data linearity indicates either assimilation of a heterogenous contaminant occured, or the LSIC non-saccharoidal granitoids had a fractional crystallization origin, or originated through fractional crystallzation with assimilation of Pontiac Metasedimentary rock.

iv) Assimilation and Fractional Crystallization: Field evidence (schliern, gradation in modal abundance of mafic minerals, cumulate textured diorites) suggest that fractional crystallization had occurred in the LSIC units and simple mixing as a dominant process controlling overall chemical variation is unlikely. Mixing is one limiting case in theAFC equation (DePaolo, 1981), where the bulk D of the element of interest equals 1, therefore, AFC rather than mixing is a more plausible process occurring in the LSIC. Analytical uncertainties in the determination of mineral isotopic compositions, uncertainties in bulk D, variability in contaminant composition (as is the case for Pontiac Metasedimentary rocks), and variability in rate of assimilation to fractional crystallization does not facilitate AFC modelling.

Tonalitic and granodioritic enclaves are not observed throughout the LSIC and it is interpreted that assimilation of Belleterre - Fugerville tonalites and Lac des Quinze gneisses are minor. Xenoliths of Pontiac sedimentary rock are observed sporadically throughout the LSIC and considered a more likely assimilant. Large xenoliths of basalt are found near the far northern boundary of the north complex of the LSIC, well away from the volcanic - LSIC contact. The total REE concentration in the non-saccharoidal granitoids declines with increasing $SiO_2$. A divergent trend toward low total REE and low $SiO_2$ is compatible with mixing between a granitoid melt and either

a mafic enclave or Belleterre volcanic rock composition. The majority of the samples defining this trend are near the southern contact of the north complex, one of which is within approximately 100 m of the contact with the volcanic rocks. The most likely assimilant producing this trend is volcanic material. The assimilation of volcanic material in the LSIC is considered minor since other samples obtained near the Belleterre belt - LSIC contact do not show evidence of contamination.

Significant variation in Cr, which is negatively correlated with $SiO_2$, Zr, K, and Rb occurs in the LSIC rocks. Fractional crystallization commonly leads to a large variation in compatible element abundances over a small range of incompatible element concentrations and produces linear variations on log-log plots for elements of widely differing igneous compatibility (Cocherie, 1986). Trace and major element relations indicate fractional crystallization is dominant over assimilation in producing the major and trace element compositional variability present in the LSIC granitoids.

### 8.1.4 Evolution of the Granitoid Magma by Fractional Crystallization

Granitoids evolve towards peralkaline compositions and increase in peraluminosity with increasing whole rock $SiO_2$ concentration (Figure 28). This variation does not represent a mixing relationship with any crustal material. This trend is the result of crystal fractionation which is marked by decreasing CaO and near constant $Al_2O_3$ at $SiO_2$ concentrations greater than 55% which increases peraluminosity whereas increasing $Na_2O$ and $K_2O$ increase peralkalinity. A decrease in $CaO/Al_2O_3$ with increasing $SiO_2$ suggests fractional crystallization of a high Ca, low Al mineral such as clinopyroxene and amphibole, removal of which would

# Alkali - Alumina Relationship for Non-Saccharoidal Granitoids

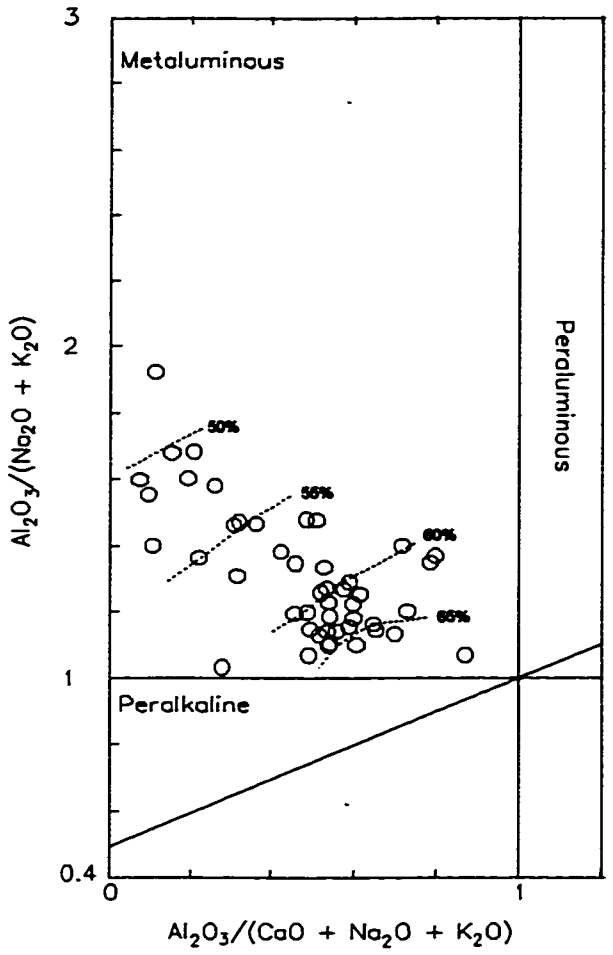


Figure 28. Non-saccharoidal granitoid samples increase in peralkalinity and peraluminosity with increasing whole rock silica. Numbers depicted on the contours represent bulk rock $SiO_2$ in wt.%

lead to increasing peraluminosity. If fractionation were dominated by clinopyroxene and amphibole, an Fe enrichment trend should be produced since both of these minerals have $Mg^{\#}$ greater than the rock from which they crystallize. A strong Fe depletion trend is observed, and is consistent over the range in silica concentration of the granitoids, suggesting that magnetite was an early liquidus phase. A positive correlation between $Na_2O/K_2O$ and $SiO_2$, and inverse relationships between $Na_2O/K_2O$ vs. Rb and $Na_2O/K_2O$ vs. Ba suggests that biotite is also crystallizing. An inverse relationship between Cr, MgO and $SiO_2$ is produced by amphibole, biotite, magnetite and clinopyroxene crystallization.

Plagioclase fractionation should lead to an increase in $CaO/Al_2O_3$, this is not observed and it is assumed that plagioclase fractionation is minor. Enrichment in Sr/Sr* partially supports this interpretation. A negative Eu anomaly is produced in rocks with low total REE. Total REE is negatively correlated with $SiO_2$ and the negative Eu/Eu* vs. ΣREE relationship (Figure 29) is probably the product of minor plagioclase fractionation. Decreasing $SiO_2$ with increasing $TiO_2$, and $P_2O_5$ and positive correlations between total REE and $TiO_2$ and $P_2O_5$ indicate that apatite and titanite were also removed from the melt.

A chondrite normalised extended element plot comparing a primitive and evolved granitoid samples can be used to show the compositional changes which occur during differentiation (Figure 30). The REE and Ba decline with fractionation and positive Zr and Sr anomalies are produced as a result of a lack of removal of zircon and plagioclase.

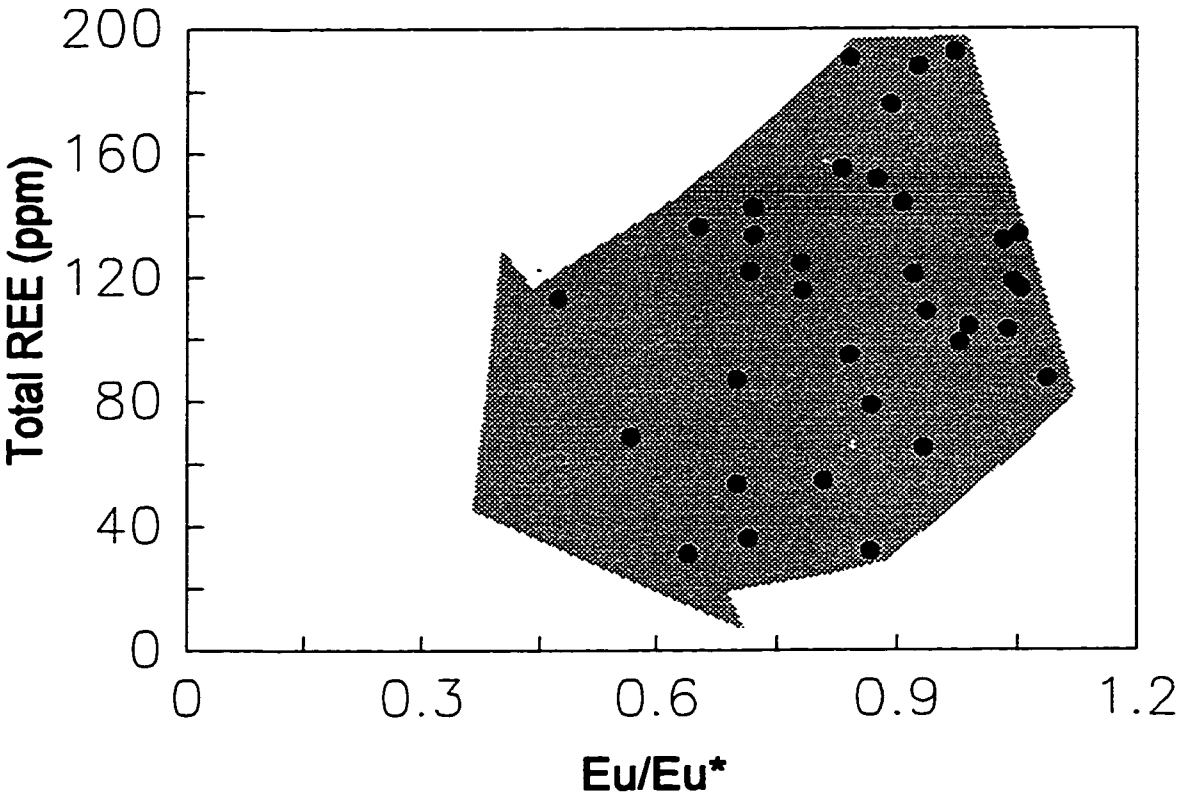


Figure 29. Total REE vs. magnitude of the Eu anomaly for non-saccharoidal granitoids. A wide range in Total REE that decreases from Eu/Eu* ~1 towards an increasingly negative Eu anomaly is observed.

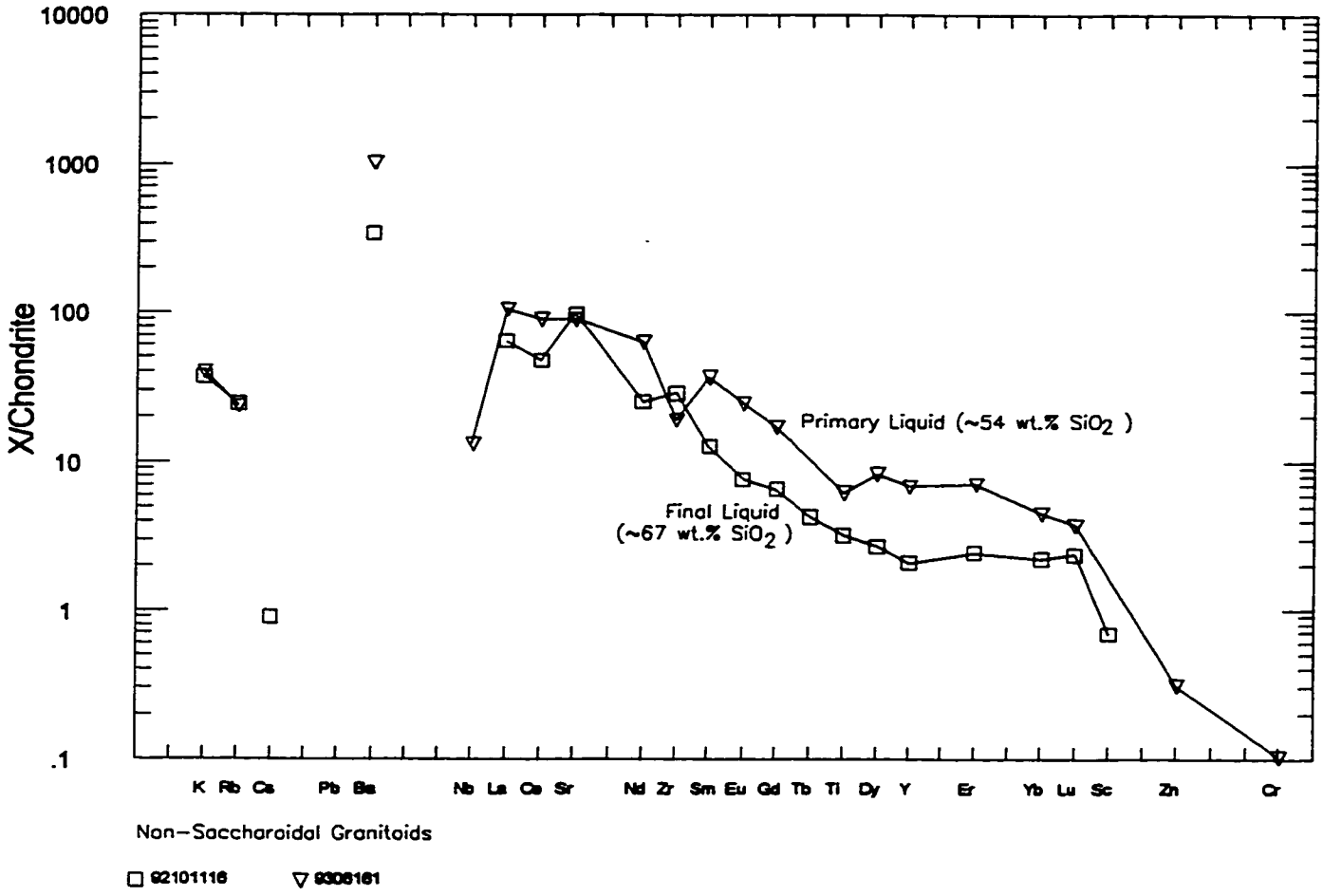


**Figure 30. Extended element plot comparing primary and evolved liquid compositions. Changes in chondrite normalized elemental abundances are produced primarily through crystal fractionation.**

## Crystallization Modelling

### Selection of Partition Coefficients

Partition coefficients have been compiled from numerous sources and are presented in Table 4. These include values from natural calc-alkaline basaltic andesites ($D_{Cr}^{Cpx}$), synthetic intermediate compositions ($D_{Zr}^{Cpx}$), natural alkali basalt ($D_{Cr}^{Zrn}$, $D_{Zr}^{Zrn}$, $D_{Cr}^{Ap}$, $D_{Sr}^{Ap}$, $D_{Sr}^{Cpx}$), natural shoshonites ($D_{Zr}^{Mag}$, $D_{Cr}^{Mag}$, $D_{Sr}^{Mag}$, $D_{Sr}^{Pl}$), natural basalts ($D_{Cr}^{Ap}$), synthetic granite ($D_{Sr}^{Ap}$), natural augite - hypersthene andesite ($D_{Zr}^{Ap}$, $D_{Zr}^{Pl}$), natural hornblende - biotite dacite ($D_{Zr}^{Bt}$, $D_{Sr}^{Bt}$), Crater Lake, Oregon dacite ($D_{Sr}^{Hbl}$, $D_{Zr}^{Hbl}$, $D_{Cr}^{Hbl}$), natural low silica rhyolite ($D_{Cr}^{Bt}$, $D_{Sr}^{Kfs}$), and natural alkali intermediate to high $SiO_2$ rocks ($D_{Zr}^{Kfs}$, $D_{Cr}^{Kfs}$, $D_{Zr}^{Zrn}$). The value of D for a specific mineral and element may be a function of liquid composition, $fO_2$ (may influence partitioning for magnetite and apatite), crystal composition (wollastonite content of pyroxene and anorthite content of plagioclase influence Zr and Sr partitioning, respectively), temperature and pressure. The quality of the D data is also method dependent. Partition coefficients determined from bulk mineral separates suffer from spurious D values resulting from inclusions of minor phases (i.e. Michael, 1988) such as (titanite, magnetite, allanite, monazite and zircon). In situ microbeam analysis overcomes this problem of contamination. Partition coefficients have been selected from available D values obtained from rock compositions best representing the LSIC granitoid compositions. Some D values of Francalanci (1989) and Irving and Frey (1984) have been utilised as a result of the data scarcity even though their D values have been determined from bulk mineral analysis and may suffer from the aforementioned contamination problems, or possible disequilibrium effects.

Table 4. Mineral - Melt Partition Coefficients (D) Applicable to the LSIC.

| | Partition Coefficient[♦] | | |
|---|---|---|---|
| Mineral | $D_{Cr}$ | $D_{Zr}$ | $D_{Sr}$ |
| Hornblende | 21[j] | 0.34[j] | 0.49[j] |
| Clinopyroxene | 40[a] | 0.27[h,c] | 0.1283[l] |
| Biotite | 8.3[d] | 0.59[k] | 0.31[k] |
| Magnetite | 14[c] | 0.45[c] | 0.15[c] |
| Apatite | 0.048[f] | 0.636[g] | 2.1[e] |
| Plagioclase | 0.43[c] | 0.15[m] | 2.23[c] |
| Zircon | 0.12[f] | 1500[b] | 0 |
| K-Feldspar | 0.01[i] | 0.17[b] | 4.5[d] |

a) Dostal et al (1983)
b) Lemarchand et al (1987)
c) Francalanci (1989)
d) Nash and Creecraft (1985)
e) Watson and Green (1981)
f) Irving and Frey (1984)
g) Fujimaki (1986)
h) Watson and Ryerson (1986)
i) Philpotts and Schnetzler (1970)
j) Sisson (1994)
k) D value from sample 63 in Ewart and Griffin (1994)
l) Hart and Dunn (1993)
m) D value from sample 23876 in Ewart and Griffin (1994)
♦ Terminology after Beattie et al (1993).

**Clinopyroxene**

Francalanci (1989) found $D_{Cr}^{Cpx}$ of 34 in calc-alkaline rocks, and $D_{Cr}^{Cpx}$ of 52-80 in shoshonitic rocks. The high $D_{Cr}^{Cpx}$ of 80 may represent disequilibrium (Francalanci, 1989), therefore the $D_{Cr}^{Cpx}$ of Dostal et al (1983) is probably applicable to the LSIC given the roughly intermediate value to that observed by Francalanci (1989). Sisson et al (1991) found $D_{Zr}^{Cpx}$ of 0.2-0.33 in rhyolites and concluded on comparison with the data of Watson and Ryerson (1986) that $D_{Zr}^{Cpx}$ does not vary significantly between intermediate and silicic rocks. The $D_{Zr}^{Cpx} = 0.27$ used (Watson and Ryerson, 1986) is similar to that observed in shoshonitic rocks (0.19-0.26), and associated calc-alkaline rocks (0.27; Francalanci, 1989), Aleutian andesites (0.291; Forsythe et al, 1994) and intermediate rocks in general (0.25; Pearce and Norry, 1979. 0.23 - 1.02; Mahood and Stimac, 1990. Lemarchand et al, 1987). Forsythe et al (1994) noted that $D_{Zr}^{Cpx}$ increases with the wollastonite content of clinopyroxene. The wollastonite content of LSIC clinopyroxenes does not vary appreciably so little change in $D_{Zr}^{Cpx}$ is expected as a result of clinopyroxene compositional variations. The $D_{Sr}^{Cpx}$ of Hart and Dunn (1993) is within the range of the $D_{Sr}^{Cpx}$ of 0.11 and 0.2 in shoshonitic rocks (Francalanci, 1989) and slightly higher than the $D_{Sr}^{Cpx} = 0.082$ in associated calc-alkaline rocks (Francalanci, 1989). This value is also similar to $D_{Sr}^{Cpx}$ in basalts (0.1; Irving and Frey, 1984) and within the broad range exhibited by alkaline series rocks in general (Lemarchand et al, 1987).

**Hornblende**

The $D_{Sr}^{Hbl}$ of Sisson (1994) is similar to the value of 0.48 obtained by Dostal et al (1983) for a low K basaltic andesite and also hematite - magnetite $fO_2$ buffered andesitic $D_{Sr}^{Hbl}$

of Green and Pearson (1986), but slightly higher than the values, 0.32 - 0.38, obtained in the fluorine free andesite experiments of Adam et al (1993). This value also lies within the range observed for alkali-basalts (Irving and Frey, 1984). $D_{Sr}^{Hbl}$ has been shown to increase slightly with increasing $SiO_2$ (Sisson, 1994) and therefore this D value may represent an upper limit given the higher $SiO_2$ concentration of the rocks which the $D_{Sr}^{Hbl}$ was derived relative to the LSIC granitoids. $D_{Zr}^{Hbl}$ has been obtained from the same sample as $D_{Sr}^{Hbl}$ and is similar to the values, 0.29 - 0.41, obtained in the fluorine free andesite experiments of Adam et al (1993). $D_{Cr}^{Hbl}$ is variable between 16 to 26 in the dacite of Sisson (1994). The $D_{Cr}^{Hbl}$ appears to increase with increasing $SiO_2$ and is higher than low-K basaltic andesites ($D_{Cr}^{Hbl}$ = 12.5; Dostal et al, 1983) and basaltic andesite of Sisson.(1994). The intermediate $D_{Cr}^{Hbl}$ of Sisson (1994) was selected, although this may represent a slight overestimate in $D_{Cr}^{Hbl}$ given the moderately higher $SiO_2$ of the dacite relative to the average granitoids of the LSIC.

**Magnetite**

$D_{Cr}^{Mag}$ was obtained from a shoshonite sample Ti-magnetite of Francalanci (1989). $D_{Cr}^{Mag}$ is typically highly variable (Lemarchand et al, 1987) with D as high as 164 in silicic rocks (Nash and Creecraft, 1985) and 50 - 153 in intermediate rocks (Leeman et al, 1978; Dostal et al, 1983). Leeman et al (1978) suggest that their $D_{Cr}^{Mag}$ probably represents maximum values due to their methods of estimating $D^{Mag}$, therefore an applicable $D_{Cr}^{Mag}$ is likely <50. The $D_{Cr}^{Mag}$ of Francalanci (1989) represents the most suitable $D_{Cr}^{Mag}$ approximation given the compositional similarities of the host rock samples. The $D_{Zr}^{Mag}$ was chosen from a shoshonite sample of Francalanci (1989). This value is within the range of the alkaline series (Lemarchand et al, 1987), slightly higher than partition coefficients (0.62-0.71)

observed in alkali basalts (Lemarchand et al, 1987) and the suggested $D_{Zr}^{Mag}$ of Pearce and Norry (1979) for intermediate rocks, and slightly lower than the $D_{Zr}^{Mag} = 0.38$ found in an andesite from Matupi, Papua New Guinea (Ewart and Griffin, 1994). Nielson et al (1995) found $D_{Zr}^{Mag}$ to be between 0.04 to 0.06 in Aleutian high Al andesite. This range of values is lower than the value used in this study, although they do note that the HFSE partitioning of magnetite is highly variable. They also note that $D_{Zr}^{Mag}$ varies inversely with magnetite alumina content. Nielson et al (1995) observed alumina contents of 3.7-4.0 wt.%, much higher than the 0-0.22 wt.% found in LSIC magnetites and therefore $D_{Zr}^{Mag}$ should be greater than the $D_{Zr}^{Mag}$ determined by Nielson et al (1995). $D_{Sr}^{Mag}$ has also been chosen from a shoshonite sample of Francalanci (1989). This value (0.15) is similar to the value of 0.11 found in an andesite from Matupi, Papua New Guinea (Ewart and Griffin, 1994).

**Apatite**

There are very few published $D^{Ap}$ values other than the REE. The $D_{Cr}^{Ap}$ of Irving and Frey (1984) from a nepheline Hawaiite and basinite were chosen as approximations to the partition coefficients applicable to the LSIC. The $D_{Zr}^{Ap}$ of Fujimaki (1986) was chosen due to the deficiency of data for this element in the Irving and Frey (1984) data set. Minor modelling errors may be introduced from the $D_{Cr}$ values since Irving and Frey (1984) observed that these phenocrysts were not in equilibrium with their host rocks. A $D_{Sr}^{Ap}$ of Watson and Green (1981) was selected for the LSIC granitoids. Watson and Green (1981) noticed that $D_{Sr}^{Ap}$ increased slightly from tholeiitic andesite to granitic compositions and that it is $H_2O$ and temperature independent. A low granite $D_{Sr}^{Ap}$ value was chosen under the assumption that the

weak compositional dependency of $D_{Sr}^{Ap}$ would lead to a true D value probably somewhere between that of a tholeiitic andesite (~1.35) and granite (~2.25).

**Plagioclase**

$D_{Cr}^{Pl}$ variability is high even within one compositional group of rocks (Lemarchand et al, 1987). Francalanci (1989) reports $D_{Cr}^{Pl}$ of 0.25 and 0.6 for two shoshonite samples. An average value of these two D values was chosen to approximate the plagioclase Cr partitioning effects in the LSIC. $D_{Sr}^{Pl}$ represents an average of two shoshonitic, and one calc-alkaline $D_{Sr}^{Pl}$ determinations (Francalanci, 1989). This value is slightly higher than the 1.67 of Dostal et al (1983) although $D_{Sr}^{Pl}$ can be quite variable with values as high as 33 in rhyolitic rocks (Nash and Creecraft, 1985). Blundy and Wood (1991) note that $D_{Sr}$ is controlled by the An content of plagioclase. Due to feldspar re-equilibration, the original An content of the feldspars is impossible to determine and an accurate comparison of LSIC plagioclase to compositions used to determine $D_{Sr}^{Pl}$ is not possible. Pressure and temperature variability is suggested to have little effect on $D_{Sr}^{Pl}$ (Blundy and Wood, 1991). The whole rock compositional similarity between the samples of Francalanci (1989) and the LSIC granitoids suggests that this $D_{Sr}^{Pl}$ value may represent the most viable estimate. $D_{Zr}^{Pl}$ was chosen from Ewart and Griffin (1994). This partition coefficient is within the range observed in rhyolites (Nash and Creecraft, 1985) and alkali volcanic rocks (Lemarchand et al, 1987) and higher than that of alkali basalts (Lemarchand et al, 1987).

**K-Feldspar**

Selection of appropriate D values for Cr, Zr, and Sr is hampered by the limited amount of data for $D^{Kfs}$. The majority of data is produced for dacite to rhyolite compositions,

probably reflecting the general rarity of K-feldspar in more mafic volcanic rocks. Nash and Creecraft (1985) found $D_{Zr}^{Kfs}$ of 0.01 to 0.04, which is comparable to $D_{Zr}^{Kfs}$ obtained by other researchers for the Bishop Tuff (Nash and Creecraft, 1985). $D_{Zr}^{Kfs}$ was selected from an average of benmoreite - trachyte samples of Lemarchand et al (1987) and is significantly higher than that obtained for rhyolitic rocks. The LSIC granitoids are equivalent to basaltic trachy-andesites to trachytes in terms of ($Na_2O+K_2O$) vs. $SiO_2$ (LeBas et al, 1986) therefore the $D_{Zr}^{Kfs}$ of Lemarchand et al (1987) probably is a more suitable $D_{Zr}^{Kfs}$ than that obtained from rhyolitic rocks. $D_{Cr}^{Kfs}$ is obtained from the data of Philpotts and Schnetzler (1970). Chromium is probably highly incompatible in K-feldspar so the D value of Philpotts and Schnetzler (1970) undoubtedly represents a suitable approximation. The $D_{Sr}^{Kfs}$ value has been obtained from a Twin Peaks rhyolite sample of Nash and Creecraft (1985) and represents the lowest $D_{Sr}^{Kfs}$ of the high silica rhyolites examined. Lower $D_{Sr}^{Kfs}$ are observed in dacitic rocks (3.9; sample AE-88. Ewart and Griffin, 1994) but $D_{Sr}^{Kfs}$ is quite variable and an approximation of $D_{Sr}^{Kfs}$ is difficult given the lack of data from rock compositions similar to the LSIC.

**Zircon**

Due to the limited number of published $D^{Zrn}$ values, $D_{Zr}^{Zrn}$ was chosen from an trachyte sample (Lemarchand et al, 1987) which probably represents a suitable approximation of $D_{Zr}^{Zrn}$ in the LSIC given the general compositional similarity. $D_{Cr}^{Zrn}$ was obtained from a basinite sample of Irving and Frey (1984) due to a lack of available D data. $D_{Sr}^{Zrn}$ could not be obtained and was arbitrarily set at 0 since it is assumed that Sr is highly incompatible in zircon.

**Biotite**

$D_{Zr}^{Bt}$ was obtained from a hornblende - biotite dacite from Papua New Guinea (Ewart and Griffin, 1994) which falls within the range of $D_{Zr}^{Bt}$ observed in alkaline rocks (Lemarchand et al, 1987; Green, 1994). The $D_{Zr}^{Bt}$ value chosen is lower than that found for rhyolitic rocks (Nash and Creecraft, 1985), but higher than that suggested by Pearce and Norry (1979) for intermediate rocks. The Pearce and Norry (1979) value represents an extrapolation from siliceous rock $D_{Zr}^{Bt}$ values and may be slightly erroneous. This $D_{Zr}^{Bt}$ represents the best estimate given the rarity of pertinent $D_{Zr}$ data for biotites. The $D_{Sr}^{Bt}$ coefficient falls within the observed range for alkaline rocks (Lemarchand et al, 1987) and high silica rocks (Nash and Creecraft, 1985). This $D_{Sr}^{Bio}$ value is roughly intermediate between the value of 0.21 found in alkali basalts (Irving and Frey, 1984) and the maximum $D_{Sr}^{Bt}$ of 0.53 observed in rhyolites (Nash and Creecraft, 1985). The $D_{Sr}^{Bt}$ chosen probably represents the best estimate of $D_{Sr}^{Bt}$ available for the LSIC. $D_{Cr}^{Bio}$ is highly variable within rocks of similar composition (Lemarchand et al, 1987. 0.06-0.3; Irving and Frey, 1984. 8.3-54; Nash and Creecraft, 1985) but appears to increase with whole rock $SiO_2$. The chosen partition coefficient represents a low value for silicic rocks but may still represent an overestimate.

**Titanite**

Titanite is considered to be an important fractionating mineral based upon the chemical variation exhibited by the LSIC granitoids. Chromium and Zr partition coefficients could not be obtained for this mineral. Chromium may substitute for Ti in titanite (Deer et al, 1962c) but $D_{Cr}^{Ttn}$ is uncertain. $D_{Zr}^{Ttn}$ may be >1 (?) given the observed Zr concentrations in titanites from carbonitites (Dawson et al, 1994) although this rock composition is not comparable to

the LSIC. Green and Pearson (1986) have determined $D_{Sr}^{Tn}$ in andesites and found Sr to be highly incompatible in titanite with $D_{Sr}^{Tn} \sim 0.2$. The $D_{Sr}^{Tn}$ is not compositionally dependent and little effect by P and T is observed although increasing $fO_2$ tends to increase $D_{Sr}^{Tn}$ (Green and Pearson, 1986). Due to deficiencies in D data for this mineral, titanite has not been included in the fractionation model.

**Application of the D Data to the LSIC Non-Saccharoidal Granitoids**

Equilibrium crystallization is considered unlikely given the compositional zoning present in some phenocrysts and the linear log-log Cr-Sr and Cr-Zr relationships, therefore the variation in Cr-Sr-Zr in the non-saccharoidal granitoids have been modelled according to the Rayleigh fractionation law defined as:

$$C_l^{el} = C_0^{el} * F^{(D-1)}$$

where $C_l^{el}$ is the trace element concentration in the liquid, $C_0^{el}$ is the trace element concentration in the initial liquid, F is the weight fraction of residual liquid, and D is the bulk partition coefficient.

**Sr - Cr Variation**

Strontium and Cr variation in bulk rocks (Figure 31a) suggests control by Fe-Mg silicates and magnetite. The fit of the Fe-Mg silicate vectors is improved if multiple, slightly compositionally differing initial melts were involved in generating the range of granitoids of the LSIC. Improved fit of the Fe-Mg silicate and magnetite vectors results if the initial melts contained slightly lower concentrations of Cr (~300+ ppm) and Sr (~700+ ppm) than the modelled initial granitoid melt. The degree of Sr enrichment in the bulk of the granitoids is

# Sr-Cr-Zr Fractional Crystallization Mineral Models

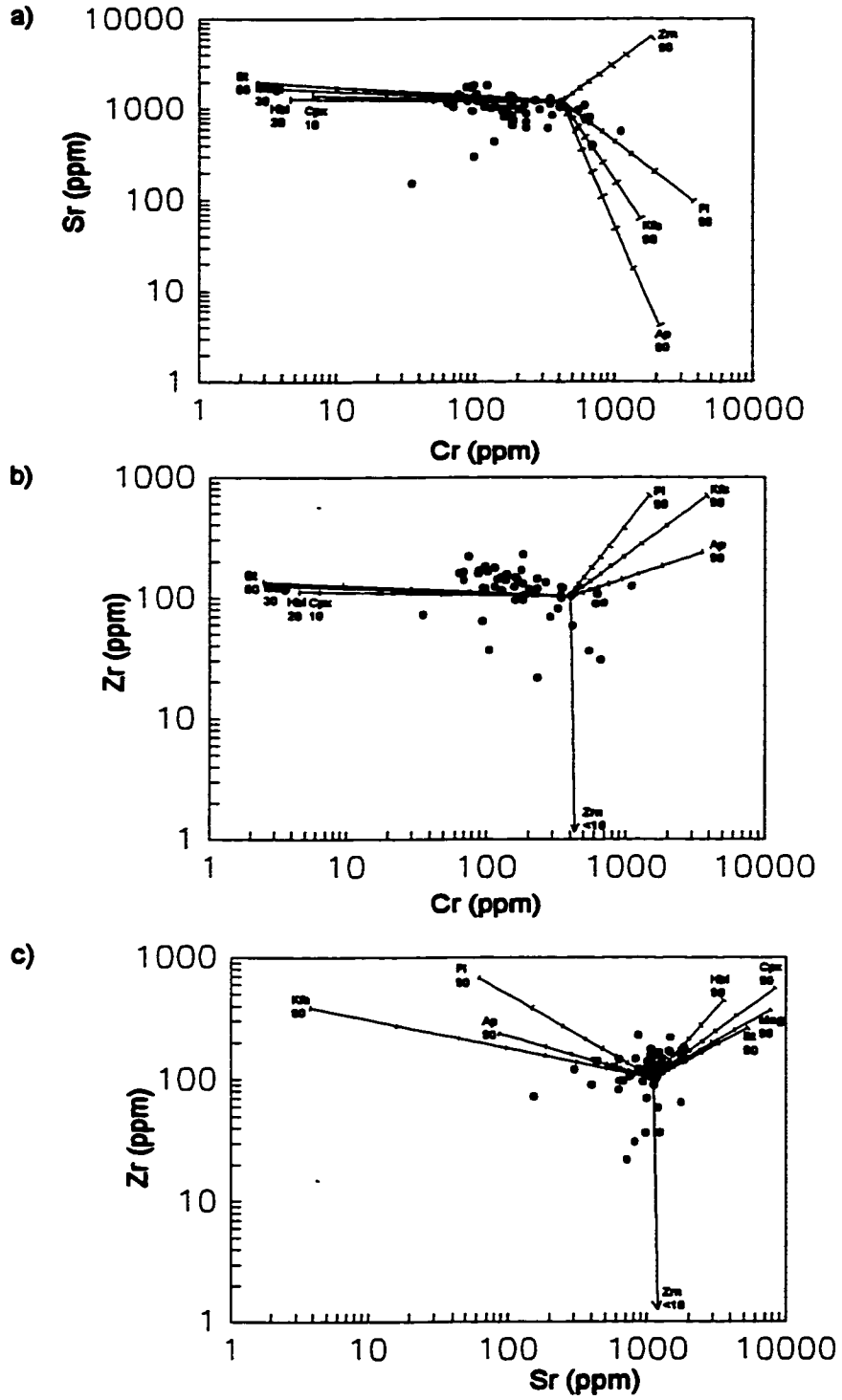


Figure 31. Mineral vectors ticked at 10% fractionation intervals with the maximum percent fractionation noted at the end of each vector. Solid circles are bulk compositions of non-saccharoidal granitoids. Plagioclase = Pl, zircon = Zrn, hornblende = Hbl, magnetite = Mag, clinopyroxene = Cpx, biotite = Bt, apatite = Ap, K-feldspar = Kfs (mineral abbreviations after Kretz, 1983). The granitoid data distribution indicates that fractionation of Fe-Mg mineral phases exerts a strong control on the compositional variability of the LSIC non-saccharoidal granitoids.

incompatible with Fe-Mg silicate and magnetite crystallization alone. The $D_{Sr}^{Hbl}$ and $D_{Sr}^{Bio}$ all may represent overestimates, as discussed in the selection of D values. Published $D_{Cr}$ is highly variable for the Fe-Mg silicates and if the $D_{Cr}$ represents overestimates, fit of the Fe-Mg silicate vectors to the granitoid data would be improved. Titanite has not been included in the model and the potential effects of this mineral should be considered given the observed fractionation of this mineral. The $D_{Sr}^{Tm}$ is low. If Cr is moderately compatible in titanite, fractionation of titanite combined with the Fe-Mg silicates could explain the bulk of the data distribution if there was slight compositional variation in the primary melts. The minor divergent array of samples towards low Cr and Sr suggests a larger influence of apatite or feldspar fractionation in these rocks.

**Zr-Cr Variation**

The granitoid data form a distribution that trends generally in the direction of the Fe-Mg silicate and magnetite fractionation vectors (Figure 31b). The fit of the Fe-Mg silicate vectors to the granitoid data cannot be improved significantly given the observed variability in biotite, hornblende, and clinopyroxene $D_{Zr}$ values obtained by various researchers. The granitoids form an array with higher Zr/Cr than the Fe-Mg silicate and magnetite partition coefficient ratios suggesting that either, or a combination of, apatite, K-feldspar, and plagioclase fractionation must be involved. The late crystallization of K-feldspar precludes its role in the fractionation process, especially at the lower $SiO_2$ concentrations of the primary granitoid melt(s). Apatite and plagioclase vector orientation suggest that apatite + Fe-Mg silicate + magnetite fractionation may exhibit a stronger control on Zr than plagioclase + Fe-Mg silicate + magnetite fractionation. Granitoid chemistry supports apatite fractionation.

While the involvement for significant plagioclase cannot be discounted from this plot, conclusive evidence from whole rock chemistry for plagioclase fractionation is not entirely recognised.

**Zr-Sr Variation**

The granitoid data does not form a distinct trend in terms of Zr - Sr (Figure 31c), although the data cluster that is developed can be resolved as the product of Fe-Mg silicate, and magnetite fractionation if initial granitoid melts are assumed to contain Sr ~700-1080 ppm, Cr ~300-410 ppm, and Zr ~90-110 ppm. Potential overestimates in $D_{Sr}$ for biotite and hornblende may also contribute to the poor fit also. Alternatively, addition of apatite and plagioclase to the fractionating assemblage could also approximate the granitoid samples in terms of Zr and Cr. More realistically, the granitoids probably result from a combination of initial melt compositional variability and apatite (± plagioclase) + Fe-Mg silicate + magnetite fractionation.

In summary, the granitoid data distribution indicates that Fe-Mg phases were the dominant fractionating minerals. The fit of the Fe-Mg silicate and magnetite vector to the granitoid data is improved if multiple, slightly compositionally differing initial melts were involved in the crystallization history of the LSIC. If it is assumed that the granitoids are a product of multiple initial melts and are the product of amphibole dominated fractionation, an approximation of the degree of fractionation required to produce the range of compositions is ~70% or less. Zircon is generally incompatible and it is enriched by ~60 % in the evolved granitoids relative to the least evolved granitoids. Assuming perfect incompatibility, a

partition coefficient of 0 provides 33 % as the minimum estimate of the extent of fractional crystallization required to achieve this enrichment.

**Evaluation of the Fractionation Modelling Results**

Modal mineralogy of the LSIC granitoids document a wide variation in the mafic mineral content, an increase in plagioclase at the expense of the mafic silicates, late increases in K-feldspar relative to plagioclase, and only a minor increase in quartz content (Figure 32). This is compatible with chemistry of the granitoids which suggests mafic silicate dominated fractionation and little evidence for feldspar fractionation. The modal Q - P - F plot for the LSIC define two trends, a slightly saturated trend subparallel to the P - F join and a quartz saturated trend originating from monzodioritic to monzonitic compositions (Figure. 8).

The slightly quartz saturated modal variation exhibited by the monzonitic series granitoids in general and is attributed to fractionation of silica rich minerals such as salitic pyroxenes (Giret et al, 1980). The removal of clinopyroxene, which is relatively high in $SiO_2$, limits the degree of silica saturation of the liquid and produces an evolutionary path essentially parallel to the P - F tie line on a modal Q - P - F plot. The fractionation of calcic amphibole (possibly in addition to magnetite and biotite) increases the $SiO_2$ content of the liquid and leads to increases in the normative quartz content of liquids (Bonin and Giret, 1984).

This can be shown graphically with the aid of the multicationic R1 - R2 plot of De La Roche et al (1980). The LSIC non-saccharoidal granitoid data, contoured for percent whole rock $SiO_2$, show an evolutionary path originating on the plane of critical silica saturation, evolving parallel to this plane with a deflection towards a high R1, low R2 coefficient

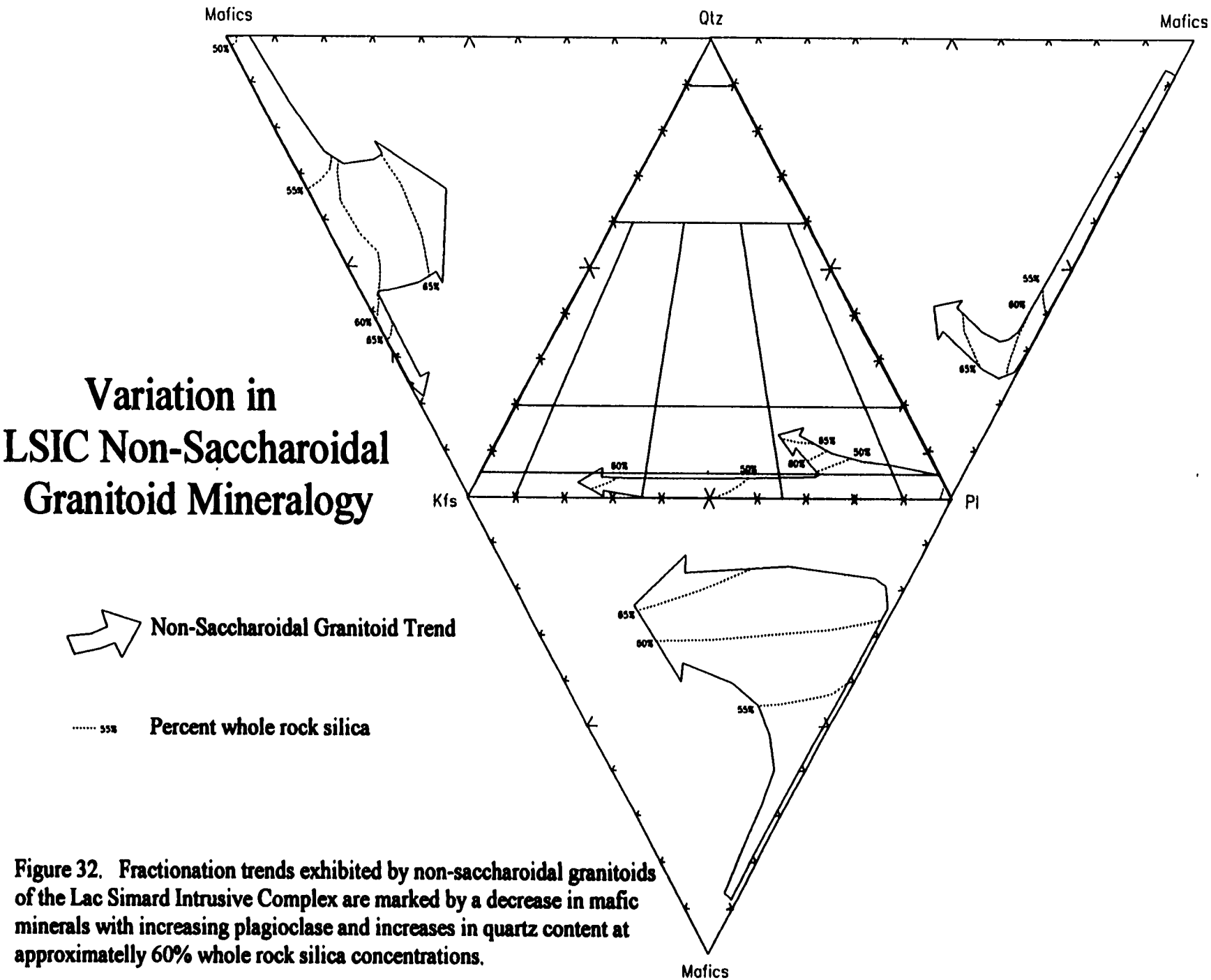


Figure 32. Fractionation trends exhibited by non-saccharoidal granitoids of the Lac Simard Intrusive Complex are marked by a decrease in mafic minerals with increasing plagioclase and increases in quartz content at approximatelly 60% whole rock silica concentrations.

(Figure 33). Mineral compositional data from the LSIC have been plotted on an R1 - R2 plot to illustrate the effects of fractional crystallization (Figure 33 inset). Fractionation of a mineral will cause the liquid composition to evolve linearly in the opposite direction of the mineral field. At silica concentrations lower than 55%, whole rock evolution is parallel to the plane of critical silica saturation and granitoid evolution is toward the albite - orthoclase field. This is in accord with petrographic observations which suggest that evolution of low $SiO_2$ granitoids is accompanied by an increase in modal plagioclase and a reduction in modal pyroxene and amphibole. Evolution along the critical plane involves removal of minerals which define the critical plane in the normative tetrahedron of Yoder and Tilley (1962) and therefore have compositions plotting on the critical silica saturation plane. The removal of clinopyroxene and amphibole is responsible for this evolution in the LSIC (Figure 33). At $SiO_2$ concentrations in excess of 55-60%, a number of rocks deviate from the plane of critical silica saturation and evolve toward the quartz pole. Removal of minerals which plot in the undersaturated portion of the R1 - R2 diagram are responsible for this variation, such as biotite, magnetite, apatite (not shown), and titanite (Figure 33). This change from clinopyroxene ± hornblende to biotite - hornblende dominated fractionation is also evident from the $SiO_2$ and $Al_2O_3$ relationship of non-saccharoidal granitoids (Figure 34). Increasing $Al_2O_3$ until 55% $SiO_2$ is the result of high Si, low Al clinopyroxene dominated fractionation whereas near constant $Al_2O_3$, as $SiO_2$ increases towards 70%, results from the removal of higher Al, Si deficient biotite and hornblende. Jakes and White (1972) found that hornblende typically occurs in calc-alkaline rocks with > ~55 wt.% $SiO_2$. This observation is compatible with fractionation style exhibited by the LSIC.

# R1 - R2 Crystal Fractionation Diagram

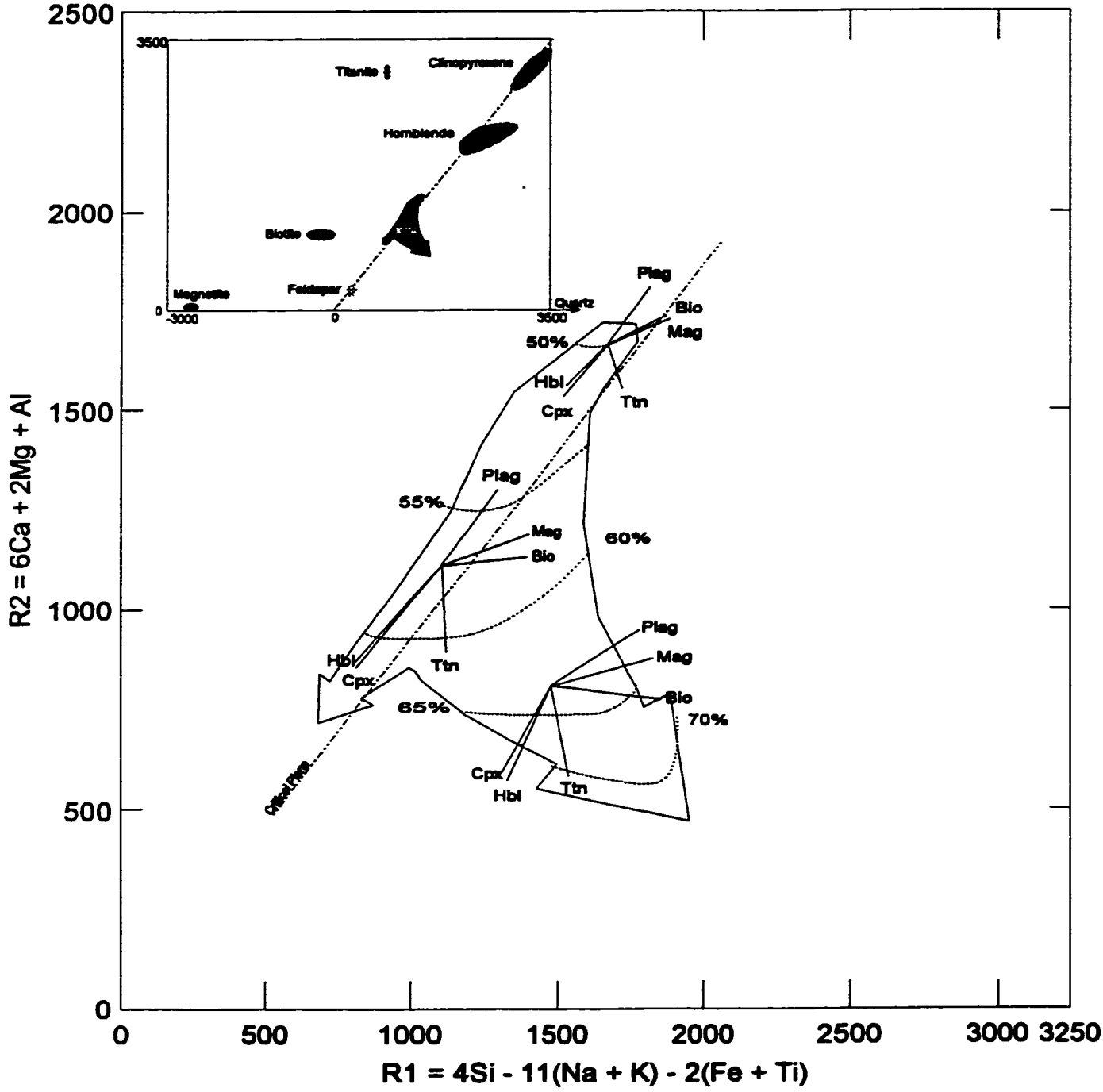


Figure 33. The effects of removal of various mineral phases one melts of various compositions is shown using multicationic parameters. Inset shows mineral fields and LSIC non-saccharoidal granitoid trend. Removal of a mineral phase causes melt composition to evolve in the direction of the mineral vector. The LSIC trend is contoured for percent whole rock silica.

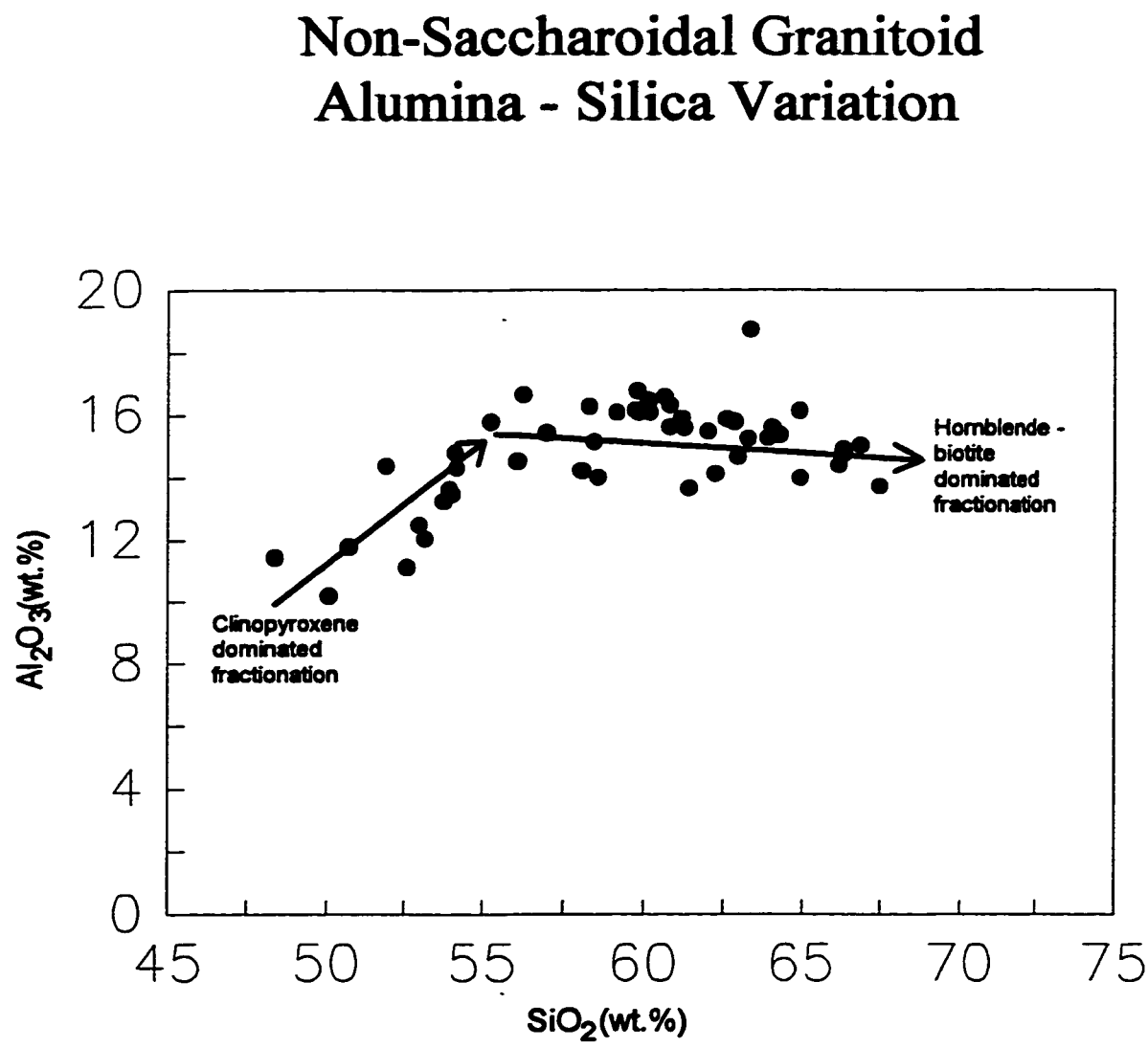


Figure 34. The effect of Cpx (+/- hornblende) dominated fractionation is evident by the steep increase in $Al_2O_3/SiO_2$ at silica concentrations lower than 55%. Above ~55% whole rock $SiO_2$, hornblende - biotite fractionation limits $Al_2O_3$ enrichment and lead to lower $Al_2O_3/SiO_2$ ratios.

The data does not suggest that all samples above ~55% $SiO_2$ are affected by Si-undersaturated mineral fractionation. Attenuation of granitoid data along the plane of critical silica saturation towards the feldspar field suggest that clinopyroxene ± amphibole dominated fractionation occurs until at least $SiO_2$ concentrations up to ~65% in some rocks. This leads to the slightly quartz saturated alkaline diorite to syenite trend evident on a modal Q -P - F plot. The curved trend toward Q on a modal Q - P - F plot originating from rocks of monzodiorite to monzonitic composition is attributed to amphibole, biotite, titanite, clinopyroxene and magnetite fractionation.

**Hornblendites and Diorites as Potential Cumulates**

Hornblendites should be composed of amphibole, clinopyroxene, magnetite, titanite, apatite, and biotite if they represent cumulates from the granitoids. Amphibole typically is a crystallization product overgrowing clinopyroxene in the hornblendites, not a discrete phase as would be expected in a cumulate. The mineralogy of hornblendites is consistent with a cumulate origin. Cumulates of granitoids should contain high REE, $P_2O_5$, $TiO_2$, Cr, Ni, and Ba and low Zr and Sr. Non-saccharoidal granitoids develop weak negative Eu anomalies during fractionation. Cumulates should exhibit slight positive Eu anomalies. Two hornblendite samples possess positive Eu anomalies but also contain the lowest concentrations of CaO and $Al_2O_3$ of the hornblendites suggesting that the development of positive Eu anomalies in the hornblendites is not the product of plagioclase accumulation. Hornblendites are typically lower in total REE than the granitoids. Granitoid REE concentrations decline with fractionation, therefore cumulates should be REE enriched. This REE enrichment is not

observed. Cumulates are commonly coarse crystalline and should exhibit cumulate type textures. Hornblendites, however, contain lower REE than the primitive granitoid sample and some hornblendites are fine grained and contain large blocks of LSIC granitoids. As previously mentioned, field relationships indicate that the hornblendites are intrusive rocks in the LSIC and do not appear to texturally represent cumulate rocks.

A range in modal mineralogy of LSIC hornblendites and diorites was utilized to test whether these rocks could be modelled by Cr, Sr, and Zr concentrations (Figure 35) as cumulate products produced during fractional crystallization of the granitoids. Hornblendites selected were a clinopyroxene hornblendite (A=$Pl_{0.02}$ $Bt_{0.03}$ $Cpx_{0.03}$ $Hbl_{0.9}$ $Mag_{0.02}$) (mineral abbreviations after Kretz, 1983) and a biotite-clinopyroxene hornblendite (B=$Pl_{0.15}$ $Bt_{0.15}$ $Cpx_{0.12}$ $Hbl_{0.53}$ $Ap_{0.05}$). Diorites selected ranged from a melanic diorite (C=$Pl_{0.1}$ $Bt_{0.14}$ $Cpx_{0.03}$ $Hbl_{0.68}$ $Ap_{0.05}$) to a relatively leucocratic diorite (D=$Pl_{0.6}$ $Bt_{0.03}$ $Cpx_{0.02}$ $Hbl_{0.3}$ $Mag_{0.02}$ $Ap_{0.03}$). Because of the dominance of hornblende in these samples, vectors for liquids that would be produced by separation of minerals in proportions of the diorites and hornblendites are roughly coincident with the hornblende vector. The leucocratic diorite has a vector approximately parallel to the granitoid data in terms of Zr-Cr (Figure 35b), although requiring high degrees of fractionation to describe the distribution, but notably divergent in terms of Sr-Cr (Figure 35a). It is unlikely that a leucocratic diorite assemblage represents a potential cumulate assemblage. Vectors B and C fit the data better than A due to the addition of apatite and greater proportions of plagioclase to the fractionating assemblage. In general, the mineralogy of the diorites and hornblendites cannot adequately be modelled as cumulates from the granitoids given the D values chosen. The mineralogy of the melanic diorite (C) is

# Sr-Cr-Zr Fractional Crystallization Models

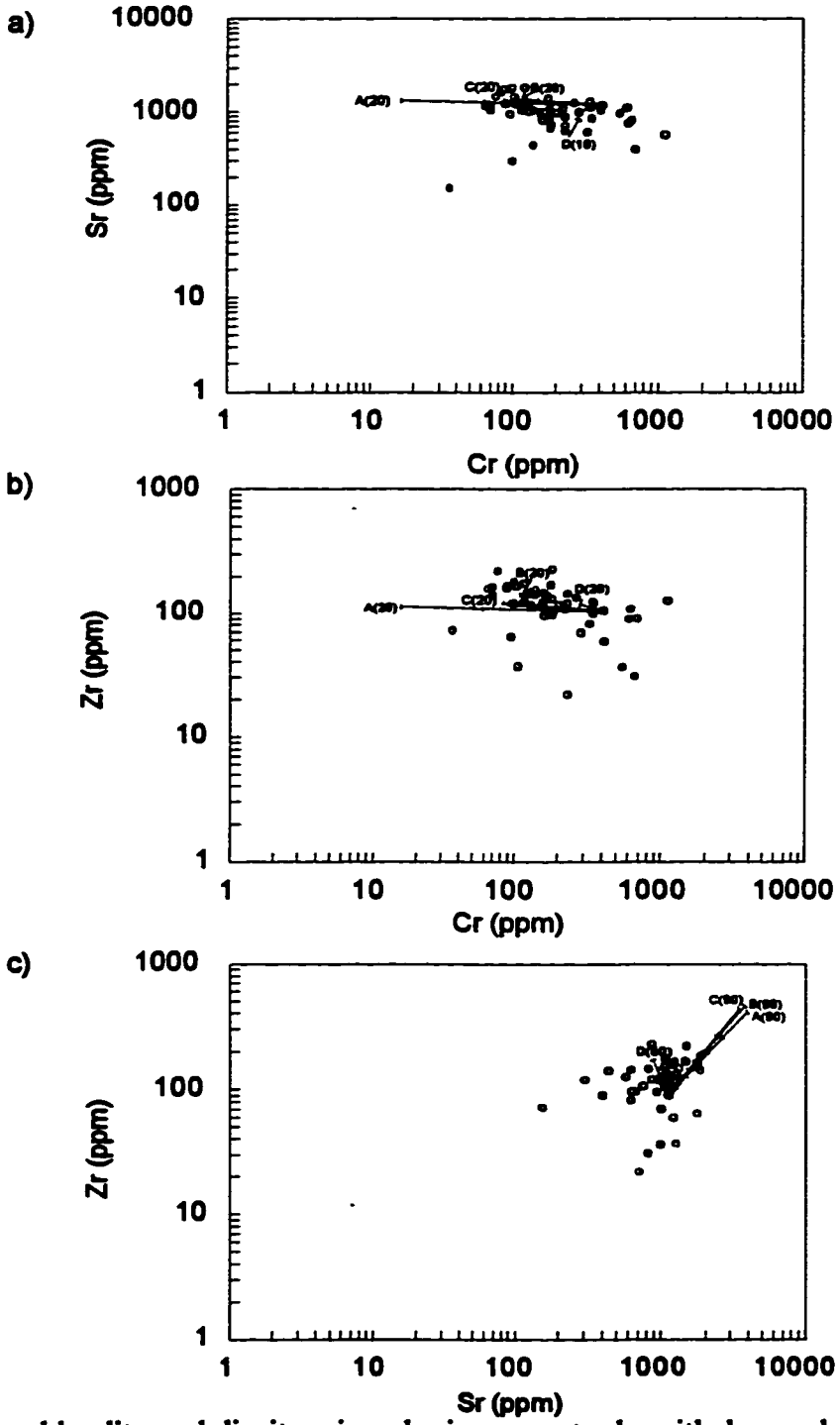


Figure 35. Hornblendite and diorite mineralogies cannot adequitly be modelled as cumulates from non-saccharoidal granitoids. Field relationships indicate that a melanocratic diorite (C ) best represents the cumulate mineralogies observed associated with the LSIC non-saccharoidal granitoids. The vector for this composition indicates that >20% fractional crystallization is required to model the range in Cr-Sr-Zr exhibited by the granitoids.

compatible with cumulate textured samples observed in the field but this vector does not fit the non-saccharoidal granitoid data well. If it assumed that D values are adequate to model fractionation in these rocks, and given the observed mineralogical similarity to cumulate textured rocks in outcrop, the extent of fractionation must exceed 20-30%, but is less than ~70%.

## Changes in Mineral Chemistry Resulting from Fractionation

Variations in mineral chemistry reflect crystallization from evolving liquid compositions. Removal of these minerals in turn modify rock chemistry. The operation of various substitutions are examined to identify how mineral chemistry affects the LSIC granitoid chemistry.

### Hornblende

Systematic compositional variations exhibited by hornblende are sympathetic to whole rock compositions and is consistent with hornblende compositions reflecting crystallization from evolving liquid compositions. These variations include a decrease in Ca, Cr, Mg and an increase in Si on a per formula unit (p.f.u.) basis with increasing rock $SiO_2$ concentration, a positive covariation between whole rock $Mg^{\#}$ ($Mg/Fe^{2+}+Mg$) and hornblende $Mg^{\#}$, and an Na decrease with increasing hornblende $Mg^{\#}$. With hornblende being the dominant ferromagnesian mineral present, the substitutions occurring in hornblende exhibit strong control on the liquid compositions.

The operation of the substitutions observed in the LSIC hornblendes with increasing evolution of the rocks of the LSIC can be examined by comparing ratios involving $Na_B$ or $Al^{IV}$

and associated coupled substitution cation against host rock normative differentiation index. This method essentially combines a binary discriminant coupled substitution plot with host rock fractionation index plot. Both richterite and riebeckite substitutions approach $Na_B$/coupled-cation ratios of 1 with differentiation accounting for the general increase in $Na_B$ with differentiation and steady decline in Ca. The Ti content of hornblende increases until a differentiation index (D.I.) of approximately 70 (~60 wt.% $SiO_2$) is reached, and then Ti is noted to decline sharply at higher D.I. The Ti-tschermakite exchange increases in importance with differentiation until D.I.=70, and then achieves a constant ratio. The observed operation of the Ti-tschermakite substitution explains the behavior of Ti in hornblende, with the decline in Ti at D.I. >70 possibly due to crystallization of titanite preferentially incorporating Ti. Aluminum tschermakite exchange appears relatively constant and increases in importance when D.I. exceeds 70, probably as a result of increasing rock $SiO_2$. The Fe-tschermakite exchange monitor continually approaches 1 as D.I. increases. The edenite substitution does not appear to increase in importance throughout the range of D.I. at the LSIC since ratios of $Al^{IV}/(Na+K)_A$ remain between 2 and ~4.

While all substitutions outlined above are variably operative, riebeckite, richterite, and Fe-tschermakite substitutions account for the general constant increase in $Na_B$ and $Fe^{3+}$ with fractionation. The Ti-tschermakite substitution is operative in more mafic host rocks and leads to a maximum hornblende Ti at D.I.~70, whereas the Al-tschermakite substitution is an increasingly important substitution in hornblendes from felsic host rocks as D.I. increases.

**Clinopyroxene**

The change in clinopyroxene substitutions with increasing host rock evolution can be examined by comparing ratios involving Na or $Al^{IV}$ and associated coupled substitution cations against host rock normative differentiation index (Thornton and Tuttle, 1960) as outlined for hornblende. Jadeite (Na - $Al^{VI}$) exchanges increase in importance with evolution of the host rocks whereas aegerine (Na - $Fe^{3+}$) exchange remains relatively constant near unity leading to an increase in $Na_{Cpx}$ with increasing D.I. which is a reflection of increasing host rock $Na_2O$. The effect of these exchanges results in a decrease of quadrilateral components with increasing D.I., and a linear trend toward Na parallel to the Q+J=2 line on a plot of Q (Wo+En+Fs) vs. Jd (2Na). No clear variations in operation of $Al^{IV}$ substitution mechanisms can be determined by this method due to data scatter. Both Ti, $Al^{IV}$, Mg, and to a lesser extent, Cr, increase with declining $Mg^{\#}_{Cpx}$ to ~0.8 equivalent to D.I.~35-40, at which a maxima is reached and concentration falls at lower $Mg^{\#}_{Cpx}$. An opposite relation is observed for Si which indicates that fassiate ($2Si+2Mg - 2Cr+2Al^{IV}$), calcium tschermakite ($2Si+2Mg - 2Al^{VI}+2Al^{VI}$), and $CaTiAl_2O_6$ ($2Si+Mg - 2Al^{IV}+Ti$) exchanges are operative until D.I.~ 35-40, at which point the substitutions are operative in an opposite sense.

This reversal in exchange direction occurs at a D.I. equivalent to the boundary between clinopyroxene hornblendite compositions and more evolved granitoids of the LSIC. If it assumed that these units were emplaced at similar P-T conditions, the discrepancy between reaction direction may be the result of differences then in bulk composition, or other crystailizing phases controlling substitution style. For crystallizing phases to control the observed variations, crystallization must commence around D.I.~ 35-40. The crystallization of

plagioclase also will reduce the Ti content of clinopyroxene through reduction in the Ca-tschermakite component by favoring the entry of Al in plagioclase, with resultant pyroxenes typically low in Ti and Ca (Barberi et al, 1971). The Ca content of LSIC pyroxenes over a D.I. range of ~30-80 varies insignificantly and cannot be attributed to plagioclase crystallization and the crystallization of plagioclase preceding pyroxene at D.I. >35 is not supported by textural evidence. The jadeite component of clinopyroxene commonly declines as a result of plagioclase crystallization. The increasing jadeite component of LSIC clinopyroxenes suggests that plagioclase was not an appreciably fractionating mineral. Magnetite crystallization can control Ti - Al of pyroxene (Gibb, 1973) by preferential incorporation of Ti in magnetite. Pyroxenes generally contain more included magnetite with increasing D.I. suggesting a link between the timing of magnetite crystallization and clinopyroxene Ti content although this relationship is too poor to be conclusive. Additionally, magnetite crystallization should dramatically reduce $Fe^{3+}$ in pyroxene which would reduce the influence of the aegerine substitution. Since both $Fe^{3+}$ and Na consistently increases as a result of the coupled Na - $Fe^{3+}$ substitution the variation in Ti cannot be attributed to magnetite fractionation. The dominant Ti phase in the LSIC is titanite, the modal percentage of which increases dramatically above D.I. = 35. This mineral is rare in clinopyroxene hornblendite units and may account for the decline in Ti at higher D.I. The entry of Ti into clinopyroxene structure is controlled by the degree of $SiO_2$ undersaturation of the liquid, $Al_2O_3$ concentration of the liquid, and varies positively with temperature (Verhoogen, 1962). Temperature is unknown and the $TiO_2/Al_2O_3$ ratio and $SiO_2$ concentration of the host rock is

incompatible to the Ti-Al variation observed in the pyroxenes from clinopyroxene hornblendites assuming bulk rock values approximate the liquid composition.

Two and three spot analysis transects across pyroxenes from diorites and clinopyroxene hornblendites revealed chemical zonation within individual grains. Large grains within the clinopyroxene hornblendites are occasionally oscillatory zoned. Zoned clinopyroxene have bright electron backscattered rims, a dark electron backscattered inner zone and bright electron backscattered, light green colored cores. The enstatite component, $Mg/Mg+Fe^{2+}$, and Cr decrease from the core to the inner zone and increase again at the rim whereas Si, ferrosalite and wollastonite components generally increase from the core to the inner zone, then decrease at the rim. Two and three spot analysis across pyroxenes from a diorite also show a crude zonation with rims generally higher in $Cr_{p.f.u}$ and XEn than core compositions. The association of mafic rim compositions and relatively evolved cores as been noted in pyroxenes from modern basinites and has been attributed to pyroxene crystallization in a fractionating magma chamber that undergoes periodic mafic melt infusions (Dobosi and Fodor, 1992). The core/rim and probe traverses of LSIC pyroxenes indicates that pyroxene compositions record a fractionation trend and zonation suggest crystallization in the presence of more mafic liquid compositions.

Clinopyroxenes from ocean floor and volcanic arc basalts are typically lower than 20 wt.% CaO (Nisbet and Pearce, 1977) due to the appearance of plagioclase on the tholeiite liquidus prior to pyroxene depleting the melt in Ca. Pyroxene from the LSIC are all in excess of 20 wt.% CaO indicating that pyroxene preceded plagioclase on the liquidus as suggested from thin section. The appearance of plagioclase on the liquidus is suppressed by high melt

$H_2O$ concentrations (Green, 1982). At a pressure range of ~2 - 14 kbar., pyroxene precedes plagioclase as a liquidus phase only when melts are $H_2O$ saturated.

### 8.1.5 Estimation of Intensive Magmatic Properties

Magmatic variables such as pressure, temperature, $fO_2$, $fH_2O$, and water content are important in determining the ultimate crystallization history of the magma. Estimation of these conditions can be made based upon the application of mineral equilibrium, mineral-bulk chemistry, and synthetic and natural based granite system studies coupled with observed textural evidence at the LSIC.

**Depth of Crystallization**

Very few barometers are applicable to the rocks of the LSIC as a result of a mineralogy that does not include two pyroxenes or garnet. One potentially useful barometer is the total Al ($Al^{TOT}$) in hornblende barometer initially formulated by Hammarstrom and Zen (1986). Pressure is related to $Al^{TOT}$ of calcic amphibole by $P=-3.92+5.03Al^{TOT}$, for P<6-8 kbar. ± 3 kbar., with the error range later modified to ±1 kbar. in a pressure range of 2-8 kbars (Hollister et al, 1987). Seven co-existing minerals are required to apply the barometer comprising of plagioclase, K-feldspar, quartz, hornblende, biotite, titanite, magnetite. Hammerstrom and Zen (1986) state that for a system of eleven chemical components ($SiO_2$, $Al_2O_3$, $TiO_2$, $Fe_2O_3$, FeO, CaO, MgO, $Na_2O$, $K_2O$, $P_2O_5$, and possibly $H_2O$), for a given set of T-P-$fO_2$-$fH_2O$ conditions, minor variations in the bulk composition of the system should be

exhibited as a change in the modal proportions of minerals, not by the change in composition of the individual phases.

Application of the $Al^{TOT}$ hornblende barometer requires that the hornblendes crystallized at $fO_2$ above the QFM buffer. Hornblendes crystallized under low $fO_2$ conditions are typically rich in Fe, Al and may undergo increased Tschermak substitution which in turn preferentially removes Mg over $Fe^{2+}$ in the M2 site of hornblende (Anderson, 1993; Anderson and Smith, 1995). These hornblendes characteristically have low $Fe^{3+}/(Fe^{3+}+Fe^{2+})$ ratios and require $Al^{VI}$ - $Fe^{3+}$ exchange to maintain C site charge balance resulting in high Al concentrations, hence erroneously high P estimates. For this reason, hornblendes with $Fe^{3+}/(Fe^{3+}+Fe^{2+})<0.25$ (Anderson and Smith, 1995) to 0.20 (Schmidt, 1992) and Fe/(Fe+Mg) ratios <0.25 (Vyhnal et al, 1991) and >0.65 (Vyhnal et al, 1991; Anderson and Smith, 1995).

The $Al^{TOT}$ in hornblende barometers have a lower pressure limit of applicability of ~2 kbar. The rational for the 2 kbar. lower limits for the application of the $Al^{TOT}$ hornblende barometer is due to crystallization in intermediate metaluminous calc-alkaline melts occurring over a narrow temperature range. Above 2 kbar., the temperature range of wet granite solidus is nearly asymptotic and varies by less than ~100°C (Hollister et al, 1987). At pressures between 0-2 kbar., the temperature range of the solidus increases dramatically to a range of approximately 300°C (Luth et al, 1964). At pressures less than 2 kbar., the temperature dependent edenite exchange ($Si^{IV}+ VAC^{A} = (Na+K)^{A}+Al^{IV}$, where $VAC^{A}$ refers to an A site vacancy) is dominant over the pressure dependant Al-tschermakite exchange ($Si^{IV}+Mg^{C} = Al^{IV}+Al^{VI}$) (Hollister et al, 1987; Poli and Schmidt, 1992) and leads to pressure underestimates.

The inflection of the wet saturated granite solidus (Luth et al, 1973) solidus occurs at a pressure slightly below 1 kbar., and it can be assumed that pressures derived from hornblendes crystallized below 1 kbar. will have increasingly large errors in pressure determinations.

A summary of applicable $Al^{TOT}$ in hornblende barometric equations is as follows:

$P = -3.92 + 5.03\ Al^{TOT} \pm 3.0$ kbar. for P = 2-8 kbar. (Hammerstrom and Zen, 1986) with error revised by Hollister et al (1987) to $\pm$ 1.0 kbar.

$P = -3.46 + 4.23\ Al^{TOT}$ (Johnson and Rutherford, 1989)

and, in order to reduce the temperature effect at lower pressures:

$P = -3.01 + 4.76Al^{TOT} - \{[T(°C) - 675]/85\} \cdot \{0.530Al^{TOT} + 0.005294[T(°C) - 675]\} \pm 0.6$ kbar. for P = 1-10 kbar. (Anderson and Smith, 1995)

Samples used to derive pressure estimates were culled from a dataset of 93 analysis based upon a selective screen. Samples analysed from obviously re-equilibrated or altered grains, recrystallized sections, and grains with Si > 7.5 p.f.u. were excluded. Although the LSIC granitoids crystallized well above the QFM buffer, as shall be discussed in following sections, hornblendes with $Fe^{3+}/Fe^{3+}+Fe^{2+} < 0.2$ were excluded, and all 28 remaining analysis met the required Fe/Fe+Mg criteria. Pressures obtained are less than the lower limits of applicability for the equations examined (Table 5). In an effort to minimize the effect of variability of solidus temperatures at low pressure, the Anderson and Smith (1995) equation represents the most suitable estimator of crystallization pressure. The temperature variable in the equation has been constrained to 700-750°C which approximately coincides to the water saturated andesite solidus of Green (1982) at pressures < 2 kbar. Pressures obtained for this

Table 5. Comparison of Pressure Estimates from Various Al in Hornblende Barometers

| | | | Pressure Estimates† | | | |
|---|---|---|---|---|---|---|
| Sample (Mineral)⊗ | Sample (Rock)∅ | $Al^{TOT}$* | P1 | P2 | P3 T°C=700 | P3 T°C=750 |
| amph-17 | 921014-9 | 0.85 | 0.356 | 0.136 | 0.885 | 0.288 |
| amph-18 | 921014-9 | 0.92 | 0.706 | 0.432 | 1.187 | 0.589 |
| amph-19 | 921014-9 | 0.797 | 0.089 | -0.089 | 0.821 | 0.081 |
| amph-20 | 921014-9 | 0.904 | 0.627 | 0.364 | 1.113 | 0.520 |
| amph-22 | 921014-9 | 0.889 | 0.552 | 0.300 | 1.044 | 0.456 |
| amph-23 | 921014-9 | 0.911 | 0.662 | 0.394 | 1.145 | 0.550 |
| amph-37 | 930619-3 | 0.866 | 0.436 | 0.203 | 0.938 | 0.357 |
| amph-38 | 930619-3 | 1.122 | 1.724 | 1.286 | 2.117 | 1.456 |
| amph-40 | 930619-3 | 1.083 | 1.527 | 1.121 | 1.937 | 1.288 |
| amph-41 | 930623-5 | 0.935 | 0.783 | 0.495 | 1.256 | 0.653 |
| amp1.1 | 921013-9 | 0.935 | 0.783 | 0.495 | 1.256 | 0.653 |
| amp1.2 | 921013-9 | 0.904 | 0.627 | 0.364 | 1.113 | 0.520 |
| amp2.2 | 921013-9 | 0.889 | 0.552 | 0.300 | 1.044 | 0.456 |
| amp3.1 | 921013-9 | 0.911 | 0.662 | 0.394 | 1.145 | 0.550 |
| amp3.2 | 921013-9 | 0.968 | 0.949 | 0.635 | 1.406 | 0.795 |
| amp6.2 | 921011-13 | 0.935 | 0.783 | 0.495 | 1.256 | 0.653 |
| amp7.1 | 921011-13 | 0.935 | 0.783 | 0.495 | 1.256 | 0.653 |
| amp8.1 | 921015-14 | 0.904 | 0.627 | 0.364 | 1.113 | 0.520 |
| amp10.1 | 921015-14 | 0.889 | 0.552 | 0.300 | 1.044 | 0.456 |
| amp11.1 | 921015-14 | 0.911 | 0.662 | 0.394 | 1.145 | 0.550 |
| amp11.2 | 921015-14 | 0.968 | 0.949 | 0.635 | 1.406 | 0.795 |
| amp12.1 | 921012-9 | 1.151 | 1.870 | 1.409 | 2.250 | 1.580 |
| amp12.2 | 921012-9 | 0.866 | 0.436 | 0.203 | 0.938 | 0.357 |
| Statistics | | | | | | |
| Avg. | | 0.93 | 0.77 | 0.48 | 1.24 | 0.64 |
| 1 Std. | | 0.08 | 0.41 | 0.34 | 0.37 | 0.35 |
| Min. | | 0.80 | 0.09 | -0.09 | 0.82 | 0.06 |
| Max. | | 1.15 | 1.87 | 1.41 | 2.25 | 1.58 |
| Med. | | 0.91 | 0.66 | 0.39 | 1.15 | 0.55 |

⊗ = Mineral compositions in Appendix 4
∅ = Sample compositions in Appendix 3
* = Total Al (p.f.u) in hornblende

† Pressure Equations

P1 = $-3.92+5.03Al^{TOT}$ for P = 2-8 kbar (Hammerstrom and Zen , 1986) ± 1.0 kbar (Hollister et al, 1987).

P2 = $-3.46+4.23Al^{TOT}$ (Johnson and Rutherford, 1989)

P3 = $-3.01+4.76Al^{TOT}-([T(°C)-675]/85).(0.530Al^{TOT}+0.005294[T(°C)-675])$ ± 0.6 kbar for P = 1-10 kbar (Anderson and Smith, 1995)

temperature range are on average 0.64 - 1.24 kbar. ± 0.6 kbar with a maximum of 2.25 kbar ± 0.6 kbar (Table 5).

Nimis (1995) formulated a clinopyroxene barometer given as:

$P = 698.443 + 4.985\ Al_T - 26.826Fe^{2+}_{M1} - 3.764Fe^{3+} + 53.989Al_{M1} + 3.948Ti + 14.651Cr - 700.431Ca - 666.629Na - 682.848Mg_{M2} - 691.138Fe^{2+}_{M2} - 688.384Mn - 6.267(Mg_{M2})^2 - 4.144(Fe^{2+}_{M2})^2$

where all elements are in a p.f.u basis. Pressure (P) is in kbar, T, M2, and M1 refer to the T, M2 and M1 sites. Clinopyroxene compositions calculated to 4 cations and sum T site and sum M1, M2 sites equal 2 respectively with a total cation deficiency <0.006 and Ca+Na > 0.45. Clinopyroxenes must also be C2/c (diopside structure) pyroxenes and host rocks must be <18 wt.% $Al_2O_3$. This barometer was formulated specifically for pyroxenes crystallized in melts of basaltic composition although it can applied as a relative barometer for rock compositions differing from basalt (Nimis, 1995) and as alkalic as leucitites. Excluding three very negative pressure estimates, the total range in pressure is ~16 kbar with a median value of 0.55 kbar (due to differing bulk rock chemistry from the experimental calibration of the barometer, this does not necessarily represent the actual crystallization depth). From a total of 21 core and rim analysis pairs, 14 pyroxenes display decreasing pressures from core to rim indicating that crystallization was most likely polybaric.

The low pressure of final crystallization from hornblende $Al^{TOT}$ differs significantly from the depth of initial melt derivation estimate discussed earlier. Hornblende crystallization occurred at crustal levels, probably in response to decreasing melt temperature and increasing melt water concentration. Clinopyroxene records polybaric crystallization and is an early

crystallizing phase relative to hornblende. Clinopyroxene crystallization probably was initiated at deeper levels, after melt extraction, but before magmatic conditions favored hornblende crystallization. This would explain the observed hornblende, clinopyroxene chemistries and discrepancies with the depth of derivation of the initial melt.

**Estimation of Water Concentration**

An approximate water content may be obtained from the minimum wt.% $H_2O$ in a melt necessary to stabilise amphibole, 2.5-3.0 wt.% (Burnham, 1979; Helz, 1982), and percent crystallization determined from where amphibole occurs in the paragenetic sequence as after Otten and Senior (1985) and Whitney (1988). As a magma ascends, cools and crystallizes, the melt fraction will tend towards $H_2O$ saturation since $H_2O$ is incompatible. The presence of early crystallized clinopyroxene indicates that the initial water contents were lower than 2.5% in some granitoids. The modal percentage of clinopyroxene is low in the granitoid rocks, generally less than 5%, indicating that the initial water concentrations were in the order of ~2.3-2.8 wt.%. This $H_2O$ undersaturation should lead to crystallization occurring over a wide temperature range and explains the high degree of intra-crystalline equilibrium of Mg and $Fe^{2+}$ between the M1 and M2 sites in clinopyroxene. An approximation of the depth of $H_2O$ saturation and final crystallization may be ~1 kbar from the granite vapour saturation surface at 750°C and melts with 2.5% $H_2O$ (Whitney, 1988), equivalent to the estimated final crystallization pressure ($Al^{TOT}_{Hbl}$) suggesting final crystallization of the LSIC under water saturated conditions. A maximum $H_2O$ concentration of ~4-6 wt.% is based upon the solubility of water in granodioritic melts (Burnham and Ohmoto, 1980) and the depth of

crystallization (~1 kbar) and granite water saturation relationship in Shelley (1993). Various authors (in Young, 1972) note that the maximum pressure dependent solubility of water in quartz syenites is equal to, or slightly less than, that for granites so the application of granite based experimental determinations of water saturation are applicable to slightly quartz saturated granitoids of the LSIC. This approximate pressure of final crystallization for granite compositions is in agreement with that obtained from LSIC amphibole compositions.

The estimated initial water concentration is similar to that observed in modern andesitic rocks. The typical range in water contents in andesitic melts is 1-5 wt.%, with the higher concentrations noted in high-K hornblende bearing andesites (Gill, 1981). Sisson and Grove (1993) suggest that the petrogenesis of high alumina calc-alkaline basalts are a product of crystallization from magmas with 4-6 wt.% $H_2O$.

Several lines of evidence support final crystallization occurring under water saturated conditions. Deuteric patch perthites are observed in some rocks, uralitization of clinopyroxene has occurred, barite has formed after biotite, hematite rims and lamella occur in magnetite, all suggesting the presence of a late magmatic to subsolidus (oxidizing) fluid phase. Ultramafics in the Pontiac sedimentary rocks at the eastern contact of the north complex are K-enriched and contain a high modal percentage of biotite, possibly as a result of a metasomatizing fluid phase derived from the LSIC.

**Estimation of Temperature**

Three independent methods of temperature estimation have been applied to the LSIC granitoids, two involving mineral composition and the third based upon bulk rock chemistry, the melt behavior of Zr, and solubility of zircon.

Crystallization temperatures have been estimated from the zircon saturation temperature equation of Watson and Harrison (1983). The zircon solubility equation has been applied by Barrie (1995) to predict melt temperatures in Archean volcanic rocks and is suitable to granitic temperature estimation provided that zircon inheritance has not occurred (Watson and Harrison, 1984) and the melt is zircon saturated. The melt saturation behavior of zircon is largely dependent upon temperature and alkali - alumina ratio which increases the Zr concentration required for saturation with zircon (Watson, 1979; Watson and Harrison, 1983). The melt concentrations of Si and Ca are of lesser importance, and the melt temperature is given by the equation below:

$\ln D_{Zr} = -3.80-0.85(M-1)+12900/T$

where $D_{zr}$ is the concentration ratio of Zr in stoichiometric zircon relative to the melt, M is the cation ratio (Na+K+2Ca)/(Al·Si), and T is temperature in Kelvin (± 30°). Other variables such as water content have negligible influence on calculated T, unless dissolved $H_2O$ is less than 2 wt.%. Water contents of the LSIC magma must have been in excess of 2 wt.% since ~ 2.5% is required to stabilize amphibole and biotite. The formulation of this equation was based partially on synthetic metaluminous samples with wt.% $SiO_2$ and melt $H_2O$ in the range of the LSIC granitoids. There are numerous limitations of the zircon thermometer to the LSIC granitoids, these are:

i) The LSIC samples may not fully represent liquid compositions in terms of Zr due to possible crystallization and removal of zircon. Zirconium increases in concentration throughout the fractionation series and only rare zircon phenocrysts have been noted in some cumulate textured diorites. The low Zr concentrations of the cumulate rocks coupled with the rarity of zircon in these rock is interpreted to represent negligible zircon removal from the melt, an inference supported by rock chemistry indicating Zr is highly incompatible in the LSIC granitoid melts. If inherited zircon is present, erroneous temperature estimates will result. The degree of crustal interaction is minor in the majority of the units of the LSIC and it is assumed that the mantle source would not contribute zircon phenocrysts to the initial granitoid partial melt.

ii) Clinopyroxene and amphibole can appreciably partition Zr but the $D_{Zr}^{Zrc/Hbl}$ and $D_{Zr}^{Zrc/Cpx}$ is so large that during zircon crystallization, the affect of clinopyroxene and hornblende crystallization on Zr concentration is probably minor. Prior to zircon crystallization, minor incorporation of Zr in other minerals may lead to temperature underestimates.

The temperature obtained from the zircon saturation thermometer will represent the temperature at which the zircon crystallized from the melt (Montel, 1993). Calculated zircon temperatures, which probably represent minimum temperatures, range up to 830°C and average ~750°C for non-saccharoidal granitoids (Table 6). The temperatures increase with increasing Zr and a positive $SiO_2$ vs. T relationship exists. Watson (1979) has shown that zircon solubility increases with peralkalinity of the liquid. It would be expected that the solubility of zircon should increase during the evolution of the LSIC magmas since

**Table 6. Estimated Crystallization Temperatures Based Upon the Solubility of Zircon in Felsic Melts**

| Sample | Rock Type** | $T_{zr}$(°C) |
|---|---|---|
| 9210102 | QMD | 761 |
| 9210105 | Mo† | 801 |
| 9210113 | Sy† | 811 |
| 92101113 | Dio | 635 |
| 92101113 | Dio | 658 |
| 92101115 | MD | 770 |
| 92101116 | Mo | 807 |
| 9210127 | Dio | 631 |
| 9210128 | MD | 677 |
| 9210129 | QMD | 786 |
| 92101210 | MD† | 787 |
| 9210131 | MD | 827 |
| 9210138 | MD† | 718 |
| 9210139 | Mo† | 735 |
| 9210147 | Sy | 710 |
| 9210157 | MD | 796 |
| 92101513 | MD | 746 |
| 92101514 | Dio | 794 |
| 9210163 | Dio | 777 |
| 9210171 | Dio | 689 |
| 9210174 | QMD | 798 |
| 9210181 | GD | 755 |
| 9210186 | QMD | 795 |
| 9210187 | QMD† | 798 |
| 9210188 | Mo† | 800 |
| 9210189 | MD† | 794 |
| 9306156 | QMD | 780 |
| 9306161 | MD† | 735 |
| 9306184 | QMD† | 786 |
| 9306187 | Dio | 623 |
| 9306193 | Mo† | 820 |
| 9306198 | Dio | 686 |
| 9306203 | Mo†£ | 746 |
| 9306222 | Sy† | 712 |
| 9306226 | MD† | 766 |
| 9306231 | Dio | 720 |
| 9306234 | QMD | 787 |
| 9306235 | Dio | 631 |
| 9306238 | Mo£ | 781 |
| 9306242 | MD† | 768 |
| 9306244 | Dio | 685 |
| 9306257 | Dio | 670 |
| 9308174 | MD† | 819 |
| 93081712 | Dio | 746 |
| 9308184 | Dio | 759 |
| 9308185 | Sy† | 762 |
| 9308187 | QMo† | 677 |
| 9308188 | Dio | 778 |
| 9308192 | Mo† | 747 |
| 9308193 | QMD | 790 |
| 9308211 | MD† | 759 |
| 9308213 | QMD | 761 |

** Rock type as presented in Appendix 1.

peralkalinity has been shown to increase with granitoid $SiO_2$. High $SiO_2$ rocks should produce lower temperature estimates than more mafic rocks which is opposite than observed. A spurious compositional control on $Zrn^T$ is discounted since rocks with equivalent temperatures have M values differing by approximately 15%.

The clinopyroxene thermometer of Mercier (1976) can be used to estimate a minimum temperature of crystallization in rocks that do not contain orthopyroxene. Application to clinopyroxenes from non-saccharoidal granitoids indicate crystallization temperatures between ~880°C - 1100°C with a distinct decline in temperature with increasing $SiO_2$. Rocks with ~53% $SiO_2$ have crystallized at ~ 1050°C+ whereas rocks with 59-61% $SiO_2$ have crystallized at ~ 880$^{+}$°C (granitoid samples contained within Table 7). This discrepancy between the temperatures derived from the pyroxene and zircon saturation thermometers probably reflects the earlier higher temperature crystallization of clinopyroxene relative to zircon, and potential underestimates in zircon saturation temperature.

The composition of biotite is used as the third method of temperature estimation. Since the $TiO_2$ content of phlogopites (and biotites) is $fO_2$ and pressure independent, and dependent upon temperature (Carmichael, 1996), it has been suggested that Ti concentrations may prove a useful thermometer (Tronnes et al, 1985; Carmichael, 1996). Luhr et al (1984) proposed a geothermometer based upon the $Ti/Fe^{2+}$ of biotites in dacitic volcanic rocks (El Chichon) that is thought to be insensitive to small changes in pressure. Uncertainty is stated at ±23°C due to minor errors in calculating $Fe^{2+}$ from microprobe data. Temperature is given by:

$$T(°K) = 838/(1.0337-Ti/Fe^{2+})$$

Table 7. Crystallization Temperatures Estimated from Clinopyroxene Compositions

| Sample (Mineral)$^{\phi}$ | Sample no. (Rock) | Equation Parameters* | | | | | T°C |
|---|---|---|---|---|---|---|---|
| | | W | Kw' | Kg" | A | Ka' | |
| px2.3 | 921012-7 | 0.4534 | 0.0943 | 1.4659 | 0.0651 | 0.0892 | 1060 |
| px3.1 | 921012-7 | 0.4353 | 0.1318 | 1.6067 | 0.0705 | 0.1053 | 1123 |
| px3.2 | 921012-7 | 0.4415 | 0.1189 | 1.5917 | 0.0785 | 0.1151 | 1103 |
| px3.3 | 921012-7 | 0.3369 | 0.3415 | 1.5416 | 0.1595 | 0.2067 | 1322 |
| px4.1 | 921012-7 | 0.4569 | 0.0872 | 1.5199 | 0.0830 | 0.1157 | 1047 |
| px4.2 | 921012-7 | 0.4550 | 0.0911 | 1.3689 | 0.0700 | 0.0891 | 1054 |
| px4.3 | 921012-7 | 0.4584 | 0.0843 | 1.3784 | 0.0615 | 0.0796 | 1039 |
| px5.1 | 921012-7 | 0.4670 | 0.0667 | 1.5106 | 0.0877 | 0.1209 | 1004 |
| px5.2 | 921012-7 | 0.4410 | 0.1200 | 1.3579 | 0.0590 | 0.0754 | 1106 |
| px6.2 | 921012-7 | 0.4581 | 0.0848 | 1.4344 | 0.0694 | 0.0926 | 1041 |
| px6.3 | 921012-7 | 0.4572 | 0.0866 | 1.3410 | 0.0482 | 0.0615 | 1043 |
| px7.1 | 921014-9 | 0.4663 | 0.0679 | 1.4114 | 0.0607 | 0.0805 | 1003 |
| px7.2 | 921014-9 | 0.4673 | 0.0660 | 1.3561 | 0.0406 | 0.0528 | 993 |
| px7.3 | 921014-9 | 0.4697 | 0.0611 | 1.3409 | 0.0454 | 0.0581 | 981 |
| px7.4 | 921014-9 | 0.4813 | 0.0375 | 1.3283 | 0.0605 | 0.0755 | 914 |
| px7.5 | 921014-9 | 0.4707 | 0.0591 | 1.3723 | 0.0393 | 0.0517 | 974 |
| px8.2 | 921014-9 | 0.4565 | 0.0880 | 1.3198 | 0.0360 | 0.0458 | 1044 |
| px8.3 | 921014-9 | 0.4581 | 0.0848 | 1.3205 | 0.0280 | 0.0360 | 1036 |
| px8.4 | 921014-9 | 0.4585 | 0.0840 | 1.2997 | 0.0380 | 0.0475 | 1036 |
| px6.1 | 921014-9 | 0.4662 | 0.0683 | 1.4744 | 0.0766 | 0.1043 | 1006 |
| px8.5 | 921014-9 | 0.4746 | 0.0512 | 1.4697 | 0.0976 | 0.1295 | 967 |
| px8.6 | 921014-9 | 0.4623 | 0.0761 | 1.2746 | 0.0329 | 0.0406 | 1016 |
| px8.7 | 921014-9 | 0.4580 | 0.0850 | 1.3280 | 0.0269 | 0.0347 | 1036 |
| px8.8 | 921014-9 | 0.4740 | 0.0524 | 1.3657 | 0.0504 | 0.0653 | 959 |
| px8.9 | 921014-9 | 0.4862 | 0.0276 | 1.4049 | 0.1172 | 0.1453 | 892 |
| px8.10 | 921014-9 | 0.4593 | 0.0823 | 1.3113 | 0.0414 | 0.0521 | 1032 |
| px8.11 | 921014-9 | 0.4637 | 0.0734 | 1.3162 | 0.0515 | 0.0643 | 1013 |
| px8.12 | 921014-9 | 0.4860 | 0.0282 | 1.2740 | 0.0642 | 0.0765 | 877 |

$\phi$ = Mineral analysis spot by SEM-EDS. See Appendix 4.

* Equation parameters defined as (Mercier, 1976):

$T = (t_1 * \ln Kw' + t_2)/D$ for temperature in Kelvin.

For garnet facies depths of derivation as supported by REE of LSIC samples:

$Kw' = (1-2W_d)/(0.862+0.276W_d)$

$Ka' = Kg'' * A * (1-A)$

$Kg'' = 3.298-1.781Mg+0.128\ln Kw'$

$A = (Al + Cr - n * Na)/2$

$n = 1$ or 0.82, or Al/Na

$W_d = Ca/(Ca+Mg+Fe^{2+}+Mn)$

$t_1 = -3168.1$

$t_2 = 53754$

$D = \ln Kw' * \ln Ka' + d_1 * \ln Kw' + 2.26 * \ln Ka' + d_2$

$d_1 = -6.208$

$d_2 = 31.037$

Table 7 continued. Crystallization Temperatures Estimated from Clinopyroxene Compositions

| Sample (Mineral)$^{\phi}$ | Sample no. (Rock) | Equation Parameters* | | | | | T°C |
|---|---|---|---|---|---|---|---|
| | | W | Kw' | Kg" | A | Ka' | |
| px9.1 | 921014-9 | 0.4851 | 0.0298 | 1.3204 | 0.0564 | 0.0702 | 882 |
| px9.2 | 921014-9 | 0.4698 | 0.0609 | 1.3190 | 0.0502 | 0.0629 | 982 |
| px10.1 | 921014-9 | 0.4717 | 0.0571 | 1.3963 | 0.0573 | 0.0755 | 974 |
| px10.2 | 921014-9 | 0.4619 | 0.0770 | 1.3438 | 0.0240 | 0.0315 | 1016 |
| px11.1 | 921014-9 | 0.4588 | 0.0833 | 1.2843 | 0.0323 | 0.0401 | 1033 |
| px11.2 | 921014-9 | 0.4565 | 0.0881 | 1.3004 | 0.0370 | 0.0463 | 1045 |
| px12.1 | 921014-9 | 0.4557 | 0.0897 | 1.3205 | 0.0334 | 0.0426 | 1048 |
| px13.1 | 921014-9 | 0.4760 | 0.0482 | 1.4210 | 0.0547 | 0.0735 | 948 |
| px13.2 | 921014-9 | 0.4579 | 0.0852 | 1.2944 | 0.0296 | 0.0371 | 1037 |
| px14.1 | 921014-9 | 0.4548 | 0.0915 | 1.3106 | 0.0275 | 0.0351 | 1051 |
| px14.2 | 921014-9 | 0.4666 | 0.0675 | 1.3073 | 0.0489 | 0.0608 | 999 |
| px15.1 | 921014-9 | 0.4555 | 0.0900 | 1.3798 | 0.0562 | 0.0732 | 1051 |
| px16.1 | 921014-9 | 0.4686 | 0.0633 | 1.3471 | 0.0575 | 0.0730 | 990 |
| px16.2 | 921014-9 | 0.4540 | 0.0931 | 1.3343 | 0.0376 | 0.0483 | 1056 |
| px16.3 | 921014-9 | 0.4527 | 0.0959 | 1.3718 | 0.0489 | 0.0637 | 1062 |
| px16.4 | 921014-9 | 0.4847 | 0.0308 | 1.3263 | 0.0617 | 0.0768 | 889 |
| px17.1 | 921018-8 | 0.4797 | 0.0408 | 1.6150 | 0.0539 | 0.0823 | 927 |
| px17.2 | 921018-8 | 0.4816 | 0.0371 | 1.5049 | 0.0572 | 0.0812 | 914 |
| px18.1 | 921018-8 | 0.4897 | 0.0207 | 1.4912 | 0.0687 | 0.0953 | 848 |
| px18.2 | 921018-8 | 0.4867 | 0.0266 | 1.4856 | 0.0605 | 0.0844 | 873 |
| px6 | 930620-3 | 0.4823 | 0.0357 | 1.7297 | 0.0454 | 0.0749 | 907 |
| px23 | 921014-11 | 0.4915 | 0.0171 | 1.4074 | 0.1151 | 0.1433 | 841 |
| px24 | 921014-11 | 0.4977 | 0.0046 | 1.2512 | 0.1388 | 0.1495 | 733 |
| px25 | 921014-11 | 0.4800 | 0.0402 | 1.5472 | 0.1385 | 0.1846 | 942 |
| px26 | 921014-11 | 0.4583 | 0.0843 | 1.3643 | 0.0290 | 0.0384 | 1035 |
| px27 | 921014-11 | 0.4551 | 0.0909 | 1.3722 | 0.0370 | 0.0489 | 1051 |
| px28 | 921014-11 | 0.4760 | 0.0484 | 1.4642 | 0.1020 | 0.1341 | 960 |
| px-a | 921014-11 | 0.4637 | 0.0733 | 1.3731 | 0.0400 | 0.0527 | 1011 |
| px-b | 921014-11 | 0.4519 | 0.0975 | 1.3900 | 0.0310 | 0.0418 | 1065 |
| px-c | 921014-11 | 0.4607 | 0.0794 | 1.3638 | 0.0310 | 0.0410 | 1024 |
| px-d | 921014-11 | 0.4620 | 0.0768 | 1.4717 | 0.0720 | 0.0983 | 1025 |
| px1.1 | 921012-7 | 0.4471 | 0.1074 | 1.5609 | 0.0561 | 0.0826 | 1084 |
| px1.2 | 921012-7 | 0.4628 | 0.0751 | 1.4812 | 0.0583 | 0.0814 | 1019 |
| px1.3 | 921012-7 | 0.4473 | 0.1069 | 1.5852 | 0.0828 | 0.1204 | 1083 |
| px2.1 | 921012-7 | 0.4636 | 0.0736 | 1.3256 | 0.0490 | 0.0617 | 1014 |
| px2.2 | 921012-7 | 0.4546 | 0.0919 | 1.3468 | 0.0365 | 0.0473 | 1053 |

$\phi$ = Mineral analysis spot by SEM-EDS. See Appendix 4.

* Equation parameters defined as (Mercier, 1976):

$T = (t_1 * \ln Kw' + t_2)/D$ for temperature in Kelvin.

For garnet facies depths of derivation as supported by REE of LSIC samples:

$Kw' = (1-2W_d)/(0.862+0.276W_d)$

$Ka' = Kg'' * A * (1-A)$

$Kg'' = 3.298-1.781Mg+0.128\ln Kw'$

$A = (Al + Cr - n * Na)/2$

$n = 1$ or 0.82, or Al/Na

$W_d = Ca/(Ca+Mg+Fe^{2+}+Mn)$

$t_1 = -3168.1$

$t_2 = 53754$

$D = \ln Kw' * \ln Ka' + d_1 * \ln Kw' + 2.26 * \ln Ka' + d_2$

$d_1 = -6.208$

$d_2 = 31.037$

Temperature calculated from one biotite analysis yielded 660°C ± 23°C. This estimate is probably too low given that it is less than the temperature of the 1 kbar granite solidus and 2 kbar wet andesite solidus of Green (1982). The error may be the result of Ti loss through titanization of biotite.

**Estimation of $fO_2$**

Graphical methods of $fO_2$ determination can be applied to obtain a relative $fO_2$ of the LSIC granitoids. Oxygen fugacity can be approximated from the Fe/(Mg+Fe) of biotite in equilibrium with K-feldspar and magnetite (Wones and Eugster, 1965). The Fe/(Mg+Fe) of biotite is 0.34 which is equivalent to $fO_2$ of $\sim 10^{-10}$, approximately the HM buffer, at 800°C for P=2.07 kbar. The $Fe^{2+}$ - $Fe^{3+}$ - Mg contents of biotite (a la Wones and Eugster, 1965) suggests an $fO_2$ at approximately the HM buffer also. The assemblage biotite+amphibole also implies that $fO_2$ was between FMQ and the HM buffers at approximately $10^{-12.5}$ at 800°C (stability curve from Wolff and Storey, 1983). The presence of titanite, magnetite, and quartz suggest $fO_2$ above the NNO buffer (TMQH $\sim 10^{-14}$ at 800°C (Wones, 1981), and TMQA $\sim 10^{-12}$ at 800°C (Noyes et al, 1983)) and less than the HM buffer. The Ti content of LSIC hornblendes are low compared to basaltic hornblendes, a feature consistent with high $fO_2$ (NNO-HM buffer) (Helz, 1973). In general, mineral chemistry reflects $fO_2$ between the NNO and MH oxygen buffers.

The fugacity of oxygen can be theoretically estimated from the equilibrium assemblage biotite + magnetite + sanidine from the biotite $fO_2$ relationship of Wones (1981) for

crystallization at $fO_2$ between the NNO and HM buffers. The $fO_2$ based upon biotite compositions can be expressed as:

$$-0.5\log fO_2 = 4819/T + 6.69 + 3\log X_{Fe2+} - \log fH_2O - \log a_{San} - \log a_{Mag} - (0.11(P-1)/T)$$

where T is temperature in Kelvin, $X_{Fe2+}$ is the number of $Fe^{2+}$ atoms in biotite divided by the number of octahedral sites in biotite (3) per formula unit, $a_{San}$ is the activity of sanidine which is equivalent to the mole fraction orthoclase in K-feldspar since T is >600°C and $X_{Or}$>0.75 (Waldbaum and Thompson, 1969). The $a_{Mag}$ term is the activity of magnetite, P is pressure in bars, and $fH_2O$ is the fugacity of water. The activity of magnetite is generally considered to be equal to one if magnetite is present although, in the case of the magnetites analyzed from the LSIC, most contain minor mole percent fractions of other spinels group endmembers, notably chromite, vanadium magnetite and trace hercynite, ulvospinel, and jacobsite. The activity of magnetite has been taken as mole fraction $Fe_3O_4$ in the analysis which ranges from 0.96-0.99 in the granitoids. Pressure has been estimated from the $Al^{TOT}$ content of hornblende to be ~1kbar.

The temperature of biotite - magnetite - K-feldspar crystallization is likely less than that obtained from clinopyroxene compositions, a mineral which crystallized early in the LSIC units. The primary LSIC magma was undersaturated with respect to water and crystallization probably occurred over a wide temperature range. Clinopyroxene is an early crystallizing phase therefore the temperature obtained from clinopyroxene thermometry may be in excess of that for the crystallization of the assemblage biotite - magnetite - K-feldspar. The stability of biotite in granitic rocks is generally limited to ≤850°C so the temperatures obtained from earlier formed clinopyroxene are not applicable to equilibrium magnetite - K-feldspar - biotite

crystallization. The temperature which will be used in the estimation of $fO_2$ can be obtained from the crystallization temperature of biotite in water saturated andesite (Green, 1982) which occurs at ~800 - 825°C.

The fugacity of water is calculated from equations presented in Burkhard (1991) and is estimated at $\log fH_2O$ ~3.1 at 1 kbar and a temperature of 800°C. For non-saccharoidal sample 930623-5 in which magnetite contains $X_{Fe2+}$ of 1.153, a calculated $fO_2$ of $10^{-13.7}$ is observed (Table 8), equivalent to ΔNNO +0.1. If it is assumed that magnetite exsolved and feldspar re-equilibrated, the compositions observed may differ from that of the original grains and $fO_2$ can be calculated with $a_{Sa} = 0.6$ and $a_{Mag} = 0.9$. The $fO_2$ calculated is ~ΔNNO -0.3 which differs insignificantly from the previous $fO_2$ value. An error of 1 kbar in the pressure estimate will produce an $fO_2$ error of $\pm 0.03$ log units whereas an error of 55°C will produce an error of $\pm 0.54$ log $fO_2$ units. The presence of titanite + magnetite + quartz (TMQ) in some of the granitoids suggests crystallization at $fO_2$ at or above the titanite + magnetite + quartz buffer. At T=800°C, the $fO_2$ of the TMQH buffer is $10^{-13.7}$, equivalent to the $fO_2$ estimate obtained from biotite equilibrium suggesting crystallization of some units of LSIC occurred at $fO_2$ equivalent to the TMQH buffer.

Intrinsically high $fO_2$ conditions, indicated by biotite equilibria and substantiated by the presence of the assemblage quartz + magnetite + titanite suggest an oxidized source. The Eu/Eu* near unity for the primary granitoids is a result of this intrinsically high $fO_2$. A constant iron depletion trend observed in the LSIC granitoids, characteristic of the calc-alkaline rocks (Miyashiro, 1974), is the product of high $fO_2$ (in conjunction with elevated $H_2O$ concentrations). Oxygen fugacity at the QFM buffer leads to magnetite crystallization ~15°C

Table 8. Calculated $fO_2$ from Biotite - K-Feldspar - Magnetite Equilibrium

| T°C | $logfH_2O^{\oplus}$ | $X_{Fe2+}/3$ | $a_{Sa}$ | $a_{Mag}$ | P(bars) | $logfO_2^{\otimes}$ |
|---|---|---|---|---|---|---|
| 800 | 3.1 | 0.38 | 0.9 | 0.99 | 1000 | -13.71 |

| $fO_2$ of buffer curves at 800°C and 1kbar $^{\theta}$ | |
|---|---|
| Buffer | $logfO_2$ |
| HM | -9.51 |
| NNO | -13.83 |
| TMQHIL | -13.72 |
| FQM | -14.51 |

⊗ Oxygen fugacity calculated from the equation of Wones (1981)
⊕ Fugacity of water calculated from the equation Burkhard (1991)
θ Equations for buffer curves taken from:
HM - Chou (1978)
NNO - Heubner and Sato (1970)
FQM - Hewitt (1978)
TMQHIL - Wones and Gilbert (1982)
See text for explanation of $a_{Sa}$, $a_{Mag}$, and $X_{Fe2+}/3$.

below the calc-alkaline basalt liquidus at $H_2O$ saturated conditions (Sisson and Grove, 1993). At the $fO_2$ ~NNO, magnetite appears on the high alumina calc-alkaline basalt liquidus (Sisson and Grove, 1993, and references therein). This is consistent with the occurrence of magnetite inclusions in clinopyroxene in the LSIC suggesting early crystallization of magnetite in the granitoid melt(s). The presence of barite indicates that the late magmatic fluid phase was probably highly oxidizing. Hattori (1989) noted that barite in the Kirkland Lake Igneous Complex has $^{87}Sr/^{86}Sr_I$ indicative of formation from a late magmatic subsolidus fluid phase at high temperature. This mineral occurs as discrete grains in biotite in LSIC in a slightly altered quartz monzodiorite similar to the Kirkland Lake Alkaline Intrusive Complex. The occurrence of barite in the LSIC supports a similar origin to barite in the Kirkland Lake Igneous Complex. The oxygen fugacity of the LSIC granitoids is consistent with magnetite series granites (Ishihara, 1977) and is slightly more reduced than the $10^{-12}$ at T>860°C identified from biotite in the Murdock Creek stock in Kirkland lake (Rowins et al, 1991). Mattioli et al (1989) found that spinel lherzolite xenoliths posses oxidation fugacities of ΔNNO -5 to ΔNNO +1 with increasing metasomatism effects. The ΔNNO ~0 for the LSIC granitoids is compatible with retention of an intrinsically oxidized mantle source signature.

## 8.2 Hornblendites

Hornblendite units of the LSIC have been suggested to represent metamorphosed Belleterre-Anglier belt mafic volcanic rocks (Avramtchev and Lebel-Drolet, 1979; Hocq, 1990). The LSIC hornblendites are chemically distinct from the volcanic rocks and are

characterised by higher Cr, $Mg^{\#}$, alkalis, and LREE than calc-alkali and tholeiitic volcanic rocks of the Belleterre belt.

The LSIC hornblendites show two compositionally distinct populations (Figure 36). Group 1 has low Zr (< 60 ppm Zr) with high Ti/Zr ~140 and $CaO/Al_2O_3$, > 1. Group 2 has high Zr (>60 ppm) with low Ti/Zr ratios (39-79), and low $CaO/Al_2O_3$ < 1. These groups are termed low and high Zr hornblendites respectively.

### 8.2.1 Origin of the High Zr Hornblendites

The high Zr group of hornblendites may be either the product of i) alteration of low Zr hornblendites, ii) lower degree partial melt products than that of the low Zr hornblendites, iii) fractionation products, iv) mixing or contamination.

i) Alteration: The involvement of a fluid and addition of elements may have formed the high Zr hornblendites. An origin through alteration requires addition of Zr and preferential mobility of Zr relative to $TiO_2$ to produce the separate hornblendite types since both hornblendite types have similar $TiO_2$ concentrations. Both Ti and Zr are generally considered immobile during alteration and moderate grades of metamorphism and therefore this is considered unlikely.

ii) Partial Melting: A lower degree of partial melting than the low Zr hornblendites is also discounted. High Zr samples are on average higher in Cr than low Zr hornblendites which is unexpected for simple partial melting of a common source.

# Hornblendite $TiO_2$ and Zr Variation

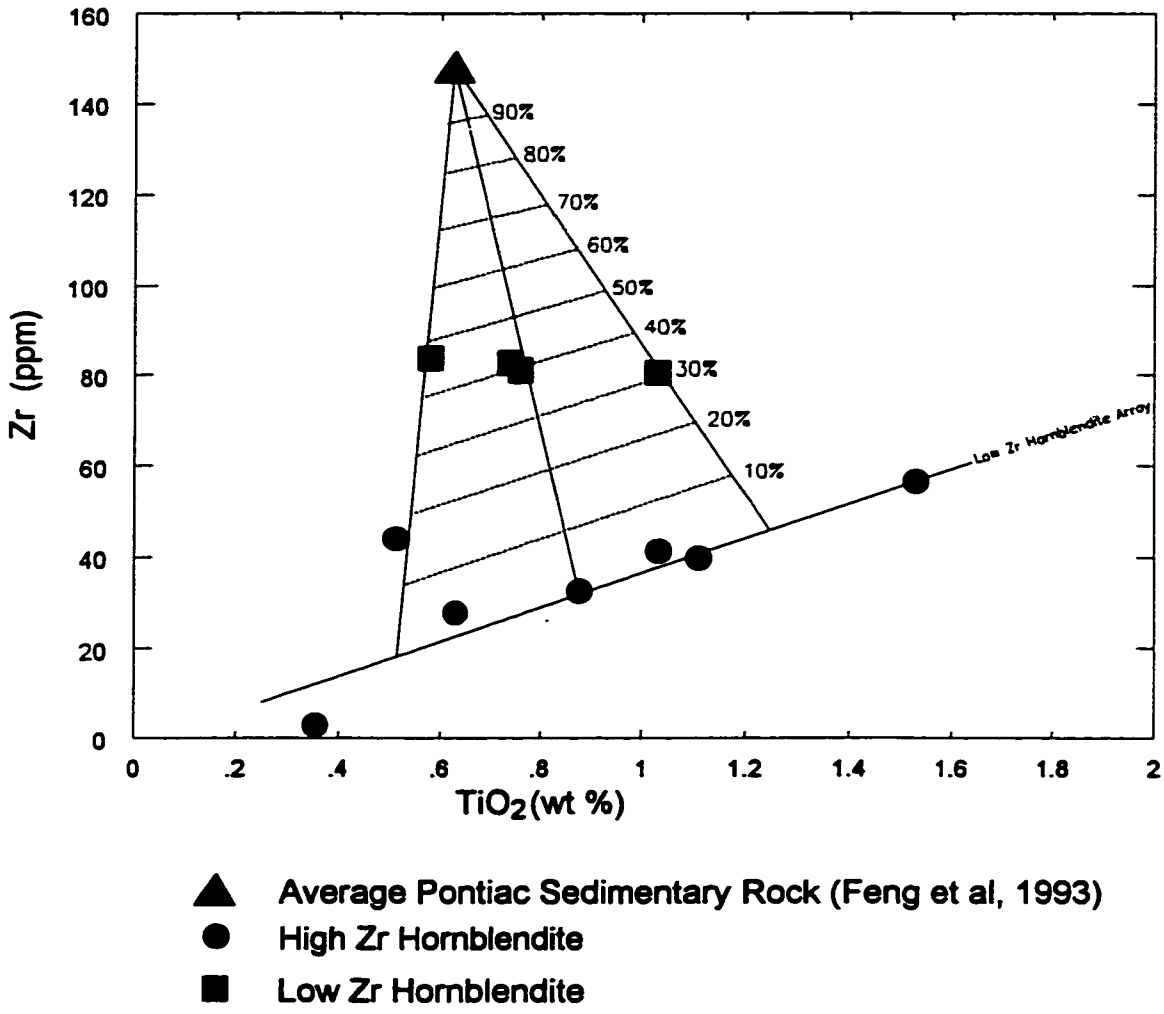


Figure 36. Two distinct clusterings of hornblendite samples are recognized. Mixing lines with an average fine grained Pontiac sedimentary rock composition (Feng et al, 1993) are marked at 10% intervals.

High Zr hornblendites are not LREE enriched relative to low Zr hornblendites and have similar $La/Yb_{CN}$.

iii) Fractional Crystallization: Fractionation is also unlikely since this process would be dominated by clinopyroxene removal. Fractionated liquids should have lower Cr/Ni ratios and $Mg^{\#}$. High Zr hornblendites have similar to higher $Mg^{\#}$ and Cr/Ni and are not related to the low Zr hornblendites by fractionation.

iii) Mixing or Contamination: Assimilation of Pontiac sedimentary rock can adequately explain many discrepancies between these two groups. High Zr samples form a low CaO, $TiO_2$ (Figure 36) trend and a low $TiO_2$, high $Al_2O_3$ trend toward an average Pontiac sedimentary rock composition (Feng et al, 1993). $CaO/Al_2O_3$ vs. major elements define mixing lines for the high Zr samples and support a crustal assimilation/mixing origin. $CaO/Al_2O_3$ vs. Ti/Zr, K/Rb and $Fe_2O_3/CaO$ vs. $SiO_2$ (Figure 37), and Zr/La vs. Ba, and Ba/Sr vs. Rb/Sr (Figure 37) also define mixing lines towards an average Pontiac sedimentary rock composition. High Zr samples are displaced towards lower K/Rb by sedimentary rock assimilation. Some trace and major element variation is inconsistent with sedimentary rock mixing, such as the necessary high Cr and $Mg^{\#}$ of the contaminant endmember, and not all element combinations produce complementary mixing relationships indicating a decoupling of trace and major elements may have occurred. It appears that high and low Zr hornblendites may have had a similar source but have undergone different extents of interaction with crustal material. The high Zr hornblendites may have experienced a longer crustal residence time relative to the low Zr samples allowing for increased

# Hornblendite - Sediment Mixing Relationships

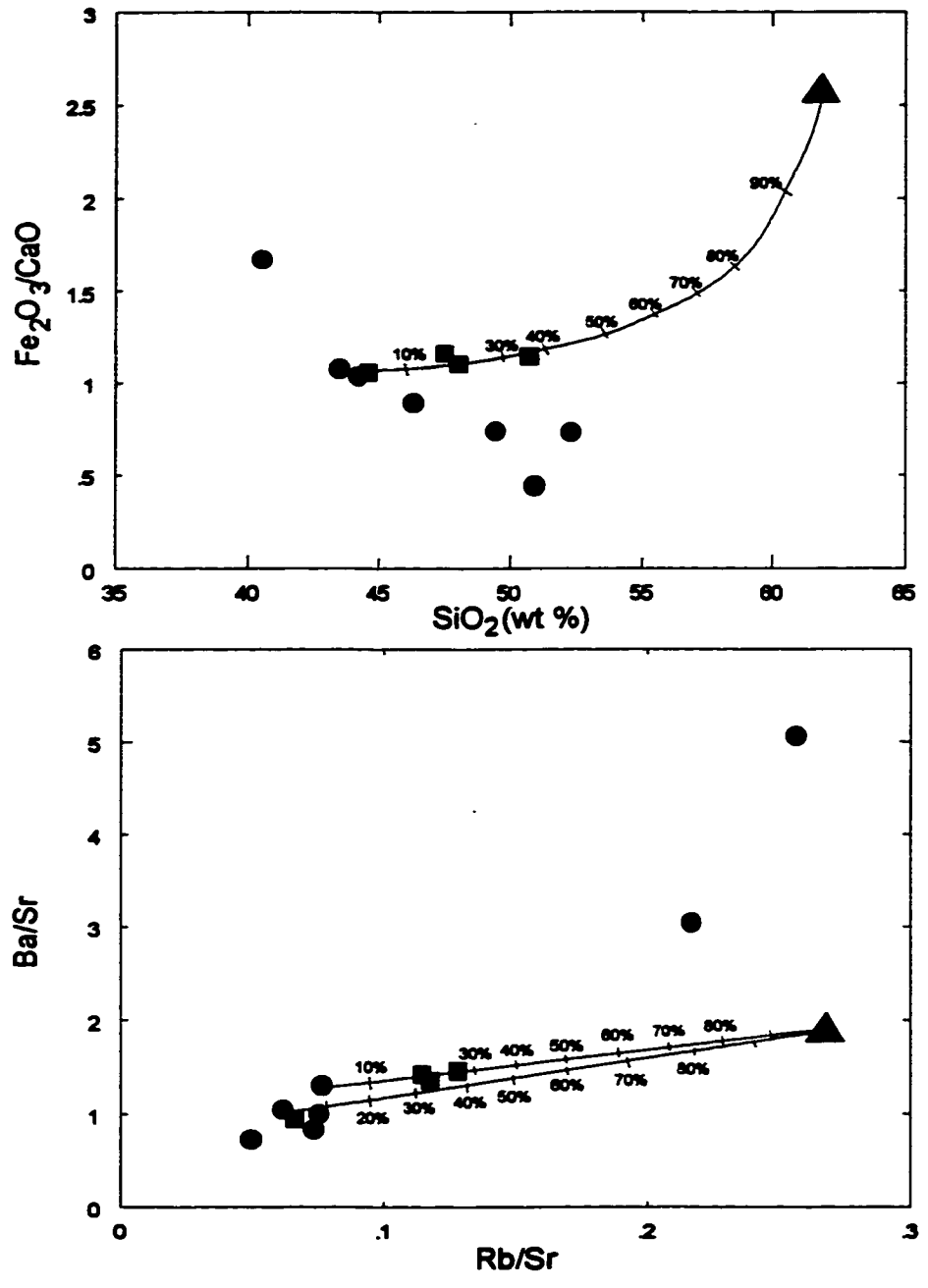


Figure 37. Ratio - oxide and ratio plots indicate that the majority of the high Zr hornblendites are the product of <~40% of a sedimentary component. Mixing curves in Ba/Sr vs. Rb/Sr and $Fe_2O_3$/CaO vs. $SiO_2$ space ticked at 10% sedimentary rock mixing.

assimilation, or were derived from a source affected by greater degrees of metasomatism from a crustal source. High Zr samples can be projected back to a composition within the bulk of the data for the low Zr samples indicating common parentage for both hornblendite types.

### 8.2.2 Origin of the Low Zr Hornblendites

Low Zr hornblendites represent uncontaminated hornblendite and therefore most suitable for determination of source and process characteristics.

**Processes Controlling Range in Low Zr Hornblendite Compositions**

The range in hornblendite compositions may be the result of either: i) assimilation, ii) partial melting, or iii) fractional crystallization.

i) Assimilation: A general increase in Ti/Zr with total REE and a positive $SiO_2$ vs. MgO relationship is observed in the low Zr hornblendites. Crustal rocks are typically lower in MgO and Ti/Zr than LSIC hornblendites and interaction should increase $SiO_2$, and lower MgO and Ti/Zr in the hornblendites. The opposite is observed in the LSIC low Zr hornblendites. The lack trace or major element evidence to suggest significant Pontiac sedimentary rock interactions outlined in the high Zr hornblendite origin discussion, indicate that the low Zr hornblendites are relatively uncontaminated by crustal material.

ii) Partial Melting: If the overall variation in hornblendite chemistry were the product of differing degrees of partial melting from a common source, it would be expected that compositions would be relatively homogenous given the high degrees of melting required to produce melts with $Mg^{\#}$ as high and $SiO_2$ contents as low as that found in the hornblendites. The LSIC hornblendites have $Mg^{\#}$ and MgO concentrations similar to komatiites suggesting these units are also the result of high degrees of partial melting. Archean komatiites are suggested to result from 30-40% partial melting of mantle peridotite (Herzberg, 1995) and similar MgO and $Mg^{\#}$ for the hornblendites suggest they may have arisen from a primary melt derived from ~ 30% partial melting. The variation in compatible element concentration is higher than that observed for incompatible elements in the hornblendites. Nickel and Cr exhibit a 3 - 4 fold concentration change whereas La and Zr exhibit <2 fold variable in concentration. The variation is more typical for that produced by fractional crystallization than partial melting.

iii) Fractional Crystallization: Least fractionated hornblendites are characterized by steep fractionated LREE profiles flattening through the HREE and no Eu anomalies. The total REE concentration increases with fractionation, as indicated by the inverse REE vs. $Mg^{\#}$ relationship, and a coherent negative $Eu/Eu^{*}$ vs. Total REE relation is observed. This suggests that a major REE partitioning phase was not fractionating and, as the degree of fractionation increased, a more pronounced negative Eu anomaly was formed indicating plagioclase was a fractionating phase. Water concentrations below saturation may have promoted the stabilization of plagioclase. An initial water

content lower than that of the granitoids is supported by higher proportions of early crystallizing anhydrous minerals and an Fe enrichment trend originating at the primitive hornblendite sample (930616-6). High melt water contents stabilize magnetite relative to plagioclase and Fe-Mg silicates (Sisson and Grove, 1993). The Fe enrichment trend probably indicates that magnetite crystallized below the liquidus temperature and Fe and Mg were controlled by high $Mg^{\#}$ minerals (i.e. clinopyroxene) which produce iron enrichment. A negative $SiO_2$ vs. $Al_2O_3$ and positive $SiO_2$ vs. $Mg^{\#}$ relationships suggest that clinopyroxene was also fractionating. This is evident when two samples from the same hornblendite intrusion are compared. Meladiorites are associated with hornblendites in two locations within the LSIC. A gradational contact is noted in one case suggesting that these two rock types may have resulted from in-situ fractionation with the meladiorites representing cumulate material.

**Derivation and Source of the Initial Hornblendite Melt**

Composition of the hornblendites is inconsistent with either residue or liquid derived from plausible crustal sources. Tholeiitic and calc-alkaline volcanic rocks from the Belleterre-Angliers belt are lower in Cr and $Mg^{\#}$ (data in Barnes et al., 1993). The degree of LREE, Sr, Ba, and $K_2O$ enrichments exhibited by the hornblendites are inconsistent with the high degree of melting required to derive hornblendites from picritic and basaltic komatiites which have similar to lower $Mg^{\#}$ (0.74 - Pontiac Subprovince komatiites (Camire et al, 1993) 0.65-0.7 - Boston Township komatiites (Xie et al, 1995) ($Mg^{\#}$ recalculated by method outlined earlier for LSIC samples). Other sources such as tonalites and sedimentary rocks

melting to produce clinopyroxene hornblendite residues are inconceivable due to the high LILE of the hornblendites.

Hornblendites are inferred to represent primary, or near primary, mantle melts based upon high $Mg^{\#}$, MgO and Ni in the range of mantle melts (Sato, 1977; Hart and Davis, 1978). An estimation of the mantle source composition can be obtained from binary element and ratio plots for low Zr samples that do not represent appreciable sedimentary rock mixtures (low Zr group) and are least fractionated. A best estimate of a primary hornblendite liquid composition is obtained from sample 930616-6 which is characterised by the lowest total REE, Zr, Rb, and Sr, second highest Cr, $Mg^{\#}$ and highest Ni of the low Zr hornblendites.

Incompatible element ratios of the primitive hornblendite should approximate that of the source. At moderate degrees of melting, Ti behaves incompatibly and the Ti/Zr ratio of the hornblendite (139) is higher than chondrite (~110). This higher than chondrite ratio may be the product of either Zr poor source or, more likely, a residual HFSE phase, as indicated by the $Zr/Zr^*$ of 0.37, is present in the source. The $Ti/Ti^*$ of the hornblendite is 1.32 suggesting that the residual phase does not contain Ti or the source was Ti enriched relative to chondrite. It is unlikely that this primitive hornblendite sample experienced significant clinopyroxene or opaque removal. The positive $Ti/Ti^*$ suggests negligible removal of a Ti phase. Removal of clinopyroxene would lower $Mg^{\#}$, Cr, and $SiO_2$ of this sample. The fact that this primitive hornblendite sample is high in $Mg^{\#}$, Cr, and $SiO_2$ (since clinopyroxene is higher in $SiO_2$ than the melt, removal should lead to constant or $SiO_2$ depletion) relative to the modified hornblendites and posses greater than chondrite Ti/Zr indicates little clinopyroxene removal occurred.

The Ti/Y ratio of 841 is significantly higher than chondrite (256), consistent with high Ti. The Zr/Y ratio of 6.04 is also higher than chondrite (2.5). Since Zr is depleted in the hornblendites, Y must be even more depleted relative to Zr. Yttrium behaves similar to an HREE because of similar radius and charge, and the positive covariation between $Gd/Yb_{CN}$ and Y attest to this behavior in the LSIC hornblendites. There is two possible means of generating the steep LREE trends in the LSIC hornblendites. The removal of amphibole, or residual amphibole will lead to an LREE enriched liquid. This liquid will have relatively flat to concave MREE to HREE patterns. The degree of LREE enrichment and $La/Yb_{CN}$ achieved in the primitive hornblendite is higher than that probably attainable through removal of amphibole alone and would require prior LREE enrichment of the source. The presence of residual or fractionating garnet does not require any assumptions on the degree of LREE enrichment of the source prior to melt generation and can be readily tested.

The depletion of Y relative to Zr coupled with a fractionated $Gd/Yb_{CN} = 2.64$ suggest that an HREE fractionating phase, such as garnet, is present in the source. Positive covariation for La/Y and Nb/Y indicate that this mineral possessed $D_Y > D_{La}$ and $D_Y > D_{Nb}$, partitioning typical of pyrope garnet. Primitive hornblendite sample 930616-6 has the highest Nb/Y and La/Y suggesting the highest residual garnet effect. Assuming a relatively compositionally homogenous source in terms of REE, the sample with the highest Cr/Y should contain the lowest ΣHREE. This variation is observed for the LSIC hornblendites and suggests that the primitive hornblendite sample (930616-6) was derived from a source with the highest percentage of residual garnet and that REE of other hornblendite samples have been affected by fractional crystallization processes. The high $SiO_2$ of the primary

hornblendite sample may be a function of melting of hydrous peridotite and relatively large degrees of melting required to melt high proportions of orthopyroxene (Herzberg, 1992) in the source. The hornblendite sample possesses very high $CaO/Al_2O_3$ = 2.01, very low $Al_2O_3/TiO_2$ = 8.58, but near chondritic $CaO/TiO_2$ of 17.34. This may be due to the combined effects residual garnet which would lower Al relative to Ti and Ca in the hornblendite melt, and might be exaggerated by large scale melting of a Ca phase, such as clinopyroxene which melts in greater proportions than olivine or orthopyroxene during partial melting. An Al depleted source is unlikely to have existed given the observed Y and $Gd/Yb_{CN}$ data indicating residual garnet. If relatively large proportions of clinopyroxene had melted out of the source compared to orthopyroxene or olivine, it would be expected that the hornblendites would posses high Cr/Ni ratios. The Cr/Ni ratio observed in the hornblendite (2.06) is not higher than that observed in Archean Al-undepleted komatiites from the Abitibi Subprovince (Lahaye et al, 1995) indicating that the $CaO/Al_2O_3$ and $Al_2O_3/TiO_2$ ratios are the result of residual garnet. The high $Gd/Yb_{CN}$ and low $Al_2O_3/TiO_2$ observed in the low Zr hornblendites has been attributed to deep mantle melting in komatiitic rocks (Tomlinson et al, 1995). An increase in HREE relative to LREE in the fractionated rocks may be due to very minor monazite fractionation, a mineral noted in hornblendite thin section, and is opposite of the relationship expected for garnet fractionation.

The higher than chondrite Ti/Al, Gd/Yb, and P/Nd < 70 for the initial hornblendite sample is consistent with derivation from a garnet lherzolite source at pressures less than 6 GPa. A higher pressure olivine - marjorite source is suggested by lower than chondrite Hf/Sm and Zr/Sm (Xie et al, 1995) although this is assumed to be the result of a residual HFSE phase

(and similar geochemical behaviour of Zr to Hf), source enrichment in REE. Ratios of La/Nb>2, $K_2O/TiO_2$>1, reflect a subduction modified source with high LILE/HFSE ratios (Ormerod et al, 1987). Within plate, and MORB rocks are typified by $K_2O/TiO_2$<0.6 and La/Nb<1.2 (Pearce, 1982; Weaver, 1991). High concentrations of Ba, Rb, $K_2O$, LREE, steep $La/Yb_{CN}$=26.7 and Zr/Zr* and Nb/Nb* <<1 at high Cr and $Mg^{\#}$ are indicative of mantle derived rocks affected by subduction related source metasomatism. Hornblendite ratios are consistent with a subduction associated enriched source composition dissimilar from either an OIB and MORB source.

Considerable elevation in Ba/Sr, Rb/Sr, and Ti/Zr from chondritic abundance is noted and might reflect the melting of mantle hydrous phases such as phlogopite. Equilibrium olivine/melt calculations indicate that the hornblendites were in equilibrium with moderately refractory mantle olivine ranging from $Fo_{87}$ to $Fo_{90}$ for $D_{Fe\text{-}Mg}^{Ol}$ = 0.3 +/- 0.03, similar to compositions observed in peridotite olivines.

**Estimation of the Depth of Initial Hornblendite Melt Derivation**

The extraction depth of the initial hornblendite melt has been examined with the pressure dependent primary peridotite melt relationship of Herzberg (1995). Low Zr hornblendites define an extensive array from the initial low Zr hornblendite plotting to the right of the peridotite solidus (Figure 38). Position of this sample relative to the peridotite solidus cannot rule out the influence of prior olivine crystallization. The maximum pressure of derivation from a mantle source for the hornblendites is ~ 6 GPa, assuming the minor displacement from the mantle melt field is solely due to olivine removal. Heavy REE increase,

# Estimation of Depth of the Mantle Source for the Initial Hornblendite Melts

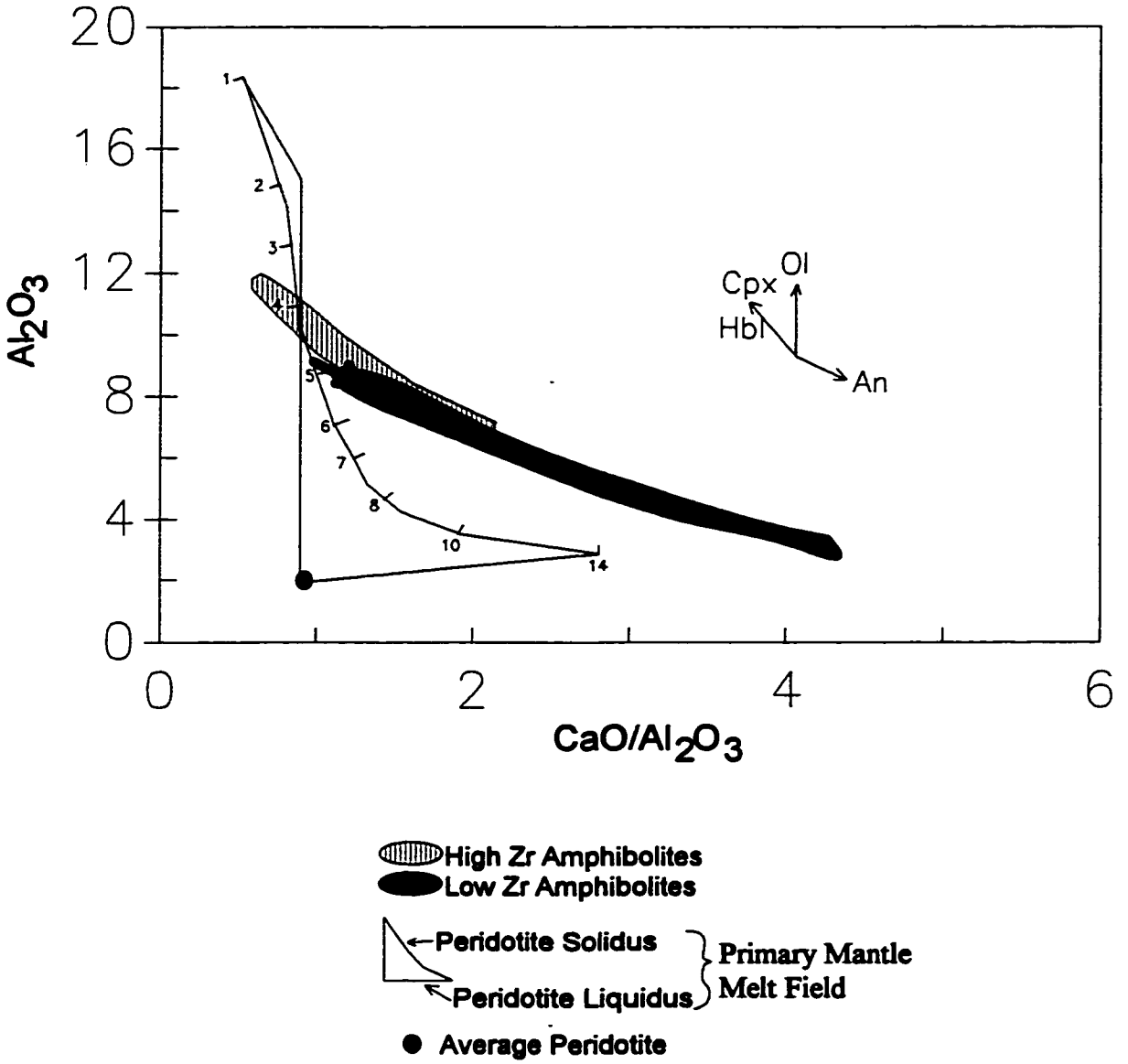


Figure 38. LSIC Hornblendite compositions compared to the pressure dependent peridotite melt field of Herzberg (1995). Fractionation vectors are approximate and represent the evolutionary direction of the liquid by removal of the specified mineral phase. The peridotite solidus marked off in gigapascals for the pressure at which a melt with the specified CaO and $Al_2O_3$ exists.

decrease in $La/Yb_{CN}$, and a decrease in Eu/Eu* suggest REE fractionating phase removal was minor, discounts garnet fractionation. The decreasing $CaO/Al_2O_3$ vs. $Al_2O_3$ trend is due to feldspar (anorthite) removal at crustal levels (stability field of feldspar). If anorthite removal is assumed, a 5 GPa source pressure results. High Zr hornblendites form an overlapping array with the low Zr hornblendites, but trend towards high $Al_2O_3$ and low $CaO/Al_2O_3$. This is interpreted to reflect crustal assimilation on high Zr hornblendite composition and derivation from a similar source as the low Zr hornblendites.

**Estimation of Temperature**

Several methods of temperature estimation have been applied, each with limitations. Three separate estimates of crystallization temperature based upon clinopyroxene compositions have been attempted. The method of Dal Negro et al (1982) derives crystallization temperature based upon intra-crystalline equilibrium of $Mg^{\#}$ between the M1 and M2 sites in clinopyroxene. This method works well for quenched minerals but clinopyroxenes from plutonic rocks tend to yield unrealistically low temperatures due to slow cooling histories of the host rocks (i.e. Faraone et al, 1988). A protracted cooling history is interpreted for the LSIC based upon the distribution of Mg and $Fe^{2+}$ between the M1 and M2 sites of LSIC clinopyroxenes and temperature cannot be determined from this method. The clinopyroxene thermometer of Bertrand and Mercier (1985) requires that the melt be in equilibrium with orthopyroxene. Clinopyroxenes from the least evolved samples of LSIC granitoids and ultramafics may be used to determine crystallization temperature in this manner

assuming that they represent melts in equilibrium with mantle peridotite. A third method involves application of the clinopyroxene thermometer of Mercier (1976).

The thermometer of Mercier (1976) tends to yield slightly higher temperatures than that of Betrand and Mercier (1985) for the same mineral analysis. The absolute variability between the temperatures obtained range from 2°C - 300°C although generally greater variability (i.e. > ~ 100°C) between estimates is observed in rim analysis than those obtained toward crystal cores. The thermometer of Bertrand and Mercier (1985) yields temperatures <800°C for some ultramafic rock samples which is unrealistically low given the high MgO (13-15%) of these rocks. The thermometer of Mercier (1976) produces slightly more realistic temperatures of approximately 1000°C ± ~ 50°C for the same minerals (see hornblendites contained within Table 7). Because of the lack of orthopyroxene in these rocks, this estimate represents minimum crystallization temperatures for pyroxene.

**Estimation of Crystallization Pressure**

The total Al in hornblende barometer applied to the granitoids is inapplicable to the clinopyroxene hornblendites due to their $SiO_2$ undersaturated nature and lack of required mineralogy. Based upon the mutually intrusive nature of the mafic and felsic units in the LSIC, it is assumed that pressures regimes of emplacement are comparable. An approximate pressure estimate can be obtained from the pressure dependency of glaucophane/crossite substitution controlling Na in the M4 (B) site of hornblende in mafic rocks (Brown, 1977). Sodium in M4 ranges up to 0.145 p.f.u indicating maximum crystallization conditions of 1-3 kbars. This is identical to values obtained for granitoid $Al^{TOT}$ in hornblende crystallization

pressures and suggests shallow level final mutual crystallization of LSIC units rather than tectonic juxtaposition.

## 8.3 Evolution and Emplacement of the LSIC Magmas

A general increase in normative olivine with increasing total REE and a weak inverse relationship between $SiO_2$ and normative olivine is observed. The primary magmas to the LSIC granitoids contain high total REE, low $SiO_2$, and are olivine normative. These samples lie on the saturated side of the "critical plane of silica saturation" in terms of normative olivine - diopside - hypersthene and fractional crystallization in the LSIC leads to quartz normative compositions.

The earliest crystallized phase in the LSIC rocks is clinopyroxene which exhibits a slight Wo enrichment trend with host rock evolution and chemistry consistent with polybaric crystallization. The dominance of pyroxene in mafic rocks of the LSIC, invariably overgrown by hornblende, and the general rarity of clinopyroxene compared to hornblende in the more evolved rocks indicates that a combination of temperature decrease and increasing melt $H_2O$ content facilitated the crystallization of hornblende at the expense of clinopyroxene. The melt was initially undersaturated in $H_2O$, but approached $H_2O$ saturation, stabilizing hornblende and biotite, and inhibiting the crystallization of plagioclase. This paragenesis is supported by mineral and whole rock chemistry. The observed paragenesis is consistent with calc-alkaline andesite melting studies (Green, 1982) to occur between 1-5 kbar which is supported by the $Al^{TOT}$ in hornblende pressure estimates < 2.3 kbar and an average value of ~1 kbar depending upon the method chosen.

The variability exhibited in the major and trace element data suggests that multiple sources may have contributed to the parent LSIC melts. This would explain the contemporaneous existence of contrasting magmas in the LSIC more adequately than a single inhomogeneous magma chamber which could give rise to both felsic and mafic melts. These melt bodies experienced similar fractional crystallization histories, part of which was polybaric and occurred prior to emplacement at ~1 kbar.

The probable melt tapping mechanism that facilitated emplacement of the LSIC is undoubtedly similar to that which allowed for emplacement of the Lac Freschette complex (Miles, 1993). Sawyer and Barnes (1994) suggest that the LSIC and other monzodiorite association intrusions in the vicinity of the Lac des Quinze complex are the product of melt intrusion into space created by extensional shearing.

The initial melt for the granitoids appears to have been derived from the lithospheric mantle within the stability field of garnet at approximately 30 kbar. The initial melts for the hornblendites also were derived from a mantle source within the stability field of garnet, possibly at up 60 kbar. It is uncertain whether the hornblendites initiated melting at shallower mantle levels to produce the initial granitoid melts, or these contrasting melts were generated by a common process. The intimate association of alkali-LREE enriched hornblendites and granitoids, which exhibit linear Harker relations, indicates a common source for both suites. That fact that this type of hornblendite appears to only be associated with shoshonitic to high-K-medium-K transitional intrusive rocks in the Pontiac Subprovince also support a common origin. High alkali abundances and elevated LREE/HREE ratios are unusual for other mafic and ultramafic hornblendites within the Pontiac Subprovince (Camire et al, 1993)

except for calc-alkaline lamprophyres. The higher percentage of anhydrous minerals present in the hornblendites indicates that the source for the hornblendites was drier than that of the granitoids.

## 8.4 Implications of High $\varepsilon Nd_T$ Secondary Minerals

The high $\varepsilon Nd_T$ associated with the epidotes are inferred to be related to alteration. The epidote REE source was the local host rock, a valid assumption considering the accepted low mobility's of the REE during alteration and a lack of evidence for pervasive host rock alteration. The timing of epidote crystallization can be evaluated from whole rock Sm/Nd and epidote $\varepsilon Nd_T$ and $\varepsilon Nd_0$. The εNd evolution of the epidote host rocks can be approximated by the Sm/Nd of the host rock and an initial $\varepsilon Nd_T$ between +2 - +4, the observed LSIC variation from primary minerals. Intersection of the epidote evolution line and host rock evolution field provides an estimate of the time of secondary mineral crystallization (Figure 39). The range in potential time of epidote crystallization obtained from this method is 1.6-2.2 Ga with an average of ~2 Ga.

Other dates for Archean rocks and minerals from the Abitibi and Pontiac Subprovince are similar to the LSIC epidote ages. Carignan et al (1993) obtained anomalous Pb-Pb dates from sulphide separates of ~1.8 - 2.2 Ga from Pontiac Subprovince Ni-Cu sulphide occurrences. Dupre et al (1984) note anomalous U-Pb ages of 2.2 Ga in spinifex textured komatiite flows in Munro township of the Abitibi Subprovince. Brevart et al (1986) found anomalous Pb-Pb dates of 2160+/-80 Ma for komatiites (Theo's Flow) from Munro Township. Gariepy at al (1984) noted lower U-Pb intercepts in populations of zircons from

**LEGEND**

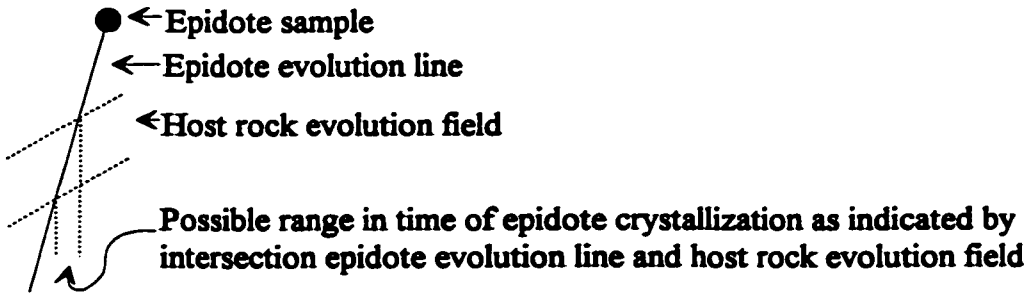


QNdfNd/Sm=−6.95 (921014−9)

Slope parameter (-6.95) for host rock sample (921014-9) used to define orientation of evolution field. Equation from DePaolo and Wasserburg (1976), where QNd = 25.13. fSm/Nd is the rock Sm/Nd enrichment factor relative to CHUR defined as: ((147Sm/144Nd rock)/0.1967)-1 (Farmer and DePaolo, 1983).

Figure 39. Epidote εNd evolution through time is compared to their respective host rock evolution fields. The evolution fields of the host rock is dependent upon the Sm/Nd ratio of the host rock and the observation that primary LSIC minerals record εNd between +2 and +4 at 2.68 Ga. The intersection of the epidote evolution lines with their host rock evolution fields suggest epidote crystallization at ~1.8 - 2 Ga. See legend for key to evolution diagram on facing page.

# Evaluation of the Timing of Epidote Crystallization

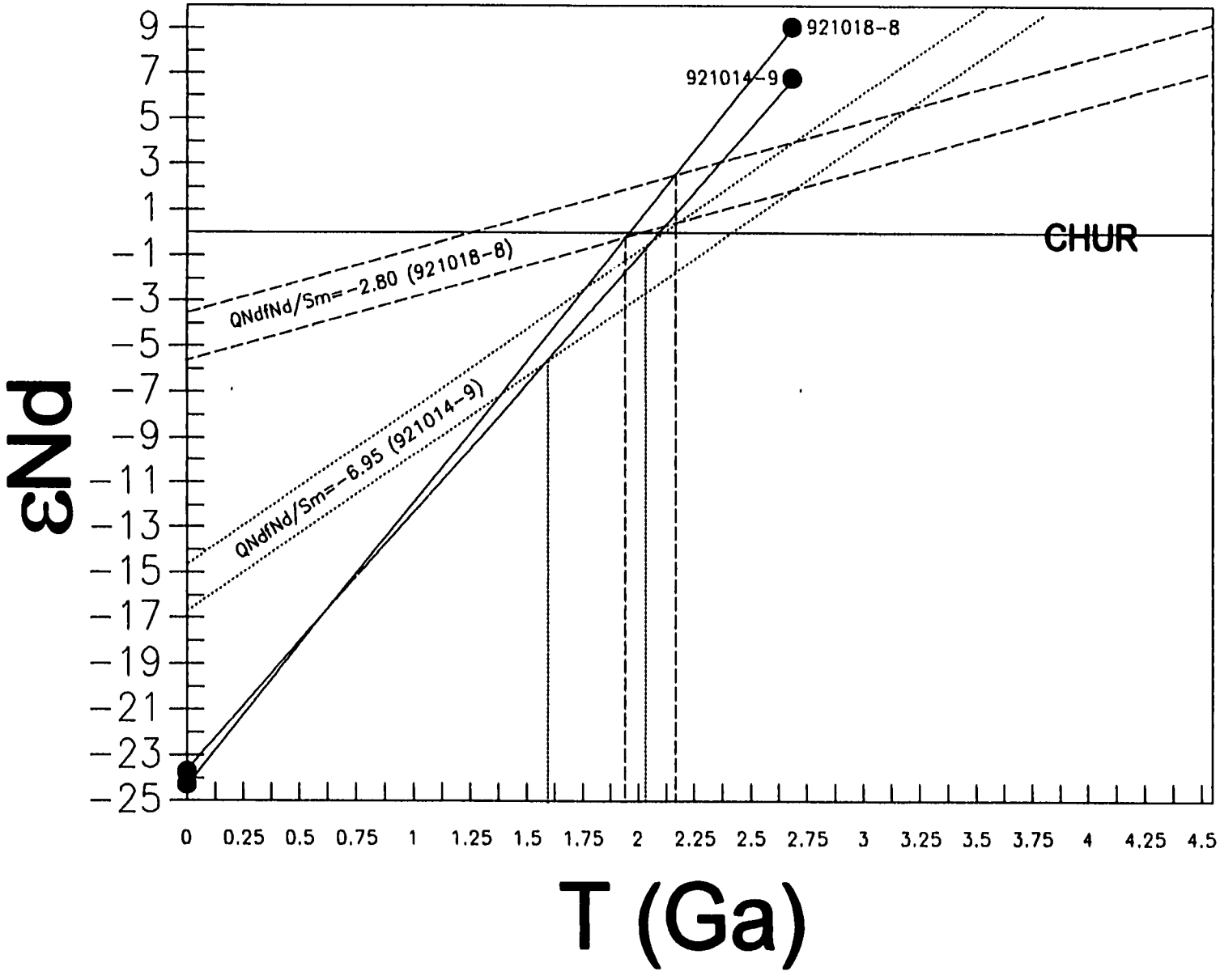

sedimentary rocks in the northern Pontiac Subprovince which yielded ages of ~2100 Ma. These young ages relative to that of the host rock ages (~2690 - ~2705 Ma; Mortensen and Card, 1993) may be attributed to a Proterozoic thermal event(s) within the Pontiac (i.e. Carignan et al, 1993).

Feng et al (1992) obtained biotite separates of Pontiac sedimentary schists approximately 10 km north of the LSIC for $^{40}Ar/^{39}Ar$ age determination. Maximum $^{40}Ar/^{39}Ar$ ages are 2023 - 2215 Ma which Feng et al (1992) suggest "has no geological implication" and "do not correspond to real geological events". Similarity in epidote crystallization ages and anomalous sulphide ages, U-Pb and Pb-Pb komatiite whole rock ages, and biotite $^{40}Ar/^{39}Ar$ ages suggests influence by a common thermal event(s). The only intrusive activity that correlates with this range of ages is Nipissing (~2110-2219 Ma; Krogh et al, 1987 and references therein. 2212 ± 2 Ma; Buchan et al, 1991) and Priessac (~2140Ma; Hanes, 1979. 2166.5 ± 1.5Ma; Buchan et al, 1991) diabase dyking (Carignan et al, 1993). It is inferred that these intrusive events may have initiated hydrothermal activity in the Pontiac Subprovince (Carignan et al, 1993). Although the ability of diabase dikes to initiate significant hydrothermal circulation is questionable (Delaney, 1987), limited, localised circulation cells may have been established which could have mobilised, Pb, U, REE on a small scale. Small scale perturbation of these isotope systems is suggested by other rocks or sulphides obtained in close vicinity to altered samples in which original crystallization ages were obtained (Dupre et al, 1984; Brevart et al, 1986).

This event was probably widespread as rocks within the Abitibi and Pontiac Subprovinces were affected at this time and suggests that diabase dyking may be the cause

isotopic age resetting. Ashwal et al. (1985) note an anomalous mineral - rock Sm-Nd isochron for slightly altered samples from the ~2.7 Ga Bad Vermilion anorthosite complex of 2.16 ± 0.05 Ga implying that the isotopic resetting event was apparently Superior Province wide. The only widespread thermal event that could lead to localised resetting of isotopic systems Superior Province wide is likely diabase dyking.

## 8.5 Origin of Enclaves

Barbarin (1995) and Tobisch et al (1995) suggest that polygenic swarms (Plate 15a, 15b) may result from either gravitational sorting and settling of enclaves, viscosity related bottlenecking of magma flow in conduits allowing for the mingling of contrasting magmas, or collection of magma globules in eddies. The association of these polygenic swarms at highly mingled contacts and areas with mafic dyking suggests that these regions may have been the locus of magma injection.

Felsic enclaves have been suggested to originate from disruption of early chilled margins by ascent of granitic magmas (Didier and Barbarin, 1990), a process compatible with the recognized contemporaneous nature of magmatism in the complex and occurrence of FME.

Monogenic swarms of MME typically are produced close to the site of magma mixing (Didier and Barbarin, 1990). The spatial association to compositionally similar mafic dykes (Plate 16a) suggests that derivation of some of the fine grained MME in the LSIC is a product of commingling of mafic and felsic magmas. The presence of disrupted dykes, forming trains of subangular to subround enclaves, also attests to the ability of contemporaneous dyking to

Plate 15a. Polygenic enclave pod exposed in outcrop. The pod is approximately 1x2 m in dimension and composed enclaves oriented generally parallel to the long axis of the pod.

Plate 15b. Close-up photograph of the polygenic enclave pod. Enclaves comprising the polygenic enclave pod are subangular and vary widely in modal abundance of amphibole and feldspar.

a)

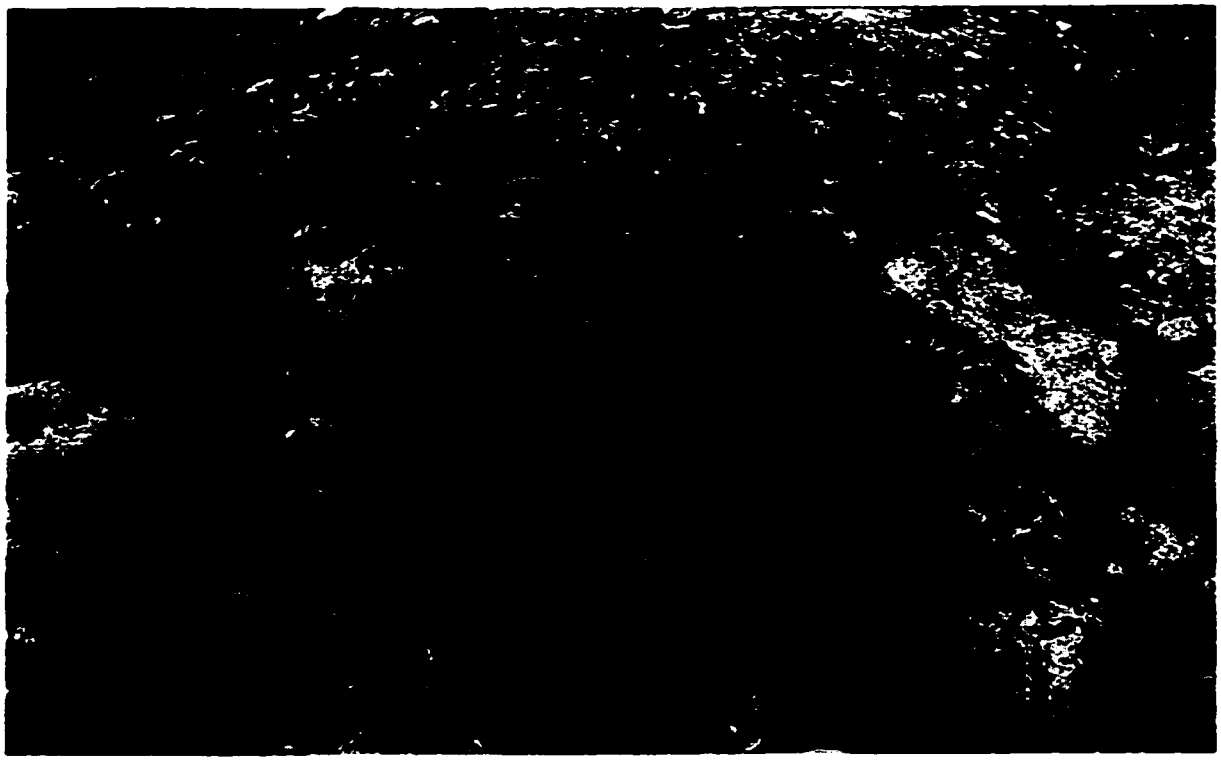

b)

Plate 16a. Mafic dyke and mafic enclave association. Mafic dyke above hammer is associated with high concentrations of mafic enclaves which appear to form a train like distribution and are similar in appearance to the mafic dyke. These enclaves are interpreted to have originated from disrupted dykes.

Plate 16b. Wispy mafic mineral patches in a granitoid of the south complex of the LSIC. Form and distribution of patches is indicative of mingling between mafic and felsic melts.

a)

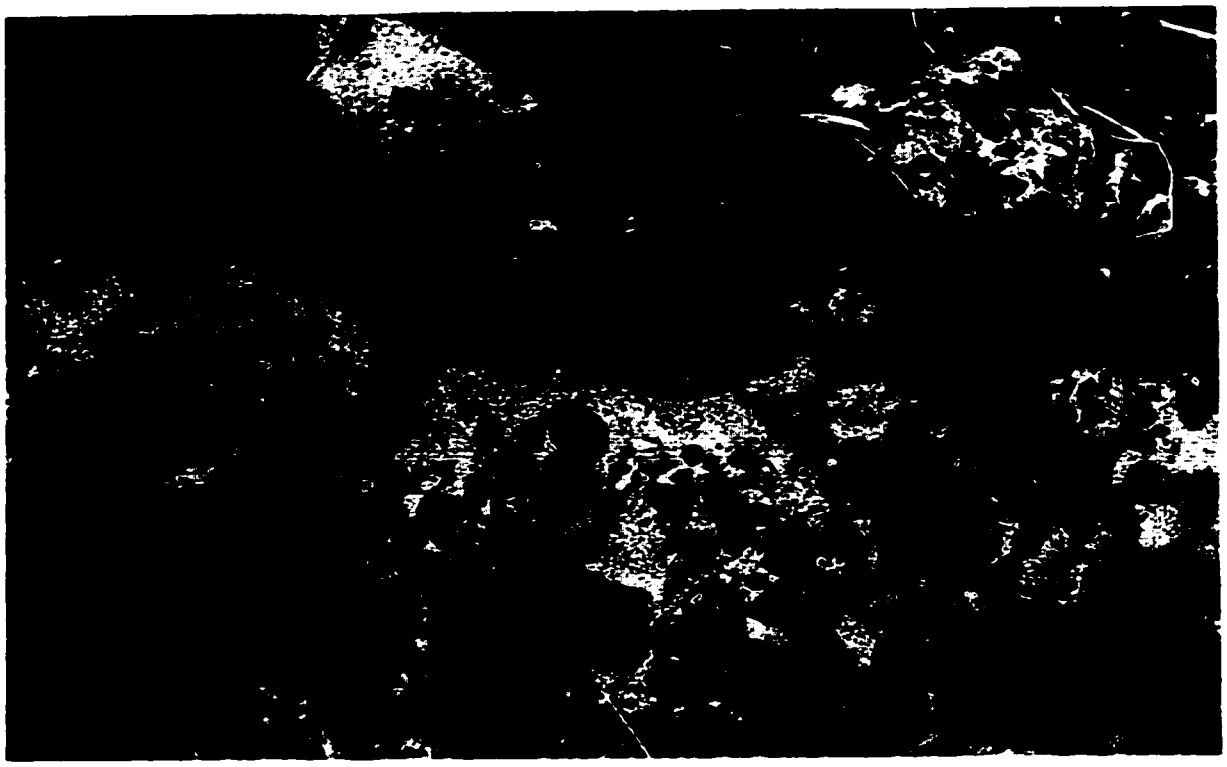

b)

produce these fine grained MME in the complex. Finer grained margins on some actinolitic MME, interpreted as chill margins, suggest that the mafic melt intruded a cooler host. Back veining and pinching of mafic dykes indicates that dyking occurred within a partially molten magma host.

Autolithic xenoliths are also present as re-incorporated cumulates and enclaves of disrupted margin material of contemporaneous magma batches. Cumulate textured coarse diorites are interpreted to represent re-incorporated cumulate material. Finer grained melano-diorites are petrographically similar to some mafic dykes but also are similar to some dioritic phases of the complex. Readily identifiable autolithic dioritic xenoliths (can be traced to a dioritic unit) are coarser grained than the dioritic MME produced through commingling.

Injections of mafic magmas appears to have taken place throughout the crystallization history of the complex and manifested as a range in mixing textures dependent on the viscosity contrast of the dyke to the felsic host. The coexistence of enclaves, dykes and amphibolitic ameboid patches suggest variable viscosity contrasts between mafic melt and the felsic host. These coexisting textures suggests that initially mafic melts intruded a relatively low viscosity felsic melt whose convectivity was high enough to allow for near complete homogenization of the mafic melt. This mingling produced mafic crystal clots of amphibole, titanite, magnetite and occasional calcic clinopyroxene, and the wispy amphibolitic patches observed in outcrop (Plate 16b). With increasing host viscosity, mafic melt injections form fine grained ovoids that may become attenuated during viscous convection of the host magma. When host viscosity is high, disrupted dykes form trains of subround to subangular enclaves that may not display fine grained chill margins. At greater viscosity, dykes do not disrupt but may pinch by tangential

shear in the mobile plastic host or, since the dyke may be less viscous than the host at this point, localize shear such that the dyke develops a strong dyke contact parallel foliation.

Actinolitic enclaves comprise up to 80% of some coarse grained (cumulate) outcrops. These enclaves are elongated, flattened, and impinge on adjacent enclaves such that dents are formed in one enclave at their contact. This feature is interpreted to result from sinking and accumulation of mafic material with compaction of the still plastic enclaves as the cumulate diorites are being generated. Enclave flattening and attenuation by deformation is not supported by the random orientations of the cumulate minerals and the lack of microstructural evidence (subgraining, broken grains, pressure solution shadows, rotation) indicating post solidus deformation did not produce the elongate enclave shapes.

## Chapter 9 Conclusions

- The LSIC does not include the granodiorites mapped by Rive (1986) to the south and east of the LSIC. These dominantly tonalitic rocks are intruded by the LSIC, are texturally similar to the Belleterre - Fugerville tonalites and are chemically equivalent to these rocks. A lack of mafic enclaves also discriminate these and other rocks from the LSIC.

- Contacts of the LSIC with the surrounding supracrustal rocks occurs are intrusive and sheared intrusive contacts between units. Xenoliths of these supracrustal rocks are typically angular and partially assimilated (sedimentary rock xenoliths) and sporadically distributed throughout the complex, although typically in higher concentration near the external contacts of the LSIC.

- The LSIC consists of multiple cogenetic mutually intrusive units that display both gradational and sharp contacts. Gradational contacts are inferred to be the result of in-situ fractionation and contact mixing between adjacent units, whereas the range of rocks types comprising the mutually intruding units reflects fractionation in either a heterogeneous lower level magma chamber, or derivation from multiple chambers.

- Granitoids are medium-K calc-alkaline to shoshonitic, generally intermediate in $SiO_2$ and the modal mineralogy of the granitoids of the LSIC define a range from diorite to syenite and quartz monzodiorite to quartz monzonite with minor granodiorite.

- Initial melts for the LSIC granitoids were dominantly shoshonitic in composition. Precursor granitoids are characterized by negative Nb/Nb*, Ti/Ti*, generally negative Zr/Zr*, and absent to weakly developed negative Eu anomalies. High Cr and $Mg^{\#}$ are indicative of primitive granitoids representing near primary mantle melts. Total REE are high and samples are high in LREE/HREE and are HREE are fractionated. High LILE/HFSE and negative HFSE anomalies indicate an arc type magmatic affinity. Chemical composition of the granitoids is inconsistent with OIB or MORB sources, and an arc source is indicated. Fractionated HREE suggest derivation from a mantle source in which garnet was residual.

- The LSIC is composed of granitoids and hornblendites which have evolved from multiple, but generally compositionally similar primary liquids. Trace element and mineral chemistry suggest that at least three parental magma compositions were involved.

- Hornblendites within the LSIC represent cogenetic units with the granitoids. The hornblendites are high in $Mg^{\#}$, MgO, Cr and represent primary mantle melts. High LREE/HREE, fractionated HREE, high LILE and negative Zr/Zr* and Nb/Nb* indicate derivation from metasomatised garnet lherzolite in a convergent margin geodynamic setting.

- Hornblendites are not cumulates composed of fractionated granitoid minerals. They represent a unique liquid composition. Hornblendite liquids have experienced differing histories of interaction with crustal material. Some intrusions (high Zr hornblendites) record assimilation of up to ~40% Pontiac sedimentary rock whereas others (low Zr hornblendites) are uncontaminated. The contamination process affecting the high Zr hornblendites is characterized by a decoupling of major and trace elements. A similar decoupling process has been observed in other locales (i.e. Banda arc and Italy) were similar rocks as the LSIC occur. In Italy, this decoupling process is the result of source metasomatism by sedimentary rock derived fluids. As an alternative process then, the non-isochemical crustal contamination effects observed in the LSIC may also be a source related feature rather than variation generated by contamination during magma emplacement

- The dominant process controlling the range in granitoid compositions is fractional crystallization. At $SiO_2$ concentrations <55 wt.%, fractionation is dominated by clinopyroxene ± hornblende. At greater $SiO_2$ concentrations, the fractionation of biotite and other silica undersaturated minerals, such as magnetite, titanite, and apatite becomes important in controlling the composition of the granitoids. The declining REE with fractionation is governed by titanite and apatite crystallization. Zircon crystallization is minor and Zr increases with fractionation. High whole rock Sr, decreasing whole rock $CaO/Al_2O_3$ and constant to increasing wollastonite components and increasing jadeite component of clinopyroxene suggest that plagioclase removal was negligible. Granitoids

evolve by fractional crystallization towards quartz normative, calc-alkaline compositions and increase in peralkalinity and peraluminosity.

- Systematic and coherent pyroxene compositional relations over a range of rock types and $SiO_2$ concentrations at the LSIC also indicate a cogenetic origin for all units of the LSIC. The decreasing pressures and zonation recorded in pyroxene grains indicate that periodic mafic magma infusion may have provided impetus for the emplacement of magma batches from magma chamber(s) to shallower levels resulting in the composite and mutually intrusive nature of the LSIC units.

- Initial granitoid melts were probably $H_2O$ undersaturated (< ~2.5 wt.% $H_2O$) and possessed initial temperatures in the order of 1000°C+. The $H_2O$ concentrations increased towards saturation with crystallization leading to the crystallization of a hydrous mineralogy, early crystallization of magnetite, and the inhibition of plagioclase crystallization. Initial hornblendite melts were dryer than granitoid melts but also approached saturation as evidenced by the abundance of hornblende and biotite. It is possible that uralitization of clinopyroxene, hematization of magnetite, titanization of amphibole and magnetite, crystallization of barite, and K-metasomatism of ultramafic units adjacent to the LSIC is the product of post solidus (oxidizing) fluid migration.

- The depth of final emplacement of the LSIC has been estimated from the total aluminum content of granitoid hornblendes at ~ 1 kbar. Clinopyroxene barometry indicates that

crystallization was likely polybaric. Whole rock chemistry of the granitoids indicates initial melt extraction occurred at a depth of approximately 3 GPa whereas hornblendite melts may have been derived at up to 6 GPa. This source was relatively oxidized since REE patterns of the initial granitoid and hornblendite melts do not possess Eu anomalies. Estimated $fO_2$ for the granitoids also suggests the magma was relatively oxidized with $fO_2$ equivalent to the TMQH buffer at 800°C. This is in accord with the observed mineral assemblage titanite+magnetite+quartz, biotite+amphibole, the low Ti contents of amphibole, and the high magnetic response of the LSIC on aeromagnetic surveys as a result of high magnetite concentrations.

- Primary minerals range from $\varepsilon Nd_T$ +1.4 - +3.9 and $^{87}Sr/^{86}Sr_I$ = 0.70080 - 0.70138. $\varepsilon Nd_T$ is within the range observed for Archean mantle derived rocks and $^{87}Sr/^{86}Sr_I$ is generally within the range of $^{87}Sr/^{86}Sr_I$ that is typically observed for ultramafic - mafic and alkaline Abitibi Subprovince rocks. $\varepsilon Nd_T$ indicate that the source for the LSIC was long term depleted in LREE, but high LILE and LREE/HFSE and high ΣREE indicate the metasomatic enrichment event predated emplacement by a short time period.

## REFERENCES


Adam, J., Green, T.H. and Sie, S.H., 1993. Proton microprobe determined partitioning of Rb, Sr, Ba, Y, Zr, Nb and Ta between experimentally produced amphiboles and silicate melts with variable F content. Chemical Geology, 109: 29-49.

Anderson, J.L. and Smith, D.R., 1993. Success and failure of the Al - in - hornblende barometer. Geological Society of America Program with Abstracts, A-41.

Anderson, J.L. and Smith, D.R., 1995. The effects of temperature and $f_{O_2}$ on the Al-in-hornblende barometer. American Mineralogist, 80: 549-559.

Aoki, K. and Kushiro, I., 1968. Some clinopyroxenes from ultramafic inclusions in Deiser Weiher, Eifel. Contributions to Mineralogy and Petrology, 18: 326-337.

Aoki, K. and Shiba, I., 1973. Pyroxenes from lherzolitic inclusions of Itinomegata, Japan. Lithos, 6: 41-51.

Arth, J.G. and Hanson, G.N., 1975. Geochemistry and origin of the early Precambrian crust of northeastern Minnesota. Geochimica et Cosmochimica Acta, 39: 325-362.

Ashwal, L.D., Wooden, J.L., Phinney, W.C. and Morrison, D.A., 1985. Sm-Nd and Rb-Sr Isotope systematics of an Archean anorthosite and related rocks from the Superior Province of the Canadian Shield. Earth and Planetary Science Letters, 74: 338-346.

Avramtchev, L. and Lebel-Drolet, S., 1981. Catalogue des Gîtes Minéraux du Québec - Région de L'Abitibi: MERQ, DPV 744, 97p.

Barbarin, B., 1995. The Enclave Swarms in some Granitoids of the Sierra Nevada Batholith, California: Indicators of Magma Interactions and Evolution. *In: The Origin of Granites and Related Rocks*, Hutton Symposium III, Abstracts. U.S. Geological Survey Circular, 1129, p13.

Barberi, F., Bizouard, H. and Varet, J., 1971. Nature of the clinopyroxene and iron enrichment in alkalic and transitional basaltic magmas. Contributions to Mineralogy and Petrology, 33: 93-107.

Barnes, S-J., Couture, J.-F., Sawyer, E.W. and Bouchaib, C., 1993. Nickel - Copper Occurrences in the Belleterre - Angliers Belt of the Pontiac Subprovince and the use of Cu-Pd Ratios in Interpreting Platinum Group Element Distributions. Economic Geology, 88: 1402-1418.

Barrie, C.T., 1990. U-Pb garnet and titanite age for the Bristol Township lamprophyre suite, western Abitibi Subprovince. Canadian Journal of Earth Sciences, 27: 1451-1456.

Barrie, C. T., and Shirey, S.B., 1991. Nd and Sr isotope systematics for the Kamiskotia - Montcalm area: implications for the formation of the late Archean crust in the western Abitibi Subprovince, Canada. Canadian Journal of Earth Sciences, 28: 30pp.

Barrie, C. T., 1995. Zircon thermometry of high-temperature rhyolites near volcanic-associated massive sulfide deposits, Abitibi Subprovince, Canada. Geology, 23: 169-172.

Barth, T.F.W., 1968. Additional Data for the two - feldspar geothermometer. Lithos, 1: 305-306.

Batchelor, R.A. and Bowden, P., 1985. Petrogenetic interpretation of granitoid rock series using multicationic parameters. Chemical Geology, 48: 43-55.

Beattie, P., Drake, M., Jones, J., Leeman, W., Longhi, J., McKay, G., Nielsen, R., Palme, H., Shaw, D., Takahashi, E. and Watson, B., 1993. Terminology for trace-element partitioning. Geochimica et Cosmochimica Acta, 57: 1605-1606.

Benn, K., Miles, W., Ghassemi, M.R. and Gillett, J., 1994. Crustal structure and kinematic framework of the northwestern Pontiac Subprovince, Quebec: an integrated structural and geophysical study. Canadian Journal of Earth Sciences, 31: 271-281.

Bertrand, P. and Mercier, J.-C.-C., 1985. The mutual solubility of coexisting ortho- and clinopyroxene; toward an absolute geothermometer for the natural system. Earth and Planetary Science Letters, 76: 109-122.

Blundy, J.D. and Wood, B.J., 1991. Crystal-chemical controls on the partitioning of Sr and Ba between plagioclase feldspar, silicate melts, and hydrothermal solutions. Geochimica et Cosmochimica Acta, 55: 193-209.

Bonin, B. and Giret, A., 1984. The plutonic alkaline series: the problem of their origin and differentiation, the role of their mineralogical assemblages. Physics of the Earth and Planetary Interiors, 35: 212-221.

Brévart, O., Dupré, B and Allègre, C.J., 1986. Lead-lead age of komatiitic lavas and limitations on the structure and evolution of the Precambrian mantle. Earth and Planetary Science Letters, 77: 293-302.

Brooks, C., Ludden, J., Pigeon, Y. and Hubregtse, J.J.M.W., 1982. Volcanism of shoshonite to High-K andesite affinity in an Archean arc environment, Oxford Lake, Manitoba. Canadian Journal of Earth Sciences, 19: 55-67.

Brown, E.H., 1977. The croissite content of Ca-Amphibole as a Guide to Pressure of Metamorphism. Journal of Petrology, 18: 53-72.

Brown, W.L. and Parsons, I., 1981. Towards a more practical two-feldspar thermometer. Contributions to Mineralogy and Petrology. 76: 369-377.

Buchan, K.L., Mortensen, J.K. and Card, K.D., 1991. U/Pb dating of emplacement and paleomagnetic remanences of Preissac dykes and Nipissing intrusions of the southern Canadian Shield. Geological Association of Canada - Mineralogical Association of Canada, Program with Abstracts, 16: A16.

Burkhard, D.J.M., 1991. Temperature and redox path of biotite-bearing intrusives: a method of estimation applied to S- and I-type granites from Australia. Earth and Planetary Science Letters, 104: 89-98.

Burnham, C.W., 1979. Magmas and hydrothermal fluids. *In* Barnes, H.L., (ed) Geochemistry of Hydrothermal Ore Deposits, 2nd edition, John Wiley and Sons, Inc., 71-136.

Burnham, C.W. and Ohmoto, H., 1980. Late-Stage Processes of Felsic Magmatism. Mining Geology Special Issue, 8: 1-11.

Camiré, G.E., Ludden, J.N., La Flèche, M.R. and Burg, J.-P., 1993. Mafic and ultramafic amphibolites from the northwestern Pontiac Subprovince: chemical characterization and implications for tectonic setting. Canadian Journal of Earth Sciences, 30: 1110-1122.

Camiré, G.E. and Burg, J.-P., 1993. Late Archaean thrusting in the northwestern Pontiac Subprovince, Canadian Shield. Precambrian Research, 61: 51-66.

Carignan, J., Machado, N. and Gariépy, C., 1993. Pb Isotope composition of Ni-Cu-Pb ore deposits in an Archean greenstone belt: Evidence for Proterozoic remobilization in the Pontiac Subprovince of Canada. Economic Geology, 88: 709-715.

Carignan, J., Machado, N. and Gariépy, C., 1995. U-Pb isotopic geochemistry of komatiites and pyroxenes from the southern Abitibi greenstone belt, Canada. Chemical Geology, 126: 17-27.

Cattell, A., Krogh, T.E. and Arndt, N.T., 1984. Conflicting Sm-Nd whole rock and U-Pb zircon ages for Archean lavas from Newton Township, Abitibi Belt, Ontario. Earth and Planetary Science Letters, 70: 280-290.

Chagnon, J.-Y., 1968. Région des lacs des Quinze et Barrière. Quebec Department of Natural Resources, Geological Report 134.

Chappell, B.W. and White, A.J.R., 1974. Two contrasting granite types. *Pacific Geology. Tokyo.* Vol. 8 p. 173-174.

Chauvel, C., Goldstein, S.L. and Hofmann, A.W., 1995. Hydration and dehydration of oceanic crust controls Pb evolution in the mantle. Chemical Geology, 126: 65-75.

Chou, I-M., 1978. Calibration of oxygen buffers at elevated P and T using the hydrogen fugacity sensor. American Mineralogist. 63: 690-703.

Cocherie, A., 1986. Systematic use of trace element distribution patterns in log-log diagrams for plutonic suites. Geochimica et Cosmochimica Acta, 50: 2517-2522.

Cooper, A.F., 1972. Progressive metamorphism of metabasic rocks from the Haast schist group of southern New Zealand. Journal of Petrology, 13: 457-492.

Condie, K.C., 1982. Archean andesites. *In*: Thorpe, R.S., (ed) *Andesites*. Wiley, Chichester.

Corfu, F., Krogh, T.E., Kwok, Y.Y., and Jensen, L.S., 1989. U-Pb zircon geochronology in the southwestern Abitibi greenstone belt, Superior Province. Canadian Journal of Earth Sciences, 26: 1747-1763.

Czamanske, G.K., and Wones, D.R., 1973. Oxidation during magmatic differentiation, Finnmarka Complex. Oslo area, Norway: Part II, The mafic silicates. Journal of Petrology, 14: 349-380.

Dal Negro, A., Carbonin, S., Molin, G.M., Cundari, A. and Piccirillo, E.M., 1982 Intracrystalline cation distribution in natural clinopyroxenes of tholeiitic, transitional, and alkaline basaltic rocks. In: S.K. Saxena (ed), *Advances in Physical Geochemistry*. Springer, New York, N.Y., 117—150.

Dawson, J.B., Smith, J.V., Steele, I.M., 1994. Trace-element distribution between coexisting perovskite, apatite and titanite from Oldoinyo Lengai, Tanzania. Chemical Geology, 117: 285-290.

De la Roche, H., Leterrier, J., Grandclaude, P., and Marchal, M., 1980. A classification of volcanic and plutonic rocks using R1 R2 -diagram and major-element analyses; its relationships with current nomenclature. Chemical Geology.29; 183-210.

Deer, W.A., Howie, R.A., and Zussman, J., 1962a. *Rock Forming Minerals*, Vol. 5. Non - Silicates. Longmans, London. p 68-77.

Deer, W.A., Howie, R.A., and Zussman, J., 1962b. *Rock Forming Minerals*, Vol. 3. Sheet Silicates. Longmans, London. p. 57.

Deer, W.A., Howie, R.A., and Zussman, J., 1962c. *Rock Forming Minerals*, Vol. 1. Ortho- and Ring Silicates. Longmans, London. p. 69-76.

Delaney, P.T., 1987. Heat Transfer during Emplacement and Cooling of Mafic Dykes. In: Halls, H.C. and Fahrig, W.F. (Eds). *Mafic dyke swarms*. Geological Association of Canada Special Paper 34, p. 31-46.

Denis, B.T., 1937. Région du Lac Simard. M.M.Q. - Rapport annuel pour l'année. 1936. Partie B.

Depaolo, D.J., and Wasserburg, G.J., 1976. Nd isotopic Variations and Petrogenetic models. Geophysical Research Letters, 3: 249-252.

DePaolo, D.J., 1981. Trace element and isotopic effects of combined wallrock assimilation and fractional crystallization. Earth and Planetary Science Letters, 53: 189-202.

Dimroth, E., Imreh, L., Rocheleau, M., Goulet, N., 1982. Evolution of the south-central part of the Archean Abitibi Belt, Quebec. Part I: Stratigraphy and paleogeographic model. 19: 1729-1758.

Dimroth, E., Imreh, L., Goulet, N. and Rocheleau, M., 1983. Evolution of the south-central segment of the Archean Abitibi Belt, Quebec. Part II: Tectonic evolution and geomechanical model. Canadian Journal of Earth Sciences, 20: 1355-1373.

Dobosi, G. and Fodor, R.V., 1992. Magma fractionation, replenishment, and mixing as inferred from green-core clinopyroxenes in Pliocene basanite, southern Slovakia. Lithos, 28: 133-150.

Dostal, J., Dupuy, C, Carron, J.P., Le Guen De Kerneizon, M. and Maury, R.C., 1983. Partition coefficients of trace elements: application to volcanic rocks of St. Vincent, West Indies. Geochimica et Cosmochimica Acta, 47: 525-533.

Dupré, B., Chauvel, C. and Arndt, T., 1984. Pb and Nd isotopic study of two Archean komatiitic flows from Alexo, Ontario. Geochimica et Cosmochimica Acta, 48: 1965-1972.

Ewart, A., 1982. The mineralogy and petrology of Tertiary - Recent orogenic volcanic rocks with special reference to the andesitic - basaltic compositional range. *In*: Thorpe, R.S., (ed) *Andesites*. Wiley, Chichester.

Ewart, A. and Griffin, W.L., 1994. Application of proton-microprobe data to trace-element partitioning in volcanic rocks. Chemical Geology, 117: 251-284.

Faraone, D., Molin, G. and Zanazzi, P.F., 1988. Clinopyroxenes from Vulcano (Aeolian Islands, Italy): Crystal chemistry and cooling history. Lithos, 22: 113-126.

Farmer, G.L., and DePaolo, D.J., 1983. Origin of Mesozoic and Tertiary granite in the western United States and implications for pre-Mesozoic crustal structure 1. Nd and Sr isotopic studies in the geocline of the Northern Great Basin. Journal of Geophysical Research. 88: 3379-3401.

Feng, R., Kerrich, R. and Maas, R., 1993. Geochemical, oxygen, and neodymium isotope compositions of metasediments from the Abitibi greenstone belt and Pontiac Subprovince, Canada: Evidence for ancient crust and Archean terrane juxtaposition. Geochimica and Cosmochimica Acta, 57: 641-658.

Feng, R., Kerrich, R., McBride, S. and Farrar, E., 1992. $^{40}Ar/^{39}Ar$ age constraints on the thermal history of the Archean Abitibi greenstone belt and the Pontiac Subprovince: implications for terrane collision, differential uplift, and overprinting of gold deposits. Canadian Journal of Earth Sciences, 29: 1389-1411.

Feng, R. and Kerrich, R., 1992. Geochemical evolution of granitoids from the Archean Abitibi Southern Volcanic Zone and the Pontiac Subprovince, Superior Province, Canada: implications for tectonic history and source regions. Chemical Geology, 98: 23-70.

Forsythe, L.M., Nielsen, R.L. and Fisk, M.R., 1994. High-field-strength element partitioning between pyroxene and basaltic to dacitic magmas. Chemical Geology, 117: 107-126.

Francalanci, L., 1989. Trace element partition coefficients for minerals in shoshonitic and calc-alkaline rocks from Stromboli Island (Aeolian Arc). Neues Jahrbuch fur Mineralogie Abhandlungen. 160; 229-247.

Fujimaki, H., 1986. Partition coefficients of Hf, Zr, and REE between zircon, apatite, and liquid. Contributions to Mineralogy and Petrology, 94: 42-45.

Gariépy, C. , Allègre, C.J. and Lajoie, J., 1984. U-Pb systematics in single zircons from the Pontiac sediments, Abitibi greenstone belt. Canadian Journal of Earth Sciences, 21: 1296-1304.

Ghandi, S.S., 1970. Petrology of the Monteregian intrusions of Mount Yamaska, Quebec. The Canadian Mineralogist, 10: 452-484.

Ghassemi, M.R., 1996. Tectonic evolution of the Late Archean Pontiac Subprovince, Superior Province, Canada: Structural, metamorphic, and geochronological studies. Ph.D. Thesis. University of Ottawa.

Gill, J.B., 1981. *Orogenic Andesites and Plate Tectonics*. New York. Springer Verlag.

Giret, A., Bonin, B., and Leger, J.M., 1980. Amphibole compositional compositional trends in oversaturated and undersaturated alkaline plutonic ring-complexes. Canadian Mineralogist. 18: 481-495.

Grand, S.P., 1987. Tomographic inversion for shear velocity beneath the North American plate. Journal of Geophysical Research, 92: 14065-14090.

Green, D.H., 1976. Experimental testing of "equilibrium" partial melting of peridotite under water-saturated, high-pressure conditions. Canadian Mineralogist, 14: 255-268.

Green, T.H., and Watson, E.B., 1982. Crystallization of apatite in natural magmas under high pressure hydrous conditions, with particular reference to "orogenic" rock series. Contributions to Mineralogy and Petrology, 97: 7-18.

Green, T.H. and Pearson, N.J., 1986. Rare-earth element partitioning between sphene and coexisting silicate liquid at high pressure and temperature. Chemical Geology, 55: 105-119.

Green, T.H., 1994. Experimental studies of trace-element partitioning applicable to igneous petrogenesis -- Sedona 16 years later. Chemical Geology, 117: 1-36.

Hammarstrom, J.M. and Zen, E.-A., 1986. Aluminum in hornblende: an empirical igneous geobarometer. American Mineralogist, 71: 1297-1313.

Hanes, J.A., 1979. An $^{40}Ar/^{39}Ar$ Geochronological Study of Precambrian Diabase Dykes: Ph.D. Thesis, University of Toronto, Toronto, Ontario; 240 p.

Hart, S.R., and Davis, K.E., 1978. Nickel partitioning between olivine and silicate melt. Earth and Planetary Science Letters. 40: 203-219

Hart, S.R. and Dunn T., 1993. Experimental Cpx/melt partitioning of 24 trace elements. Contributions to Mineralogy and Petrology, 113: 1-8.

Hattori, K., 1989. Barite-celestine intergrowths in Archean plutons: The product of oxidizing hydrothermal activity related to alkaline intrusions. American Mineralogist, 74: 1270-1277.

Hattori, K., 1993. High-sulfur magma, a product of fluid discharge from underlying mafic magma: Evidence from Mount Pinatubo, Philippines. Geology, 21: 1083-1086.

Hattori, K., Hart, S.R. and Shimizu, N., 1996. Melt and source mantle compositions in the late Archean: A study of strontium and neodymium isotope and trace elements in clinopyroxenes from shoshonitic alkaline rocks. Geochimica et Cosmochimica Acta, 60: 4551-4562.

Hawthorne, F.C., 1983. The crystal chemistry of Amphiboles. The Canadian Mineralogist. 21: 173-480.

Helz, R.T., 1973. Phase relations of basalt in their melting range at $PH_2O$ = 5kb as a function of oxygen fugacity. I. Mafic phases. Journal of Petrology, 14: 249-302.

Helz, R.T., 1982. Phase Relations and compositions of amphiboles produced in studies of the melting behavior of rocks *In* Veblin D.R., and P.H. Ribbe, (Ed). *Amphiboles: Petrology and Experimental Phase Relations*, vol. 9B, Reviews in Mineralogy, p 279-346.

Herzberg, C.T., 1992a. Depth and degree of melting of komatiites. Journal of Geophysical Research, 97: 4521-4540.

Herzberg, C., 1995. Generation of plume magmas through time: an experimental perspective. Chemical Geology, 126: 1-16.

Hewitt, D.A., 1978. A redetermination of the fayalite - magnetite - quartz equilibrium between 650° and 850°. American Journal of Science. 278: 715-724

Hocq, M., 1990. Carte lithotectonique des sous province de l'Abitibi et du Pontiac: Ministere l'Energie Ressources Quebec, DV 89-04.

Hollister, L., Grissom, C., Peters, E.K., Stowell, H.H. and Sisson, V.B., 1987. Confirmation of the empirical correlation of Al in hornblende with pressure of solidification of calc-alkaline plutons. American Mineralogist, 72: 231-239.

Huebner, J.S., and Sato, M., 1970. The oxygen fugacity - temperature relationships of manganese oxide and nickel oxide buffers. American Mineralogist. 55: 934-952.

Innocenti, F., Manetti, P., Mazzuoli, R., Pasquare, G., and Villari, L., 1982. Anatolia and north-western Iran. *In:* Thorpe, R.S., (ed) *Andesites*, Chichester, Wiley, 327-349.

Irvine, T.N., and Barager, W.R.A., 1971. A guide to the chemical classification of the common volcanic rocks, Canadian Journal of Earth Sciences. 8: 523-548.

Irving, A.J. and Frey, F.A., 1984. Trace element abundances in megacrysts and their host basalts: constraints on partition coefficients and megacryst genesis. Geochimica et Cosmochimica Acta, 48: 1201-1221.

Ishihara, S., 1977. The magnetite - series and ilmenite - series granitic rocks. Mining Geology, 27: 293-305.

Jakes, P. and White, A.J.R., 1972. Hornblende from calc-alkaline volcanic rocks of island arcs and continental margins. American Mineralogist, 57: 887-902.

Johnson, M.C., and Rutherford, M.J., 1989. Experimental calibration of the aluminum - in - hornblende geobarometer with application to Long Valley caldera (California) volcanic rocks. Geology, 17: 837-841.

Jolly, W.T., 1978. Metamorphic history of the Archean Abitibi belt. *In:* Fraser, J.A. and Heywood, W.W. (Eds). *Metamorphism in the Canadian Shield.* Geological Survey of Canada, Paper 78-10, p. 63-78.

Kretz, R., 1978. Distribution of Mg, $Fe^{+2}$, and Mn in some calcic pyroxene-hornblende-biotite-garnet gneisses and amphibolites from the Grenville Province. Journal of Geology.86: 599-619.

Kretz, R. and Jen, L.S., 1978. Effect of temperature on the distribution of Mg and $Fe^{2+}$ between calcic pyroxene and hornblende. Canadian Mineralogist, 16: 553-537.

Kretz, R., 1983. Symbols for rock-forming minerals. American Mineralogist, 68: 277-279.

Krogh, T.E., Corfu, F., Davis, D.W., Dunning, G.R., Heaman, L.M., Kamo, S.L., Machado, N., Greenough, J.D. and Nakamura, E., 1987. Precise U-Pb Isotopic Ages of Diabase Dykes and Mafic to Ultramafic Rocks Using Trace Amounts of Baddeleyite and Zircon. *In*: Halls, H.C. and Fahrig, W.F. (Eds). *Mafic dyke swarms.* Geological Association of Canada Special Paper 34, p. 147.

Lahaye, Y., Arndt, N., Byerly, G., Chauvel, C., Fourcade, S. and Gruau G., 1995. The influence of alteration on the trace element and Nd isotopic compositions of komatiites. Chemical Geology, 126: 43-64.

Lajoie, J., and Ludden, J., 1984. Petrology of the Archean Pontiac and Kewagama sediments and implications for the stratigraphy of the southern Abitibi Belt. Canadian Journal of Earth Sciences. 21: 1305-1314.

Le Bas, M.J., Le Maitre, R.W., Streckeisen, A. and Zanettin, B., 1986. A chemical classification of volcanic rocks based on the total Alkali-Silica Diagram. Journal of Petrology. Oxford, 27: 745-750.

Leeman, W.P., Ma, M.-S., Murali, A.V. and Schmitt, R.A., 1978. Empirical estimation of magnetite/liquid distribution coefficients for some transition elements. Contributions to Mineralogy and Petrology, 65: 269-272.

Le Maitre, R.W. (ed.), 1989. *A Classification of Igneous Rocks and Glossary of Terms*, Blackwell, Oxford, 193 pp.

Lemarchand, F., Villemant, B. and Calas, G., 1987. Trace element distribution coefficients in alkaline series. Geochimica et Cosmochimica Acta, 51: 1071-1081.

Leterrier, J., 1985. Mineralogical, geochemical and isotopic evolution of two Miocene mafic intrusions from the Zagros (Iran). Lithos, 18: 311-329.

Leterrier, J. and Maury, R.C., 1978. Représentation graphique de la cristallisation fractionnée des séries volcaniques. Application aux séries alcalines. Geologische Rundschau, 67: 943-952.

Luhr, J.F., Carmichael, I.S.E. and Varekamp, J.C., 1984. The 1982 Eruptions of El Chichón Volcano, Chiapas, Mexico: Mineralogy and Petrology of the anhydrite-bearing pumices. Journal of Volcanology and Geothermal Research, 23: 69-108.

Luth, W.C., Jahns, R.H., and Tuttle, O.F., 1964. The granite system at pressures of 4 to 10 kilobars. Journal of Geophysical Research. 69: 759-773.

Machado, N., Brooks, C. and Hart, S.R., 1986. Determination of initial $^{87}Sr/^{86}Sr$ and $^{143}Nd/^{144}Nd$ in primary minerals from mafic and ultramafic rocks: Experimental procedure and implications for the isotopic characteristics of the Archean mantle under the Abitibi greenstone belt, Canada. Geochimica et Cosmochimica Acta, 50: 2335-2348.

Machado, N., Rive, M., Gariepy, C., Simard, A., 1991. U-Pb geochronology of granitoids from the Pontiac Subprovince; preliminary results. Program with Abstracts - Geological Association of Canada; Mineralogical Association of Canada, 16; A78

Mahood, G.A. and Stimac, J.A., 1990. Trace-element partitioning in pantellerites and trachytes. Geochimica et Cosmochimica Acta, 54: 2257-2276.

Mattioli, G.S., Baker, M.B., Rutter, M.J., and Stolper, E.M., 1989. Upper mantle oxygen fugacity and its relationship to metasomatism. Journal of Geology, 97:521-536.

Mercier, J.-C., 1976. Single-pyroxene geothermometry and geobarometry. American Mineralogist, 61: 603-615.

Michael, P.J., 1988. Partition coefficients for rare elements in mafic minerals of high silica rhyolites; the importance of accessory mineral inclusions. Geochimica et Cosmochimica Acta.52; 275-282.

Middlemost, E.A.K., 1989. Iron oxidation ratios, norms and the classification of volcanic rocks. Chemistry Geology, 77: 19-26.

Miles, W.F., 1993. An interpretation of magnetic and gravity fields of the northwestern Pontaic Subprovince, Quebec. B.Sc. Thesis, University of Ottawa, 80pp.

MINREP. 1994. MINREP. A FORTRAN computer program to produce tables of mineral analysis with formulae and endmembers. By: G.J., Pringle. Geological Survey of Canada, Open File.

Miyashiro, A., 1974. Volcanic rock series in island arcs and active continental margins. American Journal of Science, 274: 321-355.

Montel, J.M., 1993. A model for monazite / melt equilibrium and application to the generation of granitic magmas. Chemical Geology, 110: 127-146.

Morimoto, N., 1988. Nomenclature of pyroxenes. Fortschrilleder der Mineralogie, 66. 237-252.

Morrison, G.W., 1980. Characteristics and tectonic setting of the shoshonite rock association. Lithos, 13: 97-108.

Mortensen, J.K., Theriault, R.J., and Card, K.D., 1988. U-Pb and Sr-Rb age constraints for plutonism and metamorphism in the Pontiac Subprovince and adjacent Grenville Subprovince. Program with Abstracts - Geological Association of Canada; Mineralogical Association of Canada, 13; A87

Mortensen, J.K., 1993. U-Pb geochronology of the eastern Abitibi Subprovince; Part 2, Noranda-Kirkland Lake area. Canadian Journal of Earth Sciences, 30: 29-41.

Mortensen, J.K. and Card, K.L., 1993. U-Pb Age Constraints for the Magmatic and Tectonic Evolution of the Pontiac Subprovince, Quebec. Canadian Journal of Earth Sciences, 30: 1970-1980.

Muller, D., Rock, N.M.S., and Groves, D.I., 1992. Geochemical discrimination between shoshonitic and potassic volcanic rocks in different tectonic settings: a pilot study. Mineralogy and Petrology, 46: 259-289.

Nash, W.P., and Creecraft, H.R., 1985. Partition coefficients for trace elements in silicic magmas. Geochimica et Cosmochimica Acta, 49: 2309-2322.

Nash, W.P. and Wilkinson, J.F.G., 1970. Shonkin Sag laccolith, Montana. Part 1. Mafic minerals and estimates of temperature, pressure, oxygen fugacity and silica activity: Contributions to Mineralogy and Petrology, 25: 241-269.

NewPet. 1993. NewPet for DOS from Daryl Clarke (?), Memorial University of Newfoundland, Department of Earth Sciences, Centre for Earth Resources Research.

Nielson, R.L., Forsyth, L.M., Gallahan, W.E. and Fisk, M.R., 1994. Major and Trace-element magnetite-melt equilibria. Chemical Geology, 117: 167-191.

Nimis, P., 1995. A clinopyroxene geobarometer for basaltic systems based on crystal-structure modeling. Contributions to Mineralogy and Petrology, 121: 115-125.

Nisbet, E.G., and Pearce, J.A., 1977. Clinopyroxene composition in mafic lavas from different tectonic settings. Contributions to Mineralogy and Petrology.63; 149-160

Noyes, H.J., Wones, D.R., and Frey, F.A., 1983. A tale of two plutons: Petrographic and mineralogic constraints on the petrogenesis of the Red Lake and Eagle Peak Plutons, Central Sierra Nevada, California. Journal of Geology. 91: 353-379.

Onuki, H., 1966. Mg - $Fe^{2+}$ distribution between co-existing hornblende and Ca-rich pyroxene. Journal of the Japanese Association of Mineralogy and Petrology, Economic Geology, 56: 246-255.

Ormerod, D.S., Hawkesworth,C.J., Leeman, W.P., and Menzies, M.A., 1987. The interaction between asthenosphere and lithosphere in response to the changing tectonic environment of the Western USA. Eos, Transactions, American Geophysical Union.68: 1529.

Otten, M.T. and Senior, A., 1985. Mineral chemistry and crystallization conditions of the Artfjället gabbro and dolerites (Central Swedish Caledonides). Lithos, 18: 295-310.

Pagel, M. and Leterrier, J., 1980. The subalkaline potassic magmatism of the Ballons massif (Southern Vosges, France): shoshonitic affinity. Lithos, 13: 1-10.

Peacock, M.A., 1931. Classification of igneous rock series. Journal of Geology, 39: 54-67.

Pearce, J.A. and Norry, M.J., 1979. Petrogenetic Implications of Ti, Zr, Y, and Nb Variations in Volcanic Rocks. Contributions to Mineralogy and Petrology, 69: 33-47.

Pearce, J.A., 1982. Trace element characteristics of lavas from destructive plate boundaries. *In*: Thorpe, R.S., (ed) *Andesites*, Chichester, Wiley, 525-548.

Philpotts, J.A., and Schnetzler, C.C., 1970. Phenocryst - matrix partition coefficients for K, Rb, Sr, and Ba, with implications to anorthosite and basalt genesis Geochimica et Cosmochimica Acta, 34: 307-322.

Poli, S., and Schmidt, M.W., 1992. A comment on "Calcic amphibole equilibria and a new amphibole - plagioclase geothermometer" by J.D. Blundy and T.J.B. Holland (Contrib Mineral Petrol (1990) 104: 208-224). Contributions to Mineralogy and Petrology. 111: 273-282.

Pringle, G.J., 1990. EDDI; a Fortran computer program to produce corrected electron-microprobe analyses of minerals using an energy dispersive X-ray spectrometer. *In*: Current research; Part A, National and general programs. Geological Survey, Canada: 5-8

Rapp, R.P., Watson, E.B. and Miller, C.F., 1991. Partial melting of amphibolite / eclogite and the origin of Archean trondhjemites and tonalites. Precambrian Research, 51: 1-25.

Rive, M., 1975. Géologie de la région des lacs Simard, Winawash et Décelles, comtés de Témiscamingue et de Pontiac, Min. Rich. Nat. du Québec, DP 338.

Rive, M., 1986. Cartes de compilation geologique 31M, 32D, 32E (1:125,000). Ministere l'Energie Ressources Quebec.

Rive, M., Pintson, H. and Ludden, J.N., 1990. Characteristics of late archean plutonic rocks from the Abitibi and Pontiac Subprovinces, Superior Province, Canada. *In*: Rive, M., Verpaelst, P., Gagnon, Y, Lulin, J.-M., Riverin, G. and Simard, A. (Eds). *The Northwestern Quebec Polymetallic Belt:* A summary of 60 years of mining exploration. The Canadian Institute of Mining and Metallurgy, Special Volume 43, p. 65-76.

Roeder, P.L. and Emslie, R.F., 1970. Olivine-liquid equilibrium. Contributions to Petrology and Mineralogy, 29: 275-289.

Roberts, M.P. and Clemens, J.D., 1993. Origin of high-potassium, calc-alkaline, I-type granitoids. Geology, 21: 825-828.

Rocheleau, M., and Dimroth, E., 1985. Petrology of the Archean Pontiac and Kewagama sediments and implications for the stratigraphy of the southern Abitibi belt: Discussion. Canadian Journal of Earth Sciences, 22: 1374-1377.

Rowins, S.M., 1990. Mineralogy and geochemistry of the Murdock Creek Intrusion, Kirkland Lake, Ontario. M.Sc. Thesis. University of Ottawa. 196pp.

Rowins, S.M., Lalonde, A.E., and Cameron, E.M., 1991. Magmatic oxidation in the syenitic Murdock Creek Intrusion, Kirkland Lake, Ontario; evidence from the ferromagnesian silicates. Journal of Geology. 99: 395-414.

Sato, H., 1977. Nickel content of basaltic magmas: identification of primary magmas and a measure of the degree of olivine fractionation. Lithos, 10: 113-120

Sawyer, E.W. and Barnes, S.J., 1994. Thrusting, magmatic intraplating, and metamorphic core complex development in the Archaean Belleterre-Angliers greenstone belt, Superior Province, Quebec, Canada. Precambrian Research, 68: 183-200.

Schmidt, M.W., 1992. Amphibole composition in tonalite as a function of pressure; an experimental calibration of the Al-in-hornblende barometer. Contributions to Mineralogy and Petrology. 110: 304-310.

Shcheka, S.A., Romanenko, I.M., Chubarov, V.M., and Kurentsova, N.A., 1977. Silica-bearing magnetites. Contributions to Mineralogy and Petrology. 63: 103-111

Shelley, D., 1993. *Igneous and Metamorphic rocks under the Microscope*: Classification, textures, microstructures, and mineral preferred orientations. 1st edition, Chapman and Hall. New York. 445 p.

Sisson, T.W., 1991. Pyroxene-high silica rhyolite trace element partition coefficients measured by ion microprobe. Geochimica et Cosmochimica Acta.55; 1575-1585.

Sisson, T.W., 1994. Hornblende-melt trace-element partitioning measured by ion microprobe. Chemical Geology, 117: 331-344.

Sisson, T.W. and Grove, T.L., 1993. Experimental investigations of the role of $H_2O$ in calc-alkaline differentiation and subduction zone magmatism. Contributions to Mineralogy and Petrology, 113: 143-166.

Smith, I.E.M., 1994. The monzonite alkaline association. Geological Association of Canada - Mineralogical Association of Canada, Program with Abstracts, 19: A105.

Speer, J.A., 1987. Evolution of magmatic AFM mineral assemblages in granitoid rocks: The hornblende + melt = biotite reaction in the Liberty Hill pluton, South Carolina. American Mineralogist, 72: 863-878.

Streckeisen, A., 1976. To each plutonic rock its proper name; Earth Science Reviews, 12: 1-33.

Taylor, S.R. and McClennan, S.M., 1985. *The Continental Crust: Its Composition and Evolution*, Blackwell, Oxford, 312 pp.

Thompson, J.B.Jr., 1947. Role of aluminum in rock - forming silicates: Geological Society of America, Bulletin, 58: 1232.

Thornton, C.P., and O.F. Tuttle, 1960. Chemistry of Igneous Rocks: pt. I, Differentiation Index, American Journal of Science, 258. 664-684.

Tobisch, O.T., Vernon, R.H., and McNulty, B.A., 1995. Polygenetic Microgranitoid Enclave Swarms in Granite Rocks, Central Sierra Nevada, California. In *The Origin of Granites and Related Rocks*, Hutton Symposium III, Abstracts. U.S. Geological Survey Circular, 1129, p148.

Tomlinson, K.Y., Thurston, P.C., Hughes, D.J. and Keays, R.R., 1995. The Central Wabigoon Region: Petrogenesis of Mafic-Ultramafic Rocks in the Steep Rock, Lumby Lake and Obonga Lake Greenstone Belts (Continental Drifting and Rifting in the Archean). *In*: Harrap, R. and Helmstaedt, H. (Eds). *LithoProbe Western Superior Transect Second Annual Workshop*, Lithoprobe Report. 53, p. 65-73.

Tronnes, R.G., Edgar, A.D., and Arima, M., 1985. Titanium solubility in phlogopite; an experimental study on its potential as a P-T indicator for upper mantle - lower crustal rocks. Geological Association of Canada; Mineralogical Association of Canada, Program with Abstracts, 10; A63

Ujike, O., 1984. Chemical composition of Archean Pontiac metasediments, southwestern Abitibi Belt, Superior Province. Canadian Journal of Earth Sciences, 21: 727-731.

Verhoogen, J., 1962. Distribution of titanium between silicates and oxides in igneous rocks. American Journal of Science, 260: 211-220.

Vyhnal, C.R., McSween Jr., H.Y., Speer, J.A., 1991. Hornblende chemistry in southern Apalachian granitoids: Implications for aluminum hornblende thermobarometry and magmatic epidote stability. American Mineralogist, 76: 176-188.

Watson, E.B., 1979. Zircon Saturation in Felsic Liquids: Experimental Results and Applications to Trace Element Geochemistry. Contributions to Mineralogy and Petrology, 70: 407-419.

Watson, E.B. and Green, T.H., 1981. Apatite / liquid partition coefficients for the rare earth elements and strontium. Earth and Planetary Science Letters, 56: 405-421.

Watson, E.B. and Harrison, T.M., 1983. Zircon saturation revisited: temperature and composition effects in a variety of crustal magma types. Earth and Planetary Science Letters, 64: 295-304.

Watson, E.B. and Harrison, T.M., 1984. Accessory minerals and the geochemical evolution of crustal magmatic systems: a summary and prospectus of experimental approaches. Physics of the Earth and Planetary Interiors, 35: 19-30.

Watson, E.B. and Ryerson, F.J., 1986. Partitioning of zirconium between clinopyroxene and magmatic liquids of intermediate composition. Geochimica et Cosmochimica Acta, 50: 2523-2526.

Weaver, E.B., 1991. Trace element evidence for the origin of ocean - island basalts. Geology, 19: 123-126

Westendorp, R.W., Watkinson, D.H., and Jonasson, I.R., 1991. Silicon-bearing zoned magnetite crystals and the evolution of hydrothermal fluids at the Ansil Cu-Zn mine, Rouyn-Noranda, Quebec. Economic Geology, 86: 1110-1114.

Whitney, J.A., 1988b. The origin of granite: The role and source of water in the evolution of granitic magmas: Geological Society of America, Bulletin, v. 100, pp. 1886-1897.

Wolff, J.A. and Storey, M., 1983. The Volatile Component of Some Pumice-Forming Alkaline Magmas from the Azores and Canary Islands. Contributions to Petrology and Mineralogy, 82: 66-74.

Wones, D.R. and Eugster, H.P., 1965. Stability of biotite: experiment, theory, and application. The American Mineralogist, 50: 1228-1272.

Wones, D.R., 1981. Mafic silicates as indicators of intensive variables in granitic magmas. Mining Geology 31: 191-212.

Wones, D.R., and Gilbert, M.C., 1982. Amphiboles in the igneous environment. *In* Veblin D.R., and P.H. Ribbe, (Ed). *Amphiboles: Petrology and Experimental Phase Relations*, vol. 9B, Reviews in Mineralogy, p 355-390

Wyman, D.A. and Kerrich, R., 1993. Archean Shoshonitic Lamprophyres of the Abitibi Subprovince, Canada: Petrogenesis, Age, and Tectonic Setting. Journal of Petrology, 34: 1067-1109.

Xie, Q., McCuaig, T.C. and Kerrich, R., 1995. Secular trends in the melting depths of mantle plumes: evidence from HFSE/REE systematics of Archean high-Mg lavas and modern oceanic basalts. Chemical Geology, 126: 29-42.

Yoder, H.S., and Tilley, C.E., 1962. Origin of basaltic magmas: An experimental study of natural and synthetic rock systems. Journal of Petrology, 3:342-532

Zindler, A. 1982. Nd and Sr isotopic studies of komatiites and related rocks. *In*: . N.T. Arndt and E.G. Nisbet (eds.) *Komatiites.* George Allen and Unwin, Boston. pp. 399-420.

# Appendix 1
# Sample Locations

** = Rock Type Abbreviations

Mo = Monzonite
Dio = Diorite
MD = Monzodiorite
QMD = Quartz monzodiorite
Sy = Syenite
QMo = Quartz monzonite
To = Tonalite (Belleterre - Fugerville pluton)
Vol = Belleterre belt volcanic rock
Hbldt = Hornblendite
Enc = Autolithic enclave
Dyke = Mafic dyke
GD = Granodiorite
Gra = Granite
Sed = Pontiac sedimentary rock (partially fused xenolith)
φ = La Force Ni-Cu occurence
⊕ = Lac Soufflot / Lac Maple Intrusions
Φ = Lac Devlin Intrusion
◊ = Tour de Belleterre
♥ = Lac Remigny Complex
Π = Riviere a la Loutre
Δ = Lac Freschette

**Sample Locations**

The positions of collected grab samples were obtained with the aid of a Magellan NAV PRO 5000 Global Positioning System (GPS). Error in positioning is interpreted to be approximately 20m based upon published statistics for the GPS unit, analysis of PDOP (positioning dilution of precision) obtained from the GPS unit, satellite signal qualities, and comparison of positioning information of a known location to map coordinates. Positions were outputted in the UTM (Universal Transverse Mercator) format using a NAD 27 map datum.

## UTM Co-ordinates of Samples used for Geochemical Analysis

| Sample | Rock Type** | Easting | Northing |
|---|---|---|---|
| 9210102 | QMD | 673421 | 5273342 |
| 9210103 | Enc | 673421 | 5273342 |
| 9210104 | Enc | 673421 | 5273342 |
| 9210105 | Mo† | 668880 | 5265880 |
| 9210113 | Sy† | 667148 | 5280210 |
| 9210116 | Sy[c] | 670752 | 5283380 |
| 9210117 | Dio[c] | 671100 | 5283255 |
| 9210117a | MD[c] | 671100 | 5283255 |
| 9210118 | Sy[c] | 671175 | 5283250 |
| 9210119 | Mo[c] | 673665 | 5283250 |
| 92101110 | MD[rc] | 673655 | 5282345 |
| 92101113 | Dio | 682160 | 5278640 |
| 92101113 | Dio | 682160 | 5278640 |
| 92101115 | MD | 682160 | 5278640 |
| 92101116 | Mo | 682160 | 5278640 |
| 92101116x | QMo | 682160 | 5278640 |
| 9210121 | To | 653950 | 5266350 |
| 9210127 | Dio | 653150 | 5254585 |
| 9210128 | MD | 653250 | 5254585 |
| 9210129 | QMD | 652490 | 5257710 |
| 92101210 | MD† | 651600 | 5257620 |
| 9210131 | MD | 661553 | 5269736 |
| 9210134 | Hbldt | 665082 | 5267128 |
| 9210135 | Hbldt | 664962 | 5266836 |
| 9210136 | Hbldt | 664756 | 5266940 |
| 9210137 | Vol | 664627 | 5266856 |
| 9210138 | MD† | 664750 | 5267061 |
| 9210139 | Mo† | 659396 | 5275009 |
| 9210143b | QMD† | 658714 | 5268811 |
| 9210147 | Sy | 664661 | 5266834 |
| 9210149 | Hbldt | 657316 | 5270562 |
| 92101410 | Gra | 657336 | 5270483 |
| 92101411 | Hbldt | 657423 | 5270546 |
| 9210157 | MD | 651776 | 5262825 |
| 92101513 | MD | 651527 | 5262266 |
| 92101514 | Dio | 648949 | 5257533 |
| 9210162 | Vol | 670351 | 5265817 |
| 9210163 | Dio | 670201 | 5265895 |
| 9210164 | To | 668624 | 5265713 |
| 9210171 | Dio | 651649 | 5262370 |
| 9210174 | QMD | 666805 | 5265979 |
| 9210175 | La Force | 672985 | 5262861 |
| 9210176 | To | 673073 | 5263171 |
| 9210181 | GD | 673390 | 5272343 |
| 9210186 | QMD | 673463 | 5271742 |
| 9210187 | QMD† | 678509 | 5270572 |
| 9210188 | Mo† | 664694 | 5270277 |
| 9210189 | MD† | 664786 | 5270341 |
| 9306156 | QMD | 683685 | 5271565 |
| 93061510 | To | 673380 | 5261796 |
| 93061510a | Dyke | 673380 | 5261796 |
| 9306161 | MD† | 657021 | 5273894 |
| 9306162a | Enc | 656922 | 5273655 |
| 9306164 | Enc | 656614 | 5273162 |
| 9306166 | Hbldt | 651003 | 5268382 |
| 9306171 | To | 647878 | 5261769 |
| 9306173 | Hbldt | 647985 | 5261790 |

| Sample | Rock Type** | Easting | Northing |
|---|---|---|---|
| 9306174 | Hbldt | 648055 | 5261791 |
| 93061710 | Hbldt | 650503 | 5274134 |
| 9306182 | MD† | 632129 | 5274957 |
| 9306183 | MD† | 626632 | 5276791 |
| 9306184 | QMD† | 626667 | 5294903 |
| 9306187 | Dio | 653133 | 5258231 |
| 9306193 | Mo† | 665455 | 5279661 |
| 9306196 | Mo[c] | 668552 | 5282790 |
| 9306198 | Dio | 670728 | 5282411 |
| 93061910a | Enc | 680868 | 5281515 |
| 93061911a | Enc | 675005 | 5283022 |
| 9306203 | Mo[rc] | 673035 | 5281856 |
| 9306203a | Sy† | 673035 | 5281856 |
| 9306206a | Dyke | 668413 | 5281127 |
| 9306212 | MD | 637888 | 5238106 |
| 9306222 | Sy† | 670195 | 5265757 |
| 9306226 | MD† | 672117 | 5268642 |
| 9306231 | Dio | 660154 | 5273704 |
| 9306234 | QMD | 660694 | 5273866 |
| 9306235 | Dio | 660672 | 5273779 |
| 9306238 | Mo[c] | 663753 | 5267065 |
| 9306242 | MD† | 660114 | 5271743 |
| 9306244 | Dio | 660132 | 5271660 |
| 9306254 | Hbldt | 660174 | 5271593 |
| 9306257 | Dio | 661118 | 5269380 |
| 9306257a | Dio | 661118 | 5269380 |
| 93062510 | Dyke | 672904 | 5271082 |
| 93062511 | Dyke | 672975 | 5271314 |
| 93062513 | Dyke | 672898 | 5271400 |
| 9306261a | Dio | 658486 | 5268886 |
| 9306266 | Dyke | 651553 | 5255689 |
| 9306268dyke | Dyke | 652618 | 5255081 |
| 9306268enc | Enc | 652618 | 5255081 |
| 9306271 | Dyke | 651038 | 5255753 |
| 9306273 | Dyke | 652597 | 5255168 |
| 9308173 | Gr | 669810 | 5282800 |
| 9308174 | MD† | 670444 | 5283263 |
| 93081711a | Dio | 679298 | 5282268 |
| 93081712 | Dio | 682120 | 5280334 |
| 9308182 | Vol | 685551 | 5279183 |
| 9308184 | Dio | 682041 | 5277648 |
| 9308185 | Sy† | 679954 | 5309653 |
| 9308186 | Sed | 672090 | 5274613 |
| 9308187 | QMo† | 669338 | 5272593 |
| 9308188 | Dio | 668219 | 5275023 |
| 9308191 | Hbldt | 646654 | 5263194 |
| 9308192 | Mo† | 644934 | 5263807 |
| 9308193 | QMD | 648182 | 5262896 |
| 9308193a | Sy | 648182 | 5262896 |
| 9308201 | Dio | 673972 | 5256673 |
| 9308202 | Mo | 683310 | 5248898 |
| 9308203 | MD | 683462 | 5248690 |
| 9308205 | MD† | 674155 | 5247742 |
| 9308206 | Mo† | 674279 | 5247182 |
| 9308211 | MD† | 679177 | 5265421 |
| 9308212 | Hbldt | 680994 | 5268031 |
| 9308213 | QMD | 680938 | 5268164 |

** Rock types defined on previous page.

# Appendix 2
# Thin Section Preparation and K-Feldspar Staining

**Sample Preparation**

Samples were selected based upon their representative nature of the local outcrop, lack of veining, and lack of alteration. Prior to crushing, a block of sample material was trimmed with a diamond saw to remove surface weathering affects, and washed to remove any accumulated blade material. Typically, two chips were cut from each block. One chip was used for K staining and feldspar content determination, the other for thin section preparation, and the remainder for elemental analysis. Prepared and cleaned sample blocks were crushed in a jaw crusher and powdered with a tungsten carbide ring mill.

**K Staining for Potassium Feldspar**

A total of 136 small, flat sawn chips from selected samples prepared as a thin section was etched in concentrated HF for one minute, rinsed in deionized $H_2O$, and stained with a 3:1 mixture of deionized $H_2O$ and sodium cobaltinitrate for 1 to 2 minutes.

**Thin Section Preparation**

A total of 14 chips were submitted to Geo-Ark Petrographic for the production of covered sections for transmitted light microscopy and 42 sample chips were prepared as polished sections for reflected light microscopy, energy dispersive scanning electron, and electron microscopy. The University of Ottawa thin section facility produced 15 polished and 7 covered sections.

# Appendix 3
# Whole Rock Compositions
# Major, Trace, and RE Elements

# Whole Rock Analysis

**Major and Trace Element Analysis**

A total of sixty-seven samples were analyzed for major elements and Zr, Sr, Rb, Zn, Ni, Ba, Nb, and Cr at the University of Ottawa X-ray fluorescence (XRF) laboratory by a fully automated Philips PW2400 X-ray fluorescence spectrometer. An additional forty-eight analysis were performed at the Geological Survey of Canada XRF laboratory for major elements plus S and Cu, Ni, Cr, Rb, Sr, Zr, Nb, Ba, and Pb. Further trace element analysis was performed by Instrumental Neutron Activation analysis (INAA) at Bequrel labs on 43 samples to provide Sc, Cs, Tb, Ta, Th, U, Au, Sb, As, Br, Co, and Hf. A total of nine samples were submitted as duplicates for REE analysis by INAA at Ecole Polytechnique which supplemented the trace element analysis with U, Sc, Cs, Ta, Th.

Sample fusion for XRF analysis at the GSC was performed as follows. Two grams of sample were heated at 120°C in a pre-fired ceramic crucible overnight, cooled in a desiccator, and weighed to obtain $H_2O^-$ and then fired for 1.5 hours at 1050°C, cooled in a desiccator, and weighed to obtain $H_2O^+$ and total loss on ignition (LOI). Exactly one gram of fired sample was mixed thoroughly with 5.0g of lithium tetraborate (flux), 0.05g of ammonium iodide (non-wetting agent), 0.05g ammonium nitrate (oxidant for sulphides), and 0.3g of lithium fluoride. This mixture was fused and poured as a pellet in a platinum mould.

Sample fusion method for analysis at the University of Ottawa differed from the GSC method. Exactly 1.3 grams of sample was mixed with 3.9 grams of lithium tetraborate and 0.433 grams of lithium carbonate. This mixture was fused and poured as a pellet in a platinum mould for XRF analysis.

The CIPW normative mineralogy (Appendix 3) was calculated by the CIPW module

of NEWPET (1993) with $Fe_2O_3/FeO$ estimated from ratios determined from rocks with similar magmatic affinity. (Middlemost, 1989). The Thornton and Tuttle (1960) differentiation index is included under the column "DI".

**Rare Earth Element Analysis**

Rare earth element concentrations for La, Ce, Nd, Sm, Eu, Gd, Dy, Er, Yb, and Lu of eighty-five samples were determined with the Thermo Jarrell Ash Atom Scan 25 ICP-AES at the University of Ottawa. Procedure for sample dissolution is similar to that outlined by Crock and Severson (1980) with minor modifications. Approximately 1 gram of powdered sample and 10 ml HF, 3 ml $HClO_4$ and 3 ml $HNO_3$ was added to a Teflon beaker and placed on a hot plate until dissolution was complete. The solution was then heated at low temperature until dryness was achieved. The majority of samples did not achieve full dissolution which necessitated the use of an 3:1 Li metaborate and sample fusion in graphite crucibles as outlined by Crock et al (1984). The sample was fused at 1050°C for 20 minutes and poured into a magnetically stirred beaker of 1N $HNO_3$ until complete dissolution occurred. The sample was then placed on a hot plate, dried, and brought up to 50 ml with 1N HCl and added to a 1N HCl pre-equilibrated cation exchange column with an additional 50 ml 1N HCl. A second eluent of 100 ml of 2N HCl was added after the 1N HCl elution was complete. Rare earth elements were collected with a final 250 ml 6N HCl flush and the solution dried on a hot plate at low temperature. The film of dried REE concentrate was re-dissolved with 1N $HNO_3$ and brought up to 15 ml for ICP-AES analysis.

| | Method |
|---|---|
| **Major Element Oxides** | |
| $Na_2O$ | XRF |
| MgO | XRF |
| $Al_2O_3$ | XRF |
| $SiO_2$ | XRF |
| $P_2O_5$ | XRF |
| $K_2O$ | XRF |
| CaO | XRF |
| $TiO_2$ | XRF |
| MnO | XRF |
| $Fe_2O_3$ | XRF |
| Total | |
| $H_2O$-%†† | |
| $H_2O$+%††† | |
| **Trace Elements** | |
| Sc | INAA |
| Cs | INAA |
| Ta | INAA |
| Th | INAA |
| U | INAA |
| Cr | XRF |
| Ni | XRF |
| Cu | XRF |
| Zn | XRF |
| Rb | XRF |

| | Method |
|---|---|
| **Trace Elements** | |
| Sr | XRF |
| Y | XRF/ICP |
| Zr | XRF |
| Nb | XRF |
| Ba | XRF |
| Pb | XRF |
| Sb | INAA |
| As | INAA |
| Br | INAA |
| Co | INAA |
| Hf | INAA |
| **Rare Earth Elements** | |
| La | ICP |
| Ce | ICP |
| Nd | ICP |
| Sm | ICP |
| Eu | ICP |
| Gd | ICP |
| Tb | INAA |
| Dy | ICP |
| Ho | INAA |
| Er | ICP |
| Yb | ICP |
| Lu | ICP |

† Shoshonitic Series Granitoid
£ Saccharoidal Granitoid
†† Determined from dessication at 110°C for 24 hours.
††† Loss on ignition from heating at 1050°C for 3 hours.
§ Normative Mineralogy Calculated by NEWPET (1994). The $Fe^{2+}$ /$Fe^{3+}$ ratios used in the CIPW norms were calculated using the TAS classification of the samples and the iron ratios of Middlemost (1989)
‡ Thornton and Tuttle (1960) differentiation index.
¤ Chondrite normalizations after Taylor and McClennan (1985)
¥ Mg number determined from Mg/total Fe($Fe^{2+}$ +Mg) where $Fe^{2+}$ is total Fe as $Fe^{2+}$
n.d. Not determined.

** = Rock Type abbreviations
Mo = Monzonite
Dio = Diorite
MD = Monzodiorite
QMD = Quartz monzodiorite
Sy = Syenite
QMo = Quartz monzonite
To = Tonalite (Belleterre - Fugerville)
Vol = Belleterre belt volcanic rock
Hbldt = Hornblendite
Enc = Autolithic enclave
Dyke = Mafic dyke
GD = Granodiorite
Gra = Granite
Sed = Pontiac sedimentary rock (partially fused xenolith)
φ = La Force Ni-Cu occurence
⊕ = Lac Soufflot / Lac Maple Intrusions
Φ = Lac Devlin Intrusion
◊ = Tour de Belleterre
♥ = Lac Remigny Complex
Π = Riviere a la Loutre
Δ = Lac Freschette

# Major and Trace Elements

| Sample | 9210102 | 9210103 | 9210104 | 9210105 | 9210113 | 9210116 | 9210117 | 9210117a | 9210118 |
|---|---|---|---|---|---|---|---|---|---|
| Rock Type[~] | QMD | Enc | Enc | Mo[†] | Sy[†] | Sy[£] | Dio[£] | MD[£] | Sy[£] |
| **Major Elements (%)** | | | | | | | | | |
| Oxide | | | | | | | | | |
| $Na_2O$ | 5.38 | 5.03 | 0.25 | 6.01 | 5.77 | 4.61 | 3.87 | 1.32 | 6.46 |
| MgO | 3.15 | 8.83 | 19.35 | 2.61 | 2.15 | 3.33 | 6.00 | 13.81 | 0.58 |
| $Al_2O_3$ | 14.43 | 12.63 | 2.75 | 15.81 | 14.95 | 16.58 | 15.77 | 6.56 | 18.50 |
| $SiO_2$ | 66.19 | 56.60 | 52.20 | 62.85 | 66.35 | 60.26 | 51.54 | 54.89 | 64.35 |
| $P_2O_5$ | 0.15 | 0.34 | 0.02 | 0.17 | 0.15 | 0.25 | 0.29 | 0.06 | 0.05 |
| $K_2O$ | 2.70 | 0.42 | 0.10 | 3.66 | 3.28 | 2.19 | 2.09 | 0.62 | 6.24 |
| CaO | 3.45 | 6.86 | 11.30 | 3.68 | 2.75 | 3.08 | 6.51 | 10.26 | 1.13 |
| $TiO_2$ | 0.32 | 0.67 | 0.25 | 0.46 | 0.38 | 0.68 | 0.87 | 0.51 | 0.21 |
| MnO | 0.06 | 0.15 | 0.22 | 0.06 | 0.05 | 0.17 | 0.18 | 0.16 | 0.03 |
| $Fe_2O_3$ | 3.84 | 7.81 | 9.68 | 4.62 | 3.95 | 6.97 | 11.63 | 10.86 | 2.01 |
| Total | 99.96 | 99.63 | 98.95 | 100.37 | 100.15 | 98.45 | 99.01 | 99.29 | 99.86 |
| $H_2O$-%[††] | 0.57 | 0.28 | 0.89 | 0.12 | 0.58 | 0.58 | 0.08 | 0.83 | 0.14 |
| $H_2O$+%[†††] | 0.52 | 1.43 | 1.74 | 0.54 | 0.35 | 1.93 | 1.83 | 1.26 | 0.07 |
| **Trace Elements (ppm)** | | | | | | | | | |
| Sc | 7.1 | 17 | n.d. | 8.7 | 5.7 | 13 | 28.1 | 37.1 | 2.7 |
| Cs | n.d. | 0.25 | n.d. | 0.86 | 0.8 | 1.8 | 0.8 | 0.9 | 2.9 |
| Ta | 1.9 | 1.41 | n.d. | 1.41 | 2.4 | 1.6 | 1 | 0.8 | 1.2 |
| Th | 1.4 | 2.24 | n.d. | 2.24 | 3 | 1.5 | 2.6 | 1.1 | 6.4 |
| U | 0.3 | 0.64 | n.d. | 0.64 | 0.5 | 0.4 | 0.6 | 0.4 | 1.7 |
| Cr | 158.1 | 702.0 | 1053.2 | 88.9 | 69.8 | 24.6 | 56.8 | 421.5 | 8.9 |
| Ni | n.d. | 121.0 | 144.1 | 11.8 | n.d. | 55.8 | 25.9 | 272.7 | 6.3 |
| Cu | | | | | | | | | |
| Zn | 46.6 | 109.3 | 144.1 | 72.3 | 64.3 | 154.3 | 97.2 | 90.8 | 8.8 |
| Rb | 52.1 | 17.4 | 4.9 | 75.9 | 71.3 | 146.3 | 113.4 | 22.9 | 176.5 |
| Sr | 936 | 587 | 37 | 1212 | 1192 | 1090 | 743 | 162 | 809 |
| Y | 7.1 | 7.9 | n.d. | 12.6 | 4.7 | 16.5 | 15.7 | 9.4 | 3.9 |
| Zr | 95.5 | 79.2 | 1.9 | 166.6 | 162.9 | 131.8 | 87.4 | 60.7 | 296.1 |
| Nb | n.d. | 3.5 | 2.9 | n.d. | n.d. | n.d. | n.d. | 8.4 | n.d. |
| Ba | 837 | 128 | 42 | 1409 | 1223 | 592 | 550 | 240 | 755 |
| Pb | n.d. | n.d. | n.d. | n.d. | n.d. | n.d. | n.d. | n.d. | 21.4 |
| Sb | 0.05 | 0.05 | n.d. | 0.05 | 0.05 | 0.2 | 0.2 | 0.05 | 0.05 |
| As | 0.25 | 0.25 | n.d. | 0.25 | 0.25 | 0.25 | 1 | 0.25 | 0.25 |
| Br | 0.25 | 1.1 | n.d. | 1.4 | 0.25 | 1.6 | 0.6 | 0.25 | 0.25 |
| Co | 36 | 58 | n.d. | 34 | 38 | 34 | 43 | 81 | 13 |
| Hf | 6 | 3 | n.d. | 4 | 8 | 6 | 3 | 3 | 7 |
| **Major and Trace Element Ratios** | | | | | | | | | |
| Mg#[‡] | 53 | 61 | 73 | 44 | 43 | 40 | 42 | 64 | 29 |
| $K_2O/Na_2O$ | 0.50 | 0.08 | 0.38 | 0.61 | 0.57 | 0.47 | 0.54 | 0.47 | 0.97 |
| $K_2O+Na_2O$ | 8.08 | 5.45 | 0.35 | 9.67 | 9.06 | 6.80 | 5.96 | 1.94 | 12.70 |
| K/Na | 0.33 | 0.06 | 0.25 | 0.40 | 0.37 | 0.31 | 0.35 | 0.31 | 0.64 |
| Sr/Sr* | n.d. | 1.89 | 0.41 | 2.65 | 2.98 | 3.30 | 0.99 | 0.50 | 1.98 |
| Zr/Zr* | n.d. | 0.96 | 0.04 | 1.24 | 1.53 | 1.22 | 0.38 | 0.50 | 3.36 |
| Ti/Ti* | n.d. | 1.10 | 0.47 | 0.39 | 0.52 | 0.61 | 0.52 | 0.51 | 0.30 |
| Nb/Nb* | n.d. | 0.230 | 0.88 | 0.00 | 0.00 | 0.00 | 0.00 | 0.51 | 0.00 |

| Sample | 9210119 | 92101110 | 92101113 | 92101113 | 92101115 | 92101116 | 92101116x | 9210121 | 9210123 |
|---|---|---|---|---|---|---|---|---|---|
| Rock Type[**] | Mo[f] | MD[ff] | Dio | Dio | MD | Mo | QMo | To | To |
| **Major Elements (%)** | | | | | | | | | |
| Oxide | | | | | | | | | |
| $Na_2O$ | 4.53 | 6.23 | 1.38 | 1.97 | 5.44 | 5.81 | 6.33 | 5.16 | 4.38 |
| MgO | 3.71 | 1.73 | 16.18 | 11.86 | 4.13 | 1.98 | 2.28 | 1.26 | 1.26 |
| $Al_2O_3$ | 17.61 | 18.29 | 9.57 | 10.66 | 14.68 | 15.04 | 14.76 | 16.00 | 15.26 |
| $SiO_2$ | 53.02 | 60.35 | 48.87 | 50.78 | 62.95 | 66.86 | 66.34 | 66.95 | 68.99 |
| $P_2O_5$ | 0.03 | 0.26 | 0.24 | 0.31 | 0.19 | 0.13 | 0.13 | 0.14 | 0.14 |
| $K_2O$ | 2.47 | 4.30 | 3.75 | 2.59 | 2.50 | 3.79 | 2.76 | 1.26 | 1.51 |
| CaO | 7.37 | 3.62 | 8.41 | 8.60 | 4.20 | 2.78 | 3.14 | 3.46 | 3.65 |
| $TiO_2$ | 0.86 | 0.58 | 0.57 | 0.72 | 0.40 | 0.35 | 0.36 | 0.43 | 0.39 |
| MnO | 0.15 | 0.10 | 0.17 | 0.22 | 0.07 | 0.05 | 0.06 | 0.05 | 0.05 |
| $Fe_2O_3$ | 9.46 | 4.81 | 9.48 | 11.29 | 4.73 | 3.60 | 3.86 | 3.82 | 3.50 |
| Total | 99.52 | 100.77 | 99.12 | 99.63 | 99.61 | 100.78 | 100.34 | 98.77 | 99.27 |
| $H_2O$-%[††] | 0.11 | 0.31 | 0.13 | 0.06 | 0.01 | 0.09 | 0.12 | 0.21 | 0.08 |
| $H_2O$+%[†††] | 0.52 | 0.24 | 1.57 | 1.81 | 0.63 | 0.18 | 0.21 | 1.07 | 1.13 |
| **Trace Elements (ppm)** | | | | | | | | | |
| Sc | 21.6 | 7.3 | 26.9 | n.d. | 11 | 6 | 6.8 | 5.5 | 5.2 |
| Cs | 0.9 | 3.2 | 20 | n.d. | 5.3 | 0.25 | 0.25 | n.d. | n.d. |
| Ta | n.d. | 1.8 | 0.25 | n.d. | n.d. | n.d. | n.d. | 2.1 | 2.8 |
| Th | n.d. | 10 | 3.1 | n.d. | n.d. | n.d. | n.d. | 0.4 | 3.2 |
| U | n.d. | 2.6 | 0.5 | n.d. | n.d. | n.d. | n.d. | 0.1 | 0.7 |
| Cr | 14.4 | 7.5 | 1162.5 | 775.9 | 202.5 | 64.3 | 69.8 | n.d. | n.d. |
| Ni | n.d. | n.d. | 316.7 | 258.5 | 33.0 | n.d. | 19.6 | n.d. | n.d. |
| Cu | 33.6 | 121.4 | n.d. | 572.8 | n.d. | n.d. | n.d. | n.d. | n.d. |
| Zn | 81.9 | 91.6 | 69.9 | 163.1 | 36.2 | 34.5 | 58.6 | 50.6 | 24.9 |
| Rb | 56.7 | 152.7 | 175.6 | 214.0 | 93.3 | 83.2 | 60.4 | 47.5 | 51.2 |
| Sr | 937 | 1566 | 479 | 907 | 995 | 1167 | 1061 | 764 | 405 |
| Y | 22.8 | 17.3 | 15.0 | 9.4 | 4.7 | 4.7 | 5.5 | 7.1 | 7.1 |
| Zr | 154.0 | 279.1 | 68.1 | 70.3 | 117.7 | 159.2 | 141.4 | 179.2 | 145.1 |
| Nb | n.d. | n.d. | n.d. | n.d. | n.d. | n.d. | n.d. | 5.6 | 6.3 |
| Ba | 785 | 1366 | 1102 | 1368 | 825 | 1161 | 777 | 400 | 357 |
| Pb | n.d. | n.d. | n.d. | n.d. | n.d. | n.d. | 4.6 | 1.9 | n.d. |
| Sb | 0.05 | 0.05 | 0.05 | n.d. | 0.05 | 0.05 | 0.05 | 0.05 | 0.05 |
| As | 0.5 | 0.5 | 0.25 | n.d. | 0.25 | 0.25 | 0.25 | 0.25 | 0.25 |
| Br | 0.8 | 0.25 | 0.25 | n.d. | 0.8 | 0.8 | 2.3 | 1.9 | 1.7 |
| Co | 37 | 31 | 52 | n.d. | 39 | 28 | 26 | 30 | 35 |
| Hf | 4 | 8 | 2 | n.d. | 3 | 4 | 3 | 8 | 10 |
| **Major and Trace Element Ratios** | | | | | | | | | |
| Mg#[ss] | 35 | 33 | 70 | 59 | 55 | 43 | 45 | 31 | 33 |
| $K_2O/Na_2O$ | 0.55 | 0.69 | 2.71 | 1.32 | 0.46 | 0.65 | 0.44 | 0.25 | 0.34 |
| $K_2O+Na_2O$ | 7.00 | 10.54 | 5.13 | 4.56 | 7.94 | 9.60 | 9.09 | 6.42 | 5.89 |
| K/Na | 0.36 | 0.45 | 1.78 | 0.87 | 0.30 | 0.43 | 0.29 | 0.16 | 0.23 |
| Sr/Sr* | 1.05 | 1.53 | 0.96 | n.d. | 2.83 | 2.84 | 7.92 | 3.53 | 0.78 |
| Zr/Zr* | 0.60 | 1.02 | 0.43 | n.d. | 1.15 | 1.62 | 3.77 | 2.52 | 1.08 |
| Ti/Ti* | 0.43 | 0.31 | 0.49 | n.d. | 0.44 | 0.57 | 1.26 | 0.66 | 0.37 |
| Nb/Nb* | 0.00 | 0.00 | 0.00 | n.d. | 0.00 | 0.00 | 0.00 | 0.26 | 0.19 |

| Sample | 9210127 | 9210128 | 9210129 | 92101210 | 9210131 | 9210134 | 9210135 | 9210136 | 9210137 |
|---|---|---|---|---|---|---|---|---|---|
| Rock Type* | Dio | MD | QMD | MD | MD† | Hbldt | Hbldt | Hbldt | Vol |
| **Major Elements (%)** | | | | | | | | | |
| Oxide | | | | | | | | | |
| $Na_2O$ | 3.27 | 3.38 | 6.42 | 6.84 | 5.88 | 1.69 | 1.58 | 1.76 | 2.90 |
| MgO | 9.22 | 8.50 | 2.53 | 3.34 | 2.82 | 15.81 | 15.62 | 12.18 | 7.61 |
| $Al_2O_3$ | 12.49 | 13.26 | 16.16 | 15.27 | 16.33 | 8.22 | 7.18 | 7.21 | 14.47 |
| $SiO_2$ | 52.97 | 53.74 | 64.92 | 63.27 | 60.82 | 44.56 | 46.28 | 40.46 | 47.99 |
| $P_2O_5$ | 0.33 | 0.36 | 0.17 | 0.19 | 0.25 | 0.38 | 0.14 | 0.32 | 0.10 |
| $K_2O$ | 2.24 | 2.50 | 2.65 | 2.45 | 4.14 | 1.51 | 1.18 | 0.70 | 1.00 |
| CaO | 8.50 | 7.69 | 2.89 | 3.25 | 3.51 | 12.29 | 13.23 | 13.26 | 9.24 |
| $TiO_2$ | 0.71 | 0.72 | 0.34 | 0.44 | 0.46 | 1.03 | 1.11 | 1.53 | 1.16 |
| MnO | 0.16 | 0.15 | 0.06 | 0.07 | 0.08 | 0.20 | 0.19 | 0.25 | 0.22 |
| $Fe_2O_3$ | 9.13 | 9.05 | 3.63 | 4.75 | 5.05 | 12.87 | 11.79 | 22.14 | 14.92 |
| Total | 99.40 | 99.77 | 100.10 | 100.13 | 99.86 | 99.01 | 98.69 | 100.04 | 99.81 |
| $H_2O$-%†† | 0.12 | 0.15 | 0.20 | 0.62 | 0.09 | 0.05 | 0.08 | 0.17 | 0.49 |
| $H_2O$+%††† | 1.24 | 1.38 | 0.59 | 0.40 | 0.25 | 1.41 | 1.25 | 1.09 | 1.30 |
| **Trace Elements (ppm)** | | | | | | | | | |
| Sc | 25.5 | 23.5 | 6.4 | 8.1 | 8.5 | 41 | 43 | 73 | 44.3 |
| Cs | 1.6 | 1.7 | 0.6 | 0.9 | 1.1 | 1.7 | 1.3 | 0.8 | 1.1 |
| Ta | n.d. | n.d. | n.d. | 1.7 | n.d. | 0.7 | n.d. | 0.6 | 0.6 |
| Th | n.d. | n.d. | n.d. | 2.7 | n.d. | 0.1 | n.d. | 0.1 | 0.1 |
| U | n.d. | n.d. | n.d. | 0.6 | n.d. | 0.1 | n.d. | 0.1 | 0.1 |
| Cr | 551.5 | 418.0 | 95.8 | 138.2 | 75.9 | 849.1 | 840.9 | 446.8 | 180.6 |
| Ni | 66.8 | 96.7 | 12.6 | 8.6 | 7.9 | 356.0 | 304.1 | 140.7 | 46.4 |
| Cu | n.d. | 10.4 | n.d. | n.d. | n.d. | 16.8 | 37.5 | n.d. | 111.8 |
| Zn | 106.1 | 65.9 | 28.9 | 61.9 | 70.7 | 86.0 | 73.1 | 98.8 | 97.2 |
| Rb | 75.9 | 75.0 | 68.6 | 64.9 | 79.6 | 43.9 | 32.9 | 15.5 | 58.5 |
| Sr | 975 | 1194 | 961 | 441 | 1455 | 580 | 535 | 216 | 400 |
| Y | 11.0 | 15.0 | 2.4 | 8.7 | 8.7 | 18.9 | 16.5 | 21.3 | 18.9 |
| Zr | 36.3 | 59.2 | 121.4 | 141.4 | 220.6 | 41.5 | 40.0 | 56.3 | 44.4 |
| Nb | n.d. | n.d. | n.d. | 3.5 | n.d. | n.d. | n.d. | 9.8 | 4.9 |
| Ba | 686 | 896 | 1195 | 823 | 1642 | 740 | 559 | 182 | 151 |
| Pb | n.d. | n.d. | n.d. | n.d. | n.d. | n.d. | n.d. | n.d. | n.d. |
| Sb | 0.05 | 0.05 | 0.05 | 0.05 | 0.05 | 0.05 | 0.05 | 0.05 | 0.05 |
| As | 0.25 | 0.5 | 0.25 | 0.25 | 0.25 | 0.25 | 0.25 | 0.25 | 0.25 |
| Br | 0.7 | 1.7 | 2.1 | 2.9 | 1.2 | 0.25 | 0.25 | 0.25 | 0.25 |
| Co | 50 | 47 | 25 | 37 | 31 | 76 | 73 | 100 | 72 |
| Hf | 1 | 2 | 3 | 8 | 6 | 2 | 1 | 2 | 2 |
| **Major and Trace Element Ratios** | | | | | | | | | |
| Mg#‡ | 58 | 56 | 49 | 49 | 43 | 63 | 65 | 43 | 41 |
| $K_2O/Na_2O$ | 0.68 | 0.74 | 0.41 | 0.36 | 0.70 | 0.89 | 0.75 | 0.40 | 0.35 |
| $K_2O+Na_2O$ | 5.51 | 5.88 | 9.07 | 9.30 | 10.02 | 3.20 | 2.75 | 2.46 | 3.90 |
| K/Na | 0.45 | 0.49 | 0.27 | 0.24 | 0.46 | 0.59 | 0.49 | 0.26 | 0.23 |
| Sr/Sr* | n.d. | 7.57 | 2.02 | 2.26 | 4.85 | 0.86 | 1.42 | n.d. | 3.17 |
| Zr/Zr* | n.d. | 1.20 | 0.94 | 3.00 | 2.87 | 0.16 | 0.39 | n.d. | 0.82 |
| Ti/Ti* | n.d. | 1.94 | 0.39 | 0.57 | 0.82 | 0.48 | 1.55 | n.d. | 1.10 |
| Nb/Nb* | 0.00 | 0.00 | 0.00 | 0.04 | 0.00 | 0.00 | 0.00 | n.d. | 0.60 |

| Sample | 9210138 | 9210139 | 9210143b | 9210147 | 9210149 | 92101410 | 92101411 | 9210157 | 92101513 |
|---|---|---|---|---|---|---|---|---|---|
| Rock Type** | MD† | Mo† | QMD† | Sy | Hbldt | Gra | Hbldt | MD | MD |
| Major Elements (%) | | | | | | | | | |
| Oxide | | | | | | | | | |
| $Na_2O$ | 5.56 | 3.65 | 6.46 | 2.41 | 1.86 | 5.06 | 1.61 | 6.77 | 4.66 |
| MgO | 3.41 | 6.66 | 2.64 | 11.34 | 13.34 | 0.50 | 14.68 | 3.50 | 6.51 |
| $Al_2O_3$ | 16.16 | 14.54 | 16.59 | 11.75 | 10.64 | 14.34 | 9.75 | 16.78 | 14.83 |
| $SiO_2$ | 59.75 | 56.08 | 60.65 | 52.68 | 47.97 | 73.59 | 47.53 | 59.81 | 54.11 |
| $P_2O_5$ | 0.34 | 0.41 | 0.15 | 0.45 | 0.46 | 0.04 | 0.53 | 0.19 | 0.46 |
| $K_2O$ | 3.71 | 3.64 | 3.39 | 2.35 | 3.01 | 4.44 | 2.51 | 2.06 | 1.58 |
| CaO | 4.29 | 6.78 | 3.21 | 8.08 | 9.90 | 0.75 | 10.11 | 4.06 | 7.81 |
| $TiO_2$ | 0.47 | 0.58 | 0.46 | 0.68 | 0.74 | 0.10 | 0.76 | 0.53 | 0.78 |
| MnO | 0.09 | 0.14 | 0.07 | 0.19 | 0.19 | 0.02 | 0.20 | 0.08 | 0.02 |
| $Fe_2O_3$ | 5.75 | 6.94 | 4.72 | 9.35 | 10.96 | 0.87 | 11.72 | 5.53 | 8.54 |
| Total | 100.03 | 100.05 | 98.79 | 99.73 | 99.59 | 100.02 | 99.88 | 99.66 | 99.67 |
| $H_2O$-%†† | 0.16 | 0.12 | 0.10 | 0.15 | 0.07 | 0.24 | 0.09 | 0.14 | 0.10 |
| $H_2O$+%††† | 0.59 | 0.99 | 0.34 | 2.03 | 1.47 | 0.13 | 1.87 | 0.73 | 1.05 |
| Trace Elements (ppm) | | | | | | | | | |
| Sc | 10 | 19 | 9.3 | 32.6 | 32.8 | 1.6 | 33.9 | 10 | 20.4 |
| Cs | n.d. | 0.25 | 0.25 | n.d. | 3.65 | 1.5 | 3.2 | 0.25 | 0.25 |
| Ta | 1.5 | n.d. | n.d. | 0.6 | 0.47 | 3 | n.d. | 1.9 | n.d. |
| Th | 2.4 | n.d. | n.d. | 4.9 | 4.21 | 1.1 | n.d. | 0.6 | n.d. |
| U | 0.5 | n.d. | n.d. | 1.2 | 1.04 | 0.5 | n.d. | 0.1 | n.d. |
| Cr | 93.7 | 344.2 | 115.6 | 757.4 | 924.4 | n.d. | 1030.4 | 139.6 | 266.2 |
| Ni | 20.4 | 63.6 | 20.4 | 186.2 | 237.3 | n.d. | 283.7 | n.d. | 30.6 |
| Cu | n.d. | n.d. | n.d. | n.d. | n.d. | n.d. | n.d. | n.d. | n.d. |
| Zn | 61.9 | 87.6 | 59.5 | 274.0 | 84.4 | n.d. | 104.4 | 67.5 | 65.9 |
| Rb | 71.3 | 60.4 | 64.0 | 56.7 | 100.6 | 86.9 | 91.4 | 44.8 | 25.6 |
| Sr | 1753 | 1175 | 1060 | 591 | 787 | 563 | 777 | 1067 | 1253 |
| Y | 11.8 | 19.7 | 7.9 | 17.3 | 23.6 | 0.0 | 18.1 | 8.7 | 18.9 |
| Zr | 64.4 | 105.9 | 176.2 | 109.6 | 83.7 | 52.6 | 82.2 | 156.2 | 134.7 |
| Nb | n.d. | n.d. | n.d. | n.d. | n.d. | n.d. | n.d. | n.d. | n.d. |
| Ba | 1936 | 3259 | 1571 | 1237 | 1155 | 1505 | 1087 | 983 | 1138 |
| Pb | 40.8 | n.d. | n.d. | 143.0 | n.d. | n.d. | 7.4 | n.d. | n.d. |
| Sb | 0.05 | 0.05 | 0.05 | 0.05 | n.d. | 0.05 | 0.05 | 0.05 | 0.05 |
| As | 0.8 | 0.25 | 0.25 | 0.25 | n.d. | 0.25 | 1.3 | 0.25 | 0.25 |
| Br | 1.1 | 2.1 | 2.7 | 1.3 | n.d. | 2.2 | 0.25 | 2.7 | 1.9 |
| Co | 35 | 42 | 33 | 69 | n.d. | 32 | 68 | 33 | 44 |
| Hf | 4 | 3 | 5 | 4 | n.d. | 10 | 2 | 6 | 3 |
| Major and Trace Element Ratios | | | | | | | | | |
| Mg#‡ | 45 | 57 | 44 | 63 | 63 | 44 | 63 | 47 | 51 |
| $K_2O/Na_2O$ | 0.67 | 1.00 | 0.52 | 0.97 | 1.62 | 0.88 | 1.56 | 0.30 | 0.34 |
| $K_2O+Na_2O$ | 9.27 | 7.28 | 9.85 | 4.76 | 4.87 | 9.50 | 4.13 | 8.83 | 6.24 |
| K/Na | 0.44 | 0.66 | 0.35 | 0.64 | 1.07 | 0.58 | 1.02 | 0.20 | 0.22 |
| Sr/Sr* | 3.32 | 1.28 | 1.50 | n.d. | 1.20 | n.d. | 2.37 | 1.70 | n.d. |
| Zr/Zr* | 0.41 | 0.35 | 0.93 | n.d. | 0.37 | n.d. | 0.66 | 0.90 | n.d. |
| Ti/Ti* | 0.43 | 0.28 | 0.36 | n.d. | n.d. | n.d. | 0.77 | 0.47 | n.d. |
| Nb/Nb* | 0.00 | 0.00 | 0.00 | n.d. | n.d. | n.d. | n.d. | n.d. | n.d. |

| Sample | 92101514 | 9210162 | 9210163 | 9210164 | 9210171 | 9210174 | 9210175 | 9210176 | 9210181 |
|---|---|---|---|---|---|---|---|---|---|
| Rock Type* | Dio | Vol | Dio | To | Dio | QMD | Gabbro° | To | GD |
| Major Elements (%) | | | | | | | | | |
| Oxide | | | | | | | | | |
| $Na_2O$ | 5.82 | 2.96 | 6.34 | 5.84 | 2.96 | 6.02 | 2.06 | 6.33 | 3.98 |
| MgO | 3.32 | 8.45 | 4.04 | 0.88 | 10.11 | 3.99 | 8.83 | 1.00 | 4.58 |
| $Al_2O_3$ | 15.37 | 15.54 | 15.50 | 15.86 | 11.69 | 16.10 | 11.26 | 17.12 | 16.66 |
| $SiO_2$ | 64.27 | 48.68 | 62.02 | 70.77 | 50.88 | 60.17 | 45.66 | 68.89 | 56.24 |
| $P_2O_5$ | 0.21 | 0.07 | 0.23 | 0.11 | 0.45 | 0.22 | 0.21 | 0.12 | 0.21 |
| $K_2O$ | 3.62 | 0.38 | 0.06 | 0.86 | 0.80 | 2.01 | 0.97 | 0.95 | 1.19 |
| CaO | 3.41 | 9.02 | 5.51 | 3.19 | 10.33 | 4.93 | 10.41 | 3.17 | 7.20 |
| $TiO_2$ | 0.38 | 0.91 | 0.51 | 0.28 | 0.91 | 0.52 | 1.62 | 0.38 | 0.67 |
| MnO | 0.07 | 0.19 | 0.10 | 0.03 | 0.19 | 0.08 | 0.17 | 0.02 | 0.18 |
| $Fe_2O_3$ | 4.33 | 13.04 | 5.54 | 2.65 | 10.11 | 5.45 | 19.27 | 2.46 | 8.28 |
| Total | 101.12 | 99.40 | 100.15 | 100.66 | 98.81 | 99.91 | 100.63 | 100.63 | 99.49 |
| $H_2O$-%†† | 0.16 | 0.73 | 0.23 | 0.16 | 0.13 | 0.21 | 0.12 | 0.15 | 0.12 |
| $H_2O$+%††† | 0.61 | 1.48 | 0.47 | 0.56 | 1.70 | 0.49 | 0.76 | 0.44 | 1.01 |
| Trace Elements (ppm) | | | | | | | | | |
| Sc | n.d. | 31.6 | 8.2 | 3.2 | 34.4 | 11 | 31 | 3.9 | 20 |
| Cs | n.d. | 0.25 | 0.25 | 1.4 | 0.25 | 0.6 | 0.63 | 1.3 | 1.2 |
| Ta | n.d. | 1.6 | 2 | 1.5 | 0.6 | 1 | 0.46 | 1.5 | n.d. |
| Th | n.d. | 0.1 | 1.8 | 1.4 | 0.4 | 1.3 | 1.31 | 1.5 | n.d. |
| U | n.d. | 0.1 | 0.5 | 0.3 | 0.3 | 0.4 | 0.5 | 0.1 | n.d. |
| Cr | 161.5 | 247.0 | 179.9 | n.d. | 563.8 | 176.5 | 55.4 | n.d. | 184.7 |
| Ni | 38.5 | 117.1 | n.d. | n.d. | 66.0 | 44.0 | 64.4 | n.d. | n.d. |
| Cu | n.d. | n.d. | n.d. | n.d. | n.d. | n.d. | n.d. | n.d. | n.d. |
| Zn | 53.8 | 47.4 | 102.0 | 43.4 | 165.5 | 95.6 | 115.7 | 61.9 | 123.7 |
| Rb | 83.2 | 19.2 | 17.4 | 27.4 | 21.0 | 32.9 | 19.2 | 33.8 | 36.6 |
| Sr | 824 | 106 | 1101 | 666 | 1113 | 1421 | 299 | 928 | 749 |
| Y | 8.7 | 17.3 | 6.3 | 3.9 | 16.5 | 6.3 | 11.8 | 2.4 | 11.8 |
| Zr | 147.3 | 51.1 | 131.0 | 147.3 | 117.0 | 169.5 | 34.1 | 140.7 | 105.9 |
| Nb | n.d. | 11.2 | n.d. | n.d. | n.d. | n.d. | 6.3 | n.d. | n.d. |
| Ba | 895 | 125 | 477 | 316 | 523 | 1202 | 234 | 460 | 475 |
| Pb | 10.2 | n.d. | n.d. | n.d. | 2.8 | 18.6 | n.d. | n.d. | 26.0 |
| Sb | 0.05 | 0.05 | 0.05 | 0.05 | 0.05 | 0.05 | n.d. | 0.05 | 0.8 |
| As | 0.25 | 0.6 | 4.7 | 3.3 | 2 | 1 | n.d. | 0.25 | 8 |
| Br | 1.8 | 0.25 | 1.1 | 1.5 | 0.5 | 0.25 | n.d. | 0.8 | 0.25 |
| Co | 45 | 63 | 38 | 25 | 59 | 28 | n.d. | 26 | 31 |
| Hf | 5 | 4 | 7 | 9 | 3 | 5 | n.d. | 6 | 2 |
| Major and Trace Element Ratios | | | | | | | | | |
| Mg#‡ | 51 | 47 | 50 | 31 | 58 | 50 | 39 | 36 | 43 |
| $K_2O/Na_2O$ | 0.62 | 0.13 | 0.01 | 0.15 | 0.27 | 0.33 | 0.47 | 0.15 | 0.30 |
| $K_2O+Na_2O$ | 9.44 | 3.34 | 6.40 | 6.69 | 3.76 | 8.02 | 3.03 | 7.29 | 5.17 |
| K/Na | 0.41 | 0.08 | 0.01 | 0.10 | 0.18 | 0.22 | 0.31 | 0.10 | 0.20 |
| Sr/Sr* | n.d. | 0.93 | 2.32 | 1.79 | 1.70 | 2.51 | 0.57 | n.d. | 5.36 |
| Zr/Zr* | n.d. | n.d. | 0.93 | 1.68 | 0.52 | 1.03 | 0.17 | n.d. | 2.66 |
| Ti/Ti* | n.d. | n.d. | 0.49 | 0.56 | 0.45 | 0.46 | 0.97 | n.d. | 1.90 |
| Nb/Nb* | n.d. | 1.63 | n.d. | n.d. | n.d. | n.d. | 0.30 | n.d. | n.d. |

| Sample | 9210186 | 9210187 | 9210188 | 9210189 | 9306131a | 9306156 | 93061510 | 93061510a | 9306161 |
|---|---|---|---|---|---|---|---|---|---|
| Rock Type[-] | QMD | QMD[†] | Mo[†] | MD[†] | Enc[Δ] | QMD | To | Dyke | MD[†] |
| **Major Elements (%)** | | | | | | | | | |
| Oxide | | | | | | | | | |
| $Na_2O$ | 5.74 | 6.40 | 5.55 | 6.15 | 0.28 | 4.83 | 5.38 | 2.21 | 3.23 |
| MgO | 2.85 | 2.97 | 3.44 | 3.23 | 19.88 | 3.45 | 0.66 | 13.69 | 7.48 |
| $Al_2O_3$ | 15.62 | 15.89 | 16.10 | 16.47 | 3.04 | 16.10 | 15.37 | 11.63 | 14.34 |
| $SiO_2$ | 64.05 | 62.59 | 59.15 | 60.14 | 52.55 | 74.31 | 69.86 | 51.77 | 54.17 |
| $P_2O_5$ | 0.15 | 0.18 | 0.30 | 0.33 | 0.02 | 0.17 | 0.08 | 0.49 | 0.41 |
| $K_2O$ | 2.65 | 3.07 | 3.99 | 3.48 | 0.13 | 3.14 | 1.90 | 1.76 | 4.13 |
| CaO | 4.12 | 4.07 | 4.50 | 4.08 | 11.53 | 3.40 | 2.42 | 7.75 | 6.20 |
| $TiO_2$ | 0.41 | 0.49 | 0.50 | 0.47 | 0.25 | 0.33 | 0.28 | 0.72 | 0.68 |
| MnO | 0.07 | 0.09 | 0.10 | 0.08 | 0.20 | 0.07 | 0.02 | 0.17 | 0.13 |
| $Fe_2O_3$ | 4.18 | 5.11 | 5.71 | 5.55 | 9.62 | 3.89 | 1.85 | 8.92 | 7.00 |
| Total | 100.24 | 101.31 | 99.91 | 100.60 | 99.54 | 110.53 | 99.10 | 100.61 | 99.68 |
| $H_2O$-%[††] | 0.07 | 0.19 | 0.07 | 0.08 | 0.38 | 0.15 | 0.39 | 0.35 | 0.14 |
| $H_2O$+%[†††] | 0.38 | 0.22 | 0.47 | 0.50 | 1.54 | 0.43 | 0.66 | 0.79 | 1.15 |
| | | | | | | | | | |
| **Trace Elements (ppm)** | | | | | | | | | |
| Sc | 9.1 | 8.5 | 10 | 9.4 | n.d. | n.d. | n.d. | n.d. | n.d. |
| Cs | 1.03 | 0.5 | 0.6 | 0.25 | n.d. | n.d. | n.d. | n.d. | n.d. |
| Ta | 1.54 | 0.9 | n.d. | n.d. | n.d. | n.d. | n.d. | n.d. | n.d. |
| Th | 3.23 | 1.6 | n.d. | n.d. | n.d. | n.d. | n.d. | n.d. | n.d. |
| U | 0.79 | 0.3 | n.d. | n.d. | n.d. | n.d. | n.d. | n.d. | n.d. |
| Cr | 127.9 | 101.9 | 98.5 | 87.6 | 343.2 | 182.0 | 16.8 | 1190.4 | 406.6 |
| Ni | n.d. | 52.6 | n.d. | n.d. | 179.5 | n.d. | 3.0 | 238.3 | 100.7 |
| Cu | n.d. | 5.6 | 16.0 | n.d. | n.d. | n.d. | n.d. | n.d. | n.d. |
| Zn | 41.0 | 61.9 | 95.6 | 68.3 | 113.8 | 52.7 | 42.5 | 176.0 | 143.1 |
| Rb | 69.5 | 44.8 | 64.0 | 53.0 | 3.9 | 76.6 | 34.6 | 81.1 | 80.9 |
| Sr | 1290 | 1465 | 1832 | 1760 | 55 | 668 | 889 | 426 | 1063 |
| Y | 8.7 | 10.2 | 8.7 | 5.5 | n.d. | n.d. | n.d. | n.d. | n.d. |
| Zr | 148.1 | 165.8 | 182.9 | 159.9 | 2.9 | 96.5 | 95.0 | 68.2 | 104.6 |
| Nb | n.d. | n.d. | n.d. | n.d. | 2.0 | 4.0 | 3.0 | 3.0 | 4.9 |
| Ba | 1051 | 1413 | 2041 | 2517 | 138 | 1124 | 944 | 753 | 3504 |
| Pb | n.d. | 4.6 | 0.0 | 10.2 | n.d. | n.d. | n.d. | n.d. | n.d. |
| Sb | 0.3 | 0.05 | n.d. | n.d. | n.d. | n.d. | n.d. | n.d. | n.d. |
| As | 3.1 | 0.25 | n.d. | n.d. | n.d. | n.d. | n.d. | n.d. | n.d. |
| Br | 0.25 | 0.25 | n.d. | n.d. | n.d. | n.d. | n.d. | n.d. | n.d. |
| Co | 47 | 25 | n.d. | n.d. | n.d. | n.d. | n.d. | n.d. | n.d. |
| Hf | 5 | 5 | n.d. | n.d. | n.d. | n.d. | n.d. | n.d. | n.d. |
| | | | | | | | | | |
| **Major and Trace Element Ratios** | | | | | | | | | |
| Mg#[*] | 48 | 44 | 45 | 44 | 74 | 55 | 33 | 68 | 60 |
| $K_2O/Na_2O$ | 0.46 | 0.48 | 0.72 | 0.57 | 0.45 | 0.65 | 0.35 | 0.79 | 1.28 |
| $K_2O+Na_2O$ | 8.39 | 9.46 | 9.53 | 9.62 | 0.41 | 7.98 | 7.28 | 3.97 | 7.35 |
| K/Na | 0.30 | 0.32 | 0.47 | 0.37 | 0.29 | 0.43 | 0.23 | 0.52 | 0.84 |
| Sr/Sr* | 3.12 | 2.39 | 3.58 | 7.23 | n.d. | 1.75 | n.d. | 1.64 | 1.18 |
| Zr/Zr* | 1.29 | 0.98 | 1.10 | 2.55 | n.d. | 0.90 | n.d. | 0.90 | 0.39 |
| Ti/Ti* | n.d. | 0.43 | 0.41 | 1.32 | n.d. | 0.30 | n.d. | 1.67 | 0.39 |
| Nb/Nb* | n.d. | n.d. | n.d. | n.d. | n.d. | 0.08 | n.d. | 0.10 | 0.04 |

| Sample | 9306162a | 9306164 | 9306166 | 9306171 | 9306173 | 9306174 | 93061710 | 9306182 | 9306183 |
|---|---|---|---|---|---|---|---|---|---|
| Rock Type** | Enc | Enc | Hbldt | To | Hbldt | Hbldt | Hbldt | MD†* | MD†* |
| Major Elements (%) | | | | | | | | | |
| Oxide | | | | | | | | | |
| $Na_2O$ | 0.89 | 0.23 | 0.60 | 5.23 | 3.11 | 2.97 | 0.62 | 4.32 | 5.74 |
| MgO | 14.93 | 20.30 | 19.34 | 2.80 | 11.65 | 12.15 | 18.34 | 3.97 | 3.78 |
| $Al_2O_3$ | 7.91 | 5.05 | 5.43 | 15.44 | 11.95 | 11.50 | 3.18 | 14.14 | 15.11 |
| $SiO_2$ | 49.62 | 47.85 | 49.45 | 61.37 | 50.92 | 50.65 | 52.26 | 62.24 | 60.17 |
| $P_2O_5$ | 0.08 | 0.08 | 0.14 | 0.21 | 0.32 | 0.32 | 0.04 | 0.21 | 0.24 |
| $K_2O$ | 2.80 | 0.08 | 0.53 | 2.89 | 2.84 | 2.54 | 0.21 | 3.54 | 3.21 |
| CaO | 9.34 | 8.86 | 10.96 | 3.49 | 7.11 | 7.40 | 13.32 | 3.76 | 3.59 |
| $TiO_2$ | 0.51 | 0.24 | 0.63 | 0.42 | 0.58 | 0.58 | 0.35 | 0.44 | 0.46 |
| MnO | 0.21 | 0.31 | 0.16 | 0.07 | 0.14 | 0.14 | 0.20 | 0.08 | 0.08 |
| $Fe_2O_3$ | 10.52 | 11.24 | 8.23 | 4.18 | 8.22 | 8.42 | 9.79 | 4.94 | 4.86 |
| Total | 98.39 | 98.67 | 98.50 | 97.02 | 98.44 | 98.24 | 99.99 | 98.67 | 98.33 |
| $H_2O$-%†† | 0.17 | 0.36 | 0.18 | 0.16 | 0.31 | 0.19 | 0.11 | 0.13 | 0.07 |
| $H_2O$+%††† | 0.79 | 3.53 | 2.54 | 0.40 | 0.88 | 0.96 | 1.42 | 0.58 | 0.54 |
| | | | | | | | | | |
| Trace Elements (ppm) | | | | | | | | | |
| Sc | n.d. | n.d. | n.d. | n.d. | n.d. | n.d. | n.d. | n.d. | n.d. |
| Cs | n.d. | n.d. | n.d. | n.d. | n.d. | n.d. | n.d. | n.d. | n.d. |
| Ta | n.d. | n.d. | n.d. | n.d. | n.d. | n.d. | n.d. | n.d. | n.d. |
| Th | n.d. | n.d. | n.d. | n.d. | n.d. | n.d. | n.d. | n.d. | n.d. |
| U | n.d. | n.d. | n.d. | n.d. | n.d. | n.d. | n.d. | n.d. | n.d. |
| Cr | 1591.4 | 2070.0 | 1290.3 | 122.3 | 904.9 | 941.9 | 876.4 | 230.3 | 212.7 |
| Ni | 525.8 | 1180.5 | 596.0 | 40.8 | 337.9 | 315.3 | 36.4 | 65.5 | 74.5 |
| Cu | n.d. | n.d. | n.d. | n.d. | n.d. | n.d. | n.d. | n.d. | n.d. |
| Zn | 152.5 | 213.2 | 140.0 | 62.6 | 78.0 | 81.0 | 108.3 | 65.5 | 65.6 |
| Rb | 132.7 | 7.7 | 14.6 | 76.6 | 97.8 | 92.9 | 3.9 | 99.3 | 86.5 |
| Sr | 237 | 799 | 195 | 1222 | 762 | 808 | 80 | 894 | 1724 |
| Y | n.d. | n.d. | n.d. | n.d. | n.d. | n.d. | n.d. | n.d. | n.d. |
| Zr | 18.8 | 55.7 | 27.2 | 149.1 | 89.9 | 84.0 | 3.0 | 120.1 | 127.2 |
| Nb | 1.0 | 4.8 | 3.9 | 7.0 | 8.9 | 8.9 | 1.0 | 8.9 | 8.0 |
| Ba | 2481 | 44 | 190 | 1428 | 1157 | 1145 | 59 | 1236 | 1948 |
| Pb | n.d. | n.d. | n.d. | n.d. | n.d. | n.d. | n.d. | n.d. | n.d. |
| Sb | n.d. | n.d. | n.d. | n.d. | n.d. | n.d. | n.d. | n.d. | n.d. |
| As | n.d. | n.d. | n.d. | n.d. | n.d. | n.d. | n.d. | n.d. | n.d. |
| Br | n.d. | n.d. | n.d. | n.d. | n.d. | n.d. | n.d. | n.d. | n.d. |
| Co | n.d. | n.d. | n.d. | n.d. | n.d. | n.d. | n.d. | n.d. | n.d. |
| Hf | n.d. | n.d. | n.d. | n.d. | n.d. | n.d. | n.d. | n.d. | n.d. |
| | | | | | | | | | |
| Major and Trace Element Ratios | | | | | | | | | |
| Mg#‡ | 66 | 71 | 76 | 48 | 66 | 67 | 72 | 53 | 52 |
| $K_2O/Na_2O$ | 3.14 | 0.33 | 0.89 | 0.55 | 0.91 | 0.85 | 0.33 | 0.82 | 0.56 |
| $K_2O+Na_2O$ | 3.69 | 0.31 | 1.14 | 8.12 | 5.95 | 5.51 | 0.83 | 7.86 | 8.95 |
| K/Na | 2.07 | 0.22 | 0.58 | 0.36 | 0.60 | 0.56 | 0.22 | 0.54 | 0.37 |
| Sr/Sr* | 0.41 | 1.85 | 0.68 | 1.95 | 1.25 | n.d. | 0.77 | 1.78 | 3.11 |
| Zr/Zr* | 0.10 | 0.51 | 0.37 | 0.88 | 0.51 | n.d. | 0.07 | 0.86 | 0.82 |
| Ti/Ti* | 0.34 | 0.33 | 1.32 | 0.36 | 0.43 | n.d. | 0.67 | 0.40 | 0.38 |
| Nb/Nb* | 0.01 | 0.40 | 0.21 | 0.10 | 0.14 | n.d. | 0.17 | 0.15 | 0.11 |

| Sample | 9306184 | 9306187 | 9306193 | 9306196 | 9306198 | 93061910a | 93061911a | 9306203 | 9306203a |
|---|---|---|---|---|---|---|---|---|---|
| Rock Type[*] | QMD[†] | Dio | Mo[†] | Mo[‡] | Dio | Enc | Enc | Mo[†‡] | Sy[†] |
| **Major Elements (%)** | | | | | | | | | |
| Oxide | | | | | | | | | |
| $Na_2O$ | 5.32 | 3.35 | 4.71 | 4.73 | 4.46 | 0.59 | 0.33 | 6.76 | 5.52 |
| MgO | 3.52 | 9.96 | 4.25 | 0.95 | 6.83 | 16.09 | 20.01 | 0.90 | 4.57 |
| $Al_2O_3$ | 15.92 | 12.04 | 15.46 | 15.38 | 14.39 | 3.66 | 2.37 | 18.42 | 13.68 |
| $SiO_2$ | 61.20 | 53.14 | 56.97 | 67.75 | 51.90 | 51.09 | 54.66 | 61.29 | 61.44 |
| $P_2O_5$ | 0.24 | 0.37 | 0.37 | 0.05 | 0.26 | 0.05 | 0.01 | 0.15 | 0.12 |
| $K_2O$ | 2.82 | 2.06 | 4.06 | 5.00 | 1.13 | 0.82 | 0.65 | 4.01 | 3.86 |
| CaO | 3.31 | 7.82 | 4.39 | 1.70 | 8.41 | 11.67 | 12.12 | 2.63 | 4.49 |
| $TiO_2$ | 0.48 | 0.82 | 0.57 | 0.21 | 0.83 | 0.25 | 0.16 | 0.35 | 0.45 |
| MnO | 0.10 | 0.15 | 0.11 | 0.03 | 0.15 | 0.26 | 0.22 | 0.07 | 0.11 |
| $Fe_2O_3$ | 4.56 | 8.50 | 6.16 | 1.82 | 8.97 | 12.46 | 8.05 | 3.36 | 4.71 |
| Total | 99.21 | 99.73 | 96.37 | 96.46 | 96.70 | 98.11 | 100.18 | 98.86 | 99.71 |
| $H_2O$-%[††] | 0.19 | 0.18 | 0.13 | 0.14 | 0.14 | 0.38 | 0.11 | 0.22 | 0.10 |
| $H_2O$+%[†††] | 1.17 | 1.03 | 0.75 | 0.42 | 1.01 | 0.61 | 1.31 | 0.18 | 0.44 |
| **Trace Elements (ppm)** | | | | | | | | | |
| Sc | n.d. | n.d. | n.d. | n.d. | n.d. | n.d. | n.d. | n.d. | n.d. |
| Cs | n.d. | n.d. | n.d. | n.d. | n.d. | n.d. | n.d. | n.d. | n.d. |
| Ta | n.d. | n.d. | n.d. | n.d. | n.d. | n.d. | n.d. | n.d. | n.d. |
| Th | n.d. | n.d. | n.d. | n.d. | n.d. | n.d. | n.d. | n.d. | n.d. |
| U | n.d. | n.d. | n.d. | n.d. | n.d. | n.d. | n.d. | n.d. | n.d. |
| Cr | 157.8 | 660.8 | 180.4 | 45.7 | 287.6 | 661.3 | 881.3 | 19.9 | 230.7 |
| Ni | 25.6 | 105.7 | 54.5 | 15.9 | 38.5 | 104.9 | 171.5 | 9.0 | 25.9 |
| Cu | n.d. | n.d. | n.d. | n.d. | n.d. | n.d. | n.d. | n.d. | n.d. |
| Zn | 72.0 | 106.7 | 84.2 | 25.9 | 108.7 | 329.6 | 139.0 | 62.7 | 86.5 |
| Rb | 64.1 | 62.2 | 70.4 | 91.5 | 49.4 | 115.8 | 55.2 | 131.5 | 86.5 |
| Sr | 1016 | 815 | 867 | 924 | 998 | 56 | 55 | 2663 | 715 |
| Y | n.d. | n.d. | n.d. | n.d. | n.d. | n.d. | n.d. | n.d. | n.d. |
| Zr | 124.3 | 30.6 | 227.9 | 92.5 | 70.2 | 2.0 | 1.0 | 75.7 | 21.9 |
| Nb | 6.9 | 3.0 | 8.9 | 5.0 | 4.0 | n.d. | n.d. | 6.0 | 4.0 |
| Ba | 1930 | 754 | 2387 | 1189 | 445 | 168 | 178 | 1667 | 867 |
| Pb | n.d. | n.d. | n.d. | n.d. | n.d. | n.d. | n.d. | n.d. | n.d. |
| Sb | n.d. | n.d. | n.d. | n.d. | n.d. | n.d. | n.d. | n.d. | n.d. |
| As | n.d. | n.d. | n.d. | n.d. | n.d. | n.d. | n.d. | n.d. | n.d. |
| Br | n.d. | n.d. | n.d. | n.d. | n.d. | n.d. | n.d. | n.d. | n.d. |
| Co | n.d. | n.d. | n.d. | n.d. | n.d. | n.d. | n.d. | n.d. | n.d. |
| Hf | n.d. | n.d. | n.d. | n.d. | n.d. | n.d. | n.d. | n.d. | n.d. |
| **Major and Trace Element Ratios** | | | | | | | | | |
| Mg#[§] | 52 | 62 | 49 | 42 | 51 | 64 | 77 | 27 | 57 |
| $K_2O/Na_2O$ | 0.53 | 0.62 | 0.86 | 1.06 | 0.25 | 1.38 | 2.00 | 0.59 | 0.70 |
| $K_2O+Na_2O$ | 8.14 | 5.41 | 8.77 | 9.73 | 5.58 | 1.42 | 0.98 | 10.78 | 9.38 |
| K/Na | 0.35 | 0.41 | 0.57 | 0.70 | 0.17 | 0.91 | 1.32 | 0.39 | 0.46 |
| Sr/Sr* | 1.49 | n.d. | 0.96 | 4.15 | 1.87 | 0.61 | 0.75 | 3.47 | 1.45 |
| Zr/Zr* | 0.63 | n.d. | 0.86 | 1.08 | 0.39 | 0.06 | 0.02 | 0.38 | 0.15 |
| Ti/Ti* | 0.36 | n.d. | 0.31 | 0.27 | 0.48 | 0.37 | 0.23 | 0.28 | 0.38 |
| Nb/Nb* | 0.09 | n.d. | 0.09 | 0.16 | 0.12 | n.d. | n.d. | 0.07 | 0.08 |

| Sample | 9306206a | 9306212 | 9306222 | 9306226 | 9306231 | 9306234 | 9306235 | 9306238 | 9306242 |
|---|---|---|---|---|---|---|---|---|---|
| Rock Type[~] | Dyke | MD[††] | Sy[†] | MD[†] | Dio | QMD | Dio | Mo[‡] | MD[†] |
| **Major Elements (%)** | | | | | | | | | |
| Oxide | | | | | | | | | |
| $Na_2O$ | 1.97 | 5.27 | 3.71 | 6.30 | 3.06 | 5.51 | 1.97 | 5.73 | 5.49 |
| MgO | 12.29 | 2.17 | 6.98 | 2.88 | 12.17 | 2.08 | 13.16 | 2.89 | 4.18 |
| $Al_2O_3$ | 9.81 | 16.77 | 13.64 | 15.63 | 11.14 | 13.75 | 9.66 | 14.24 | 16.29 |
| $SiO_2$ | 48.63 | 61.89 | 53.93 | 60.82 | 52.57 | 67.48 | 47.79 | 63.54 | 58.27 |
| $P_2O_5$ | 0.40 | 0.24 | 0.47 | 0.18 | 0.29 | 0.17 | 0.47 | 0.11 | 0.31 |
| $K_2O$ | 1.55 | 4.41 | 2.92 | 3.22 | 2.70 | 2.84 | 2.00 | 3.66 | 2.40 |
| CaO | 9.73 | 2.92 | 6.28 | 3.70 | 6.71 | 2.21 | 9.31 | 2.80 | 4.04 |
| $TiO_2$ | 0.90 | 0.32 | 0.79 | 0.52 | 0.54 | 0.34 | 0.63 | 0.36 | 0.50 |
| MnO | 0.18 | 0.06 | 0.14 | 0.08 | 0.13 | 0.07 | 0.17 | 0.06 | 0.08 |
| $Fe_2O_3$ | 10.79 | 3.68 | 8.50 | 4.87 | 7.86 | 3.03 | 10.07 | 4.11 | 5.35 |
| Total | 99.49 | 98.99 | 99.71 | 99.07 | 98.50 | 98.45 | 98.25 | 98.51 | 98.71 |
| $H_2O$-%[†††] | 0.54 | 0.22 | 0.15 | 0.11 | 0.14 | 0.05 | 1.51 | 0.24 | 0.22 |
| $H_2O$+%[†††] | 2.27 | 0.66 | 1.90 | 0.44 | 0.76 | 0.75 | 1.19 | 0.40 | 1.22 |
| **Trace Elements (ppm)** | | | | | | | | | |
| Sc | n.d. | n.d. | n.d. | n.d. | n.d. | n.d. | n.d. | n.d. | n.d. |
| Cs | n.d. | n.d. | n.d. | n.d. | n.d. | n.d. | n.d. | n.d. | n.d. |
| Ta | n.d. | n.d. | n.d. | n.d. | n.d. | n.d. | n.d. | n.d. | n.d. |
| Th | n.d. | n.d. | n.d. | n.d. | n.d. | n.d. | n.d. | n.d. | n.d. |
| U | n.d. | n.d. | n.d. | n.d. | n.d. | n.d. | n.d. | n.d. | n.d. |
| Cr | 1026.1 | 113.0 | 329.1 | 130.3 | 1107.9 | 98.2 | 819.9 | 138.1 | 223.7 |
| Ni | 122.4 | 18.8 | 75.4 | 20.9 | 362.7 | 30.7 | 205.2 | 56.6 | 37.4 |
| Cu | n.d. | n.d. | n.d. | n.d. | n.d. | n.d. | n.d. | n.d. | n.d. |
| Zn | 179.8 | 81.3 | 106.8 | 77.6 | 74.3 | 90.3 | 93.4 | 68.6 | 76.9 |
| Rb | 150.6 | 137.8 | 63.7 | 59.7 | 85.2 | 55.5 | 63.2 | 90.4 | 61.1 |
| Sr | 1183 | 1162 | 621 | 1012 | 574 | 302 | 561 | 1030 | 1110 |
| Y | n.d. | n.d. | n.d. | n.d. | n.d. | n.d. | n.d. | n.d. | n.d. |
| Zr | 50.5 | 198.2 | 82.3 | 116.4 | 125.8 | 120.0 | 72.0 | 130.1 | 109.4 |
| Nb | 1.0 | 5.0 | 2.9 | 3.0 | 6.9 | 5.0 | 5.8 | 6.0 | 4.9 |
| Ba | 723 | 1624 | 1267 | 1467 | 1512 | 978 | 885 | 1677 | 1445 |
| Pb | n.d. | n.d. | n.d. | n.d. | n.d. | n.d. | n.d. | n.d. | n.d. |
| Sb | n.d. | n.d. | n.d. | n.d. | n.d. | n.d. | n.d. | n.d. | n.d. |
| As | n.d. | n.d. | n.d. | n.d. | n.d. | n.d. | n.d. | n.d. | n.d. |
| Br | n.d. | n.d. | n.d. | n.d. | n.d. | n.d. | n.d. | n.d. | n.d. |
| Co | n.d. | n.d. | n.d. | n.d. | n.d. | n.d. | n.d. | n.d. | n.d. |
| Hf | n.d. | n.d. | n.d. | n.d. | n.d. | n.d. | n.d. | n.d. | n.d. |
| **Major and Trace Element Ratios** | | | | | | | | | |
| Mg#[¥] | 61 | 45 | 53 | 45 | 68 | 49 | 64 | 49 | 52 |
| $K_2O/Na_2O$ | 0.79 | 0.84 | 0.79 | 0.51 | 0.88 | 0.52 | 1.01 | 0.64 | 0.44 |
| $K_2O+Na_2O$ | 3.53 | 9.68 | 6.63 | 9.52 | 5.76 | 8.34 | 3.98 | 9.39 | 7.89 |
| K/Na | 0.52 | 0.55 | 0.52 | 0.34 | 0.58 | 0.34 | 0.67 | 0.42 | 0.29 |
| Sr/Sr* | 2.94 | n.d. | 1.00 | 2.20 | 1.60 | 0.64 | 0.94 | 3.18 | 1.39 |
| Zr/Zr* | 0.38 | n.d. | 0.42 | 0.93 | 1.14 | 1.02 | 0.32 | 1.43 | 0.50 |
| Ti/Ti* | 0.60 | n.d. | 0.51 | 0.60 | 0.64 | 0.43 | 0.32 | 0.52 | 0.34 |
| Nb/Nb* | 0.02 | n.d. | 0.05 | 0.05 | 0.13 | 0.09 | 0.12 | 0.11 | 0.06 |

| Sample | 9306244 | 9306254 | 9306257 | 9306257a | 93062510 | 93062511 | 93062513 | 9306261a | 9306266 |
|---|---|---|---|---|---|---|---|---|---|
| Rock Type* | Dio | Hbldt | Dio | Dio | Dyke | Dyke | Dyke | Dio | Dyke |
| **Major Elements (%)** | | | | | | | | | |
| Oxide | | | | | | | | | |
| $Na_2O$ | 2.53 | 1.78 | 2.94 | 0.19 | 4.74 | 0.96 | 6.79 | 1.22 | 3.70 |
| MgO | 12.13 | 12.44 | 11.97 | 0.13 | 7.13 | 13.70 | 4.95 | 16.77 | 5.83 |
| $Al_2O_3$ | 11.43 | 6.92 | 10.21 | 18.74 | 12.48 | 2.72 | 14.06 | 8.04 | 13.86 |
| $SiO_2$ | 48.36 | 44.28 | 50.07 | 63.36 | 55.68 | 51.90 | 61.54 | 49.67 | 55.47 |
| $P_2O_5$ | 0.42 | 0.89 | 0.46 | 0.06 | 0.24 | 0.29 | 0.14 | 0.19 | 0.55 |
| $K_2O$ | 1.65 | 1.11 | 1.12 | 15.91 | 1.30 | 0.28 | 1.57 | 2.45 | 3.91 |
| CaO | 8.04 | 14.20 | 8.28 | 1.37 | 7.55 | 12.34 | 4.33 | 9.29 | 6.28 |
| $TiO_2$ | 0.79 | 1.03 | 0.57 | 0.14 | 0.77 | 1.00 | 0.41 | 0.89 | 0.68 |
| MnO | 0.18 | 0.23 | 0.17 | 0.02 | 0.14 | 0.27 | 0.06 | 0.17 | 0.14 |
| $Fe_2O_3$ | 10.10 | 14.90 | 9.72 | 1.28 | 8.42 | 14.01 | 4.30 | 10.45 | 7.35 |
| Total | 96.77 | 96.50 | 96.50 | 102.01 | 99.32 | 96.37 | 99.09 | 100.56 | 99.62 |
| $H_2O$-%†† | 0.22 | 0.15 | 0.17 | 0.26 | 0.14 | 0.23 | 0.29 | 0.14 | 0.24 |
| $H_2O$+%††† | 2.58 | 0.33 | 2.47 | 0.29 | 0.49 | 0.52 | 0.44 | 1.20 | 1.17 |
| **Trace Elements (ppm)** | | | | | | | | | |
| Sc | n.d. | n.d. | n.d. | n.d. | n.d. | n.d. | n.d. | n.d. | n.d. |
| Cs | n.d. | n.d. | n.d. | n.d. | n.d. | n.d. | n.d. | n.d. | n.d. |
| Ta | n.d. | n.d. | n.d. | n.d. | n.d. | n.d. | n.d. | n.d. | n.d. |
| Th | n.d. | n.d. | n.d. | n.d. | n.d. | n.d. | n.d. | n.d. | n.d. |
| U | n.d. | n.d. | n.d. | n.d. | n.d. | n.d. | n.d. | n.d. | n.d. |
| Cr | 699.6 | 486.6 | 610.2 | 35.8 | 404.4 | 472.4 | 371.2 | 1333.9 | 291.8 |
| Ni | 201.1 | 163.2 | 288.1 | 16.9 | 21.9 | 83.4 | 19.9 | 169.7 | 46.3 |
| Cu | n.d. | n.d. | n.d. | n.d. | n.d. | n.d. | n.d. | n.d. | n.d. |
| Zn | 128.3 | 158.2 | 115.8 | 1.0 | 87.4 | 253.1 | 55.6 | 89.8 | 98.6 |
| Rb | 51.5 | 33.8 | 38.0 | 282.4 | 19.9 | 6.0 | 24.8 | 95.7 | 71.0 |
| Sr | 401 | 516 | 1117 | 154 | 722 | 208 | 256 | 140 | 1342 |
| Y | n.d. | n.d. | n.d. | n.d. | n.d. | n.d. | n.d. | n.d. | 17.5 |
| Zr | 90.4 | 80.6 | 89.5 | 72.6 | 60.6 | 53.6 | 74.4 | 17.8 | 141.0 |
| Nb | 7.8 | 7.0 | 2.9 | 1.0 | 3.0 | 5.0 | 3.0 | 1.0 | 5.9 |
| Ba | 1549 | 493 | 675 | 1513 | 766 | 118 | 644 | 284 | 1939 |
| Pb | n.d. | n.d. | n.d. | n.d. | n.d. | n.d. | n.d. | n.d. | n.d. |
| Sb | n.d. | n.d. | n.d. | n.d. | n.d. | n.d. | n.d. | n.d. | n.d. |
| As | n.d. | n.d. | n.d. | n.d. | n.d. | n.d. | n.d. | n.d. | n.d. |
| Br | n.d. | n.d. | n.d. | n.d. | n.d. | n.d. | n.d. | n.d. | n.d. |
| Co | n.d. | n.d. | n.d. | n.d. | n.d. | n.d. | n.d. | n.d. | n.d. |
| Hf | n.d. | n.d. | n.d. | n.d. | n.d. | n.d. | n.d. | n.d. | n.d. |
| **Major and Trace Element Ratios** | | | | | | | | | |
| Mg#‡ | 62 | 53 | 63 | 12 | 54 | 57 | 61 | 69 | 52 |
| $K_2O/Na_2O$ | 0.65 | 0.63 | 0.38 | 84.21 | 0.27 | 0.29 | 0.23 | 2.00 | 1.06 |
| $K_2O+Na_2O$ | 4.18 | 2.90 | 4.06 | 16.10 | 6.04 | 1.24 | 8.36 | 3.67 | 7.61 |
| K/Na | 0.43 | 0.41 | 0.25 | 55.41 | 0.18 | 0.19 | 0.15 | 1.32 | 0.70 |
| Sr/Sr* | 0.61 | n.d. | 2.04 | 1.13 | 2.80 | n.d. | 1.78 | 0.42 | 1.24 |
| Zr/Zr* | 0.39 | n.d. | 0.49 | 2.20 | 0.65 | n.d. | 1.46 | 0.15 | 0.46 |
| Ti/Ti* | 0.38 | n.d. | 0.38 | 0.50 | 0.71 | n.d. | 0.75 | 0.64 | 0.35 |
| Nb/Nb* | 0.13 | n.d. | 0.07 | 0.03 | 0.10 | n.d. | 0.14 | 0.05 | 0.06 |

| Sample | 9306268dyke | 9306268enc | 9306271 | 9306273 | 9306173 | 9306174 | 93061711a | 93061712 | 9306182 |
|---|---|---|---|---|---|---|---|---|---|
| Rock Type* | Dyke | Enc | Dyke | Dyke | Gr | MD† | Dio | Dio | Vol |
| **Major Elements (%)** | | | | | | | | | |
| Oxide | | | | | | | | | |
| $Na_2O$ | 3.72 | 0.59 | 2.80 | 1.72 | 5.97 | 5.94 | 2.16 | 5.54 | 0.99 |
| MgO | 11.48 | 18.04 | 11.35 | 9.22 | 2.74 | 1.93 | 11.76 | 5.33 | 21.95 |
| $Al_2O_3$ | 11.63 | 3.36 | 12.46 | 16.28 | 14.65 | 17.75 | 8.23 | 15.17 | 8.99 |
| $SiO_2$ | 51.54 | 54.59 | 51.61 | 45.62 | 65.67 | 58.58 | 46.40 | 58.42 | 45.95 |
| $P_2O_5$ | 0.71 | 0.02 | 0.39 | 0.06 | 0.13 | 0.24 | 0.17 | 0.25 | 0.00 |
| $K_2O$ | 0.43 | 0.48 | 2.94 | 1.42 | 3.07 | 4.36 | 1.10 | 1.98 | 4.20 |
| CaO | 7.36 | 11.85 | 7.22 | 11.24 | 2.83 | 3.23 | 10.87 | 5.23 | 4.87 |
| $TiO_2$ | 0.76 | 0.35 | 0.69 | 0.81 | 0.30 | 0.51 | 1.18 | 0.50 | 0.22 |
| MnO | 0.14 | 0.16 | 0.14 | 0.17 | 0.06 | 0.10 | 0.20 | 0.09 | 0.24 |
| $Fe_2O_3$ | 8.44 | 8.58 | 8.30 | 11.07 | 3.38 | 4.62 | 15.12 | 5.70 | 10.06 |
| Total | 99.16 | 99.30 | 99.78 | 100.10 | 99.45 | 99.25 | 98.31 | 99.40 | 100.10 |
| $H_2O$-%†† | 0.29 | 0.23 | 0.20 | 0.12 | 0.11 | 0.02 | 0.13 | 0.25 | 0.07 |
| $H_2O$+%††† | 2.34 | 0.85 | 1.24 | 2.23 | 0.32 | 1.54 | 0.80 | 0.86 | 1.98 |
| **Trace Elements (ppm)** | | | | | | | | | |
| Sc | n.d. | n.d. | n.d. | n.d. | n.d. | n.d. | n.d. | n.d. | n.d. |
| Cs | n.d. | n.d. | n.d. | n.d. | n.d. | n.d. | n.d. | n.d. | n.d. |
| Ta | n.d. | n.d. | n.d. | n.d. | n.d. | n.d. | n.d. | n.d. | n.d. |
| Th | n.d. | n.d. | n.d. | n.d. | n.d. | n.d. | n.d. | n.d. | n.d. |
| U | n.d. | n.d. | n.d. | n.d. | n.d. | n.d. | n.d. | n.d. | n.d. |
| Cr | 857.6 | 963.4 | 757.9 | 449.2 | 160.3 | 62.0 | 1389.5 | 346.8 | 2535.8 |
| Ni | 129.5 | 29.7 | 153.8 | 115.2 | 14.9 | 11.8 | 256.2 | 37.7 | 881.5 |
| Cu | n.d. | n.d. | n.d. | n.d. | n.d. | n.d. | n.d. | n.d. | n.d. |
| Zn | 140.2 | 102.9 | 94.6 | 83.0 | 36.8 | 94.5 | 246.3 | 67.4 | 135.2 |
| Rb | 13.6 | 12.9 | 89.7 | 78.1 | 73.7 | 129.9 | 28.8 | 60.4 | 697.4 |
| Sr | 924 | 114 | 751 | 269 | 743 | 1684 | 72 | 1137 | 51 |
| Y | 22.8 | n.d. | 14.5 | n.d. | n.d. | n.d. | n.d. | n.d. | n.d. |
| Zr | 99.3 | 4.0 | 59.1 | 18.6 | 79.7 | 191.9 | 2.0 | 100.1 | 2.0 |
| Nb | 6.8 | 2.0 | 3.9 | 1.0 | 3.0 | 7.9 | 2.0 | 4.0 | 4.9 |
| Ba | 443 | 161 | 1834 | 218 | 991 | 1563 | 201 | 724 | 323 |
| Pb | n.d. | n.d. | n.d. | n.d. | n.d. | n.d. | n.d. | n.d. | n.d. |
| Sb | n.d. | n.d. | n.d. | n.d. | n.d. | n.d. | n.d. | n.d. | n.d. |
| As | n.d. | n.d. | n.d. | n.d. | n.d. | n.d. | n.d. | n.d. | n.d. |
| Br | n.d. | n.d. | n.d. | n.d. | n.d. | n.d. | n.d. | n.d. | n.d. |
| Co | n.d. | n.d. | n.d. | n.d. | n.d. | n.d. | n.d. | n.d. | n.d. |
| Hf | n.d. | n.d. | n.d. | n.d. | n.d. | n.d. | n.d. | n.d. | n.d. |
| **Major and Trace Element Ratios** | | | | | | | | | |
| Mg#* | 65 | 74 | 65 | 53 | 53 | 37 | 52 | 56 | 75 |
| $K_2O/Na_2O$ | 0.12 | 0.82 | 1.05 | 0.82 | 0.51 | 0.73 | 0.51 | 0.36 | 4.25 |
| $K_2O+Na_2O$ | 4.15 | 1.08 | 5.74 | 3.13 | 9.04 | 10.30 | 3.26 | 7.52 | 5.19 |
| K/Na | 0.08 | 0.54 | 0.69 | 0.54 | 0.34 | 0.48 | 0.34 | 0.24 | 2.79 |
| Sr/Sr* | 0.71 | 0.48 | 1.17 | 3.20 | n.d. | n.d. | 0.12 | n.d. | 3.34 |
| Zr/Zr* | 0.27 | 0.05 | 0.31 | 0.43 | n.d. | n.d. | 0.01 | n.d. | 0.24 |
| Ti/Ti* | 0.29 | 0.51 | 0.48 | 0.86 | n.d. | n.d. | 0.89 | n.d. | 1.02 |
| Nb/Nb* | 0.11 | 0.17 | 0.05 | 0.11 | n.d. | n.d. | 0.09 | n.d. | 0.65 |

| Sample | 9306184 | 9306185 | 9306186 | 9306187 | 9306188 | 9306191 | 9306192 | 9306193 | 9306193a |
|---|---|---|---|---|---|---|---|---|---|
| Rock Type** | Dio | Sy† | Sed | QMo† | Dio | Hbldt | Mo† | QMD | Sy |
| **Major Elements (%)** | | | | | | | | | |
| Oxide | | | | | | | | | |
| $Na_2O$ | 5.50 | 4.80 | 4.08 | 6.11 | 7.79 | 0.89 | 3.93 | 4.68 | 2.49 |
| MgO | 5.82 | 4.61 | 4.27 | 2.42 | 2.96 | 17.35 | 6.27 | 2.68 | 9.85 |
| $Al_2O_3$ | 15.81 | 14.23 | 15.43 | 15.60 | 16.10 | 8.52 | 13.49 | 15.29 | 11.79 |
| $SiO_2$ | 55.24 | 58.04 | 60.47 | 61.29 | 59.86 | 43.43 | 54.04 | 63.90 | 50.71 |
| $P_2O_5$ | 0.27 | 0.38 | 0.22 | 0.14 | 0.19 | 0.52 | 0.52 | 0.19 | 0.43 |
| $K_2O$ | 1.51 | 2.76 | 1.91 | 4.20 | 0.60 | 2.07 | 3.17 | 3.20 | 2.71 |
| CaO | 5.83 | 5.92 | 5.19 | 3.46 | 4.74 | 10.18 | 6.73 | 3.22 | 7.41 |
| $TiO_2$ | 0.54 | 0.69 | 0.59 | 0.40 | 0.51 | 0.88 | 0.79 | 0.39 | 0.66 |
| MnO | 0.11 | 0.10 | 0.09 | 0.06 | 0.07 | 0.17 | 0.13 | 0.06 | 0.14 |
| $Fe_2O_3$ | 6.44 | 6.26 | 5.88 | 3.89 | 4.97 | 10.95 | 8.14 | 3.76 | 8.13 |
| Total | 98.48 | 98.75 | 99.09 | 98.25 | 98.71 | 97.94 | 98.78 | 98.69 | 96.71 |
| $H_2O$-%†† | 0.14 | 0.04 | 0.13 | 0.10 | 0.09 | 0.05 | 0.20 | 0.12 | 1.98 |
| $H_2O$+%††† | 0.93 | 0.64 | 0.59 | 0.19 | 0.34 | 2.48 | 1.07 | 0.80 | 2.00 |
| **Trace Elements (ppm)** | | | | | | | | | |
| Sc | n.d. | n.d. | n.d. | n.d. | n.d. | n.d. | n.d. | n.d. | n.d. |
| Cs | n.d. | n.d. | n.d. | n.d. | n.d. | n.d. | n.d. | n.d. | n.d. |
| Ta | n.d. | n.d. | n.d. | n.d. | n.d. | n.d. | n.d. | n.d. | n.d. |
| Th | n.d. | n.d. | n.d. | n.d. | n.d. | n.d. | n.d. | n.d. | n.d. |
| U | n.d. | n.d. | n.d. | n.d. | n.d. | n.d. | n.d. | n.d. | n.d. |
| Cr | 343.2 | 167.8 | 210.5 | 104.7 | 121.5 | 1304.3 | 230.0 | 115.9 | 622.8 |
| Ni | 119.7 | 33.8 | 62.5 | 38.9 | 57.7 | 415.0 | 45.4 | 43.6 | 205.4 |
| Cu | n.d. | n.d. | n.d. | n.d. | n.d. | n.d. | n.d. | n.d. | n.d. |
| Zn | 87.0 | 71.5 | 74.5 | 64.8 | 70.7 | 104.2 | 93.8 | 56.5 | 99.8 |
| Rb | 33.6 | 79.4 | 60.6 | 54.8 | 12.9 | 77.0 | 53.3 | 72.3 | 73.9 |
| Sr | 1310 | 1008 | 671 | 1227 | 1830 | 300 | 626 | 1150 | 766 |
| Y | n.d. | n.d. | n.d. | n.d. | n.d. | n.d. | n.d. | n.d. | n.d. |
| Zr | 122.7 | 140.0 | 131.0 | 36.9 | 143.4 | 32.1 | 144.1 | 123.8 | 108.4 |
| Nb | 5.9 | 7.0 | 6.9 | 5.0 | 5.0 | 6.8 | 7.9 | 5.9 | 6.7 |
| Ba | 871 | 1053 | 936 | 1810 | 2259 | 1516 | 1394 | 1878 | 1819 |
| Pb | n.d. | n.d. | n.d. | n.d. | n.d. | n.d. | n.d. | n.d. | n.d. |
| Sb | n.d. | n.d. | n.d. | n.d. | n.d. | n.d. | n.d. | n.d. | n.d. |
| As | n.d. | n.d. | n.d. | n.d. | n.d. | n.d. | n.d. | n.d. | n.d. |
| Br | n.d. | n.d. | n.d. | n.d. | n.d. | n.d. | n.d. | n.d. | n.d. |
| Co | n.d. | n.d. | n.d. | n.d. | n.d. | n.d. | n.d. | n.d. | n.d. |
| Hf | n.d. | n.d. | n.d. | n.d. | n.d. | n.d. | n.d. | n.d. | n.d. |
| **Major and Trace Element Ratios** | | | | | | | | | |
| Mg#‡ | 55 | 50 | 50 | 46 | 45 | 69 | 51 | 50 | 63 |
| $K_2O/Na_2O$ | 0.28 | 0.58 | 0.47 | 0.69 | 0.08 | 2.34 | 0.81 | 0.68 | 1.09 |
| $K_2O+Na_2O$ | 7.01 | 7.56 | 5.99 | 10.31 | 8.38 | 2.96 | 7.10 | 7.88 | 5.19 |
| K/Na | 0.18 | 0.38 | 0.31 | 0.45 | 0.05 | 1.54 | 0.53 | 0.45 | 0.72 |
| Sr/Sr* | n.d. | n.d. | 1.33 | n.d. | n.d. | 0.55 | n.d. | 2.10 | 1.05 |
| Zr/Zr* | n.d. | n.d. | 0.85 | n.d. | n.d. | 0.18 | n.d. | 0.79 | 0.48 |
| Ti/Ti* | n.d. | n.d. | 0.48 | n.d. | n.d. | 0.74 | n.d. | 0.33 | 0.39 |
| Nb/Nb* | n.d. | n.d. | 0.15 | n.d. | n.d. | 0.11 | n.d. | 0.07 | 0.09 |

| Sample | 9308201 | 9308202 | 9308203 | 9308205 | 9308206 | 9308211 | 9308212 | 9308213 |
|---|---|---|---|---|---|---|---|---|
| Rock Type** | Dio* | Mo* | MD* | MD† | Mo† | MD† | Hbldt | QMD |
| **Major Elements (%)** | | | | | | | | |
| Oxide | | | | | | | | |
| $Na_2O$ | 4.17 | 3.69 | 4.11 | 4.46 | 3.51 | 4.52 | 1.07 | 5.15 |
| MgO | 6.33 | 9.01 | 7.07 | 3.66 | 2.87 | 5.93 | 15.22 | 3.14 |
| $Al_2O_3$ | 14.57 | 11.83 | 13.97 | 16.30 | 14.56 | 14.01 | 5.49 | 14.00 |
| $SiO_2$ | 56.15 | 54.50 | 55.44 | 54.13 | 60.96 | 58.54 | 50.94 | 64.95 |
| $P_2O_5$ | 0.31 | 0.78 | 0.29 | 0.56 | 0.31 | 0.25 | 0.50 | 0.15 |
| $K_2O$ | 1.49 | 4.42 | 2.16 | 4.29 | 4.43 | 2.51 | 2.26 | 3.13 |
| CaO | 6.67 | 6.54 | 6.72 | 5.81 | 4.46 | 5.24 | 14.54 | 3.09 |
| $TiO_2$ | 0.60 | 0.49 | 0.60 | 0.68 | 0.50 | 0.48 | 0.51 | 0.30 |
| MnO | 0.10 | 0.08 | 0.13 | 0.13 | 0.09 | 0.10 | 0.13 | 0.06 |
| $Fe_2O_3$ | 6.48 | 5.17 | 7.41 | 7.29 | 5.32 | 6.02 | 6.42 | 3.69 |
| Total | 98.92 | 98.13 | 99.54 | 98.86 | 98.38 | 98.76 | 98.33 | 98.62 |
| $H_2O$-%†† | 0.00 | 0.20 | 0.06 | 0.59 | 0.22 | 0.18 | 0.18 | 0.26 |
| $H_2O$+%††† | 1.78 | 0.92 | 1.25 | 0.56 | 0.79 | 0.70 | 0.78 | 0.43 |
| **Trace Elements (ppm)** | | | | | | | | |
| Sc | n.d. | n.d. | n.d. | n.d. | n.d. | n.d. | n.d. | n.d. |
| Cs | n.d. | n.d. | n.d. | n.d. | n.d. | n.d. | n.d. | n.d. |
| Ta | n.d. | n.d. | n.d. | n.d. | n.d. | n.d. | n.d. | n.d. |
| Th | n.d. | n.d. | n.d. | n.d. | n.d. | n.d. | n.d. | n.d. |
| U | n.d. | n.d. | n.d. | n.d. | n.d. | n.d. | n.d. | n.d. |
| Cr | 223.9 | 529.8 | 458.9 | 51.4 | 52.5 | 355.8 | 540.7 | 178.7 |
| Ni | 114.9 | 129.5 | 44.4 | 15.8 | 14.8 | 125.9 | 207.0 | 55.6 |
| Cu | n.d. | n.d. | n.d. | n.d. | n.d. | n.d. | n.d. | n.d. |
| Zn | 78.6 | 56.3 | 103.6 | 85.0 | 69.3 | 70.4 | 74.3 | 48.7 |
| Rb | 40.3 | 156.2 | 59.2 | 137.4 | 164.3 | 61.4 | 87.1 | 80.4 |
| Sr | 946 | 751 | 912 | 1222 | 823 | 864 | 401 | 630 |
| Y | n.d. | n.d. | n.d. | n.d. | n.d. | n.d. | n.d. | n.d. |
| Zr | 71.7 | 86.0 | 78.9 | 222.4 | 218.7 | 120.9 | 44.6 | 97.3 |
| Nb | 4.9 | 6.9 | 3.0 | 11.9 | 10.9 | 6.9 | 4.0 | 5.0 |
| Ba | 722 | 2596 | 1242 | 1741 | 1573 | 803 | 1215 | 1161 |
| Pb | n.d. | n.d. | n.d. | n.d. | n.d. | n.d. | n.d. | n.d. |
| Sb | n.d. | n.d. | n.d. | n.d. | n.d. | n.d. | n.d. | n.d. |
| As | n.d. | n.d. | n.d. | n.d. | n.d. | n.d. | n.d. | n.d. |
| Br | n.d. | n.d. | n.d. | n.d. | n.d. | n.d. | n.d. | n.d. |
| Co | n.d. | n.d. | n.d. | n.d. | n.d. | n.d. | n.d. | n.d. |
| Hf | n.d. | n.d. | n.d. | n.d. | n.d. | n.d. | n.d. | n.d. |
| **Major and Trace Element Ratios** | | | | | | | | |
| Mg#¥ | 57 | 71 | 57 | 41 | 43 | 58 | 77 | 54 |
| $K_2O/Na_2O$ | 0.36 | 1.20 | 0.53 | 0.96 | 1.26 | 0.55 | 2.11 | 0.61 |
| $K_2O+Na_2O$ | 5.67 | 8.11 | 6.27 | 8.75 | 7.95 | 7.03 | 3.33 | 8.28 |
| K/Na | 0.24 | 0.79 | 0.35 | 0.63 | 0.83 | 0.37 | 1.39 | 0.40 |
| Sr/Sr* | n.d. | n.d. | n.d. | 0.86 | n.d. | 3.02 | 1.18 | 2.77 |
| Zr/Zr* | n.d. | n.d. | n.d. | 0.55 | n.d. | 1.23 | 0.32 | 1.53 |
| Ti/Ti* | n.d. | n.d. | n.d. | 0.25 | n.d. | 0.55 | 0.46 | 0.56 |
| Nb/Nb* | n.d. | n.d. | n.d. | 0.10 | n.d. | 0.20 | 0.10 | 0.13 |

# Rare Earth Elements and CIPW Normative Mineralogy

| Sample | 9210102 | 9210103 | 9210104 | 9210105 | 9210113 | 9210116 | 9210117 | 9210117a | 9210118 |
|---|---|---|---|---|---|---|---|---|---|
| Rock Type[-] | QMD | Enc | Enc | Mo[†] | Sy[†] | Sy[£] | Dio[£] | MD[£] | Sy[£] |
| **Rare Earth Elements (ppm)** | | | | | | | | | |
| La | | 16.0 | 2.3 | 25.5 | 19.5 | 13.9 | 30.1 | 9.8 | 26.4 |
| Ce | | 32.8 | 6.5 | 52.0 | 41.1 | 30.6 | 70.5 | 26.9 | 48.8 |
| Nd | | 14.1 | 6.0 | 19.3 | 18.7 | 17.1 | 38.3 | 19.1 | 16.4 |
| Sm | | 2.6 | 1.7 | 5.0 | 3.3 | 3.7 | 7.4 | 4.2 | 2.5 |
| Eu | | 0.5 | 0.4 | 0.9 | 0.9 | 1.0 | 1.6 | 0.9 | 0.7 |
| Gd | | 2.1 | 1.5 | 7.2 | 2.0 | 3.1 | 4.8 | 2.9 | 1.5 |
| Tb | | n.d. | n.d. | 0.4 | n.d. | n.d. | n.d. | n.d. | n.d. |
| Dy | | 1.4 | 1.4 | 1.3 | 1.4 | 2.7 | 3.0 | 2.1 | 1.2 |
| Ho | | n.d. | n.d. | 0.2 | n.d. | n.d. | n.d. | n.d. | n.d. |
| Er | | 0.8 | 0.7 | n.d. | n.d. | 1.2 | 1.6 | n.d. | n.d. |
| Yb | | 0.7 | 0.5 | 1.0 | 0.6 | 1.5 | 1.2 | 0.8 | 1.0 |
| Lu | | 0.1 | 0.1 | 0.0 | 0.1 | 0.2 | 0.2 | 0.1 | 0.2 |
| Sum REE | | 71.1 | 21.1 | 112.9 | 87.6 | 75.0 | 158.6 | 67.0 | 96.7 |
| **Rare Earth Element Ratios** | | | | | | | | | |
| Eu/Eu* | | 0.65 | 0.80 | 0.47 | 1.09 | 0.90 | 0.83 | 0.81 | 1.11 |
| $(La/Lu)_{CN}$* | | 13.9963 | 4.21 | 87.89 | 18.72 | 6.05 | 16.67 | 8.39 | 15.13 |
| $(Gd/Yb)_{CN}$* | | n.d. | 2.36 | 5.56 | 2.59 | 1.67 | 3.24 | 2.89 | 1.22 |
| $(La/Yb)_{CN}$* | | 14.81 | 3.05 | 16.47 | 21.35 | 6.29 | 17.06 | 8.07 | 17.92 |
| $(Sm/Nd)_{CN}$* | | 0.57 | 0.86 | 0.80 | 0.53 | 0.66 | 0.80 | 0.68 | 0.48 |
| **CIPW Normative Mineralogy[§]** | | | | | | | | | |
| Quartz | 14.19 | 0.66 | 4.31 | 4.41 | 12.5 | 12.33 | 0 | 7.05 | 0 |
| Corundum | 0 | 0 | 0 | 0 | 0 | 1.45 | 0 | 0 | 0 |
| Zircon | 0.02 | 0.02 | 0 | 0.03 | 0.03 | 0.03 | 0.02 | 0.01 | 0.06 |
| Orthoclase | 16 | 2.5 | 0.58 | 21.69 | 19.43 | 12.99 | 12.38 | 3.67 | 36.94 |
| Albite | 45.49 | 42.58 | 2.14 | 50.84 | 48.86 | 39 | 32.76 | 11.2 | 54.65 |
| Anorthite | 7.29 | 10.64 | 6.1 | 5.38 | 5.22 | 14.22 | 19.53 | 10.13 | 3.09 |
| Leucite | 0 | 0 | 0 | 0 | 0 | 0 | 0 | 0 | 0 |
| Nepheline | 0 | 0 | 0 | 0 | 0 | 0 | 0 | 0 | 0 |
| Diopside | 7.43 | 17.07 | 39.48 | 10.01 | 6.56 | 0 | 9.2 | 32.3 | 2.14 |
| Hypersthene | 5.49 | 19.77 | 37.88 | 2.99 | 3.33 | 11.89 | 9.79 | 27.93 | 0.47 |
| Olivine | 0 | 0 | 0 | 0 | 0 | 0 | 6.07 | 0 | 0.34 |
| Chromite | 0 | 0 | 0 | 0 | 0 | 0 | 0 | 0 | 0 |
| Magnetite | 2.53 | 3.09 | 3.83 | 3.05 | 2.6 | 3.67 | 5.37 | 4.3 | 1.32 |
| Chromite | 0.03 | 0.15 | 0.23 | 0.02 | 0.02 | 0.01 | 0.01 | 0.09 | 0 |
| Ilmenite | 0.61 | 1.28 | 0.48 | 0.88 | 0.71 | 1.3 | 1.85 | 0.97 | 0.39 |
| Apatite | 0.37 | 0.82 | 0.05 | 0.41 | 0.36 | 0.59 | 0.88 | 0.14 | 0.13 |
| Pyrite | 0.03 | 0.04 | 0 | 0.06 | 0.04 | 0.06 | 0.04 | 0.06 | 0.05 |
| Total | 99.49 | 98.6 | 95.07 | 99.77 | 99.65 | 97.53 | 97.52 | 97.85 | 99.58 |
| DI[‡] | 75.68 | 45.74 | 7.03 | 76.94 | 80.79 | 64.32 | 45.14 | 21.92 | 91.59 |

| Sample | 9210119 | 92101110 | 92101113 | 92101113 | 92101115 | 92101116 | 92101116x | 9210121 | 9210123 |
|---|---|---|---|---|---|---|---|---|---|
| Rock Type[a] | Mo[c] | MD[nc] | Dio | Dio | MD | Mo | QMo | To | To |
| **Rare Earth Elements (ppm)** | | | | | | | | | |
| La | 42.6 | 48.6 | 22.0 | n.d. | 21.8 | 23.5 | 7.2 | 10.7 | 26.0 |
| Ce | 90.0 | 107.0 | 51.4 | n.d. | 39.8 | 45.6 | 13.7 | 20.6 | 54.8 |
| Nd | 42.7 | 47.1 | 23.1 | n.d. | 14.9 | 17.7 | 6.3 | 10.9 | 23.4 |
| Sm | 8.3 | 8.5 | 5.9 | n.d. | 3.8 | 2.9 | 1.2 | 2.5 | 4.1 |
| Eu | 1.8 | 2.0 | 0.8 | n.d. | 0.7 | 0.7 | 0.2 | 0.8 | 0.9 |
| Gd | 5.9 | 4.9 | 4.7 | n.d. | 2.7 | 2.0 | 0.9 | 2.0 | 2.9 |
| Tb | n.d. | n.d. | n.d. | n.d. | 0.3 | 0.3 | n.d. | n.d. | n.d. |
| Dy | 3.6 | 3.4 | 2.3 | n.d. | 1.9 | 1.0 | 0.6 | 1.5 | 1.9 |
| Ho | n.d. | n.d. | n.d. | n.d. | n.d. | n.d. | n.d. | n.d. | n.d. |
| Er | 2.3 | 2.0 | 1.7 | n.d. | n.d. | 0.6 | 0.7 | n.d. | 1.0 |
| Yb | 1.7 | 1.6 | 1.1 | n.d. | 1.0 | 0.6 | 0.3 | 0.6 | 1.0 |
| Lu | 0.3 | 0.2 | 0.1 | n.d. | 0.1 | 0.1 | 0.0 | 0.1 | 0.2 |
| Sum REE | 199.2 | 225.4 | 113.0 | n.d. | 87.0 | 94.9 | 31.2 | 49.7 | 116.1 |
| **Rare Earth Element Ratios** | | | | | | | | | |
| Eu/Eu* | 0.77 | 0.95 | 0.44 | n.d. | 0.70 | 0.84 | 0.84 | 1.16 | 0.82 |
| $(La/Lu)_{CN}$* | 16.34 | 22.99 | 22.88 | n.d. | 25.12 | 26.74 | 16.50 | 9.23 | 16.92 |
| $(Gd/Yb)_{CN}$* | 2.72 | 2.48 | 3.48 | n.d. | 2.14 | 2.91 | 2.62 | 2.51 | 2.37 |
| $(La/Yb)_{CN}$* | 16.50 | 20.29 | 13.61 | n.d. | 14.26 | 28.50 | 16.61 | 11.28 | 18.04 |
| $(Sm/Nd)_{CN}$* | 0.60 | 0.56 | 0.79 | n.d. | 0.78 | 0.50 | 0.59 | 0.70 | 0.54 |
| **CIPW Normative Mineralogy[§]** | | | | | | | | | |
| Quartz | 0 | 0 | 0 | 0 | 8.83 | 11.46 | 10.99 | 22.26 | 27.58 |
| Corundum | 0 | 0 | 0 | 0 | 0 | 0 | 0 | 0.09 | 0.05 |
| Zircon | 0.03 | 0.06 | 0.01 | 0.01 | 0.02 | 0.03 | 0.03 | 0.04 | 0.03 |
| Orthoclase | 14.62 | 25.49 | 22.21 | 15.4 | 14.79 | 22.43 | 16.32 | 7.49 | 8.94 |
| Albite | 36.01 | 51.68 | 8.63 | 16.66 | 46.04 | 49.13 | 53.55 | 43.62 | 37.05 |
| Anorthite | 20.49 | 9.3 | 8.82 | 12.61 | 8.29 | 3.82 | 3.74 | 16.61 | 17.42 |
| Leucite | 0 | 0 | 0 | 0 | 0 | 0 | 0 | 0 | 0 |
| Nepheline | 1.26 | 0.57 | 1.67 | 0 | 0 | 0 | 0 | 0 | 0 |
| Diopside | 13.4 | 6.32 | 25.22 | 23.14 | 9.38 | 7.83 | 9.17 | 0 | 0 |
| Hypersthene | 0 | 0 | 0 | 11.35 | 7.26 | 2.17 | 2.42 | 4.93 | 4.84 |
| Olivine | 6.34 | 1.77 | 25.59 | 13.47 | 0 | 0 | 0 | 0 | 0 |
| Chromite | 0 | 0 | 0 | 0 | 0 | 0 | 0 | 0 | 0 |
| Magnetite | 4.37 | 3.17 | 3.75 | 2.96 | 3.12 | 2.37 | 2.55 | 2.02 | 1.85 |
| Chromite | 0 | 0 | 0.25 | 0.17 | 0.04 | 0.01 | 0.02 | 0 | 0 |
| Ilmenite | 1.63 | 1.09 | 1.07 | 1.36 | 0.76 | 0.67 | 0.68 | 0.81 | 0.73 |
| Apatite | 0.07 | 0.64 | 0.58 | 0.74 | 0.46 | 0.31 | 0.32 | 0.34 | 0.34 |
| Pyrite | 0.05 | 0.05 | 0.05 | 0.07 | 0.03 | 0.07 | 0.05 | 0.05 | 0.02 |
| Total | 98.27 | 100.14 | 97.86 | 97.97 | 99.03 | 100.3 | 99.84 | 98.26 | 98.84 |
| DI[$] | 51.89 | 77.74 | 32.51 | 32.06 | 69.66 | 83.02 | 80.86 | 73.37 | 73.55 |

| Sample | 9210127 | 9210128 | 9210129 | 92101210 | 9210131 | 9210134 | 9210135 | 9210136 | 9210137 |
|---|---|---|---|---|---|---|---|---|---|
| Rock Type** | Dio | MD | QMD | MD | MD† | Hbldt | Hbldt | Hbldt | Vol |
| Rare Earth Elements (ppm) | | | | | | | | | |
| La | 21.0 | 6.5 | 22.4 | 68.3 | 14.0 | 18.0 | 19.2 | n.d. | 3.9 |
| Ce | 38.0 | 15.6 | 48.8 | 56.9 | 30.1 | 54.7 | 38.8 | n.d. | 10.2 |
| Nd | n.d. | 7.7 | 22.3 | 3.2 | 14.4 | 39.6 | 17.8 | n.d. | 7.5 |
| Sm | 4.4 | 1.7 | 4.0 | 3.7 | 2.2 | 8.8 | 3.2 | n.d. | 2.1 |
| Eu | 1.0 | 0.4 | 1.0 | 1.2 | 0.6 | 2.0 | 0.8 | n.d. | 0.9 |
| Gd | n.d. | 1.4 | 2.4 | 7.6 | 1.8 | 7.4 | 2.0 | n.d. | 3.2 |
| Tb | n.d. | 0.5 | n.d. | n.d. | n.d. | n.d. | 0.7 | n.d. | n.d. |
| Dy | n.d. | 1.0 | 1.6 | 0.8 | 0.8 | 4.5 | 1.4 | n.d. | 3.5 |
| Ho | n.d. | n.d. | n.d. | n.d. | n.d. | n.d. | n.d. | n.d. | n.d. |
| Er | n.d. | 0.8 | 0.9 | n.d. | 0.5 | 2.9 | 0.7 | n.d. | 2.4 |
| Yb | n.d. | 0.6 | 0.7 | 0.8 | 0.6 | 1.8 | 0.6 | n.d. | 2.2 |
| Lu | n.d. | 0.1 | 0.1 | 0.0 | 0.1 | 0.2 | 0.1 | n.d. | 0.3 |
| Sum REE | 64.4 | 36.2 | 104.4 | 142.5 | 65.2 | 139.9 | 85.0 | n.d. | 36.2 |
| Rare Earth Element Ratios | | | | | | | | | |
| Eu/Eu* | n.d. | 0.71 | 0.99 | 0.72 | 0.93 | 0.78 | 1.02 | n.d. | 1.01 |
| $(La/Lu)_{CN}$* | n.d. | 6.94 | 18.07 | 333.80 | 13.36 | 8.43 | 25.93 | n.d. | 1.19 |
| $(Gd/Yb)_{CN}$* | n.d. | 1.79 | 2.68 | 7.83 | 2.39 | 3.32 | 2.70 | n.d. | 1.18 |
| $(La/Yb)_{CN}$* | n.d. | 7.07 | 20.87 | 58.92 | 15.31 | 6.74 | 21.84 | n.d. | 1.20 |
| $(Sm/Nd)_{CN}$* | n.d. | 0.68 | 0.55 | 3.54 | 0.47 | 0.68 | 0.55 | n.d. | 0.86 |
| CIPW Normative Mineralogy§ | | | | | | | | | |
| Quartz | 0 | 0 | 8.6 | 4.41 | 1.07 | 0 | 0 | 0 | 0 |
| Corundum | 0 | 0 | 0 | 0 | 0 | 0 | 0 | 0 | 0 |
| Zircon | 0.01 | 0.01 | 0.02 | 0.03 | 0.04 | 0.01 | 0.01 | 0.01 | 0.01 |
| Orthoclase | 13.27 | 14.82 | 15.89 | 14.53 | 24.48 | 8.83 | 6.96 | 0 | 5.95 |
| Albite | 27.69 | 28.6 | 54.33 | 57.89 | 49.76 | 1.33 | 5.27 | 0 | 24.5 |
| Anorthite | 12.79 | 13.65 | 7.5 | 3.72 | 6 | 10.4 | 9.04 | 9.73 | 23.53 |
| Leucite | 0 | 0 | 0 | 0 | 0 | 0 | 0 | 3.24 | 0 |
| Nepheline | 0 | 0 | 0 | 0 | 0 | 7.03 | 4.37 | 8.06 | 0 |
| Diopside | 22.11 | 18.26 | 5.07 | 9.15 | 8.51 | 38.87 | 44.79 | 39.88 | 17.95 |
| Hypersthene | 9.3 | 12.52 | 4.95 | 5.31 | 4.43 | 0 | 0 | 0 | 3.67 |
| Olivine | 6.51 | 4.2 | 0 | 0 | 0 | 24.15 | 20.81 | 26.13 | 15.66 |
| Chromite | 0 | 0 | 0 | 0 | 0 | 0 | 0 | 1.73 | 0 |
| Magnetite | 4.21 | 4.18 | 2.4 | 3.13 | 3.33 | 3.39 | 3.11 | 4.38 | 3.94 |
| Chromite | 0.12 | 0.09 | 0.02 | 0.03 | 0.02 | 0.18 | 0.18 | 0.1 | 0.04 |
| Ilmenite | 1.35 | 1.37 | 0.64 | 0.83 | 0.87 | 1.96 | 2.11 | 2.9 | 2.2 |
| Apatite | 0.79 | 0.86 | 0.41 | 0.46 | 0.62 | 0.9 | 0.33 | 0.76 | 0.23 |
| Pyrite | 0.05 | 0.05 | 0.03 | 0.04 | 0.07 | 0.07 | 0.06 | 0.06 | 0.06 |
| Total | 96.21 | 96.6 | 99.65 | 99.54 | 99.2 | 97.23 | 97.06 | 96.97 | 97.74 |
| DI‡ | 40.96 | 43.42 | 78.62 | 76.83 | 75.31 | 17.29 | 16.62 | 8.06 | 30.45 |

| Sample | 9210138 | 9210139 | 9210143b | 9210147 | 9210149 | 92101410 | 92101411 | 9210157 | 92101513 |
|---|---|---|---|---|---|---|---|---|---|
| Rock Type[-] | MD[†] | Mo[†] | QMD[†] | Sy | Hbldt | Gra | Hbldt | MD | MD |
| **Rare Earth Elements (ppm)** | | | | | | | | | |
| La | 25.1 | 30.3 | 30.3 | n.d. | 28.1 | n.d. | 11.4 | 27.0 | 35.0 |
| Ce | 51.6 | 81.4 | 73.0 | n.d. | 59.0 | n.d. | 27.1 | 63.1 | 69.0 |
| Nd | 25.9 | 49.3 | 33.0 | n.d. | 35.0 | n.d. | 19.1 | 30.0 | n.d. |
| Sm | 5.1 | 9.7 | 5.8 | n.d. | 7.9 | n.d. | 4.3 | 5.4 | 9.1 |
| Eu | 1.4 | 2.4 | 1.3 | n.d. | 2.2 | n.d. | 1.1 | 1.4 | 3.0 |
| Gd | 3.1 | 6.3 | 3.7 | n.d. | n.d. | n.d. | 4.4 | 3.2 | n.d. |
| Tb | n.d. | 0.8 | n.d. | n.d. | 0.9 | n.d. | 0.9 | n.d. | 0.9 |
| Dy | 2.0 | 4.1 | 2.2 | n.d. | 4.3 | n.d. | 2.4 | 2.1 | n.d. |
| Ho | n.d. | n.d. | n.d. | n.d. | 0.8 | n.d. | n.d. | n.d. | n.d. |
| Er | 1.1 | 2.1 | 1.6 | n.d. | n.d. | n.d. | 1.1 | 1.1 | n.d. |
| Yb | 0.8 | 1.4 | 1.0 | n.d. | 1.8 | n.d. | 0.9 | 0.8 | 1.0 |
| Lu | 0.1 | 0.2 | 0.1 | n.d. | 0.3 | n.d. | 0.1 | 0.1 | n.d. |
| Sum REE | 116.3 | 188.0 | 152.0 | n.d. | 140.2 | n.d. | 72.8 | 134.2 | 118.0 |
| **Rare Earth Element Ratios** | | | | | | | | | |
| Eu/Eu* | 1.05 | 0.93 | 0.87 | n.d. | n.d. | n.d. | 0.74 | 1.05 | n.d. |
| $(La/Lu)_{CN}$* | 26.24 | 16.76 | 24.22 | n.d. | 11.67 | n.d. | 9.17 | 25.62 | n.d. |
| $(Gd/Yb)_{CN}$* | 3.05 | 3.72 | 3.04 | n.d. | 0.00 | n.d. | 4.11 | 3.25 | 0.00 |
| $(La/Yb)_{CN}$* | 20.79 | 14.86 | 20.99 | n.d. | 10.85 | n.d. | 8.97 | 23.01 | 23.65 |
| $(Sm/Nd)_{CN}$* | 0.61 | 0.61 | 0.54 | n.d. | 0.69 | n.d. | 0.69 | 0.56 | n.d. |
| **CIPW Normative Mineralogy[§]** | | | | | | | | | |
| Quartz | 0.64 | 0 | 0.87 | 0 | 0 | 24.75 | 0 | 0 | 0 |
| Corundum | 0 | 0 | 0 | 0 | 0 | 0 | 0 | 0 | 0 |
| Zircon | 0.01 | 0.02 | 0.04 | 0.02 | 0.02 | 0.01 | 0.02 | 0.03 | 0.03 |
| Orthoclase | 21.97 | 21.53 | 20.04 | 13.91 | 17.85 | 26.28 | 14.89 | 12.21 | 9.35 |
| Albite | 47 | 30.84 | 54.64 | 20.41 | 8.65 | 42.84 | 9.84 | 57.29 | 39.44 |
| Anorthite | 8.28 | 12.68 | 6.34 | 14.34 | 11.8 | 3.37 | 11.95 | 9.35 | 14.92 |
| Leucite | 0 | 0 | 0 | 0 | 0 | 0 | 0 | 0 | 0 |
| Nepheline | 0 | 0 | 0 | 0 | 3.84 | 0 | 2.07 | 0 | 0 |
| Diopside | 9.64 | 15.59 | 7.48 | 18.68 | 28 | 0.53 | 28.32 | 8.18 | 17.29 |
| Hypersthene | 6.96 | 11.92 | 4.31 | 20.32 | 0 | 1.18 | 0 | 6.96 | 5.4 |
| Olivine | 0 | 0.74 | 0 | 4.57 | 22.24 | 0 | 25.18 | 0.46 | 5.57 |
| Chromite | 0 | 0 | 0 | 0 | 0 | 0 | 0 | 0 | 0 |
| Magnetite | 3.03 | 3.66 | 3.11 | 3.7 | 2.89 | 0.58 | 3.09 | 2.92 | 3.94 |
| Chromite | 0.02 | 0.07 | 0.02 | 0.16 | 0.2 | 0 | 0.22 | 0.03 | 0.06 |
| Ilmenite | 0.89 | 1.11 | 0.88 | 1.29 | 1.41 | 0.18 | 1.43 | 1.02 | 1.47 |
| Apatite | 0.82 | 0.99 | 0.36 | 1.06 | 1.1 | 0.11 | 1.25 | 0.46 | 1.1 |
| Pyrite | 0.03 | 0.03 | 0.07 | 0.04 | 0.07 | 0.05 | 0.04 | 0.03 | 0.03 |
| Total | 99.3 | 99.18 | 98.17 | 98.49 | 98.07 | 99.88 | 98.3 | 98.95 | 98.59 |
| DI[‡] | 69.61 | 52.37 | 75.55 | 34.32 | 30.34 | 93.87 | 26.8 | 69.5 | 48.79 |

| Sample | 92101514 | 9210162 | 9210163 | 9210164 | 9210171 | 9210174 | 9210175 | 9210176 | 9210181 |
|---|---|---|---|---|---|---|---|---|---|
| Rock Type[a] | Dio | Vol | Dio | To | Dio | QMD | Gabbro[b] | To | GD |
| **Rare Earth Elements (ppm)** | | | | | | | | | |
| La | n.d. | 3.4 | 18.1 | 20.9 | 30.4 | 22.8 | 16.3 | n.d. | 5.6 |
| Ce | n.d. | 9.1 | 45.6 | 40.4 | 61.4 | 54.9 | 45.6 | n.d. | 13.4 |
| Nd | n.d. | 6.8 | 23.7 | 16.5 | 33.7 | 28.0 | 29.0 | n.d. | 7.0 |
| Sm | n.d. | n.d. | 4.4 | 2.5 | 8.1 | 5.2 | 7.7 | n.d. | 1.2 |
| Eu | n.d. | 0.7 | 1.1 | 0.8 | 2.1 | 1.4 | 1.8 | n.d. | 0.4 |
| Gd | n.d. | 2.9 | 2.9 | 1.3 | 8.8 | 3.2 | 9.8 | n.d. | 1.3 |
| Tb | n.d. | n.d. | n.d. | n.d. | n.d. | n.d. | 0.7 | n.d. | 0.3 |
| Dy | n.d. | 3.2 | 2.0 | 0.9 | 3.7 | 2.1 | 2.3 | n.d. | 1.2 |
| Ho | n.d. | n.d. | n.d. | n.d. | n.d. | n.d. | 0.6 | n.d. | n.d. |
| Er | n.d. | 2.3 | n.d. | 0.4 | n.d. | n.d. | n.d. | n.d. | 1.1 |
| Yb | n.d. | 2.0 | 0.9 | 0.4 | 1.6 | 0.9 | 1.1 | n.d. | 0.7 |
| Lu | n.d. | 0.3 | 0.2 | 0.1 | 0.6 | 0.2 | 0.2 | n.d. | 0.1 |
| Sum REE | n.d. | 30.6 | 99.0 | 84.1 | 150.4 | 118.6 | 115.1 | n.d. | 32.2 |
| **Rare Earth Element Ratios** | | | | | | | | | |
| Eu/Eu* | n.d. | n.d. | 0.96 | 1.27 | 0.76 | 1.04 | 0.63 | n.d. | 0.87 |
| $(La/Lu)_{CN}$* | n.d. | 1.12 | 12.44 | 39.80 | 5.62 | 15.16 | 7.16 | n.d. | 4.99 |
| $(Gd/Yb)_{CN}$* | n.d. | 1.18 | 2.48 | 2.95 | 4.31 | 2.91 | 6.99 | n.d. | 1.51 |
| $(La/Yb)_{CN}$* | n.d. | 1.15 | 12.97 | 38.51 | 12.48 | 17.50 | 9.75 | n.d. | 5.52 |
| $(Sm/Nd)_{CN}$* | n.d. | 0.00 | 0.57 | 0.47 | 0.74 | 0.57 | 0.82 | n.d. | 0.52 |
| **CIPW Normative Mineralogy[c]** | | | | | | | | | |
| Quartz | 6.46 | 0 | 8.64 | 25.45 | 0 | 2.79 | 0 | 19.82 | 6.1 |
| Corundum | 0 | 0 | 0 | 0 | 0 | 0 | 0 | 0.04 | 0 |
| Zircon | 0.03 | 0.01 | 0.03 | 0.03 | 0.02 | 0.03 | 0.01 | 0.03 | 0.02 |
| Orthoclase | 21.43 | 2.22 | 0.34 | 5.06 | 4.75 | 11.88 | 5.75 | 5.84 | 7.07 |
| Albite | 49.25 | 25.06 | 53.67 | 49.4 | 25.06 | 50.9 | 17.43 | 53.6 | 33.67 |
| Anorthite | 5.14 | 28 | 13.71 | 14.59 | 16.26 | 11.06 | 18.63 | 15.42 | 24.13 |
| Leucite | 0 | 0 | 0 | 0 | 0 | 0 | 0 | 0 | 0 |
| Nepheline | 0 | 0 | 0 | 0 | 0 | 0 | 0 | 0 | 0 |
| Diopside | 8.7 | 13.34 | 10.19 | 0.68 | 26.2 | 10.23 | 26.21 | 0 | 8.65 |
| Hypersthene | 5.42 | 12.16 | 8.7 | 2.52 | 11.57 | 7.82 | 2.73 | 3.47 | 13.56 |
| Olivine | 0 | 11.36 | 0 | 0 | 7.9 | 0 | 18.52 | 0 | 0 |
| Chromite | 0 | 0 | 0 | 0 | 0 | 0 | 0 | 0 | 0 |
| Magnetite | 2.85 | 3.44 | 2.56 | 1.75 | 2.67 | 2.87 | 5.06 | 1.3 | 3.27 |
| Chromite | 0.03 | 0.05 | 0.04 | 0 | 0.12 | 0.04 | 0.01 | 0 | 0.04 |
| Ilmenite | 0.72 | 1.72 | 0.96 | 0.53 | 1.72 | 0.96 | 3.06 | 0.72 | 1.27 |
| Apatite | 0.5 | 0.17 | 0.55 | 0.26 | 1.06 | 0.53 | 0.49 | 0.28 | 0.49 |
| Pyrite | 0.04 | 0.05 | 0.04 | 0.03 | 0.05 | 0.05 | 0.06 | 0 | 0.09 |
| Total | 100.58 | 97.61 | 99.41 | 100.32 | 97.42 | 99.19 | 97.99 | 100.33 | 98.35 |
| DI[d] | 77.14 | 27.3 | 62.65 | 79.91 | 29.81 | 65.57 | 23.18 | 79.06 | 46.84 |

| Sample | 9210186 | 9210187 | 9210188 | 9210189 | 9306131a | 9306156 | 93061510 | 93061510a | 9306161 |
|---|---|---|---|---|---|---|---|---|---|
| Rock Type[~] | QMD | QMD[†] | Mc[†] | MD[†] | Enc[A] | QMD | To | Dyke | MD[†] |
| **Rare Earth Elements (ppm)** | | | | | | | | | |
| La | 21.6 | 27.6 | 28.7 | 12.7 | n.d. | 20.0 | n.d. | 10.9 | 38.8 |
| Ce | 41.0 | 61.1 | 54.4 | 25.7 | n.d. | 39.5 | n.d. | 25.3 | 87.0 |
| Nd | 20.0 | 29.6 | 23.1 | 11.1 | n.d. | 17.7 | n.d. | 12.8 | 44.9 |
| Sm | 3.5 | 5.1 | 6.4 | 1.9 | n.d. | 3.5 | n.d. | 2.4 | 8.5 |
| Eu | 1.1 | 1.3 | 1.2 | 0.4 | n.d. | 0.8 | n.d. | 0.6 | 2.1 |
| Gd | n.d. | 3.0 | 4.3 | 1.2 | n.d. | 2.6 | n.d. | 1.3 | 5.2 |
| Tb | 0.3 | n.d. | 0.3 | 0.3 | n.d. | n.d. | n.d. | n.d. | n.d. |
| Dy | 1.5 | 2.2 | 2.4 | 0.8 | n.d. | 2.4 | n.d. | 0.7 | 3.2 |
| Ho | 0.3 | n.d. | n.d. | n.d. | n.d. | n.d. | n.d. | n.d. | n.d. |
| Er | n.d. | 1.1 | n.d. | n.d. | n.d. | 1.6 | n.d. | 0.3 | 1.8 |
| Yb | 0.8 | 0.9 | 1.0 | 0.5 | n.d. | 1.7 | n.d. | 0.2 | 1.1 |
| Lu | 0.1 | 0.1 | 0.1 | 0.1 | n.d. | 0.2 | n.d. | 0.0 | 0.1 |
| Sum REE | 90.1 | 132.1 | 121.9 | 54.6 | n.d. | 90.1 | n.d. | 54.6 | 192.7 |
| **Rare Earth Element Ratios** | | | | | | | | | |
| Eu/Eu* | n.d. | 1.03 | 0.72 | 0.81 | n.d. | 0.82 | n.d. | 1.09 | 0.97 |
| $(La/Lu)_{CN}$* | 22.42 | 21.88 | 48.93 | 22.71 | n.d. | 8.65 | n.d. | 44.03 | 27.97 |
| $(Gd/Yb)_{CN}$* | 0.00 | 2.77 | 3.53 | 2.09 | n.d. | 1.23 | n.d. | 4.25 | 3.76 |
| $(La/Yb)_{CN}$* | 19.46 | 20.96 | 19.83 | 18.38 | n.d. | 8.01 | n.d. | 29.39 | 23.31 |
| $(Sm/Nd)_{CN}$* | 0.54 | 0.53 | 0.85 | 0.53 | n.d. | 0.80 | n.d. | 0.58 | 0.58 |
| **CIPW Normative Mineralogy[§]** | | | | | | | | | |
| Quartz | 9.45 | 3.09 | 0 | 0 | 3.21 | 22.16 | 24.96 | 0 | 0 |
| Corundum | 0 | 0 | 0 | 0 | 0 | 0 | 0.06 | 0 | 0 |
| Zircon | 0.03 | 0.03 | 0.04 | 0.03 | 0 | 0.02 | 0.02 | 0.01 | 0.02 |
| Orthoclase | 15.71 | 18.13 | 23.6 | 20.57 | 0.75 | 18.61 | 11.24 | 10.43 | 24.41 |
| Albite | 48.56 | 54.13 | 46.92 | 52.02 | 2.4 | 40.91 | 45.54 | 18.74 | 27.3 |
| Anorthite | 9.08 | 5.62 | 7.33 | 7.15 | 6.65 | 13.01 | 12.09 | 16.61 | 12.57 |
| Leucite | 0 | 0 | 0 | 0 | 0 | 0 | 0 | 0 | 0 |
| Nepheline | 0 | 0 | 0 | 0 | 0 | 0 | 0 | 0 | 0 |
| Diopside | 8.81 | 11.38 | 11.47 | 9.77 | 39.96 | 2.62 | 0 | 15.14 | 13.4 |
| Hypersthene | 4.08 | 3.46 | 2.35 | 4.56 | 38.99 | 8.54 | 1.99 | 23.21 | 7.87 |
| Olivine | 0 | 0 | 2.69 | 0.36 | 0 | 0 | 0 | 9 | 6.33 |
| Chromite | 0 | 0 | 0 | 0 | 0 | 0 | 0 | 0 | 0 |
| Magnetite | 2.76 | 3.37 | 3.01 | 3.66 | 3.81 | 2.56 | 1.22 | 2.35 | 3.23 |
| Chromite | 0.03 | 0.02 | 0.02 | 0.02 | 0.07 | 0.04 | 0 | 0.26 | 0.09 |
| Ilmenite | 0.78 | 0.94 | 0.95 | 0.89 | 0.48 | 0.82 | 0.53 | 1.37 | 1.29 |
| Apatite | 0.37 | 0.44 | 0.72 | 0.8 | 0.05 | 0.41 | 0.19 | 1.18 | 1.01 |
| Pyrite | 0.05 | 0.04 | 0.05 | 0.06 | 0 | 0 | 0 | 0 | 0 |
| Total | 99.7 | 100.67 | 99.16 | 99.9 | 96.37 | 109.5 | 97.84 | 96.3 | 97.52 |
| DI[‡] | 73.72 | 75.35 | 70.52 | 72.59 | 6.36 | 81.68 | 81.74 | 29.17 | 51.71 |

| Sample | 9306162a | 9306164 | 9306166 | 9306171 | 9306173 | 9306174 | 93061710 | 9306182 | 9306183 |
|---|---|---|---|---|---|---|---|---|---|
| Rock Type[-] | Enc | Enc | Hbldt | To | Hbldt | Hbldt | Hbldt | MD[tv] | MD[tv] |
| Rare Earth Elements (ppm) | | | | | | | | | |
| La | 21.4 | 29.5 | 15.8 | 31.6 | 29.0 | n.d. | 5.0 | 25.2 | 24.0 |
| Ce | 54.4 | 49.2 | 30.4 | 64.7 | 60.9 | n.d. | 9.4 | 51.2 | 55.7 |
| Nd | 29.7 | 18.2 | 13.1 | 29.1 | 29.2 | n.d. | 5.4 | 23.6 | 26.4 |
| Sm | 5.9 | 3.5 | 2.2 | 5.3 | 5.7 | n.d. | 1.9 | 4.4 | 4.9 |
| Eu | 1.5 | 0.6 | 0.6 | 1.3 | 1.3 | n.d. | 0.4 | 1.1 | 1.3 |
| Gd | 4.2 | 2.7 | 1.3 | 3.2 | 3.7 | n.d. | 2.2 | 2.9 | 3.2 |
| Tb | n.d. | n.d. | n.d. | n.d. | n.d. | n.d. | n.d. | n.d. | n.d. |
| Dy | 3.0 | 1.5 | 0.8 | 2.1 | 2.7 | n.d. | 1.4 | 2.1 | 2.3 |
| Ho | n.d. | n.d. | n.d. | n.d. | n.d. | n.d. | n.d. | n.d. | n.d. |
| Er | 1.8 | 0.8 | 0.4 | 1.3 | 1.5 | n.d. | 0.7 | 1.3 | 1.4 |
| Yb | 1.6 | 0.5 | 0.4 | 0.9 | 1.2 | n.d. | 0.6 | 1.0 | 1.1 |
| Lu | 0.2 | 0.0 | 0.0 | 0.1 | 0.2 | n.d. | 0.0 | 0.2 | 0.1 |
| Sum REE | 123.6 | 106.2 | 65.0 | 139.5 | 135.3 | n.d. | 27.1 | 112.9 | 120.5 |
| | | | | | | | | | |
| Rare Earth Element Ratios | | | | | | | | | |
| Eu/Eu* | 0.94 | 0.57 | 1.11 | 0.93 | 0.90 | n.d. | 0.53 | 0.91 | 0.97 |
| $(La/Lu)_{CN}$* | 11.60 | 157.52 | 32.86 | 27.00 | 18.36 | n.d. | 19.02 | 16.49 | 17.63 |
| $(Gd/Yb)_{CN}$* | 2.16 | 4.76 | 2.64 | 2.97 | 2.53 | n.d. | 2.76 | 2.27 | 2.38 |
| $(La/Yb)_{CN}$* | 9.20 | 43.80 | 26.73 | 24.73 | 16.50 | n.d. | 5.27 | 16.41 | 14.86 |
| $(Sm/Nd)_{CN}$* | 0.61 | 0.59 | 0.53 | 0.56 | 0.60 | n.d. | 1.10 | 0.58 | 0.57 |
| | | | | | | | | | |
| CIPW Normative Mineralogy[§] | | | | | | | | | |
| Quartz | 0 | 0 | 0 | 6.42 | 0 | 0 | 1.4 | 10.69 | 2.11 |
| Corundum | 0 | 0 | 0 | 0 | 0 | 0 | 0 | 0 | 0 |
| Zircon | 0 | 0 | 0 | 0.03 | 0.01 | 0.01 | 0 | 0.02 | 0.02 |
| Orthoclase | 16.61 | 0.51 | 3.34 | 17.31 | 17.5 | 15.63 | 1.22 | 21.34 | 19.42 |
| Albite | 7.54 | 1.52 | 4.94 | 44.67 | 24.52 | 24.74 | 5.25 | 37.04 | 49.19 |
| Anorthite | 9.33 | 13.58 | 11.54 | 10.63 | 10.99 | 11.5 | 5.28 | 8.98 | 6.51 |
| Leucite | 0 | 0 | 0 | 0 | 0 | 0 | 0 | 0 | 0 |
| Nepheline | 0 | 0 | 0 | 0 | 1.57 | 0.64 | 0 | 0 | 0 |
| Diopside | 29.8 | 25.08 | 34.24 | 4.84 | 18.57 | 19.29 | 48.01 | 7.15 | 8.52 |
| Hypersthene | 14.14 | 44.07 | 30.26 | 7.03 | 0 | 0 | 31.22 | 8.31 | 8.1 |
| Olivine | 14.33 | 5.55 | 9.01 | 0 | 19.25 | 20.52 | 0 | 0 | 0 |
| Chromite | 0 | 0 | 0 | 0 | 0 | 0 | 0 | 0 | 0 |
| Magnetite | 2.77 | 2.99 | 2.24 | 2.24 | 3.79 | 3.33 | 3.87 | 3.29 | 2.56 |
| Chromite | 0.34 | 0.41 | 0.26 | 0.03 | 0.23 | 0.23 | 0.19 | 0.05 | 0.05 |
| Ilmenite | 0.96 | 0.55 | 1.39 | 0.81 | 1.2 | 1.2 | 0.67 | 0.85 | 0.89 |
| Apatite | 0.19 | 0.2 | 0.35 | 0.51 | 0.78 | 0.78 | 0.09 | 0.5 | 0.61 |
| Pyrite | 0 | 0 | 0 | 0 | 0 | 0 | 0 | 0 | 0 |
| Total | 96.04 | 94.48 | 97.58 | 96.5 | 98.41 | 97.88 | 97.2 | 96.22 | 97.96 |
| DI[‡] | 24.15 | 2.03 | 8.28 | 70.4 | 43.59 | 41.01 | 7.87 | 69.07 | 70.72 |

| Sample | 9306184 | 9306187 | 9306193 | 9306196 | 9306198 | 93061910a | 93061911a | 9306203 | 9306203a |
|---|---|---|---|---|---|---|---|---|---|
| Rock Type[a] | QMD[†] | Dio | Mo[†] | Mo[‡] | Dio | Enc | Enc | Mo[†‡] | Sy[†] |
| **Rare Earth Elements (ppm)** | | | | | | | | | |
| La | 28.1 | n.d. | 36.3 | 7.0 | 23.6 | 2.4 | 1.3 | 37.5 | 24.9 |
| Ce | 66.1 | n.d. | 88.2 | 19.0 | 53.3 | 7.2 | 4.1 | 79.6 | 54.6 |
| Nd | 33.6 | n.d. | 44.1 | 12.5 | 25.6 | 5.6 | 6.4 | 35.5 | 21.4 |
| Sm | 6.3 | n.d. | 8.4 | 3.1 | 6.8 | 1.2 | 2.5 | 5.9 | 5.0 |
| Eu | 1.4 | n.d. | 1.8 | 0.9 | 1.6 | 0.3 | 0.4 | 1.5 | 1.1 |
| Gd | 3.7 | n.d. | 5.1 | 2.7 | 5.4 | 1.4 | 2.7 | 3.2 | 3.5 |
| Tb | n.d. | n.d. | n.d. | n.d. | n.d. | n.d. | n.d. | n.d. | n.d. |
| Dy | 2.5 | n.d. | 3.4 | 2.0 | 3.9 | 1.3 | 2.0 | 2.2 | 2.4 |
| Ho | n.d. | n.d. | n.d. | n.d. | n.d. | n.d. | n.d. | n.d. | n.d. |
| Er | 1.2 | n.d. | 1.8 | | 2.3 | 0.5 | 1.3 | 1.2 | 1.5 |
| Yb | 1.0 | n.d. | 1.4 | 0.5 | 1.9 | 0.8 | 0.8 | 0.9 | 1.1 |
| Lu | 0.1 | n.d. | 0.2 | 0.1 | 0.2 | 0.1 | 0.0 | 0.1 | 0.1 |
| Sum REE | 144.1 | n.d. | 190.8 | 47.9 | 124.6 | 21.0 | 21.8 | 167.8 | 115.7 |
| **Rare Earth Element Ratios** | | | | | | | | | |
| Eu/Eu* | 0.91 | n.d. | 0.84 | 0.96 | 0.78 | 0.64 | 0.46 | 1.07 | 0.78 |
| $(La/Lu)_{CN}$* | 20.99 | n.d. | 20.61 | 11.65 | 15.54 | 1.97 | 2.74 | 33.35 | 26.97 |
| $(Gd/Yb)_{CN}$* | 3.01 | n.d. | 3.05 | 4.10 | 2.31 | 1.38 | 2.68 | 2.88 | 2.48 |
| $(La/Yb)_{CN}$* | 18.84 | n.d. | 17.96 | 8.62 | 8.38 | 1.97 | 1.03 | 28.05 | 14.72 |
| $(Sm/Nd)_{CN}$* | 0.58 | n.d. | 0.59 | 0.77 | 0.82 | 0.67 | 1.19 | 0.51 | 0.72 |
| **CIPW Normative Mineralogy[§]** | | | | | | | | | |
| Quartz | 7.37 | 0 | 0 | 16.16 | 0 | 0.7 | 3.56 | 0.2 | 2.14 |
| Corundum | 0 | 0 | 0 | 0 | 0 | 0 | 0 | 0 | 0 |
| Zircon | 0.02 | 0.01 | 0.04 | 0.02 | 0.01 | 0 | 0 | 0.02 | 0 |
| Orthoclase | 16.7 | 12.23 | 24.39 | 30.24 | 6.66 | 4.9 | 3.87 | 23.77 | 22.84 |
| Albite | 44.96 | 28.34 | 40.16 | 40.81 | 37.72 | 5.03 | 2.75 | 57.22 | 46.7 |
| Anorthite | 11.36 | 11.75 | 9.9 | 6.16 | 15.96 | 4.88 | 3.07 | 8.17 | 1.13 |
| Leucite | 0 | 0 | 0 | 0 | 0 | 0 | 0 | 0 | 0 |
| Nepheline | 0 | 0 | 0 | 0 | 0 | 0 | 0 | 0 | 0 |
| Diopside | 3.53 | 20.02 | 8.38 | 2.11 | 19.71 | 42.32 | 45.05 | 4.31 | 16.44 |
| Hypersthene | 9.41 | 13.67 | 7.96 | 1.96 | 1.54 | 33.57 | 35.73 | 1.14 | 5.05 |
| Olivine | 0 | 4.97 | 1.54 | 0 | 8.43 | 0 | 0 | 0 | 0 |
| Chromite | 0 | 0 | 0 | 0 | 0 | 0 | 0 | 0 | 0 |
| Magnetite | 2.4 | 3.92 | 3.22 | 1.21 | 4.14 | 3.29 | 3.19 | 2.21 | 3.11 |
| Chromite | 0.03 | 0.14 | 0.04 | 0.01 | 0.06 | 0.14 | 0.19 | 0 | 0.05 |
| Ilmenite | 0.92 | 1.56 | 1.11 | 0.4 | 1.56 | 0.47 | 0.3 | 0.66 | 0.85 |
| Apatite | 0.56 | 0.87 | 0.92 | 0.12 | 0.81 | 0.12 | 0.02 | 0.37 | 0.29 |
| Pyrite | 0 | 0 | 0 | 0 | 0 | 0 | 0 | 0 | 0 |
| Total | 97.3 | 97.46 | 97.67 | 99.24 | 98.44 | 95.42 | 97.73 | 98.06 | 98.81 |
| DI[‡] | 69.05 | 40.57 | 64.55 | 87.21 | 44.4 | 10.63 | 10.18 | 81.19 | 71.88 |

| Sample | 9306206a | 9306212 | 9306222 | 9306226 | 9306231 | 9306234 | 9306235 | 9306238 | 9306242 |
|---|---|---|---|---|---|---|---|---|---|
| Rock Type[-] | Dyke | MD[††] | Sy[†] | MD[†] | Dio | QMD | Dio | Mo[£] | MD[†] |
| **Rare Earth Elements (ppm)** | | | | | | | | | |
| La | 19.9 | n.d. | 28.3 | 23.4 | 16.3 | 27.9 | 23.8 | 16.6 | 39.0 |
| Ce | 41.8 | n.d. | 60.3 | 47.5 | 34.8 | 51.1 | 55.6 | 33.1 | 81.4 |
| Nd | 18.6 | n.d. | 30.6 | 21.5 | 17.7 | 20.6 | 30.6 | 15.2 | 37.5 |
| Sm | 5.2 | n.d. | 6.6 | 3.9 | 3.7 | 3.6 | 9.0 | 2.9 | 6.9 |
| Eu | 1.1 | n.d. | 1.6 | 1.0 | 0.8 | 0.8 | 1.7 | 0.8 | 1.5 |
| Gd | 4.8 | n.d. | 4.4 | 2.4 | 2.3 | 2.1 | 7.1 | 1.9 | 4.1 |
| Tb | n.d. | n.d. | n.d. | n.d. | n.d. | n.d. | n.d. | n.d. | n.d. |
| Dy | 3.8 | n.d. | 3.1 | 1.6 | 1.6 | 1.4 | 4.4 | 1.3 | 2.8 |
| Ho | n.d. | n.d. | n.d. | n.d. | n.d. | n.d. | n.d. | n.d. | n.d. |
| Er | 2.0 | n.d. | | 0.9 | 0.8 | 0.8 | 2.3 | 0.8 | 1.3 |
| Yb | 1.8 | n.d. | 1.3 | 0.7 | 0.6 | 0.6 | 1.7 | 0.7 | 1.1 |
| Lu | 0.2 | n.d. | 0.2 | 0.1 | 0.1 | 0.1 | 0.1 | 0.1 | 0.1 |
| Sum REE | 99.1 | n.d. | 136.4 | 103.0 | 78.8 | 109.0 | 136.4 | 73.4 | 175.8 |
| **Rare Earth Element Ratios** | | | | | | | | | |
| Eu/Eu* | 0.70 | n.d. | 0.92 | 1.04 | 0.87 | 0.94 | 0.85 | 0.99 | 0.89 |
| $(La/Lu)_{CN}$* | 12.00 | n.d. | 17.39 | 26.69 | 20.47 | 33.88 | 16.62 | 18.38 | 27.47 |
| $(Gd/Yb)_{CN}$* | 2.14 | n.d. | 2.82 | 2.86 | 2.90 | 2.62 | 3.37 | 2.36 | 2.95 |
| $(La/Yb)_{CN}$* | 7.50 | n.d. | 14.97 | 23.29 | 17.53 | 29.74 | 9.44 | 17.28 | 23.55 |
| $(Sm/Nd)_{CN}$* | 0.85 | n.d. | 0.67 | 0.56 | 0.64 | 0.54 | 0.90 | 0.59 | 0.56 |
| **CIPW Normative Mineralogy[§]** | | | | | | | | | |
| Quartz | 0 | 5.66 | 0 | 2.07 | 0 | 17.8 | 0 | 7.54 | 3.44 |
| Corundum | 0 | 0 | 0 | 0 | 0 | 0 | 0 | 0 | 0 |
| Zircon | 0.01 | 0.04 | 0.02 | 0.02 | 0.01 | 0.02 | 0.01 | 0.02 | 0.02 |
| Orthoclase | 9.25 | 26.12 | 17.28 | 19.07 | 16.55 | 17.03 | 12.28 | 22.06 | 14.23 |
| Albite | 16.69 | 44.61 | 31.41 | 53.26 | 26.75 | 47.06 | 16.96 | 48.92 | 46.43 |
| Anorthite | 13.34 | 9.15 | 11.99 | 4.92 | 9.33 | 4.42 | 12.32 | 2.79 | 12.8 |
| Leucite | 0 | 0 | 0 | 0 | 0 | 0 | 0 | 0 | 0 |
| Nepheline | 0 | 0 | 0 | 0 | 0 | 0 | 0.22 | 0 | 0 |
| Diopside | 26.45 | 3.71 | 13.34 | 10.34 | 18.36 | 4.51 | 26.02 | 8.78 | 4.78 |
| Hypersthene | 11.33 | 4.77 | 14.83 | 3.62 | 6.03 | 3.95 | 0 | 4.43 | 9.68 |
| Olivine | 12.45 | 0 | 1.14 | 0 | 15.58 | 0 | 22.9 | 0 | 0 |
| Chromite | 0 | 0 | 0 | 0 | 0 | 0 | 0 | 0 | 0 |
| Magnetite | 2.84 | 2.42 | 3.92 | 3.21 | 3.62 | 2.05 | 2.67 | 2.72 | 3.53 |
| Chromite | 0.22 | 0.02 | 0.07 | 0.03 | 0.26 | 0.02 | 0.19 | 0.03 | 0.05 |
| Ilmenite | 1.72 | 0.6 | 1.51 | 0.96 | 1.09 | 0.68 | 1.31 | 0.7 | 0.95 |
| Apatite | 0.95 | 0.58 | 1.13 | 0.43 | 0.69 | 0.41 | 1.14 | 0.27 | 0.74 |
| Pyrite | 0 | 0 | 0 | 0 | 0 | 0 | 0 | 0 | 0 |
| Total | 95.25 | 97.69 | 96.62 | 97.96 | 98.28 | 97.96 | 96.02 | 98.26 | 96.85 |
| DI[‡] | 25.94 | 76.39 | 48.69 | 74.4 | 43.3 | 81.91 | 29.46 | 78.52 | 64.1 |

| Sample | 9306244 | 9306254 | 9306257 | 9306257a | 93062510 | 93062511 | 93062513 | 9306261a | 9306266 |
|---|---|---|---|---|---|---|---|---|---|
| Rock Type** | Dio | Hbldt | Dio | Dio | Dyke | Dyke | Dyke | Dio | Dyke |
| **Rare Earth Elements (ppm)** | | | | | | | | | |
| La | 21.8 | n.d. | 23.4 | 7.9 | 10.7 | n.d. | 6.5 | 10.5 | 48.2 |
| Ce | 57.8 | n.d. | 50.4 | 15.7 | 23.2 | n.d. | 13.1 | 29.6 | 105.8 |
| Nd | 36.3 | n.d. | 28.5 | 5.7 | 13.8 | n.d. | 7.6 | 17.9 | 52.8 |
| Sm | 8.0 | n.d. | 6.2 | 1.0 | 3.4 | n.d. | 1.8 | 4.0 | 9.7 |
| Eu | 2.0 | n.d. | 1.6 | 0.3 | 1.0 | n.d. | 0.6 | 0.9 | 2.2 |
| Gd | 5.9 | n.d. | 4.4 | 0.8 | 3.0 | n.d. | 1.5 | 3.1 | 6.0 |
| Tb | n.d. | n.d. | n.d. | n.d. | n.d. | n.d. | n.d. | n.d. | n.d. |
| Dy | 4.3 | n.d. | 3.1 | 0.6 | 2.6 | n.d. | 1.2 | 2.3 | 3.6 |
| Ho | n.d. | n.d. | n.d. | n.d. | n.d. | n.d. | n.d. | n.d. | n.d. |
| Er | 2.3 | n.d. | 1.9 | | 1.3 | n.d. | 0.7 | 1.3 | 1.6 |
| Yb | 1.9 | n.d. | 1.3 | 0.3 | 1.3 | n.d. | 0.6 | 1.1 | 1.1 |
| Lu | 0.3 | n.d. | 0.2 | 0.0 | 0.2 | n.d. | 0.1 | 0.1 | 0.1 |
| Sum REE | 140.6 | n.d. | 120.9 | 32.4 | 60.6 | n.d. | 33.7 | 70.9 | 231.2 |
| **Rare Earth Element Ratios** | | | | | | | | | |
| Eu/Eu* | 0.89 | n.d. | 0.92 | 1.02 | 0.98 | n.d. | 1.03 | 0.80 | 0.89 |
| $(La/Lu)_{CN}$* | 8.99 | n.d. | 13.67 | 17.35 | 6.24 | n.d. | 8.72 | 7.55 | 39.35 |
| $(Gd/Yb)_{CN}$* | 2.49 | n.d. | 2.80 | 2.01 | 1.96 | n.d. | 2.06 | 2.33 | 4.33 |
| $(La/Yb)_{CN}$* | 7.73 | n.d. | 12.49 | 15.81 | 5.74 | n.d. | 7.43 | 6.55 | 29.08 |
| $(Sm/Nd)_{CN}$* | 0.68 | n.d. | 0.67 | 0.56 | 0.76 | n.d. | 0.73 | 0.68 | 0.56 |
| **CIPW Normative Mineralogy§** | | | | | | | | | |
| Quartz | 0 | 0 | 0 | 0 | 0.28 | 4.98 | 2.91 | 0 | 0.32 |
| Corundum | 0 | 0 | 0 | 0 | 0 | 0 | 0 | 0 | 0 |
| Zircon | 0.01 | 0.01 | 0.01 | 0.01 | 0.01 | 0.01 | 0.01 | 0 | 0.03 |
| Orthoclase | 10.01 | 6.72 | 6.8 | 89.56 | 7.7 | 1.65 | 9.28 | 14.5 | 23.16 |
| Albite | 21.63 | 1.08 | 25.61 | 0 | 40.1 | 8.15 | 57.44 | 10.35 | 31.28 |
| Anorthite | 16.02 | 7.97 | 11.92 | 3.28 | 8.96 | 2.28 | 3.34 | 9.22 | 9.73 |
| Leucite | 0 | 0 | 0 | 3.61 | 0 | 0 | 0 | 0 | 0 |
| Nepheline | 0 | 7.71 | 0 | 0.87 | 0 | 0 | 0 | 0 | 0 |
| Diopside | 17.85 | 47.81 | 21.88 | 3.02 | 21.94 | 46.06 | 13.77 | 28.53 | 15.04 |
| Hypersthene | 5.66 | 0 | 10.5 | 0 | 12.65 | 26.24 | 7.09 | 9.41 | 11.23 |
| Olivine | 19.17 | 17.79 | 13.62 | 0.45 | 0 | 0 | 0 | 21.03 | 0 |
| Chromite | 0 | 0 | 0 | 0 | 0 | 0 | 0 | 0 | 0 |
| Magnetite | 2.65 | 2.96 | 2.57 | 0 | 3.89 | 3.7 | 2.83 | 2.76 | 3.86 |
| Chromite | 0.17 | 0.1 | 0.14 | 0.01 | 0.09 | 0.1 | 0.06 | 0.29 | 0.06 |
| Ilmenite | 1.62 | 2.21 | 1.22 | 0.26 | 1.45 | 1.9 | 0.77 | 1.31 | 1.29 |
| Apatite | 1.04 | 2.13 | 1.09 | 0.2 | 0.57 | 0.68 | 0.33 | 0.44 | 1.33 |
| Pyrite | 0 | 0 | 0 | 0 | 0 | 0 | 0 | 0 | 0 |
| Total | 95.84 | 96.49 | 95.36 | 101.27 | 97.64 | 95.74 | 97.86 | 97.83 | 97.34 |
| DI‡ | 31.64 | 15.51 | 32.41 | 90.43 | 48.08 | 14.78 | 69.63 | 24.85 | 54.76 |

| Sample | 9306268dyke | 9306268enc | 9306271 | 9306273 | 9306173 | 9306174 | 93061711a | 93061712 | 9306182 |
|---|---|---|---|---|---|---|---|---|---|
| Rock Type* | Dyke | Enc | Dyke | Dyke | Gr | MD† | Dio | Dio | Vol |
| **Rare Earth Elements (ppm)** | | | | | | | | | |
| La | 71.3 | 7.1 | 30.4 | 3.3 | n.d. | n.d. | 20.6 | n.d. | 1.6 |
| Ce | 142.3 | 20.6 | 62.7 | 7.0 | n.d. | n.d. | 52.9 | n.d. | 1.3 |
| Nd | 57.7 | 13.0 | 31.4 | 4.8 | n.d. | n.d. | 30.6 | n.d. | 0.9 |
| Sm | 13.0 | 2.9 | 6.1 | 2.1 | n.d. | n.d. | 6.1 | n.d. | 0.4 |
| Eu | 2.7 | 0.7 | 1.5 | 0.5 | n.d. | n.d. | 1.5 | n.d. | 0.1 |
| Gd | 9.3 | 2.3 | 4.4 | 3.3 | n.d. | n.d. | 4.5 | n.d. | 0.9 |
| Tb | n.d. | n.d. | n.d. | n.d. | n.d. | n.d. | n.d. | n.d. | n.d. |
| Dy | 5.1 | 1.5 | 3.0 | 3.6 | n.d. | n.d. | 2.8 | n.d. | 0.8 |
| Ho | n.d. | n.d. | n.d. | n.d. | n.d. | n.d. | n.d. | n.d. | n.d. |
| Er | 2.5 | 0.4 | 1.4 | 2.4 | n.d. | n.d. | 1.4 | n.d. | 0.4 |
| Yb | 1.6 | 0.5 | 1.0 | 2.1 | n.d. | n.d. | 0.9 | n.d. | 0.4 |
| Lu | 0.2 | 0.0 | 0.1 | 0.1 | n.d. | n.d. | 0.1 | n.d. | 0.0 |
| Sum REE | 305.6 | 48.9 | 142.2 | 29.3 | n.d. | n.d. | 121.4 | n.d. | 6.7 |
| **Rare Earth Element Ratios** | | | | | | | | | |
| Eu/Eu* | 0.74 | 0.82 | 0.91 | 0.63 | n.d. | n.d. | 0.87 | n.d. | 0.45 |
| $(La/Lu)_{CN}$* | 47.43 | 16.92 | 25.66 | 2.55 | n.d. | n.d. | 18.78 | n.d. | 3.80 |
| $(Gd/Yb)_{CN}$* | 4.76 | 4.06 | 3.64 | 1.30 | n.d. | n.d. | 4.17 | n.d. | 1.67 |
| $(La/Yb)_{CN}$* | 30.42 | 10.60 | 20.77 | 1.08 | n.d. | n.d. | 16.07 | n.d. | 2.51 |
| $(Sm/Nd)_{CN}$* | 0.69 | 0.68 | 0.60 | 1.33 | n.d. | n.d. | 0.61 | n.d. | 1.38 |
| **CIPW Normative Mineralogy‡** | | | | | | | | | |
| Quartz | 0 | 5.36 | 0 | 0 | 10.81 | 0 | 0 | 1.83 | 0 |
| Corundum | 0 | 0 | 0 | 0 | 0 | 0 | 0 | 0 | 0 |
| Zircon | 0.02 | 0 | 0.01 | 0 | 0.02 | 0.04 | 0 | 0.02 | 0 |
| Orthoclase | 2.53 | 2.87 | 17.39 | 8.4 | 18.16 | 25.82 | 6.51 | 11.74 | 25.1 |
| Albite | 31.46 | 5.02 | 23.68 | 12.96 | 50.55 | 48.96 | 16.7 | 46.86 | 1.69 |
| Anorthite | 13.82 | 5.08 | 12.8 | 32.53 | 4.12 | 8.96 | 9.52 | 10.72 | 7.58 |
| Leucite | 0 | 0 | 0 | 0 | 0 | 0 | 0 | 0 | 0 |
| Nepheline | 0 | 0 | 0 | 0.86 | 0 | 0.72 | 0.85 | 0 | 3.62 |
| Diopside | 14.79 | 42.43 | 16.85 | 18.62 | 7.6 | 5.29 | 35.14 | 11.33 | 13.19 |
| Hypersthene | 20.82 | 32.05 | 7.05 | 0 | 4.25 | 0 | 0 | 10.9 | 0 |
| Olivine | 6.44 | 0 | 13.28 | 18.2 | 0 | 3.32 | 19.78 | 0 | 40.86 |
| Chromite | 0 | 0 | 0 | 0 | 0 | 0 | 0 | 0 | 0 |
| Magnetite | 2.23 | 3.39 | 3.83 | 2.92 | 2.23 | 2.44 | 3.99 | 3.01 | 3.96 |
| Chromite | 0.18 | 0.21 | 0.16 | 0.1 | 0.03 | 0.01 | 0.3 | 0.07 | 0.55 |
| Ilmenite | 1.44 | 0.66 | 1.31 | 1.54 | 0.57 | 0.97 | 2.24 | 0.94 | 0.41 |
| Apatite | 1.69 | 0.05 | 0.95 | 0.14 | 0.31 | 0.58 | 0.4 | 0.59 | 0 |
| Pyrite | 0 | 0 | 0 | 0 | 0 | 0 | 0 | 0 | 0 |
| Total | 95.43 | 97.12 | 97.32 | 98.27 | 98.64 | 97.13 | 95.43 | 97.81 | 96.77 |
| DI‡ | 33.99 | 13.25 | 41.07 | 22.22 | 79.52 | 75.5 | 24.06 | 60.23 | 30.41 |

| Sample | 9306184 | 9306185 | 9306186 | 9306187 | 9306188 | 9306191 | 9306192 | 9306193 | 9306193a |
|---|---|---|---|---|---|---|---|---|---|
| Rock Type[~] | Dio | Sy[†] | Sed | QMo[†] | Dio | Hbldt | Mo[†] | QMD | Sy |
| Rare Earth Elements (ppm) | | | | | | | | | |
| La | n.d. | n.d. | 20.4 | n.d. | n.d. | 21.4 | n.d. | 32.9 | 28.5 |
| Ce | n.d. | n.d. | 48.3 | n.d. | n.d. | 49.3 | n.d. | 62.7 | 70.2 |
| Nd | n.d. | n.d. | 25.3 | n.d. | n.d. | 28.6 | n.d. | 23.1 | 36.2 |
| Sm | n.d. | n.d. | 5.1 | n.d. | n.d. | 5.7 | n.d. | 5.7 | 7.5 |
| Eu | n.d. | n.d. | 1.2 | n.d. | n.d. | 1.3 | n.d. | 1.1 | 1.7 |
| Gd | n.d. | n.d. | 3.4 | n.d. | n.d. | 3.9 | n.d. | 3.8 | 5.2 |
| Tb | n.d. | n.d. | n.d. | n.d. | n.d. | n.d. | n.d. | n.d. | n.d. |
| Dy | n.d. | n.d. | 2.4 | n.d. | n.d. | 2.3 | n.d. | 2.3 | 3.3 |
| Ho | n.d. | n.d. | n.d. | n.d. | n.d. | n.d. | n.d. | n.d. | n.d. |
| Er | n.d. | n.d. | 1.2 | n.d. | n.d. | n.d. | n.d. | 1.0 | 1.5 |
| Yb | n.d. | n.d. | 1.0 | n.d. | n.d. | 0.7 | n.d. | 1.0 | 1.1 |
| Lu | n.d. | n.d. | 0.1 | n.d. | n.d. | 0.1 | n.d. | 0.1 | 0.1 |
| Sum REE | n.d. | n.d. | 108.4 | n.d. | n.d. | 113.2 | n.d. | 133.7 | 155.3 |
| Rare Earth Element Ratios | | | | | | | | | |
| Eu/Eu* | n.d. | n.d. | 0.90 | n.d. | n.d. | 0.81 | n.d. | 0.72 | 0.83 |
| $(La/Lu)_{CN}$* | n.d. | n.d. | 18.80 | n.d. | n.d. | 35.25 | n.d. | 52.17 | 23.25 |
| $(Gd/Yb)_{CN}$* | n.d. | n.d. | 2.78 | n.d. | n.d. | 4.59 | n.d. | 3.11 | 3.79 |
| $(La/Yb)_{CN}$* | n.d. | n.d. | 13.82 | n.d. | n.d. | 20.86 | n.d. | 22.21 | 17.49 |
| $(Sm/Nd)_{CN}$* | n.d. | n.d. | 0.61 | n.d. | n.d. | 0.61 | n.d. | 0.76 | 0.64 |
| CIPW Normative Mineralogy[§] | | | | | | | | | |
| Quartz | 0 | 3.12 | 11.72 | 1.14 | 0.46 | 0 | 0 | 14.01 | 0 |
| Corundum | 0 | 0 | 0 | 0 | 0 | 0 | 0 | 0 | 0 |
| Zircon | 0.02 | 0.02 | 0.02 | 0.01 | 0.03 | 0 | 0.02 | 0.02 | 0.01 |
| Orthoclase | 9.13 | 16.64 | 11.41 | 25.42 | 3.59 | 12.82 | 19.1 | 19.24 | 16.49 |
| Albite | 47.2 | 40.93 | 34.94 | 52.05 | 65.28 | 0.77 | 33.67 | 39.99 | 21.37 |
| Anorthite | 14.3 | 9.51 | 18.24 | 3.15 | 7.59 | 14.4 | 10.55 | 11.44 | 14.03 |
| Leucite | 0 | 0 | 0 | 0 | 0 | 0 | 0 | 0 | 0 |
| Nepheline | 0 | 0 | 0 | 0 | 0 | 3.69 | 0 | 0 | 0 |
| Diopside | 10.51 | 14.23 | 5.1 | 10.96 | 12.01 | 27.94 | 16.18 | 3.25 | 17.05 |
| Hypersthene | 4.79 | 8.02 | 12.06 | 2.11 | 3.95 | 0 | 6.09 | 6.42 | 13.1 |
| Olivine | 6.44 | 0 | 0 | 0 | 0 | 30.35 | 5.17 | 0 | 7.46 |
| Chromite | 0 | 0 | 0 | 0 | 0 | 0 | 0 | 0 | 0 |
| Magnetite | 2.99 | 3.32 | 2.73 | 2.58 | 2.64 | 2.87 | 3.71 | 2.51 | 3.2 |
| Chromite | 0.09 | 0.04 | 0.05 | 0.03 | 0.03 | 0.31 | 0.06 | 0.03 | 0.15 |
| Ilmenite | 1.09 | 1.36 | 1.17 | 0.76 | 1 | 1.83 | 1.56 | 0.77 | 1.35 |
| Apatite | 0.66 | 0.93 | 0.55 | 0.37 | 0.46 | 1.28 | 1.28 | 0.48 | 1.06 |
| Pyrite | 0 | 0 | 0 | 0 | 0 | 0 | 0 | 0 | 0 |
| Total | 97.24 | 96.1 | 97.99 | 96.57 | 97.05 | 96.26 | 97.38 | 96.15 | 95.28 |
| DI[‡] | 56.33 | 60.89 | 58.07 | 78.61 | 69.33 | 17.28 | 52.77 | 73.24 | 37.86 |

| Sample | 9308201 | 9308202 | 9308203 | 9308205 | 9308206 | 9308211 | 9308212 | 9308213 |
|---|---|---|---|---|---|---|---|---|
| Rock Type** | Dio● | Mo● | MD● | MD[N] | Mo[N] | MD† | Hbldt | QMD |
| **Rare Earth Elements (ppm)** | | | | | | | | |
| La | n.d. | n.d. | n.d. | 71.0 | n.d. | 13.0 | 11.5 | 11.4 |
| Ce | n.d. | n.d. | n.d. | 146.2 | n.d. | 29.6 | 29.8 | 23.6 |
| Nd | n.d. | n.d. | n.d. | 65.8 | n.d. | 13.3 | 18.7 | 10.5 |
| Sm | n.d. | n.d. | n.d. | 13.5 | n.d. | 3.9 | 5.6 | 2.1 |
| Eu | n.d. | n.d. | n.d. | 3.0 | n.d. | 0.7 | 1.1 | 0.6 |
| Gd | n.d. | n.d. | n.d. | 8.8 | n.d. | 3.5 | 4.4 | 3.1 |
| Tb | n.d. | n.d. | n.d. | n.d. | n.d. | n.d. | n.d. | n.d. |
| Dy | n.d. | n.d. | n.d. | 5.2 | n.d. | 2.2 | 2.4 | 1.2 |
| Ho | n.d. | n.d. | n.d. | n.d. | n.d. | n.d. | n.d. | n.d. |
| Er | n.d. | n.d. | n.d. | 2.6 | n.d. | 1.4 | 0.8 | 0.6 |
| Yb | n.d. | n.d. | n.d. | 1.9 | n.d. | 1.2 | 0.7 | 0.7 |
| Lu | n.d. | n.d. | n.d. | 0.2 | n.d. | 0.1 | 0.0 | 0.1 |
| Sum REE | n.d. | n.d. | n.d. | 318.2 | n.d. | 68.8 | 75.0 | 53.7 |
| **Rare Earth Element Ratios** | | | | | | | | |
| Eu/Eu* | n.d. | n.d. | n.d. | 0.83 | n.d. | 0.57 | 0.65 | 0.70 |
| $(La/Lu)_{CN}$* | n.d. | n.d. | n.d. | 39.01 | n.d. | 16.97 | 28.45 | 18.02 |
| $(Gd/Yb)_{CN}$* | n.d. | n.d. | n.d. | 3.76 | n.d. | 2.34 | 5.05 | 3.50 |
| $(La/Yb)_{CN}$* | n.d. | n.d. | n.d. | 25.39 | n.d. | 7.23 | 10.96 | 10.86 |
| $(Sm/Nd)_{CN}$* | n.d. | n.d. | n.d. | 0.63 | n.d. | 0.89 | 0.92 | 0.61 |
| **CIPW Normative Mineralogy§** | | | | | | | | |
| Quartz | 3.87 | 0 | 0.76 | 0 | 10.77 | 4.06 | 0 | 13.11 |
| Corundum | 0 | 0 | 0 | 0 | 0 | 0 | 0 | 0 |
| Zircon | 0.01 | 0.01 | 0.02 | 0.04 | 0.04 | 0.02 | 0 | 0.02 |
| Orthoclase | 9.01 | 27.46 | 12.8 | 25.82 | 26.62 | 15.31 | 14.38 | 18.87 |
| Albite | 35.98 | 27.17 | 34.73 | 33.47 | 30.23 | 39 | 8.01 | 44.03 |
| Anorthite | 16.78 | 3.06 | 13.37 | 12.24 | 11.17 | 10.74 | 3.91 | 5.93 |
| Leucite | 0 | 0 | 0 | 0 | 0 | 0 | 0 | 0 |
| Nepheline | 0 | 2.77 | 0 | 2.53 | 0 | 0 | 0.66 | 0 |
| Diopside | 11.57 | 20.44 | 14.99 | 11.27 | 7.95 | 11.16 | 53.01 | 6.99 |
| Hypersthene | 14.76 | 0 | 15.29 | 0 | 6.51 | 13.19 | 0 | 5.94 |
| Olivine | 0 | 12.02 | 0 | 5.63 | 0 | 0 | 15.61 | 0 |
| Chromite | 0 | 0 | 0 | 0 | 0 | 0 | 0 | 0 |
| Magnetite | 3.03 | 2.75 | 3.42 | 3.79 | 2.82 | 3.22 | 2.2 | 2.47 |
| Chromite | 0.06 | 0.13 | 0.1 | 0.01 | 0.01 | 0.09 | 0.11 | 0.04 |
| Ilmenite | 1.21 | 0.98 | 1.14 | 1.31 | 0.98 | 0.96 | 1.09 | 0.6 |
| Apatite | 0.8 | 1.91 | 0.68 | 1.38 | 0.77 | 0.64 | 1.2 | 0.36 |
| Pyrite | 0 | 0 | 0 | 0 | 0 | 0 | 0 | 0 |
| Total | 97.08 | 98.69 | 97.31 | 97.49 | 97.87 | 98.39 | 100.17 | 98.36 |
| DI‡ | 48.86 | 57.4 | 48.29 | 61.82 | 67.62 | 58.37 | 23.05 | 76.01 |

# Appendix 4
# Mineral Compositions

**Mineral Chemistry**

Mineral chemistry was determined at Carleton University for biotite/phlogopite, amphibole, clinopyroxene, plagioclase, potassium feldspar, allanite, zircon, epidote, titanite, and magnetite from a variety of rock types from the LSIC. All minerals were analyzed by a JEOL JSM 6400 wavelength-dispersive scanning electron microscope operating at 15kV beam accelerating potential, and 0.8nA beam current with collection times of 100 seconds. The SEM data were recalculated to structural formula using the JEOL resident software or MINREP (1994), a mineral formulae recalculation program produced by the Geological Survey of Canada. Additional analysis were performed for amphibole, clinopyroxene, and plagioclase on a Cambridge Microscan 5 energy dispersive X-ray spectrometer electron microprobe interfaced to a Ortec Si detector. Operating conditions were set at 20 kV beam accelerating potential, 75° takeoff angle, and 3.5 nA beam current measured on Faraday cup for 120 second count times. Raw X-ray spectra were processed to structural formula by the FORTRAN program EDDI (Pringle, 1989). A variety of natural and synthetic minerals were used for calibration. For Hornblende, Kakanui hornblende USM 143965 was used.

# Hornblende Compositions

| Sample (Min.) | amph1.1 | amph1.2 | amph2.1 | amph2.2 | amph3.1 | amph3.2 | amph3.3 | amph4.1 | amph4.2 |
|---|---|---|---|---|---|---|---|---|---|
| Sample (Rock) | 921012-7 | 921012-7 | 921012-7 | 921012-7 | 921012-7 | 921012-7 | 921012-7 | 921012-7 | 921012-7 |
| Rock Type | Dio | Dio | Dio | Dio | Dio | Dio | Dio | Dio | Dio |
| Amph. Type | Act. Hbl | Act. Hbl | Act. Hbl | Actinolite | Actinolite | Actinolite | Actinolite | Actinolite | Actinolite |
| Oxide % | | | | | | | | | |
| $SiO_2$ | 51.07 | 50.63 | 51.55 | 52.98 | 55.78 | 55.79 | 55.61 | 52.24 | 52.31 |
| $Al_2O_3$ | 3.9 | 4.24 | 4.12 | 3.58 | 0.76 | 0.67 | 0.55 | 2.47 | 2.48 |
| $TiO_2$ | 0.21 | 0.18 | 0.36 | 0.43 | 0.12 | 0.15 | 0.13 | 0.13 | 0.1 |
| $Cr_2O_3$ | 0.03 | 0.16 | 0.06 | 0.26 | 0.13 | 0.15 | 0.18 | 0.05 | 0 |
| $Fe_2O_3$ | 3.57 | 1.48 | 1.46 | 0 | 1.37 | 1.17 | 1.67 | 1.04 | 2.48 |
| FeO | 9.51 | 10.9 | 10.71 | 11.67 | 4.07 | 5.18 | 5.58 | 10.06 | 8.93 |
| MnO | 0.13 | 0.1 | 0.1 | 0.1 | 0.16 | 0.13 | 0.11 | 0.1 | 0.1 |
| MgO | 15.49 | 15.4 | 15.39 | 14.99 | 20.96 | 20.48 | 20.01 | 16.91 | 16.72 |
| CaO | 11.86 | 12.47 | 12.04 | 12.22 | 13.09 | 12.93 | 12.95 | 13.06 | 12.46 |
| $Na_2O$ | 1.13 | 1.15 | 1.06 | 0.71 | 0.3 | 0.55 | 0.4 | 0.74 | 0.75 |
| $K_2O$ | 0.46 | 0.37 | 0.5 | 0.31 | 0.17 | 0.14 | 0.13 | 0.22 | 0.15 |
| Cl | 0 | 0.01 | 0.01 | 0 | 0.01 | 0.02 | 0 | 0.01 | 0 |
| Sum | 97.36 | 97.09 | 97.36 | 97.25 | 96.94 | 97.36 | 97.52 | 97.03 | 96.48 |
| | | | | | | | | | |
| T Site Occupancy | | | | | | | | | |
| Si | 7.402 | 7.382 | 7.462 | 7.644 | 7.822 | 7.827 | 7.816 | 7.565 | 7.586 |
| $Al^{IV}$ | 0.598 | 0.618 | 0.538 | 0.356 | 0.126 | 0.111 | 0.091 | 0.422 | 0.414 |
| Sum | 8 | 8 | 8 | 8 | 7.948 | 7.938 | 7.907 | 7.987 | 8 |
| | | | | | | | | | |
| C Site Occupancy | | | | | | | | | |
| $Al^{VI}$ | 0.068 | 0.111 | 0.165 | 0.253 | 0 | 0 | 0 | 0 | 0.01 |
| Ti | 0.023 | 0.02 | 0.041 | 0.047 | 0.013 | 0.016 | 0.014 | 0.014 | 0.011 |
| Cr | 0.003 | 0.018 | 0.007 | 0.03 | 0.014 | 0.017 | 0.02 | 0.006 | 0 |
| $Fe^{3+}$ | 0.389 | 0.162 | 0.159 | 0 | 0.145 | 0.124 | 0.187 | 0.113 | 0.271 |
| $Fe^{2+}$ | 1.153 | 1.329 | 1.296 | 1.406 | 0.477 | 0.607 | 0.656 | 1.218 | 1.083 |
| Mn | 0.016 | 0.012 | 0.012 | 0.012 | 0.019 | 0.015 | 0.013 | 0.012 | 0.012 |
| Mg | 3.347 | 3.347 | 3.321 | 3.224 | 4.386 | 4.283 | 4.192 | 3.65 | 3.614 |
| Sum | 4.999 | 4.999 | 5.001 | 4.974 | 5.054 | 5.062 | 5.082 | 5.013 | 5.001 |
| | | | | | | | | | |
| B Site Occupancy | | | | | | | | | |
| Ca | 1.842 | 1.948 | 1.867 | 1.889 | 1.967 | 1.944 | 1.95 | 2.026 | 1.936 |
| Na | 0.158 | 0.052 | 0.133 | 0.111 | 0.033 | 0.056 | 0.05 | 0 | 0.064 |
| Sum | 2 | 2 | 2 | 2 | 2 | 2 | 2 | 2.026 | 2 |
| | | | | | | | | | |
| A Site Occupancy | | | | | | | | | |
| Na | 0.16 | 0.273 | 0.164 | 0.068 | 0.049 | 0.084 | 0.059 | 0.206 | 0.147 |
| K | 0.089 | 0.069 | 0.092 | 0.057 | 0.03 | 0.025 | 0.023 | 0.041 | 0.028 |
| Sum | 0.249 | 0.342 | 0.256 | 0.145 | 0.079 | 0.119 | 0.082 | 0.249 | 0.175 |
| | | | | | | | | | |
| OH Site Occupancy | | | | | | | | | |
| Cl | 0 | 0.002 | 0.002 | 0 | 0.002 | 0.005 | 0 | 0.002 | 0 |
| Sum | 0 | 0.002 | 0.002 | 0 | 0.002 | 0.005 | 0 | 0.002 | 0 |
| | | | | | | | | | |
| Ratios | | | | | | | | | |
| Fm | 0.315 | 0.308 | 0.305 | 0.304 | 0.124 | 0.148 | 0.169 | 0.267 | 0.273 |
| Na+K | 0.407 | 0.394 | 0.389 | 0.256 | 0.112 | 0.175 | 0.132 | 0.249 | 0.239 |
| $Mg^{\#}(Fe_{tot})$ | 0.685 | 0.682 | 0.695 | 0.696 | 0.876 | 0.854 | 0.831 | 0.733 | 0.727 |
| $Fe^{3+}/Fe^{2+}$ | 0.337 | 0.122 | 0.123 | 0.000 | 0.304 | 0.204 | 0.300 | 0.093 | 0.250 |
| $Al_{tot}$ | 0.666 | 0.729 | 0.703 | 0.609 | 0.126 | 0.111 | 0.091 | 0.422 | 0.424 |

Hornblende compositions based upon $[C]_{5}[B]_{2}[A][T]_{8}O_{22}$

$Mg^{\#} = Mg/(Mg+Fe^{2+}+Fe^{3+})$

$Al_{tot} = Al^{IV}+Al^{VI}$

$Fm = Fe_{tot}/(Fe_{tot}+Mg)$

Proportions $Fe^{3+}$ and $Fe^{2+}$ calculated assuming hornblende stoichiometry and electrostatic neutrality.

Abbreviations Si. Eden. = Silicic Edenite., Eden. Hbl. = Edenitic Hornblende., Mg. Hbl. = Magnesio Hornblende, Act. Hbl. = Actinolitic Hornblende.

** = Rock Type defined in Appendix 1

| Sample (Min.) | amph5.1 | amph5.2 | amph6.1 | amph6.2 | amph6.3 | amph6.4 | amph6.5 | amph6.6 | amph6.7 |
|---|---|---|---|---|---|---|---|---|---|
| Sample (Rock) | 921012-7 | 921012-7 | 921010-4 | 921010-4 | 921010-4 | 921010-4 | 921010-4 | 921010-4 | 921010-4 |
| Rock Type | Dio | Dio | Enc | Enc | Enc | Enc | Enc | Enc | Enc |
| Amph. Type | Actinolite | Actinolite | Tremolite. | Actinolite | Actinolite | Actinolite | Actinolite | Actinolite | Actinolite |
| Oxide % | | | | | | | | | |
| $SiO_2$ | 55.67 | 55.09 | 56.91 | 56.3 | 55.68 | 55.84 | 55.42 | 54.96 | 56.39 |
| $Al_2O_3$ | 0.7 | 0.77 | 0.2 | 0.58 | 1.1 | 0.49 | 0.51 | 0.76 | 0.34 |
| $TiO_2$ | 0.1 | 0.18 | 0.13 | 0.11 | 0.11 | 0.09 | 0.09 | 0.1 | 0.13 |
| $Cr_2O_3$ | 0.08 | 0.14 | 0 | 0 | 0 | 0 | 0 | 0 | 0 |
| $Fe_2O_3$ | 0.96 | 1.09 | 4.06 | 3.47 | 2.31 | 2 | 1.56 | 0.99 | 3.96 |
| FeO | 6.48 | 5.65 | 1.87 | 3.33 | 4.75 | 4.5 | 5.1 | 5.72 | 3.1 |
| MnO | 0.09 | 0.11 | 0.33 | 0.25 | 0.25 | 0.24 | 0.18 | 0.25 | 0.32 |
| MgO | 19.5 | 19.99 | 21.61 | 20.94 | 20.25 | 20.67 | 20.47 | 19.83 | 20.75 |
| CaO | 12.95 | 12.96 | 12.61 | 12.95 | 13.14 | 13.09 | 13.44 | 13.06 | 12.46 |
| $Na_2O$ | 0.24 | 0.42 | 0.33 | 0.23 | 0.24 | 0.35 | 0.07 | 0.24 | 0.43 |
| $K_2O$ | 0.09 | 0.12 | 0.16 | 0.14 | 0.14 | 0.15 | 0.13 | 0.11 | 0.16 |
| Cl | 0 | 0 | 0 | 0 | 0 | 0 | 0 | 0 | 0 |
| Sum | 96.86 | 96.52 | 96.21 | 96.3 | 97.97 | 97.22 | 96.97 | 96.06 | 96.04 |
| | | | | | | | | | |
| T Site Occupancy | | | | | | | | | |
| Si | 7.873 | 7.812 | 7.841 | 7.796 | 7.768 | 7.814 | 7.814 | 7.833 | 7.827 |
| $Al^{IV}$ | 0.117 | 0.129 | 0.032 | 0.095 | 0.181 | 0.081 | 0.085 | 0.128 | 0.056 |
| Sum | 7.99 | 7.941 | 7.873 | 7.891 | 7.949 | 7.895 | 7.899 | 7.961 | 7.883 |
| | | | | | | | | | |
| C Site Occupancy | | | | | | | | | |
| $Al^{VI}$ | 0 | 0 | 0 | 0 | 0 | 0 | 0 | 0 | 0 |
| Ti | 0.011 | 0.019 | 0.013 | 0.011 | 0.012 | 0.01 | 0.01 | 0.011 | 0.014 |
| Cr | 0.009 | 0.016 | 0 | 0 | 0 | 0 | 0 | 0 | 0 |
| $Fe^{3+}$ | 0.102 | 0.116 | 0.421 | 0.362 | 0.243 | 0.211 | 0.166 | 0.106 | 0.414 |
| $Fe^{2+}$ | 0.767 | 0.67 | 0.215 | 0.385 | 0.554 | 0.529 | 0.602 | 0.682 | 0.359 |
| Mn | 0.011 | 0.013 | 0.039 | 0.029 | 0.03 | 0.029 | 0.021 | 0.03 | 0.038 |
| Mg | 4.111 | 4.226 | 4.438 | 4.322 | 4.212 | 4.327 | 4.302 | 4.211 | 4.293 |
| Sum | 5.011 | 5.06 | 5.126 | 5.109 | 5.051 | 5.106 | 5.101 | 5.04 | 5.118 |
| | | | | | | | | | |
| B Site Occupancy | | | | | | | | | |
| Ca | 1.962 | 1.969 | 1.862 | 1.921 | 1.964 | 1.97 | 2.03 | 1.997 | 1.853 |
| Na | 0.038 | 0.031 | 0.068 | 0.062 | 0.036 | 0.03 | 0 | 0.003 | 0.116 |
| Sum | 2 | 2 | 1.95 | 1.983 | 2 | 2 | 2.03 | 2 | 1.969 |
| | | | | | | | | | |
| A Site Occupancy | | | | | | | | | |
| Na | 0.028 | 0.064 | 0 | 0 | 0.029 | 0.065 | 0.019 | 0.063 | 0 |
| K | 0.016 | 0.022 | 0.028 | 0.025 | 0.025 | 0.027 | 0.023 | 0.02 | 0.028 |
| Sum | 0.044 | 0.106 | 0.028 | 0.025 | 0.054 | 0.092 | 0.042 | 0.083 | 0.028 |
| | | | | | | | | | |
| OH Site Occupancy | | | | | | | | | |
| Cl | 0 | 0 | 0 | 0 | 0 | 0 | 0 | 0 | 0 |
| Sum | 0 | 0 | 0 | 0 | 0 | 0 | 0 | 0 | 0 |
| | | | | | | | | | |
| Ratios | | | | | | | | | |
| Fm | 0.174 | 0.157 | 0.125 | 0.147 | 0.159 | 0.146 | 0.151 | 0.158 | 0.153 |
| Na+K | 0.062 | 0.137 | 0.116 | 0.087 | 0.090 | 0.122 | 0.042 | 0.086 | 0.144 |
| $Mg^{\#}(Fe_{tot})$ | 0.826 | 0.843 | 0.875 | 0.853 | 0.841 | 0.854 | 0.849 | 0.842 | 0.847 |
| $Fe^{3+}/Fe^{2+}$ | 0.133 | 0.173 | 1.958 | 0.940 | 0.439 | 0.399 | 0.276 | 0.155 | 1.153 |
| $Al_{tot}$ | 0.117 | 0.129 | 0.032 | 0.095 | 0.181 | 0.081 | 0.085 | 0.128 | 0.056 |

Hornblende compositions based upon $[C]_{5}[B]_{2}[A][T]_{8}O_{23}$

$Mg^{\#} = Mg/(Mg+Fe^{2+}+Fe^{3+})$

$Al_{tot} = Al^{IV}+Al^{VI}$

$Fm = Fe_{tot}/(Fe_{tot}+Mg)$

Proportions $Fe^{3+}$ and $Fe^{2+}$ calculated assuming hornblende stoichiometry and electrostatic neutrality.

Abbreviations Si. Eden. = Silicic Edenite., Eden. Hbl. = Edenitic Hornblende., Mg. Hbl. = Magnesio Hornblende, Act. Hbl. = Actinolitic Hornblende.

** = Rock Type defined in Appendix 1

| Sample (Min.) | amph6.8 | amph7.1 | amph7.2 | amph8.1 | amph8.2 | amph9.1 | amph9.2 | amph10.1 | amph10.2 |
|---|---|---|---|---|---|---|---|---|---|
| Sample (Rock) | 921010-4 | 921018-8 | 921018-8 | 921018-8 | 921018-8 | 921018-8 | 921018-8 | 921018-8 | 921018-8 |
| Rock Type | Enc | Mo | Mo† | Mo† | Mo† | Mo† | Mo† | Mo† | Mo† |
| Amph. Type | Actinolite | Act. Hbl | Edenite | Edenite | Mg. Hbl. | Edenite | Edenite | Edenite | Edenite |
| Oxide % | | | | | | | | | |
| $SiO_2$ | 56.21 | 50.65 | 49.24 | 49.17 | 48.86 | 48.33 | 49.29 | 48.66 | 49.33 |
| $Al_2O_3$ | 0.73 | 4.13 | 4.82 | 5.04 | 5.36 | 4.89 | 4.96 | 5.14 | 4.78 |
| $TiO_2$ | 0.06 | 0.44 | 0.57 | 0.59 | 0.55 | 0.48 | 0.53 | 0.55 | 0.41 |
| $Cr_2O_3$ | 0 | 0.02 | 0.02 | 0.03 | 0.06 | 0.09 | 0.03 | 0.06 | 0.01 |
| $Fe_2O_3$ | 2.89 | 3.99 | 4.81 | 4.97 | 4.96 | 4.53 | 4.3 | 5.47 | 4.83 |
| FeO | 3.36 | 10.77 | 9.73 | 10.25 | 10.47 | 10.63 | 10.76 | 10.17 | 10.01 |
| MnO | 0.18 | 0.16 | 0.17 | 0.19 | 0.24 | 0.17 | 0.15 | 0.2 | 0.19 |
| MgO | 20.97 | 14.57 | 14.27 | 14.14 | 13.79 | 13.68 | 14.05 | 13.87 | 14.37 |
| CaO | 12.94 | 11.86 | 11.23 | 11.36 | 11.52 | 11.32 | 11.44 | 11.23 | 11.36 |
| $Na_2O$ | 0.22 | 1.15 | 1.45 | 1.59 | 1.38 | 1.45 | 1.59 | 1.64 | 1.64 |
| $K_2O$ | 0.12 | 0.43 | 0.53 | 0.59 | 0.56 | 0.55 | 0.54 | 0.59 | 0.53 |
| Cl | 0 | 0 | 0 | 0 | 0 | 0 | 0 | 0 | 0 |
| Sum | 97.72 | 98.17 | 96.84 | 97.92 | 97.77 | 96.12 | 97.66 | 97.58 | 97.46 |
| | | | | | | | | | |
| T Site Occupancy | | | | | | | | | |
| Si | 7.812 | 7.338 | 7.23 | 7.172 | 7.146 | 7.192 | 7.206 | 7.136 | 7.215 |
| $Al^{IV}$ | 0.12 | 0.662 | 0.77 | 0.828 | 0.854 | 0.808 | 0.792 | 0.864 | 0.785 |
| Sum | 7.932 | 8 | 8 | 8 | 8 | 8 | 8 | 8 | 8 |
| | | | | | | | | | |
| C Site Occupancy | | | | | | | | | |
| $Al^{VI}$ | 0 | 0.043 | 0.084 | 0.039 | 0.07 | 0.05 | 0.066 | 0.024 | 0.039 |
| Ti | 0.006 | 0.048 | 0.063 | 0.065 | 0.06 | 0.054 | 0.058 | 0.061 | 0.045 |
| Cr | 0 | 0.002 | 0.002 | 0.003 | 0.009 | 0.011 | 0.003 | 0.007 | 0.001 |
| $Fe^{3+}$ | 0.302 | 0.435 | 0.532 | 0.545 | 0.545 | 0.507 | 0.473 | 0.604 | 0.532 |
| $Fe^{2+}$ | 0.393 | 1.305 | 1.195 | 1.25 | 1.281 | 1.323 | 1.316 | 1.248 | 1.225 |
| Mn | 0.021 | 0.02 | 0.021 | 0.023 | 0.03 | 0.021 | 0.019 | 0.025 | 0.024 |
| Mg | 4.345 | 3.147 | 3.123 | 3.075 | 3.006 | 3.035 | 3.063 | 3.032 | 3.133 |
| Sum | 5.069 | 5 | 5 | 5 | 5.001 | 5.001 | 4.998 | 5.001 | 4.999 |
| | | | | | | | | | |
| B Site Occupancy | | | | | | | | | |
| Ca | 1.927 | 1.841 | 1.767 | 1.775 | 1.805 | 1.805 | 1.793 | 1.765 | 1.78 |
| Na | 0.059 | 0.159 | 0.233 | 0.225 | 0.195 | 0.195 | 0.207 | 0.235 | 0.22 |
| Sum | 1.986 | 2 | 2 | 2 | 2 | 2 | 2 | 2 | 2 |
| | | | | | | | | | |
| A Site Occupancy | | | | | | | | | |
| Na | 0 | 0.184 | 0.18 | 0.225 | 0.196 | 0.223 | 0.244 | 0.231 | 0.245 |
| K | 0.021 | 0.079 | 0.099 | 0.11 | 0.104 | 0.104 | 0.101 | 0.11 | 0.099 |
| Sum | 0.021 | 0.243 | 0.279 | 0.335 | 0.3 | 0.327 | 0.345 | 0.341 | 0.344 |
| | | | | | | | | | |
| OH Site Occupancy | | | | | | | | | |
| Cl | 0 | 0 | 0 | 0 | 0 | 0 | 0 | 0 | 0 |
| Sum | 0 | 0 | 0 | 0 | 0 | 0 | 0 | 0 | 0 |
| | | | | | | | | | |
| Ratios | | | | | | | | | |
| Fm | 0.138 | 0.356 | 0.356 | 0.369 | 0.378 | 0.376 | 0.369 | 0.379 | 0.359 |
| Na+K | 0.080 | 0.402 | 0.512 | 0.560 | 0.495 | 0.522 | 0.552 | 0.576 | 0.564 |
| $Mg^{\#}(Fe_{tot})$ | 0.862 | 0.644 | 0.644 | 0.631 | 0.622 | 0.624 | 0.631 | 0.621 | 0.641 |
| $Fe^{3+}/Fe^{2+}$ | 0.768 | 0.333 | 0.445 | 0.436 | 0.425 | 0.383 | 0.359 | 0.484 | 0.434 |
| $Al_{tot}$ | 0.120 | 0.705 | 0.834 | 0.867 | 0.924 | 0.858 | 0.858 | 0.888 | 0.824 |

Hornblende compositions based upon $[C]_2[B]_2[A][T]_8O_{22}$

$Mg^{\#} = Mg/(Mg+Fe^{2+}+Fe^{3+})$

$Al_{tot} = Al^{IV}+Al^{VI}$

$Fm = Fe_{tot}/(Fe_{tot}+Mg)$

Proportions $Fe^{3+}$ and $Fe^{2+}$ calculated assuming hornblende stoichiometry and electrostatic neutrality.

Abbreviations Si. Eden. = Silicic Edenite., Eden. Hbl. = Edenitic Hornblende., Mg. Hbl. = Magnesio Hornblende, Act. Hbl. = Actinolitic Hornblende.

** = Rock Type defined in Appendix 1

| Sample (Min.) | amph11.1 | amph11.3 | amph12.1 | amph12.2 | amph13.1 | amph13.2 | amph14.1 | amph15.1 | amph16.1 |
|---|---|---|---|---|---|---|---|---|---|
| Sample (Rock) | 921018-8 | 921018-8 | 921018-8 | 921018-8 | 921018-8 | 921018-8 | 921014-9 | 921014-9 | 921014-9 |
| Rock Type | Mo | Mo | Mo† | Mo† | Mo† | Mo† | Hbldt | Hbldt | Hbldt |
| Amph. Type | Mg. Hbl | Edenite | Si. Edenite | Edenite | Mg. Hbl | Act. Hbl. | Edenite | Mg. Hbl | Edenite |
| Oxide % | | | | | | | | | |
| $SiO_2$ | 49 | 48.49 | 49.31 | 49.21 | 49.48 | 49.54 | 47.84 | 50.86 | 48.4 |
| $Al_2O_3$ | 4.88 | 5.06 | 4.78 | 5.04 | 4.78 | 4.74 | 7.95 | 4.85 | 6.99 |
| $TiO_2$ | 0.41 | 0.52 | 0.39 | 0.48 | 0.38 | 0.39 | 0.23 | 0.24 | 0.33 |
| $Cr_2O_3$ | 0 | 0.01 | 0 | 0.02 | 0.02 | 0 | 0 | 0.33 | 0.34 |
| $Fe_2O_3$ | 4.71 | 4.18 | 3.41 | 2.89 | 3.44 | 3.24 | 4.8 | 4.85 | 2.97 |
| FeO | 10.47 | 10.22 | 11 | 11.5 | 11.19 | 11.03 | 7.68 | 6.72 | 8.54 |
| MnO | 0.19 | 0.16 | 0.21 | 0.19 | 0.17 | 0.15 | 0.07 | 0.11 | 0.08 |
| MgO | 14.02 | 14.16 | 14.05 | 14.11 | 14.29 | 14.38 | 15.23 | 16.94 | 15.53 |
| CaO | 11.63 | 11.37 | 11.53 | 11.86 | 11.94 | 11.85 | 12.11 | 12.58 | 12.04 |
| $Na_2O$ | 1.31 | 1.61 | 1.45 | 1.44 | 1.39 | 1.39 | 1.53 | 0.87 | 1.84 |
| $K_2O$ | 0.51 | 0.55 | 0.5 | 0.54 | 0.46 | 0.46 | 0.62 | 0.39 | 0.54 |
| Cl | 0.01 | 0 | 0 | 0 | 0 | 0 | 0.01 | 0 | 0.01 |
| Sum | 97.14 | 96.33 | 96.63 | 97.28 | 97.54 | 97.17 | 96.07 | 96.54 | 97.61 |
| | | | | | | | | | |
| T Site Occupancy | | | | | | | | | |
| Si | 7.204 | 7.18 | 7.274 | 7.227 | 7.243 | 7.265 | 6.897 | 7.228 | 7.01 |
| $Al^{IV}$ | 0.796 | 0.82 | 0.726 | 0.773 | 0.757 | 0.735 | 1.103 | 0.772 | 0.99 |
| Sum | 8 | 8 | 8 | 8 | 8 | 8 | 8 | 8 | 8 |
| | | | | | | | | | |
| C Site Occupancy | | | | | | | | | |
| $Al^{VI}$ | 0.05 | 0.063 | 0.105 | 0.1 | 0.068 | 0.084 | 0.248 | 0.04 | 0.203 |
| Ti | 0.045 | 0.058 | 0.043 | 0.053 | 0.042 | 0.043 | 0.025 | 0.026 | 0.036 |
| Cr | 0 | 0.001 | 0 | 0.002 | 0.002 | 0 | 0 | 0.037 | 0.039 |
| $Fe^{3+}$ | 0.521 | 0.466 | 0.379 | 0.32 | 0.379 | 0.358 | 0.521 | 0.497 | 0.323 |
| $Fe^{2+}$ | 1.287 | 1.285 | 1.357 | 1.412 | 1.37 | 1.353 | 0.926 | 0.799 | 1.035 |
| Mn | 0.024 | 0.02 | 0.026 | 0.024 | 0.021 | 0.019 | 0.009 | 0.013 | 0.01 |
| Mg | 3.073 | 3.126 | 3.09 | 3.089 | 3.118 | 3.144 | 3.273 | 3.589 | 3.353 |
| Sum | 5 | 4.999 | 5 | 5 | 5 | 5.001 | 5.002 | 5.001 | 4.999 |
| | | | | | | | | | |
| B Site Occupancy | | | | | | | | | |
| Ca | 1.832 | 1.804 | 1.823 | 1.866 | 1.873 | 1.862 | 1.871 | 1.916 | 1.869 |
| Na | 0.168 | 0.196 | 0.177 | 0.134 | 0.127 | 0.138 | 0.129 | 0.084 | 0.131 |
| Sum | 2 | 2 | 2 | 2 | 2 | 2 | 2 | 2 | 2 |
| | | | | | | | | | |
| A Site Occupancy | | | | | | | | | |
| Na | 0.205 | 0.266 | 0.238 | 0.276 | 0.268 | 0.257 | 0.299 | 0.156 | 0.386 |
| K | 0.096 | 0.104 | 0.094 | 0.101 | 0.086 | 0.086 | 0.114 | 0.071 | 0.1 |
| Sum | 0.301 | 0.37 | 0.332 | 0.377 | 0.354 | 0.343 | 0.413 | 0.227 | 0.486 |
| | | | | | | | | | |
| OH Site Occupancy | | | | | | | | | |
| Cl | 0.002 | 0 | 0 | 0 | 0 | 0 | 0.002 | 0 | 0.002 |
| Sum | 0.002 | 0 | 0 | 0 | 0 | 0 | 0.002 | 0 | 0.002 |
| | | | | | | | | | |
| Ratios | | | | | | | | | |
| Fm | 0.370 | 0.356 | 0.360 | 0.359 | 0.359 | 0.352 | 0.307 | 0.285 | 0.288 |
| Na+K | 0.469 | 0.566 | 0.509 | 0.511 | 0.481 | 0.481 | 0.542 | 0.311 | 0.617 |
| $Mg^{\#}(Fe_{tot})$ | 0.630 | 0.644 | 0.640 | 0.641 | 0.641 | 0.648 | 0.693 | 0.735 | 0.712 |
| $Fe^{3+}/Fe^{2+}$ | 0.405 | 0.368 | 0.279 | 0.227 | 0.277 | 0.265 | 0.563 | 0.622 | 0.312 |
| $Al_{tot}$ | 0.846 | 0.883 | 0.831 | 0.873 | 0.825 | 0.819 | 1.351 | 0.812 | 1.193 |

Hornblende compositions based upon $[C]_{5}[B]_{2}[A][T]_{8}O_{23}$

$Mg^{\#} = Mg/(Mg+Fe^{2+}+Fe^{3+})$

$Al_{tot} = Al^{IV}+Al^{VI}$

$Fm = Fe_{tot}/(Fe_{tot}+Mg)$

Proportions $Fe^{3+}$ and $Fe^{2+}$ calculated assuming hornblende stoichiometry and electrostatic neutrality.

Abbreviations Si. Eden. = Silicic Edenite., Eden. Hbl. = Edenitic Hornblende., Mg. Hbl. = Magnesio Hornblende, Act. Hbl. = Actinolitic Hornblende.

** = Rock Type defined in Appendix 1

| Sample (Min.) | amph17.1 | amph18.1 | amph19.2 | amph20.1 | amph21.1 | amph22.1 | amph23.1 | amph24.1 | amph25.1 |
|---|---|---|---|---|---|---|---|---|---|
| Sample (Rock) | 921014-9 | 921014-9 | 921014-9 | 921014-9 | 921014-9 | 921014-9 | 921014-9 | 921014-9 | 921014-9 |
| Rock Type | Hbldt | Hbldt | Hbldt | Hbldt | Hbldt | Hbldt | Hbldt | Hbldt | Hbldt |
| Amph. Type | Edenite | Edenite | Edenite | Edenite | Edenite | Mg. Hbl. | Mg. Hbl. | Edenite | Edenite |
| Oxide % | | | | | | | | | |
| $SiO_2$ | 48.1 | 47.17 | 48.53 | 48.08 | 47.99 | 50.6 | 50.4 | 49.86 | 49.06 |
| $Al_2O_3$ | 6.8 | 7.83 | 7.06 | 7.6 | 7.55 | 5.75 | 5.65 | 6.6 | 6.35 |
| $TiO_2$ | 0.48 | 0.35 | 0.48 | 0.22 | 0.45 | 0.3 | 0.34 | 0.37 | 0.45 |
| $Cr_2O_3$ | 0.22 | 0.24 | 0.13 | 0.09 | 0.26 | 0.05 | 0.15 | 0.12 | 0.24 |
| $Fe_2O_3$ | 2.85 | 4.45 | 2.2 | 4.62 | 3.49 | 3.62 | 2.88 | 3.37 | 4.15 |
| FeO | 8.89 | 8.25 | 9.57 | 7.85 | 8.81 | 7.28 | 8.22 | 8.28 | 7.37 |
| MnO | 0.09 | 0.12 | 0.08 | 0.14 | 0.06 | 0.06 | 0.07 | 0.1 | 0.1 |
| MgO | 15.32 | 14.9 | 15.28 | 15.3 | 15.21 | 16.41 | 16.53 | 16.01 | 16.09 |
| CaO | 12.02 | 11.98 | 12.27 | 12.01 | 12.1 | 12.26 | 12.5 | 12.27 | 12.04 |
| $Na_2O$ | 1.75 | 1.76 | 1.69 | 1.68 | 1.83 | 0.97 | 1.36 | 1.59 | 1.58 |
| $K_2O$ | 0.57 | 0.68 | 0.62 | 0.65 | 0.62 | 0.55 | 0.46 | 0.54 | 0.53 |
| Cl | 0.03 | 0 | 0.03 | 0.02 | 0.02 | 0 | 0 | 0 | 0.05 |
| Sum | 97.12 | 97.71 | 97.94 | 96.26 | 96.39 | 96.07 | 96.58 | 96.91 | 96.01 |
| | | | | | | | | | |
| T Site Occupancy | | | | | | | | | |
| Si | 7.015 | 6.858 | 7.023 | 6.927 | 6.921 | 7.218 | 7.185 | 7.077 | 7.053 |
| $Al^{IV}$ | 0.985 | 1.142 | 0.977 | 1.073 | 1.079 | 0.782 | 0.815 | 0.923 | 0.947 |
| Sum | 8 | 8 | 8 | 8 | 8 | 8 | 8 | 8 | 8 |
| | | | | | | | | | |
| C Site Occupancy | | | | | | | | | |
| $Al^{VI}$ | 0.184 | 0.2 | 0.227 | 0.218 | 0.204 | 0.185 | 0.134 | 0.186 | 0.129 |
| Ti | 0.053 | 0.038 | 0.052 | 0.024 | 0.049 | 0.032 | 0.036 | 0.04 | 0.049 |
| Cr | 0.025 | 0.028 | 0.015 | 0.01 | 0.03 | 0.006 | 0.017 | 0.014 | 0.027 |
| $Fe^{3+}$ | 0.313 | 0.487 | 0.239 | 0.5 | 0.379 | 0.41 | 0.309 | 0.382 | 0.449 |
| $Fe^{2+}$ | 1.084 | 1.003 | 1.159 | 0.945 | 1.082 | 0.869 | 0.96 | 0.966 | 0.886 |
| Mn | 0.011 | 0.015 | 0.01 | 0.017 | 0.007 | 0.01 | 0.008 | 0.012 | 0.012 |
| Mg | 3.331 | 3.229 | 3.296 | 3.286 | 3.27 | 3.489 | 3.513 | 3.401 | 3.446 |
| Sum | 5.001 | 5 | 4.998 | 5 | 5.001 | 5.001 | 4.997 | 5.001 | 5 |
| | | | | | | | | | |
| B Site Occupancy | | | | | | | | | |
| Ca | 1.878 | 1.866 | 1.903 | 1.854 | 1.87 | 1.874 | 1.909 | 1.874 | 1.855 |
| Na | 0.122 | 0.134 | 0.097 | 0.146 | 0.13 | 0.126 | 0.091 | 0.126 | 0.145 |
| Sum | 2 | 2 | 2 | 2 | 2 | 2 | 2 | 2 | 2 |
| | | | | | | | | | |
| A Site Occupancy | | | | | | | | | |
| Na | 0.373 | 0.362 | 0.377 | 0.323 | 0.382 | 0.142 | 0.29 | 0.313 | 0.295 |
| K | 0.106 | 0.122 | 0.114 | 0.119 | 0.114 | 0.1 | 0.084 | 0.098 | 0.097 |
| Sum | 0.479 | 0.484 | 0.491 | 0.442 | 0.496 | 0.242 | 0.374 | 0.411 | 0.392 |
| | | | | | | | | | |
| OH Site Occupancy | | | | | | | | | |
| Cl | 0.007 | 0 | 0.007 | 0.005 | 0.005 | 0 | 0 | 0 | 0.012 |
| Sum | 0.007 | 0 | 0.007 | 0.005 | 0.005 | 0 | 0 | 0 | 0.012 |
| | | | | | | | | | |
| Ratios | | | | | | | | | |
| Fm | 0.295 | 0.316 | 0.298 | 0.305 | 0.306 | 0.268 | 0.268 | 0.284 | 0.279 |
| Na+K | 0.601 | 0.618 | 0.588 | 0.588 | 0.626 | 0.368 | 0.465 | 0.537 | 0.537 |
| $Mg^{\#}(Fe_{tot})$ | 0.705 | 0.684 | 0.702 | 0.695 | 0.694 | 0.732 | 0.732 | 0.718 | 0.721 |
| $Fe^{3+}/Fe^{2+}$ | 0.289 | 0.486 | 0.206 | 0.529 | 0.357 | 0.472 | 0.315 | 0.367 | 0.507 |
| $Al_{tot}$ | 1.169 | 1.342 | 1.204 | 1.291 | 1.283 | 0.967 | 0.949 | 1.109 | 1.076 |

Hornblende compositions based upon $(C)_2(B)_2(A)(T)_8O_{22}$

$Mg^{\#} = Mg/(Mg+Fe^{2+}+Fe^{3+})$

$Al_{tot} = Al^{IV}+Al^{VI}$

$Fm = Fe_{tot}/(Fe_{tot}+Mg)$

Proportions $Fe^{3+}$ and $Fe^{2+}$ calculated assuming hornblende stoichiometry and electrostatic neutrality.

Abbreviations Si. Eden. = Silicic Edenite., Eden. Hbl. = Edenitic Hornblende., Mg. Hbl. = Magnesio Hornblende, Act. Hbl. = Actinolitic Hornblende.

** = Rock Type defined in Appendix 1

| Sample (Min.) | amph25.2 | amph-1 | amph-4 | amph-5 | amph-7 | amph-8 | amph-11 | amph-13 | amph-15 |
|---|---|---|---|---|---|---|---|---|---|
| Sample (Rock) | 921014-8 | 930620-3 | 930620-3 | 930620-3 | 930620-3 | 930620-3 | 930620-3 | 930620-3 | 921018-6 |
| Rock Type | Hbldt | Mo$^{c}$ | Mo$^{c}$ | Mo$^{c}$ | Mo$^{c}$ | Mo$^{c}$ | Mo$^{c}$ | Mo$^{c}$ | QMD |
| Amph. Type | Edenite | Act. Hbl. | Actinolite | Actinolite | Actinolite | Edenite | Actinolite | Actinolite | Edenite |
| Oxide % | | | | | | | | | |
| $SiO_2$ | 48.61 | 51.77 | 52.84 | 53.54 | 51.93 | 48.36 | 52.87 | 54.31 | 45.71 |
| $Al_2O_3$ | 6.61 | 3.74 | 2.58 | 1.86 | 3.61 | 5.84 | 2.67 | 2.58 | 8.36 |
| $TiO_2$ | 0.39 | 0 | 0 | 0 | 0 | 0.13 | 0 | 0 | 0.94 |
| $Cr_2O_3$ | 0.17 | 0 | 0 | 0 | 0 | 0 | 0 | 0 | 0 |
| $Fe_2O_3$ | 2.4 | 3.41 | 3.8 | 2.16 | 0.39 | 2.78 | 4.1 | 1.55 | 3.63 |
| FeO | 9.04 | 10.5 | 9.31 | 9.88 | 13.32 | 12.96 | 9.18 | 10.81 | 13.5 |
| MnO | 0.08 | 0.79 | 0.77 | 0.84 | 0.79 | 0.81 | 0.83 | 0.82 | 0.39 |
| MgO | 15.35 | 14.47 | 15.13 | 15.49 | 14.03 | 12.64 | 15.19 | 15.73 | 11.2 |
| CaO | 12.03 | 12.11 | 12.2 | 12.35 | 12.5 | 12.01 | 12.29 | 12.48 | 11.89 |
| $Na_2O$ | 1.62 | 0.69 | 0 | 0 | 0.86 | 1.38 | 0 | 0.71 | 1.2 |
| $K_2O$ | 0.51 | 0.25 | 0.26 | 0.15 | 0.29 | 0.62 | 0.24 | 0.14 | 0.88 |
| Cl | 0 | 0 | 0 | 0 | 0 | 0 | 0 | 0 | 0 |
| Sum | 96.79 | 97.73 | 96.89 | 96.27 | 97.72 | 97.55 | 97.37 | 99.13 | 97.7 |
| T Site Occupancy | | | | | | | | | |
| Si | 7.09 | 7.497 | 7.655 | 7.784 | 7.568 | 7.159 | 7.627 | 7.696 | 6.805 |
| $Al^{IV}$ | 0.91 | 0.503 | 0.345 | 0.216 | 0.432 | 0.841 | 0.373 | 0.302 | 1.195 |
| Sum | 8 | 8 | 8 | 8 | 8 | 8 | 8 | 8 | 8 |
| C Site Occupancy | | | | | | | | | |
| $Al^{VI}$ | 0.226 | 0.135 | 0.096 | 0.103 | 0.188 | 0.178 | 0.081 | 0.129 | 0.272 |
| Ti | 0.043 | 0 | 0 | 0 | 0 | 0.014 | 0 | 0 | 0.105 |
| Cr | 0.02 | 0 | 0 | 0 | 0 | 0 | 0 | 0 | 0 |
| $Fe^{3+}$ | 0.264 | 0.372 | 0.414 | 0.236 | 0.042 | 0.309 | 0.445 | 0.166 | 0.407 |
| $Fe^{2+}$ | 1.102 | 1.272 | 1.129 | 1.201 | 1.624 | 1.607 | 1.108 | 1.282 | 1.681 |
| Mn | 0.007 | 0.097 | 0.094 | 0.103 | 0.096 | 0.102 | 0.101 | 0.096 | 0.049 |
| Mg | 3.336 | 3.124 | 3.267 | 3.357 | 3.048 | 2.789 | 3.267 | 3.324 | 2.486 |
| Sum | 5 | 5 | 5 | 5 | 5 | 4.999 | 5.002 | 4.999 | 5 |
| B Site Occupancy | | | | | | | | | |
| Ca | 1.88 | 1.879 | 1.894 | 1.924 | 1.952 | 1.905 | 1.9 | 1.895 | 1.897 |
| Na | 0.12 | 0.121 | 0 | 0 | 0.048 | 0.095 | 0 | 0.105 | 0.103 |
| Sum | 2 | 2 | 1.894 | 1.924 | 2 | 2 | 1.9 | 2 | 2 |
| A Site Occupancy | | | | | | | | | |
| Na | 0.338 | 0.073 | 0 | 0 | 0.195 | 0.301 | 0 | 0.09 | 0.243 |
| K | 0.095 | 0.046 | 0.048 | 0.028 | 0.054 | 0.117 | 0.044 | 0.025 | 0.167 |
| Sum | 0.433 | 0.119 | 0.048 | 0.028 | 0.249 | 0.418 | 0.044 | 0.115 | 0.41 |
| OH Site Occupancy | | | | | | | | | |
| Cl | 0 | 0 | 0 | 0 | 0 | 0 | 0 | 0 | 0 |
| Sum | 0 | 0 | 0 | 0 | 0 | 0 | 0 | 0 | 0 |
| Ratios | | | | | | | | | |
| Fm | 0.290 | 0.345 | 0.321 | 0.300 | 0.353 | 0.407 | 0.322 | 0.303 | 0.456 |
| Na+K | 0.553 | 0.240 | 0.048 | 0.028 | 0.297 | 0.513 | 0.044 | 0.220 | 0.513 |
| $Mg^{g}(Fe_{tot})$ | 0.710 | 0.655 | 0.679 | 0.700 | 0.647 | 0.593 | 0.678 | 0.697 | 0.544 |
| $Fe^{3+}/Fe^{2+}$ | 0.240 | 0.292 | 0.367 | 0.197 | 0.026 | 0.192 | 0.402 | 0.129 | 0.242 |
| $Al_{tot}$ | 1.136 | 0.638 | 0.441 | 0.319 | 0.620 | 1.019 | 0.454 | 0.431 | 1.467 |

Hornblende compositions based upon $[C]_5[B]_2[A][T]_8O_{22}$

$Mg^{g} = Mg/(Mg+Fe^{2+}+Fe^{3+})$

$Al_{tot} = Al^{IV}+Al^{VI}$

$Fm = Fe_{tot}/(Fe_{tot}+Mg)$

Proportions $Fe^{3+}$ and $Fe^{2+}$ calculated assuming hornblende stoichiometry and electrostatic neutrality.

Abbreviations Si. Eden. = Silicic Edenite., Eden. Hbl. = Edenitic Hornblende., Mg. Hbl. = Magnesio Hornblende, Act. Hbl. = Actinolitic Hornblende.

** = Rock Type defined in Appendix 1

| Sample (Min.) | amph-16 | amph-17 | amph-18 | amph-19 | amph-20 | amph-21 | amph-22 | amph-23 | amph-36 |
|---|---|---|---|---|---|---|---|---|---|
| Sample (Rock) | 921018-6 | 921014-3 | 921014-3 | 921014-3 | 921014-3 | 921014-3 | 921014-3 | 921014-3 | 930619-3 |
| Rock Type | QMD | QMD | QMD | QMD | QMD | QMD | QMD | QMD | QMD |
| Amph. Type | Edenite | Edenite | Edenite | Sl. Eden | Edenite | Sl. Eden. | Edenite | Mg. Hbl. | Mg. Hbl. |
| Oxide % | | | | | | | | | |
| $SiO_2$ | 45.21 | 49.2 | 49.25 | 50.06 | 48.6 | 50.18 | 48.94 | 49.36 | 47.29 |
| $Al_2O_3$ | 9 | 4.93 | 5.38 | 4.67 | 5.28 | 4.55 | 5.17 | 5.29 | 6.55 |
| $TiO_2$ | 0.85 | 0.78 | 0.9 | 0.73 | 0.96 | 0.62 | 0.88 | 0.85 | 0.91 |
| $Cr_2O_3$ | 0 | 0 | 0 | 0 | 0 | 0.14 | 0 | 0 | 0 |
| $Fe_2O_3$ | 4.55 | 3.92 | 4.68 | 3.96 | 6.16 | 2.25 | 4.47 | 4.17 | 3.41 |
| FeO | 13.19 | 11.83 | 10.85 | 11.26 | 9.66 | 12.58 | 10.96 | 11.86 | 13.42 |
| MnO | 0.43 | 0.3 | 0.34 | 0.32 | 0.3 | 0.32 | 0.33 | 0.33 | 0.33 |
| MgO | 11.02 | 13.56 | 13.73 | 14.07 | 13.83 | 13.81 | 13.83 | 13 | 11.69 |
| CaO | 12.04 | 11.54 | 11.35 | 11.58 | 11.21 | 11.4 | 11.06 | 11.47 | 11.69 |
| $Na_2O$ | 1.14 | 1.56 | 1.53 | 1.48 | 1.39 | 1.34 | 2.02 | 1.06 | 0.99 |
| $K_2O$ | 0.95 | 0.58 | 0.66 | 0.57 | 0.71 | 1.34 | 0.63 | 0.64 | 0.72 |
| Cl | 0.07 | 0 | 0 | 0 | 0 | 0 | 0 | 0 | 0 |
| Sum | 98.45 | 98.2 | 98.67 | 98.72 | 98.1 | 98.53 | 98.33 | 98.03 | 97 |
| | | | | | | | | | |
| T Site Occupancy | | | | | | | | | |
| Si | 6.701 | 7.193 | 7.145 | 7.251 | 7.068 | 7.315 | 7.138 | 7.214 | 7.051 |
| $Al^{IV}$ | 1.299 | 0.807 | 0.855 | 0.749 | 0.904 | 0.685 | 0.862 | 0.786 | 0.949 |
| Sum | 8 | 8 | 8 | 8 | 7.992 | 8 | 8 | 8 | 8 |
| | | | | | | | | | |
| C Site Occupancy | | | | | | | | | |
| $Al^{VI}$ | 0.273 | 0.043 | 0.065 | 0.048 | 0 | 0.097 | 0.027 | 0.125 | 0.202 |
| Ti | 0.095 | 0.086 | 0.098 | 0.079 | 0.107 | 0.068 | 0.097 | 0.093 | 0.102 |
| Cr | 0 | 0 | 0 | 0 | 0 | 0.016 | 0 | 0 | 0 |
| $Fe^{3+}$ | 0.507 | 0.431 | 0.511 | 0.431 | 0.676 | 0.246 | 0.49 | 0.459 | 0.382 |
| $Fe^{2+}$ | 1.635 | 1.447 | 1.317 | 1.363 | 1.178 | 1.533 | 1.339 | 1.45 | 1.673 |
| Mn | 0.054 | 0.037 | 0.042 | 0.039 | 0.037 | 0.04 | 0.041 | 0.041 | 0.042 |
| Mg | 2.435 | 2.855 | 2.869 | 3.037 | 3.007 | 3.001 | 3.007 | 2.832 | 2.598 |
| Sum | 4.999 | 4.999 | 5.002 | 4.997 | 5.005 | 5.001 | 5.001 | 5 | 4.999 |
| | | | | | | | | | |
| B Site Occupancy | | | | | | | | | |
| Ca | 1.912 | 1.808 | 1.764 | 1.797 | 1.752 | 1.781 | 1.732 | 1.796 | 1.868 |
| Na | 0.088 | 0.192 | 0.236 | 0.203 | 0.248 | 0.219 | 0.268 | 0.204 | 0.132 |
| Sum | 2 | 2 | 2 | 2 | 2 | 2 | 2 | 2 | 2 |
| | | | | | | | | | |
| A Site Occupancy | | | | | | | | | |
| Na | 0.24 | 0.25 | 0.194 | 0.213 | 0.145 | 0.16 | 0.303 | 0.096 | 0.154 |
| K | 0.18 | 0.108 | 0.122 | 0.105 | 0.132 | 0.249 | 0.117 | 0.119 | 0.137 |
| Sum | 0.42 | 0.358 | 0.316 | 0.318 | 0.277 | 0.409 | 0.42 | 0.215 | 0.291 |
| | | | | | | | | | |
| OH Site Occupancy | | | | | | | | | |
| Cl | 0.018 | 0 | 0 | 0 | 0 | 0 | 0 | 0 | 0 |
| Sum | 0.018 | 0 | 0 | 0 | 0 | 0 | 0 | 0 | 0 |
| | | | | | | | | | |
| Ratios | | | | | | | | | |
| Fm | 0.468 | 0.389 | 0.381 | 0.371 | 0.381 | 0.372 | 0.378 | 0.403 | 0.442 |
| Na+K | 0.508 | 0.550 | 0.552 | 0.521 | 0.525 | 0.628 | 0.688 | 0.419 | 0.423 |
| $Mg^B(Fe_{tot})$ | 0.532 | 0.611 | 0.619 | 0.629 | 0.619 | 0.628 | 0.622 | 0.597 | 0.558 |
| $Fe^{3+}/Fe^{2+}$ | 0.310 | 0.298 | 0.388 | 0.316 | 0.574 | 0.160 | 0.366 | 0.317 | 0.228 |
| $Al_{tot}$ | 1.572 | 0.850 | 0.920 | 0.797 | 0.904 | 0.782 | 0.889 | 0.911 | 1.151 |

Hornblende compositions based upon $[C]_5[B]_2[A][T]_8O_{22}$

$Mg^B = Mg/(Mg+Fe^{2+}+Fe^{3+})$

$Al_{tot} = Al^{IV}+Al^{VI}$

$Fm = Fe_{tot}/(Fe_{tot}+Mg)$

Proportions $Fe^{3+}$ and $Fe^{2+}$ calculated assuming hornblende stoichiometry and electrostatic neutrality.

Abbreviations Sl. Eden. = Silicic Edenite., Eden. Hbl. = Edenitic Hornblende., Mg. Hbl. = Magnesio Hornblende, Act. Hbl. = Actinolitic Hornblende.

** = Rock Type defined in Appendix 1

| Sample (Min.) | amph-37 | amph-38 | amph-39 | amph-40 | amph-41 | amp1.1 | amp1.2 | amp2.1 | amp2.2 |
|---|---|---|---|---|---|---|---|---|---|
| Sample (Rock) | 930619-3 | 930619-3 | 930619-3 | 930619-3 | 930623-5 | 921013-9 | 921013-9 | 921013-9 | 921013-9 |
| Rock Type | QMD | QMD | QMD | QMD | Dio | Mo† | Mo† | Mo† | Mo† |
| Amph. Type | Mg. Hbl. | Mg. Hbl. | Mg. Hbl. | Mg. Hbl. | Mg. Hbl. | Mg. Hbl. | Mg. Hbl. | Act. Hbl. | Edenite |
| Oxide % | | | | | | | | | |
| $SiO_2$ | 49.44 | 48.21 | 49.25 | 48.06 | 49.71 | 49.63 | 49.43 | 51.1 | 48.42 |
| $Al_2O_3$ | 5.04 | 6.51 | 5.55 | 6.26 | 5.5 | 5.95 | 5.59 | 4.84 | 6.35 |
| $TiO_2$ | 0.81 | 1.06 | 0.93 | 1.06 | 0.48 | 0.76 | 0.78 | 0.57 | 0.81 |
| $Cr_2O_3$ | 0.12 | 0.11 | 0 | 0 | 0.12 | 0.14 | 0 | 0 | 0 |
| $Fe_2O_3$ | 4.12 | 4.36 | 3.1 | 4.75 | 4.42 | 3.61 | 3.09 | 3.74 | 4.44 |
| FeO | 10.51 | 11.45 | 12.24 | 11.47 | 6.94 | 9.87 | 10.35 | 9.46 | 9.28 |
| MnO | 0.3 | 0.28 | 0.37 | 0.29 | 0.16 | 0.27 | 0.34 | 0.25 | 0.3 |
| MgO | 14.07 | 12.78 | 13.13 | 12.68 | 16.26 | 14.28 | 14.01 | 15.06 | 14.4 |
| CaO | 11.9 | 11.86 | 11.62 | 11.8 | 12.24 | 11.73 | 11.73 | 11.88 | 11.66 |
| $Na_2O$ | 0.95 | 0.74 | 1.24 | 0.76 | 0.91 | 1.09 | 0.89 | 0.93 | 1.42 |
| $K_2O$ | 0.51 | 0.66 | 0.59 | 0.61 | 0.52 | 0.53 | 0.57 | 0.46 | 0.65 |
| Cl | 0 | 0 | 0 | 0 | 0 | 0 | 0 | 0 | 0 |
| Sum | 97.77 | 96.06 | 96.02 | 97.76 | 97.26 | 97.86 | 96.78 | 96.29 | 97.73 |
| T Site Occupancy | | | | | | | | | |
| Si | 7.205 | 7.048 | 7.198 | 7.056 | 7.168 | 7.184 | 7.24 | 7.331 | 7.045 |
| $Al^{IV}$ | 0.795 | 0.952 | 0.802 | 0.944 | 0.832 | 0.816 | 0.76 | 0.669 | 0.955 |
| Sum | 8 | 8 | 8 | 8 | 8 | 8 | 8 | 8 | 8 |
| C Site Occupancy | | | | | | | | | |
| $Al^{VI}$ | 0.071 | 0.17 | 0.154 | 0.139 | 0.103 | 0.199 | 0.205 | 0.149 | 0.134 |
| Ti | 0.089 | 0.119 | 0.102 | 0.119 | 0.052 | 0.083 | 0.086 | 0.081 | 0.089 |
| Cr | 0.014 | 0.013 | 0 | 0 | 0.014 | 0.016 | 0 | 0 | 0 |
| $Fe^{3+}$ | 0.452 | 0.48 | 0.341 | 0.525 | 0.48 | 0.393 | 0.341 | 0.403 | 0.487 |
| $Fe^{2+}$ | 1.281 | 1.4 | 1.496 | 1.406 | 0.837 | 1.195 | 1.268 | 1.135 | 1.129 |
| Mn | 0.037 | 0.035 | 0.046 | 0.036 | 0.02 | 0.033 | 0.042 | 0.03 | 0.037 |
| Mg | 3.057 | 2.785 | 2.861 | 2.774 | 3.495 | 3.061 | 3.059 | 3.221 | 3.123 |
| Sum | 5.001 | 5.002 | 5 | 5.001 | 5.001 | 5 | 5.001 | 4.999 | 4.999 |
| B Site Occupancy | | | | | | | | | |
| Ca | 1.858 | 1.858 | 1.82 | 1.856 | 1.891 | 1.819 | 1.841 | 1.826 | 1.818 |
| Na | 0.142 | 0.142 | 0.18 | 0.144 | 0.109 | 0.181 | 0.159 | 0.174 | 0.182 |
| Sum | 2 | 2 | 2 | 2 | 2 | 2 | 2 | 2 | 2 |
| A Site Occupancy | | | | | | | | | |
| Na | 0.126 | 0.068 | 0.171 | 0.072 | 0.145 | 0.125 | 0.094 | 0.065 | 0.219 |
| K | 0.095 | 0.127 | 0.11 | 0.114 | 0.096 | 0.096 | 0.107 | 0.084 | 0.121 |
| Sum | 0.221 | 0.195 | 0.281 | 0.186 | 0.241 | 0.223 | 0.201 | 0.169 | 0.34 |
| OH Site Occupancy | | | | | | | | | |
| Cl | 0 | 0 | 0 | 0 | 0 | 0 | 0 | 0 | 0 |
| Sum | 0 | 0 | 0 | 0 | 0 | 0 | 0 | 0 | 0 |
| Ratios | | | | | | | | | |
| Fm | 0.362 | 0.403 | 0.391 | 0.411 | 0.274 | 0.34 | 0.345 | 0.323 | 0.341 |
| Na+K | 0.363 | 0.337 | 0.461 | 0.330 | 0.350 | 0.404 | 0.360 | 0.343 | 0.522 |
| $Mg^{\#}(Fe_{tot})$ | 0.638 | 0.597 | 0.609 | 0.589 | 0.726 | 0.680 | 0.655 | 0.677 | 0.659 |
| $Fe^{3+}/Fe^{2+}$ | 0.353 | 0.343 | 0.228 | 0.373 | 0.573 | 0.329 | 0.269 | 0.355 | 0.431 |
| $Al_{tot}$ | 0.866 | 1.122 | 0.956 | 1.063 | 0.935 | 1.015 | 0.965 | 0.818 | 1.089 |

Hornblende compositions based upon $[C]_5[B]_2[A][T]_8O_{23}$

$Mg^{\#} = Mg/(Mg+Fe^{2+}+Fe^{3+})$

$Al_{tot} = Al^{IV}+Al^{VI}$

$Fm = Fe_{tot}/(Fe_{tot}+Mg)$

Proportions $Fe^{3+}$ and $Fe^{2+}$ calculated assuming hornblende stoichiometry and electrostatic neutrality.

Abbreviations Si. Eden. = Silicic Edenite., Eden. Hbl. = Edenitic Hornblende., Mg. Hbl. = Magnesio Hornblende, Act. Hbl. = Actinolitic Hornblende.

** = Rock Type defined in Appendix 1

| Sample (Min.) | amp3.1 | amp3.2 | amp4.1 | amp5.1 | amp5.2 | amp6.1 | amp6.2 | amp7.1 | amp8.1 |
|---|---|---|---|---|---|---|---|---|---|
| Sample (Rock) | 921013-9 | 921013-9 | 921011-16x | 921011-16x | 921011-16x | 921011-13 | 921011-13 | 921011-13 | 921015-14 |
| Rock Type | Mo† | Mo† | QMo | QMo | QMo | Dio | Dio | Dio | Dio |
| Amph. Type | Mg. Hbl. | Si. Eden. | Si. Eden. | Act. Hbl. | Act. Hbl. | Act. Hbl. | Mg. Hbl. | Mg. Hbl. | Mg. Hbl. |
| Oxide % | | | | | | | | | |
| $SiO_2$ | 47.72 | 48.01 | 49.03 | 49.59 | 50.03 | 49.88 | 48.05 | 48.33 | 49.27 |
| $Al_2O_3$ | 7.12 | 6.76 | 4.84 | 4.59 | 4.32 | 5.82 | 6.57 | 6.44 | 5.7 |
| $TiO_2$ | 1.01 | 0.84 | 0.69 | 0.69 | 0.44 | 0.29 | 0.34 | 0.36 | 0.53 |
| $Cr_2O_3$ | 0.17 | 0 | 0 | 0.17 | 0 | 0.24 | 0.42 | 0.3 | 0 |
| $Fe_2O_3$ | 5.45 | 4.57 | 4.96 | 4.13 | 4.5 | 2.02 | 4.35 | 4.2 | 6.12 |
| FeO | 9.06 | 9.74 | 11.42 | 11.59 | 11.43 | 11.06 | 9.67 | 9.71 | 8.78 |
| MnO | 0.26 | 0.27 | 0.37 | 0.28 | 0.3 | 0.24 | 0.32 | 0.24 | 0.27 |
| MgO | 13.69 | 13.62 | 12.73 | 13.37 | 13.36 | 14.36 | 13.82 | 14.1 | 13.69 |
| CaO | 11.66 | 11.78 | 10.73 | 11.27 | 11.29 | 12.12 | 12 | 12.13 | 11.89 |
| $Na_2O$ | 0.97 | 0.88 | 1.41 | 1.31 | 1.11 | 1.17 | 0.99 | 0.97 | 0 |
| $K_2O$ | 0.71 | 0.67 | 0.68 | 0.61 | 0.57 | 0.48 | 0.57 | 0.6 | 0.57 |
| Cl | 0 | 0 | 0 | 0 | 0 | 0 | 0 | 0 | 0 |
| Sum | 97.84 | 97.14 | 96.86 | 97.6 | 97.35 | 97.48 | 97.1 | 97.38 | 96.82 |
| T Site Occupancy | | | | | | | | | |
| Si | 6.946 | 7.035 | 7.257 | 7.275 | 7.343 | 7.262 | 7.049 | 7.064 | 7.199 |
| $Al^{IV}$ | 1.054 | 0.965 | 0.743 | 0.725 | 0.657 | 0.738 | 0.951 | 0.936 | 0.801 |
| Sum | 8 | 8 | 8 | 8 | 8 | 8 | 8 | 8 | 8 |
| C Site Occupancy | | | | | | | | | |
| $Al^{VI}$ | 0.168 | 0.202 | 0.101 | 0.069 | 0.09 | 0.226 | 0.185 | 0.174 | 0.181 |
| Ti | 0.111 | 0.093 | 0.077 | 0.076 | 0.049 | 0.032 | 0.038 | 0.04 | 0.058 |
| Cr | 0.02 | 0 | 0 | 0.02 | 0 | 0.026 | 0.049 | 0.035 | 0 |
| $Fe^{3+}$ | 0.597 | 0.504 | 0.552 | 0.455 | 0.497 | 0.222 | 0.48 | 0.462 | 0.673 |
| $Fe^{2+}$ | 1.103 | 1.193 | 1.413 | 1.422 | 1.403 | 1.346 | 1.187 | 1.187 | 1.073 |
| Mn | 0.032 | 0.034 | 0.046 | 0.035 | 0.037 | 0.03 | 0.04 | 0.03 | 0.033 |
| Mg | 2.97 | 2.975 | 2.809 | 2.924 | 2.923 | 3.116 | 3.022 | 3.072 | 2.982 |
| Sum | 5.001 | 5.001 | 4.998 | 5.001 | 4.999 | 5 | 5.001 | 5 | 5 |
| B Site Occupancy | | | | | | | | | |
| Ca | 1.822 | 1.849 | 1.702 | 1.771 | 1.776 | 1.891 | 1.886 | 1.9 | 1.862 |
| Na | 0.178 | 0.151 | 0.298 | 0.229 | 0.224 | 0.109 | 0.114 | 0.1 | 0 |
| Sum | 2 | 2 | 2 | 2 | 2 | 2 | 2 | 2 | 1.862 |
| A Site Occupancy | | | | | | | | | |
| Na | 0.096 | 0.099 | 0.107 | 0.144 | 0.092 | 0.221 | 0.168 | 0.175 | 0 |
| K | 0.132 | 0.125 | 0.128 | 0.114 | 0.107 | 0.089 | 0.107 | 0.112 | 0.106 |
| Sum | 0.228 | 0.224 | 0.235 | 0.258 | 0.199 | 0.31 | 0.275 | 0.287 | 0.106 |
| OH Site Occupancy | | | | | | | | | |
| Cl | 0 | 0 | 0 | 0 | 0 | 0 | 0 | 0 | 0 |
| Sum | 0 | 0 | 0 | 0 | 0 | 0 | 0 | 0 | 0 |
| Ratios | | | | | | | | | |
| Fm | 0.364 | 0.363 | 0.412 | 0.391 | 0.394 | 0.335 | 0.356 | 0.349 | 0.369 |
| Na+K | 0.408 | 0.375 | 0.533 | 0.487 | 0.423 | 0.419 | 0.389 | 0.387 | 0.106 |
| $Mg^{\#}(Fe_{tot})$ | 0.636 | 0.637 | 0.588 | 0.609 | 0.606 | 0.665 | 0.644 | 0.651 | 0.631 |
| $Fe^{3+}/Fe^{2+}$ | 0.541 | 0.422 | 0.391 | 0.320 | 0.354 | 0.165 | 0.404 | 0.389 | 0.627 |
| $Al_{tot}$ | 1.222 | 1.167 | 0.844 | 0.794 | 0.747 | 0.964 | 1.136 | 1.110 | 0.982 |

Hornblende compositions based upon $[C]_{5}[B]_{2}[A][T]_{8}O_{23}$

$Mg^{\#} = Mg/(Mg+Fe^{2+}+Fe^{3+})$

$Al_{tot} = Al^{IV}+Al^{VI}$

$Fm = Fe_{tot}/(Fe_{tot}+Mg)$

Proportions $Fe^{3+}$ and $Fe^{2+}$ calculated assuming hornblende stoichiometry and electrostatic neutrality.

Abbreviations Si. Eden. = Silicic Edenite., Eden. Hbl. = Edenitic Hornblende., Mg. Hbl. = Magnesio Hornblende, Act. Hbl. = Actinolitic Hornblende.

** = Rock Type defined in Appendix 1

| Sample (Min.) | amp9.1 | amp10.1 | amp11.2 | amp12.1 | amp12.2 | amp13.2 |
|---|---|---|---|---|---|---|
| Sample (Rock) | 921015-14 | 921015-14 | 921015-14 | 921012-9 | 921012-9 | 921012-9 |
| Rock Type | Dio | Dio | Dio | QMD | QMD | QMD |
| Amph. Type | Actinolite | Edenite | Act. Hbl | Mg. Hbl. | Mg. Hbl. | Actinolite |
| Oxide % | | | | | | |
| $SiO_2$ | 55.75 | 48.29 | 49.06 | 49.73 | 49.28 | 55.91 |
| $Al_2O_3$ | 0.5 | 6.3 | 5.09 | 5.56 | 5.63 | 0.71 |
| $TiO_2$ | 0 | 0.99 | 0.66 | 0.6 | 0.68 | 0 |
| $Cr_2O_3$ | 0.12 | 0 | 0.14 | 0 | 0 | 0 |
| $Fe_2O_3$ | 0.26 | 4.34 | 4.89 | 4.17 | 5.55 | 1.19 |
| FeO | 12.12 | 10.66 | 8.24 | 9.96 | 9.39 | 10.93 |
| MnO | 0.29 | 0.43 | 0.29 | 0.3 | 0.39 | 0.24 |
| MgO | 15.79 | 13.46 | 14.6 | 14.17 | 14.11 | 16.48 |
| CaO | 12.58 | 11.48 | 11.54 | 11.82 | 11.58 | 12.74 |
| $Na_2O$ | 0 | 1.5 | 0.79 | 0.92 | 1.15 | 0 |
| $K_2O$ | 0 | 0.6 | 0.47 | 0.5 | 0.56 | 0 |
| Cl | 0 | 0 | 0 | 0 | 0.07 | 0 |
| Sum | 97.41 | 96.05 | 95.77 | 97.73 | 98.39 | 98.2 |
| | | | | | | |
| T Site Occupancy | | | | | | |
| Si | 8.003 | 7.048 | 7.227 | 7.217 | 7.133 | 7.939 |
| $Al^{IV}$ | 0 | 0.952 | 0.773 | 0.783 | 0.867 | 0.061 |
| Sum | 8.003 | 8 | 8 | 8 | 8 | 8 |
| | | | | | | |
| C Site Occupancy | | | | | | |
| $Al^{VI}$ | 0.085 | 0.132 | 0.111 | 0.168 | 0.094 | 0.058 |
| Ti | 0 | 0.109 | 0.073 | 0.065 | 0.074 | 0 |
| Cr | 0.014 | 0 | 0.016 | 0 | 0 | 0 |
| $Fe^{3+}$ | 0.028 | 0.476 | 0.542 | 0.455 | 0.604 | 0.127 |
| $Fe^{2+}$ | 1.456 | 1.301 | 1.015 | 1.209 | 1.137 | 1.298 |
| Mn | 0.035 | 0.053 | 0.036 | 0.037 | 0.048 | 0.029 |
| Mg | 3.379 | 2.929 | 3.206 | 3.066 | 3.045 | 3.488 |
| Sum | 4.997 | 5 | 4.999 | 5 | 5.002 | 5 |
| | | | | | | |
| B Site Occupancy | | | | | | |
| Ca | 1.935 | 1.795 | 1.822 | 1.838 | 1.796 | 1.938 |
| Na | 0 | 0.205 | 0.178 | 0.162 | 0.204 | 0 |
| Sum | 1.935 | 2 | 2 | 2 | 2 | 1.938 |
| | | | | | | |
| A Site Occupancy | | | | | | |
| Na | 0 | 0.22 | 0.048 | 0.097 | 0.119 | 0 |
| K | 0 | 0.112 | 0.088 | 0.093 | 0.103 | 0 |
| Sum | 0 | 0.332 | 0.136 | 0.19 | 0.222 | 0 |
| | | | | | | |
| OH Site Occupancy | | | | | | |
| Cl | 0 | 0 | 0 | 0 | 0.017 | 0 |
| Sum | 0 | 0 | 0 | 0 | 0.017 | 0 |
| | | | | | | |
| Ratios | | | | | | |
| Fm | 0.305 | 0.378 | 0.327 | 0.352 | 0.364 | 0.29 |
| Na+K | 0.000 | 0.537 | 0.314 | 0.352 | 0.426 | 0.000 |
| $Mg^{\#}(Fe_{tot})$ | 0.695 | 0.622 | 0.673 | 0.648 | 0.636 | 0.710 |
| $Fe^{3+}/Fe^{2+}$ | 0.019 | 0.366 | 0.534 | 0.376 | 0.531 | 0.098 |
| $Al_{tot}$ | 0.085 | 1.084 | 0.884 | 0.951 | 0.961 | 0.119 |

Hornblende compositions based upon $[C]_5[B]_2[A][T]_8O_{23}$

$Mg^{\#} = Mg/(Mg+Fe^{2+}+Fe^{3+})$

$Al_{tot} = Al^{IV}+Al^{VI}$

$Fm = Fe_{tot}/(Fe_{tot}+Mg)$

Proportions $Fe^{3+}$ and $Fe^{2+}$ calculated assuming hornblende stoichiometry and electrostatic neutrality.

Abbreviations Si. Eden. = Silicic Edenite., Eden. Hbl. = Edenitic Hornblende., Mg. Hbl. = Magnesio Hornblende, Act. Hbl. = Actinolitic Hornblende.

** = Rock Type defined in Appendix 1

# Clinopyroxene Compositions

| Sample (Min.) | px2.3 | px3.1 | px3.2 | px4.1 | px4.2 | px4.3 | px5.1 | px5.2 | px6.2 |
|---|---|---|---|---|---|---|---|---|---|
| Sample (Rock) | 921012-7 | 921012-7 | 921012-7 | 921012-7 | 921012-7 | 921012-7 | 921012-7 | 921012-7 | 921012-7 |
| Rock Type** | Dio | Dio | Dio | Dio | Dio | Dio | Dio | Dio | Dio |
| Cpx Type | Augite | | Augite | Cr-Augite | Cr-Endiopside | Cr-Salite | Cr-Salite | Cr-Endiopside | $Fe^{3+}$, Cr-Augite |
| Oxide % | | | | | | | | | |
| $SiO_2$ | 51.53 | 51.71 | 51.63 | 51.99 | 53.29 | 52.49 | 51.87 | 52.43 | 52.69 |
| $Al_2O_3$ | 2.21 | 2.38 | 2.44 | 1.96 | 1.34 | 1.27 | 2.38 | 1.36 | 1.4 |
| $Fe_2O_3$ | 1.48 | 0.74 | 2.13 | 3.53 | 2.17 | 2.04 | 2.67 | 0.96 | 3.86 |
| $TiO_2$ | 0.45 | 0.56 | 0.57 | 0.39 | 0.28 | 0.25 | 0.43 | 0.21 | 0.3 |
| $Cr_2O_3$ | 0.2 | 0.14 | 0.15 | 0.73 | 1.12 | 1.09 | 0.49 | 0.76 | 0.44 |
| MgO | 15.39 | 14.38 | 14.48 | 14.92 | 16.72 | 16.3 | 14.62 | 16.81 | 15.82 |
| FeO | 5.3 | 7.96 | 6.82 | 4.66 | 2.81 | 3.4 | 4.76 | 3.65 | 3.14 |
| MnO | 0.07 | 0.16 | 0.13 | 0.12 | 0.08 | 0.1 | 0.1 | 0 | 0.12 |
| CaO | 21.23 | 20.34 | 20.2 | 20.61 | 21.29 | 21.5 | 21.15 | 20.7 | 20.78 |
| $Na_2O$ | 0.44 | 0.53 | 0.78 | 1.01 | 0.86 | 0.61 | 0.97 | 0.61 | 1.11 |
| Sum | 98.3 | 98.92 | 99.33 | 99.94 | 99.96 | 99.05 | 99.44 | 97.49 | 99.66 |
| T Site Occupancy | | | | | | | | | |
| Si | 1.93 | 1.939 | 1.926 | 1.923 | 1.948 | 1.943 | 1.925 | 1.961 | 1.941 |
| $Al^{IV}$ | 0.07 | 0.061 | 0.074 | 0.077 | 0.052 | 0.055 | 0.075 | 0.039 | 0.059 |
| $Fe^{3+}$ | 0 | 0 | 0 | 0 | 0 | 0.002 | 0 | 0 | 0 |
| Sum | 2 | 2 | 2 | 2 | 2 | 2 | 2 | 2 | 2 |
| M1 Site Occupancy | | | | | | | | | |
| $Al^{VI}$ | 0.028 | 0.044 | 0.033 | 0.009 | 0.006 | 0 | 0.029 | 0.021 | 0.002 |
| $Fe^{3+}$ | 0.042 | 0.021 | 0.06 | 0.096 | 0.06 | 0.055 | 0.075 | 0.027 | 0.107 |
| $Ti^{4+}$ | 0.013 | 0.016 | 0.016 | 0.011 | 0.008 | 0.007 | 0.012 | 0.006 | 0.008 |
| Cr | 0.006 | 0.004 | 0.004 | 0.021 | 0.032 | 0.032 | 0.014 | 0.022 | 0.013 |
| Mg | 0.859 | 0.804 | 0.805 | 0.823 | 0.894 | 0.9 | 0.809 | 0.924 | 0.869 |
| $Fe^{2+}$ | 0.052 | 0.111 | 0.082 | 0.038 | 0 | 0.006 | 0.061 | 0 | 0.001 |
| Mn | 0 | 0 | 0 | 0 | 0 | 0 | 0 | 0 | 0 |
| Sum | 1 | 1 | 1 | 1 | 1 | 1 | 1 | 1 | 1 |
| M2 Site Occupancy | | | | | | | | | |
| Mg | 0 | 0 | 0 | 0 | 0.017 | 0 | 0 | 0.013 | 0 |
| $Fe^{2+}$ | 0.114 | 0.139 | 0.131 | 0.106 | 0.086 | 0.099 | 0.087 | 0.114 | 0.096 |
| Mn | 0.002 | 0.006 | 0.004 | 0.004 | 0.002 | 0.003 | 0.003 | 0 | 0.004 |
| Ca | 0.852 | 0.817 | 0.808 | 0.817 | 0.834 | 0.853 | 0.841 | 0.829 | 0.82 |
| Na | 0.032 | 0.039 | 0.056 | 0.072 | 0.061 | 0.044 | 0.07 | 0.044 | 0.079 |
| Sum | 1 | 1.001 | 0.999 | 0.999 | 1 | 0.999 | 1.001 | 1 | 0.999 |
| Mole % Endmembers | | | | | | | | | |
| Wo | 44.35 | 43.06 | 42.75 | 43.32 | 44.06 | 44.47 | 44.83 | 43.47 | 43.23 |
| En | 44.72 | 42.35 | 42.59 | 43.64 | 48.12 | 46.92 | 43.12 | 49.13 | 45.81 |
| Fs | 10.83 | 14.28 | 14.44 | 12.83 | 7.71 | 8.45 | 11.89 | 7.39 | 10.75 |
| Mn | 0.1 | 0.32 | 0.21 | 0.21 | 0.11 | 0.16 | 0.16 | 0 | 0.21 |
| Ratios | | | | | | | | | |
| $Mg\#(Fe^{2+})$ | 0.84 | 0.76 | 0.79 | 0.85 | 0.91 | 0.90 | 0.85 | 0.89 | 0.90 |
| $Mg\#(Fe_{tot})$ | 0.81 | 0.75 | 0.75 | 0.77 | 0.86 | 0.85 | 0.78 | 0.87 | 0.81 |
| $Fe^{3+}/Fe^{2+}$ | 0.25 | 0.08 | 0.28 | 0.68 | 0.70 | 0.54 | 0.51 | 0.24 | 1.10 |
| D.I. | 40.96 | 40.96 | 40.96 | 40.96 | 40.96 | 40.96 | 40.96 | 40.96 | 40.96 |

Clinopyroxene compositions based upon $[M1][M2][T]_2O_6$.

$Mg\#(Fe^{2+}) = Mg/(Fe^{2+}+Mg)$

$Mg\#(Fe_{tot}) = Mg/(Fe^{2+}+Fe^{3+}+Mg)$

Clinopyroxene type classified from Wo - En - Fs quadrilateral.

Proportions $Fe^{3+}$ and $Fe^{2+}$ calculated assuming Cpx stoichiometry and electrostatic neutrality.

** = Rock Type defined in Appendix 1

| Sample (Min.) | px8.3 | px7.1 | px7.2 | px7.3 | px7.4 | px7.5 | px8.2 | px8.3 | px8.4 |
|---|---|---|---|---|---|---|---|---|---|
| Sample (Rock) | 921012-7 | 921014-9 | 921014-9 | 921014-9 | 921014-9 | 921014-9 | 921014-9 | 921014-9 | 921014-9 |
| Rock Type** | Dio | Hbldt | Hbldt | Hbldt | Hbldt | Hbldt | Hbldt | Hbldt | Hbldt |
| Cpx Type | Cr-Diopside | Salite | Diopside | Diopside | Diopside | Diopside | Diopside | Diopside | Diopside |
| Oxide % | | | | | | | | | |
| $SiO_2$ | 52.53 | 52.73 | 53 | 53.92 | 52.83 | 53 | 53.42 | 54.4 | 54.03 |
| $Al_2O_3$ | 1.14 | 2.04 | 1.28 | 1.14 | 1.36 | 1 | 1.13 | 0.83 | 1.07 |
| $Fe_2O_3$ | 1.29 | 1.3 | 0.75 | 0.55 | 2.04 | 0 | 0 | 0 | 1.32 |
| $TiO_2$ | 0.32 | 0.48 | 0.4 | 0.37 | 0.35 | 0.41 | 0.29 | 0.37 | 0.36 |
| $Cr_2O_3$ | 0.86 | 0.28 | 0.26 | 0.63 | 0.56 | 0.47 | 0.63 | 0.39 | 0.61 |
| MgO | 16.69 | 15.82 | 16.25 | 16.55 | 15.78 | 15.81 | 17.1 | 17.25 | 17.55 |
| FeO | 3.52 | 4.5 | 4.21 | 3.85 | 2.69 | 4.42 | 4.03 | 4.13 | 3.16 |
| MnO | 0.07 | 0.09 | 0.04 | 0 | 0.19 | 0.13 | 0.09 | 0.06 | 0.14 |
| CaO | 21.9 | 22.36 | 22.73 | 23.04 | 22.46 | 22.72 | 22.69 | 23.03 | 22.86 |
| $Na_2O$ | 0.36 | 0.44 | 0.3 | 0.41 | 0.78 | 0.34 | 0.08 | 0.15 | 0.25 |
| Sum | 98.68 | 100.04 | 99.22 | 100.46 | 99.04 | 98.3 | 99.46 | 100.61 | 101.35 |
| | | | | | | | | | |
| T Site Occupancy | | | | | | | | | |
| Si | 1.949 | 1.936 | 1.958 | 1.964 | 1.953 | 1.975 | 1.962 | 1.974 | 1.949 |
| $Al^{IV}$ | 0.05 | 0.064 | 0.042 | 0.036 | 0.047 | 0.025 | 0.038 | 0.026 | 0.045 |
| $Fe^{3+}$ | 0.001 | 0 | 0 | 0 | 0 | 0 | 0 | 0 | 0.006 |
| Sum | 2 | 2 | 2 | 2 | 2 | 2 | 2 | 2 | 2 |
| | | | | | | | | | |
| M1 Site Occupancy | | | | | | | | | |
| $Al^{VI}$ | 0 | 0.024 | 0.014 | 0.013 | 0.012 | 0.019 | 0.011 | 0.01 | 0 |
| $Fe^{3+}$ | 0.035 | 0.036 | 0.021 | 0.015 | 0.057 | 0 | 0 | 0 | 0.03 |
| $Ti^{4+}$ | 0.009 | 0.013 | 0.011 | 0.01 | 0.01 | 0.011 | 0.008 | 0.01 | 0.01 |
| Cr | 0.025 | 0.008 | 0.008 | 0.018 | 0.016 | 0.014 | 0.018 | 0.011 | 0.017 |
| Mg | 0.923 | 0.866 | 0.895 | 0.898 | 0.87 | 0.878 | 0.936 | 0.933 | 0.943 |
| $Fe^{2+}$ | 0.008 | 0.053 | 0.051 | 0.046 | 0.035 | 0.078 | 0.027 | 0.036 | 0 |
| Mn | 0 | 0 | 0 | 0 | 0 | 0 | 0 | 0 | 0 |
| Sum | 1 | 1 | 1 | 1 | 1 | 1 | 1 | 1 | 1 |
| | | | | | | | | | |
| M2 Site Occupancy | | | | | | | | | |
| Mg | 0 | 0 | 0 | 0 | 0 | 0 | 0 | 0 | 0.001 |
| $Fe^{2+}$ | 0.101 | 0.085 | 0.079 | 0.071 | 0.048 | 0.06 | 0.097 | 0.069 | 0.095 |
| Mn | 0.002 | 0.003 | 0.001 | 0 | 0.006 | 0.004 | 0.003 | 0.002 | 0.004 |
| Ca | 0.871 | 0.88 | 0.9 | 0.899 | 0.89 | 0.907 | 0.893 | 0.896 | 0.883 |
| Na | 0.026 | 0.031 | 0.021 | 0.029 | 0.056 | 0.025 | 0.006 | 0.011 | 0.017 |
| Sum | 1 | 0.999 | 1.001 | 0.999 | 1 | 0.996 | 0.999 | 0.998 | 1 |
| | | | | | | | | | |
| Mole % Endmembers | | | | | | | | | |
| Wo | 44.87 | 45.76 | 46.22 | 46.6 | 46.69 | 47.07 | 45.65 | 45.81 | 45.01 |
| En | 47.55 | 45.03 | 45.97 | 46.55 | 45.65 | 45.56 | 47.85 | 47.7 | 48.11 |
| Fs | 7.47 | 9.05 | 7.76 | 6.84 | 7.35 | 7.16 | 6.34 | 6.39 | 6.68 |
| Mn | 0.1 | 0.16 | 0.05 | 0 | 0.31 | 0.21 | 0.15 | 0.1 | 0.2 |
| | | | | | | | | | |
| Ratios | | | | | | | | | |
| $Mg\#(Fe^{2+})$ | 0.89 | 0.86 | 0.87 | 0.88 | 0.91 | 0.86 | 0.88 | 0.88 | 0.91 |
| $Mg\#(Fe_{tot})$ | 0.86 | 0.83 | 0.86 | 0.87 | 0.86 | 0.86 | 0.88 | 0.88 | 0.88 |
| $Fe^{3+}/Fe^{2+}$ | 0.33 | 0.26 | 0.16 | 0.13 | 0.69 | 0.00 | 0.00 | 0.00 | 0.38 |
| D.I. | 40.96 | 30.34 | 30.34 | 30.34 | 30.34 | 30.34 | 30.34 | 30.34 | 30.34 |

Clinopyroxene compositions based upon $[M1][M2][T]_2O_6$.

$Mg\#(Fe^{2+}) = Mg/(Fe^{2+}+Mg)$

$Mg\#(Fe_{tot}) = Mg/(Fe^{2+}+Fe^{3+}+Mg)$

Clinopyroxene type classified from Wo - En - Fs quadrilateral.

Proportions $Fe^{3+}$ and $Fe^{2+}$ calculated assuming Cpx stoichiometry and electrostatic neutrality.

** = Rock Type defined in Appendix 1

| Sample (Min.) | px6.1 | px6.5 | px6.6 | px6.7 | px6.8 | px6.9 | px6.10 | px6.11 | px6.12 |
|---|---|---|---|---|---|---|---|---|---|
| Sample (Rock) | 921014-9 | 921014-9 | 921014-9 | 921014-9 | 921014-9 | 921014-9 | 921014-9 | 921014-9 | 921014-9 |
| Rock Type** | Hbldt | Hbldt | Hbldt | Hbldt | Hbldt | Hbldt | Hbldt | Hbldt | Hbldt |
| Cpx Type | Salite | Salite | Diopside | Diopside | Diopside | Salite | Diopside | Diopside | Diopside |
| Oxide % | | | | | | | | | |
| $SiO_2$ | 52.32 | 52.42 | 54.21 | 54.14 | 53.57 | 50.4 | 53.32 | 52.64 | 54.24 |
| $Al_2O_3$ | 1.55 | 3.36 | 1.01 | 0.92 | 1.27 | 3.89 | 1.08 | 1.14 | 1.31 |
| $Fe_2O_3$ | 2.99 | 0.54 | 0.33 | 0 | 1.3 | 2.76 | 0.97 | 2.14 | 3.2 |
| $TiO_2$ | 0.33 | 0.56 | 0.28 | 0.32 | 0.34 | 0.68 | 0.33 | 0.38 | 0.34 |
| $Cr_2O_3$ | 0.93 | 0.51 | 0.47 | 0.31 | 0.26 | 0.51 | 0.58 | 0.59 | 0.58 |
| MgO | 15.05 | 14.89 | 17.6 | 17.11 | 15.97 | 14.49 | 17.1 | 16.77 | 16.45 |
| FeO | 4.16 | 5.11 | 3.23 | 4.44 | 3.77 | 3.4 | 3.27 | 2.39 | 1.89 |
| MnO | 0.09 | 0.05 | 0 | 0 | 0.07 | 0.14 | 0.04 | 0.17 | 0.08 |
| CaO | 21.19 | 22.36 | 23.22 | 23.05 | 22.75 | 21.7 | 22.4 | 21.9 | 22.92 |
| $Na_2O$ | 0.99 | 0.61 | 0.17 | 0.1 | 0.65 | 0.81 | 0.33 | 0.62 | 1.01 |
| Sum | 99.62 | 100.41 | 100.52 | 100.39 | 99.95 | 98.78 | 99.42 | 98.74 | 101.82 |
| | | | | | | | | | |
| T Site Occupancy | | | | | | | | | |
| Si | 1.937 | 1.919 | 1.965 | 1.971 | 1.963 | 1.878 | 1.958 | 1.947 | 1.947 |
| $Al^{IV}$ | 0.063 | 0.081 | 0.035 | 0.029 | 0.037 | 0.122 | 0.042 | 0.05 | 0.053 |
| $Fe^{3+}$ | 0 | 0 | 0 | 0 | 0 | 0 | 0 | 0.003 | 0 |
| Sum | 2 | 2 | 2 | 2 | 2 | 2 | 2 | 2 | 2 |
| | | | | | | | | | |
| M1 Site Occupancy | | | | | | | | | |
| $Al^{VI}$ | 0.005 | 0.064 | 0.008 | 0.01 | 0.018 | 0.049 | 0.005 | 0 | 0.002 |
| $Fe^{3+}$ | 0.083 | 0.015 | 0.009 | 0 | 0.036 | 0.077 | 0.027 | 0.057 | 0.066 |
| $Ti^{4+}$ | 0.009 | 0.015 | 0.008 | 0.009 | 0.009 | 0.019 | 0.009 | 0.011 | 0.009 |
| Cr | 0.027 | 0.015 | 0.013 | 0.009 | 0.008 | 0.015 | 0.017 | 0.017 | 0.016 |
| Mg | 0.831 | 0.813 | 0.951 | 0.929 | 0.873 | 0.805 | 0.936 | 0.915 | 0.88 |
| $Fe^{2+}$ | 0.045 | 0.078 | 0.011 | 0.043 | 0.056 | 0.035 | 0.006 | 0 | 0.007 |
| Mn | 0 | 0 | 0 | 0 | 0 | 0 | 0 | 0 | 0 |
| Sum | 1 | 1 | 1 | 1 | 1 | 1 | 1 | 1 | 1 |
| | | | | | | | | | |
| M2 Site Occupancy | | | | | | | | | |
| Mg | 0 | 0 | 0 | 0 | 0 | 0 | 0 | 0.01 | 0 |
| $Fe^{2+}$ | 0.084 | 0.078 | 0.067 | 0.092 | 0.06 | 0.071 | 0.094 | 0.074 | 0.044 |
| Mn | 0.003 | 0.002 | 0 | 0 | 0.002 | 0.004 | 0.001 | 0.005 | 0.002 |
| Ca | 0.841 | 0.877 | 0.902 | 0.899 | 0.893 | 0.866 | 0.881 | 0.868 | 0.882 |
| Na | 0.071 | 0.043 | 0.012 | 0.007 | 0.046 | 0.059 | 0.023 | 0.044 | 0.07 |
| Sum | 0.999 | 1 | 1.001 | 0.998 | 1.001 | 1 | 0.999 | 1.001 | 0.998 |
| | | | | | | | | | |
| Mole % Endmembers | | | | | | | | | |
| Wo | 44.57 | 47.07 | 46.02 | 45.8 | 46.51 | 46.61 | 45.3 | 44.93 | 46.4 |
| En | 44.04 | 43.64 | 48.52 | 47.33 | 45.47 | 43.33 | 48.12 | 47.88 | 46.29 |
| Fs | 11.23 | 9.18 | 5.46 | 6.88 | 7.92 | 9.85 | 6.53 | 6.94 | 7.21 |
| Mn | 0.16 | 0.11 | 0 | 0 | 0.1 | 0.22 | 0.05 | 0.26 | 0.11 |
| | | | | | | | | | |
| Ratios | | | | | | | | | |
| $Mg\#(Fe^{2+})$ | 0.87 | 0.84 | 0.91 | 0.87 | 0.88 | 0.88 | 0.90 | 0.93 | 0.95 |
| $Mg\#(Fe_{tot})$ | 0.80 | 0.83 | 0.90 | 0.87 | 0.85 | 0.81 | 0.88 | 0.87 | 0.87 |
| $Fe^{3+}/Fe^{2+}$ | 0.64 | 0.10 | 0.09 | 0.00 | 0.31 | 0.73 | 0.27 | 0.81 | 1.69 |
| D.I. | 30.34 | 30.34 | 30.34 | 30.34 | 30.34 | 30.34 | 30.34 | 30.34 | 30.34 |

Clinopyroxene compositions based upon $[M1][M2][T]_2O_6$.

$Mg\#(Fe^{2+}) = Mg/(Fe^{2+}+Mg)$

$Mg\#(Fe_{tot}) = Mg/(Fe^{2+}+Fe^{3+}+Mg)$

Clinopyroxene type classified from Wo - En - Fs quadrilateral.

Proportions $Fe^{3+}$ and $Fe^{2+}$ calculated assuming Cpx stoichiometry and electrostatic neutrality.

** = Rock Type defined in Appendix 1

| Sample (Min.) | px9.1 | px9.2 | px10.1 | px10.2 | px11.1 | px11.2 | px12.1 | px13.1 | px13.2 |
|---|---|---|---|---|---|---|---|---|---|
| Sample (Rock) | 921014-9 | 921014-9 | 921014-9 | 921014-9 | 921014-9 | 921014-9 | 921014-9 | 921014-9 | 921014-9 |
| Rock Type** | Hbldt | Hbldt | Hbldt | Hbldt | Hbldt | Hbldt | Hbldt | Hbldt | Hbldt |
| Cpx Type | Diopside | Diopside | Salite | Diopside | Diopside | Diopside | Diopside | Salite | Diopside |
| Oxide % | | | | | | | | | |
| $SiO_2$ | 53.31 | 53.23 | 52.17 | 52.95 | 54.04 | 53.41 | 53.85 | 53.3 | 53.19 |
| $Al_2O_3$ | 1.01 | 1.11 | 1.94 | 0.97 | 0.88 | 1.03 | 0.86 | 1.31 | 0.82 |
| $Fe_2O_3$ | 2.49 | 0.87 | 0.86 | 0 | 1.09 | 0.11 | 0 | 0 | 0.43 |
| $TiO_2$ | 0.27 | 0.33 | 0.46 | 0.28 | 0.22 | 0.33 | 0.34 | 0.36 | 0.31 |
| $Cr_2O_3$ | 0.77 | 0.93 | 0.34 | 0.16 | 0.38 | 0.88 | 0.5 | 0.63 | 0.88 |
| MgO | 15.72 | 16.61 | 15.55 | 16.44 | 17.57 | 17.34 | 17.13 | 15.14 | 17.26 |
| FeO | 2.74 | 3.16 | 4.59 | 4.62 | 2.99 | 3.7 | 3.89 | 4.9 | 3.44 |
| MnO | 0.35 | 0.09 | 0.07 | 0.05 | 0.06 | 0.08 | 0.02 | 0.21 | 0.27 |
| CaO | 22.88 | 22.72 | 22.58 | 22.77 | 22.74 | 22.71 | 22.52 | 22.78 | 22.72 |
| $Na_2O$ | 0.8 | 0.44 | 0.33 | 0 | 0.27 | 0.06 | 0.25 | 0.59 | 0.07 |
| Sum | 100.34 | 99.49 | 99.89 | 99.24 | 100.24 | 99.67 | 99.36 | 99.22 | 99.17 |
| | | | | | | | | | |
| T Site Occupancy | | | | | | | | | |
| Si | 1.952 | 1.956 | 1.939 | 1.973 | 1.965 | 1.957 | 1.976 | 1.974 | 1.96 |
| $Al^{IV}$ | 0.044 | 0.044 | 0.061 | 0.027 | 0.035 | 0.043 | 0.024 | 0.026 | 0.036 |
| $Fe^{3+}$ | 0.004 | 0 | 0 | 0 | 0 | 0 | 0 | 0 | 0.004 |
| Sum | 2 | 2 | 2 | 2 | 2 | 2 | 2 | 2 | 2 |
| | | | | | | | | | |
| M1 Site Occupancy | | | | | | | | | |
| $Al^{VI}$ | 0 | 0.004 | 0.024 | 0.016 | 0.003 | 0.001 | 0.013 | 0.031 | 0 |
| $Fe^{3+}$ | 0.065 | 0.024 | 0.024 | 0 | 0.03 | 0.003 | 0 | 0 | 0.008 |
| $Ti^{4+}$ | 0.007 | 0.009 | 0.013 | 0.008 | 0.006 | 0.009 | 0.009 | 0.01 | 0.009 |
| Cr | 0.022 | 0.027 | 0.01 | 0.005 | 0.011 | 0.025 | 0.015 | 0.018 | 0.019 |
| Mg | 0.858 | 0.91 | 0.862 | 0.913 | 0.95 | 0.947 | 0.937 | 0.836 | 0.948 |
| $Fe^{2+}$ | 0.048 | 0.026 | 0.067 | 0.058 | 0 | 0.015 | 0.026 | 0.105 | 0.016 |
| Mn | 0 | 0 | 0 | 0 | 0 | 0 | 0 | 0 | 0 |
| Sum | 1 | 1 | 1 | 1 | 1 | 1 | 1 | 1 | 1 |
| | | | | | | | | | |
| M2 Site Occupancy | | | | | | | | | |
| Mg | 0 | 0 | 0 | 0 | 0.002 | 0 | 0 | 0 | 0 |
| $Fe^{2+}$ | 0.036 | 0.071 | 0.076 | 0.086 | 0.091 | 0.098 | 0.093 | 0.047 | 0.09 |
| Mn | 0.011 | 0.003 | 0.002 | 0.002 | 0.002 | 0.002 | 0.001 | 0.007 | 0.008 |
| Ca | 0.898 | 0.895 | 0.899 | 0.909 | 0.886 | 0.892 | 0.885 | 0.904 | 0.897 |
| Na | 0.057 | 0.031 | 0.024 | 0 | 0.019 | 0.006 | 0.018 | 0.042 | 0.005 |
| Sum | 1.002 | 1 | 1.001 | 0.997 | 1 | 0.998 | 0.997 | 1 | 1 |
| | | | | | | | | | |
| Mole % Endmembers | | | | | | | | | |
| Wo | 46.77 | 46.4 | 46.58 | 46.19 | 45.18 | 45.58 | 45.57 | 47.6 | 45.51 |
| En | 44.69 | 47.17 | 44.66 | 46.39 | 48.55 | 48.39 | 48.25 | 44.02 | 48.1 |
| Fs | 7.97 | 6.27 | 8.65 | 7.32 | 6.17 | 5.93 | 6.13 | 8 | 5.99 |
| Mn | 0.57 | 0.16 | 0.1 | 0.1 | 0.1 | 0.1 | 0.05 | 0.37 | 0.41 |
| | | | | | | | | | |
| Ratios | | | | | | | | | |
| $Mg\#(Fe^{2+})$ | 0.91 | 0.90 | 0.86 | 0.86 | 0.91 | 0.89 | 0.89 | 0.85 | 0.90 |
| $Mg\#(Fe_{tot})$ | 0.85 | 0.88 | 0.84 | 0.86 | 0.89 | 0.89 | 0.89 | 0.85 | 0.89 |
| $Fe^{3+}/Fe^{2+}$ | 0.82 | 0.25 | 0.17 | 0.00 | 0.33 | 0.03 | 0.00 | 0.00 | 0.11 |
| D.I. | 30.34 | 30.34 | 30.34 | 30.34 | 30.34 | 30.34 | 30.34 | 30.34 | 30.34 |

Clinopyroxene compositions based upon $[M1][M2][T]_2O_6$.

$Mg\#(Fe^{2+}) = Mg/(Fe^{2+}+Mg)$

$Mg\#(Fe_{tot}) = Mg/(Fe^{2+}+Fe^{3+}+Mg)$

Clinopyroxene type classified from Wo - En - Fs quadrilateral.

Proportions $Fe^{3+}$ and $Fe^{2+}$ calculated assuming Cpx stoichiometry and electrostatic neutrality.

** = Rock Type defined in Appendix 1

| Sample (Min.) | px14.1 | px14.2 | px15.1 | px16.1 | px16.2 | px16.3 | px16.4 | px17.1 | px17.2 |
|---|---|---|---|---|---|---|---|---|---|
| Sample (Rock) | 921014-9 | 921014-9 | 921014-9 | 921014-9 | 921014-9 | 921014-9 | 921014-9 | 921018-8 | 921018-8 |
| Rock Type** | Hbldt | Hbldt | Hbldt | Hbldt | Hbldt | Hbldt | Hbldt | Mo† | Mo† |
| Cpx Type | Diopside | Diopside | Augite | Diopside | Diopside | Diopside | Salite | Salite | Salite |
| Oxide % | | | | | | | | | |
| $SiO_2$ | 53.47 | 52.87 | 52.69 | 52.79 | 53.34 | 53.89 | 52.47 | 52.19 | 52.48 |
| $Al_2O_3$ | 0.73 | 1.26 | 1.06 | 1.84 | 0.86 | 0.96 | 1.5 | 0.77 | 0.86 |
| $Fe_2O_3$ | 0 | 1.51 | 2.46 | 1.52 | 0.86 | 0 | 2.15 | 2.4 | 2.75 |
| $TiO_2$ | 0.3 | 0.35 | 0.32 | 0.42 | 0.25 | 0.26 | 0.42 | 0.15 | 0.35 |
| $Cr_2O_3$ | 0.48 | 0.64 | 0.58 | 0.63 | 0.42 | 0.92 | 0.65 | 0.29 | 0.35 |
| MgO | 17.15 | 16.63 | 16.34 | 16.45 | 16.91 | 16.71 | 15.56 | 12.65 | 13.78 |
| FeO | 4 | 2.76 | 3 | 3.43 | 3.54 | 4.2 | 3.03 | 6.81 | 4.96 |
| MnO | 0 | 0.14 | 0.21 | 0.19 | 0.14 | 0.15 | 0.19 | 0.59 | 0.5 |
| CaO | 22.5 | 22.44 | 21.12 | 22.7 | 21.94 | 22.04 | 22.72 | 21.56 | 21.78 |
| $Na_2O$ | 0.16 | 0.41 | 0.62 | 0.31 | 0.45 | 0.49 | 0.67 | 1.07 | 1.12 |
| Sum | 98.79 | 99.21 | 98.62 | 100.28 | 98.71 | 99.64 | 99.36 | 98.48 | 98.95 |
| | | | | | | | | | |
| T Site Occupancy | | | | | | | | | |
| Si | 1.975 | 1.947 | 1.955 | 1.93 | 1.972 | 1.976 | 1.94 | 1.979 | 1.967 |
| $Al^{IV}$ | 0.025 | 0.053 | 0.045 | 0.07 | 0.028 | 0.024 | 0.06 | 0.021 | 0.033 |
| $Fe^{3+}$ | 0 | 0 | 0 | 0 | 0 | 0 | 0 | 0 | 0 |
| Sum | 2 | 2 | 2 | 2 | 2 | 2 | 2 | 2 | 2 |
| | | | | | | | | | |
| M1 Site Occupancy | | | | | | | | | |
| $Al^{VI}$ | 0.007 | 0.002 | 0.002 | 0.009 | 0.009 | 0.018 | 0.005 | 0.013 | 0.005 |
| $Fe^{3+}$ | 0 | 0.042 | 0.069 | 0.042 | 0.024 | 0 | 0.06 | 0.069 | 0.077 |
| $Ti^{4+}$ | 0.008 | 0.01 | 0.009 | 0.012 | 0.007 | 0.007 | 0.012 | 0.004 | 0.01 |
| Cr | 0.014 | 0.019 | 0.017 | 0.018 | 0.012 | 0.027 | 0.019 | 0.009 | 0.01 |
| Mg | 0.944 | 0.924 | 0.903 | 0.897 | 0.932 | 0.913 | 0.857 | 0.715 | 0.77 |
| $Fe^{2+}$ | 0.027 | 0.003 | 0 | 0.022 | 0.016 | 0.035 | 0.047 | 0.19 | 0.128 |
| Mn | 0 | 0 | 0 | 0 | 0 | 0 | 0 | 0 | 0 |
| Sum | 1 | 1 | 1 | 1 | 1 | 1 | 1 | 1 | 1 |
| | | | | | | | | | |
| M2 Site Occupancy | | | | | | | | | |
| Mg | 0 | 0 | 0.001 | 0 | 0 | 0 | 0 | 0 | 0 |
| $Fe^{2+}$ | 0.097 | 0.082 | 0.093 | 0.083 | 0.093 | 0.094 | 0.047 | 0.026 | 0.028 |
| Mn | 0 | 0.004 | 0.007 | 0.006 | 0.004 | 0.005 | 0.006 | 0.019 | 0.016 |
| Ca | 0.891 | 0.886 | 0.84 | 0.889 | 0.869 | 0.866 | 0.9 | 0.876 | 0.875 |
| Na | 0.011 | 0.029 | 0.059 | 0.022 | 0.032 | 0.035 | 0.048 | 0.079 | 0.081 |
| Sum | 0.999 | 1.001 | 1 | 1 | 0.998 | 1 | 1.001 | 1 | 1 |
| | | | | | | | | | |
| Mole % Endmembers | | | | | | | | | |
| Wo | 45.48 | 45.65 | 43.91 | 45.85 | 44.84 | 45.27 | 46.95 | 46.23 | 46.2 |
| En | 48.19 | 47.6 | 47.26 | 46.26 | 48.09 | 47.73 | 44.71 | 37.73 | 40.65 |
| Fs | 6.33 | 6.54 | 8.47 | 7.58 | 6.86 | 6.74 | 8.03 | 15.04 | 12.3 |
| Mn | 0 | 0.21 | 0.37 | 0.31 | 0.21 | 0.26 | 0.31 | 1 | 0.84 |
| | | | | | | | | | |
| Ratios | | | | | | | | | |
| $Mg\#(Fe^{2+})$ | 0.88 | 0.92 | 0.91 | 0.90 | 0.90 | 0.88 | 0.90 | 0.77 | 0.83 |
| $Mg\#(Fe_{tot})$ | 0.88 | 0.88 | 0.85 | 0.86 | 0.88 | 0.88 | 0.85 | 0.72 | 0.77 |
| $Fe^{3+}/Fe^{2+}$ | 0.00 | 0.49 | 0.74 | 0.40 | 0.22 | 0.00 | 0.64 | 0.32 | 0.49 |
| D.I. | 30.34 | 30.34 | 30.34 | 30.34 | 30.34 | 30.34 | 30.34 | 70.52 | 70.52 |

Clinopyroxene compositions based upon $[M1][M2][T]_2O_6$.

$Mg\#(Fe^{2+}) = Mg/(Fe^{2+}+Mg)$

$Mg\#(Fe_{tot}) = Mg/(Fe^{2+}+Fe^{3+}+Mg)$

Clinopyroxene type classified from Wo - En - Fs quadrilateral.

Proportions $Fe^{3+}$ and $Fe^{2+}$ calculated assuming Cpx stoichiometry and electrostatic neutrality.

** = Rock Type defined in Appendix 1

| Sample (Min.) | px18.1 | px18.2 | px19.1 | px19.2 | px3 | px6 | px24 | px25 | px26 |
|---|---|---|---|---|---|---|---|---|---|
| Sample (Rock) | 921018-6 | 921018-6 | 921018-6 | 921018-6 | 930620-3 | 930620-3 | 921014-11 | 921014-11 | 921014-11 |
| Rock Type** | Mo† | Mo† | Mo† | Mo† | Mo‡ | Mo‡ | Hbldt | Hbldt | Hbldt |
| Cpx Type | Na-Salite | Na-Salite | Salite | Salite | Na-Salite | Salite | Salite | Salite | Diopside |
| Oxide % | | | | | | | | | |
| $SiO_2$ | 52.86 | 52.89 | 52.43 | 52.22 | 53.45 | 53.11 | 49.7 | 48.75 | 53.81 |
| $Al_2O_3$ | 0.77 | 0.74 | 0.35 | 0.29 | 0.29 | 0.8 | 5.34 | 6.15 | 1.26 |
| $Fe_2O_3$ | 4.89 | 4.03 | 4.84 | 2.94 | 4.02 | 1.69 | 4.31 | 0.75 | 0 |
| $TiO_2$ | 0.25 | 0.22 | 0.09 | 0.15 | 0 | 0 | 0.83 | 1.11 | 0.31 |
| $Cr_2O_3$ | 0.32 | 0.23 | 0.19 | 0.22 | 0 | 0 | 0.27 | 0.2 | 0.14 |
| MgO | 13.31 | 13.64 | 12.84 | 12.58 | 11.03 | 11.46 | 13.94 | 13.51 | 16.68 |
| FeO | 4.21 | 4.48 | 4.53 | 6.47 | 7 | 9.21 | 3.62 | 6.76 | 5.02 |
| MnO | 0.67 | 0.44 | 0.6 | 0.67 | 1.24 | 1.03 | 0.23 | 0 | 0.16 |
| CaO | 21.44 | 21.64 | 22.57 | 23.12 | 22.33 | 22.32 | 22.21 | 22.24 | 23.05 |
| $Na_2O$ | 1.6 | 1.36 | 1.21 | 0.71 | 1.56 | 0.93 | 0.66 | 0 | 0 |
| Sum | 100.32 | 99.69 | 99.65 | 99.37 | 100.92 | 100.55 | 101.11 | 99.47 | 100.43 |
| T Site Occupancy | | | | | | | | | |
| Si | 1.96 | 1.968 | 1.965 | 1.971 | 1.995 | 1.991 | 1.821 | 1.82 | 1.964 |
| $Al^{IV}$ | 0.034 | 0.032 | 0.015 | 0.013 | 0.005 | 0.009 | 0.179 | 0.18 | 0.036 |
| $Fe^{3+}$ | 0.006 | 0 | 0.02 | 0.016 | 0 | 0 | 0 | 0 | 0 |
| Sum | 2 | 2 | 2 | 2 | 2 | 2 | 2 | 2 | 2 |
| M1 Site Occupancy | | | | | | | | | |
| $Al^{VI}$ | 0 | 0 | 0 | 0 | 0.008 | 0.026 | 0.052 | 0.091 | 0.018 |
| $Fe^{3+}$ | 0.13 | 0.113 | 0.116 | 0.067 | 0.113 | 0.048 | 0.119 | 0.021 | 0 |
| $Ti^{4+}$ | 0.007 | 0.006 | 0.003 | 0.004 | 0 | 0 | 0.023 | 0.031 | 0.009 |
| Cr | 0.009 | 0.007 | 0.006 | 0.007 | 0 | 0 | 0.008 | 0.006 | 0.004 |
| Mg | 0.736 | 0.757 | 0.717 | 0.708 | 0.614 | 0.641 | 0.762 | 0.752 | 0.906 |
| $Fe^{2+}$ | 0.118 | 0.117 | 0.142 | 0.204 | 0.219 | 0.285 | 0.036 | 0.099 | 0.061 |
| Mn | 0 | 0 | 0.016 | 0.01 | 0.039 | 0 | 0 | 0 | 0 |
| Sum | 1 | 1 | 1 | 1 | 0.993 | 1 | 1 | 1 | 1 |
| M2 Site Occupancy | | | | | | | | | |
| Mg | 0 | 0 | 0 | 0 | 0 | 0 | 0 | 0 | 0 |
| $Fe^{2+}$ | 0.013 | 0.022 | 0 | 0 | 0 | 0.004 | 0.075 | 0.112 | 0.092 |
| Mn | 0.021 | 0.014 | 0.003 | 0.011 | 0 | 0.033 | 0.007 | 0 | 0.005 |
| Ca | 0.852 | 0.863 | 0.906 | 0.935 | 0.893 | 0.897 | 0.872 | 0.889 | 0.902 |
| Na | 0.115 | 0.1 | 0.088 | 0.052 | 0.113 | 0.068 | 0.047 | 0 | 0 |
| Sum | 1.001 | 0.999 | 0.997 | 0.998 | 1.006 | 1.002 | 1.001 | 1.001 | 0.999 |
| Mole % Endmembers | | | | | | | | | |
| Wo | 45.42 | 45.76 | 47.19 | 47.92 | 47.55 | 47.01 | 46.61 | 47.46 | 45.83 |
| En | 39.23 | 40.14 | 37.34 | 36.29 | 32.69 | 33.6 | 40.73 | 40.15 | 46.14 |
| Fs | 14.23 | 13.36 | 14.48 | 14.71 | 17.68 | 17.66 | 12.29 | 12.39 | 7.77 |
| Mn | 1.12 | 0.74 | 0.99 | 1.08 | 2.08 | 1.73 | 0.37 | 0 | 0.25 |
| Ratios | | | | | | | | | |
| $Mg\#(Fe^{2+})$ | 0.85 | 0.84 | 0.83 | 0.78 | 0.74 | 0.69 | 0.87 | 0.78 | 0.86 |
| $Mg\#(Fe_{tot})$ | 0.73 | 0.75 | 0.72 | 0.71 | 0.65 | 0.66 | 0.77 | 0.76 | 0.86 |
| $Fe^{3+}/Fe^{2+}$ | 1.04 | 0.81 | 0.96 | 0.41 | 0.52 | 0.17 | 1.07 | 0.10 | 0.00 |
| D.I. | 70.52 | 70.52 | 70.52 | 70.52 | 81.19 | 81.19 | 26.8 | 26.8 | 26.8 |

Clinopyroxene compositions based upon $[M1][M2][T]_2O_6$.

$Mg\#(Fe^{2+}) = Mg/(Fe^{2+}+Mg)$

$Mg\#(Fe_{tot}) = Mg/(Fe^{2+}+Fe^{3+}+Mg)$

Clinopyroxene type classified from Wo - En - Fs quadrilateral.

Proportions $Fe^{3+}$ and $Fe^{2+}$ calculated assuming Cpx stoichiometry and electrostatic neutrality.

** = Rock Type defined in Appendix 1

| Sample (Min.) | px27 | px28 | px-a | px-b | px-c | px-d | px1.1 | px1.2 | px1.3 |
|---|---|---|---|---|---|---|---|---|---|
| Sample (Rock) | 921014-11 | 921014-11 | 921014-11 | 921014-11 | 921014-11 | 921014-11 | 921012-7 | 921012-7 | 921012-7 |
| Rock Type** | Hbldt | Hbldt | Hbldt | Hbldt | Hbldt | Hbldt | Dio | Dio | Dio |
| Cpx Type | Diopside | Salite | Salite | Salite | Diopside | Salite | Augite | Augite | Augite |
| Oxide % | | | | | | | | | |
| $SiO_2$ | 53.95 | 50.26 | 53.3 | 53.96 | 53.94 | 51.8 | 52.64 | 52.2 | 52.03 |
| $Al_2O_3$ | 1.56 | 4.47 | 1.66 | 1.27 | 1.17 | 3.13 | 1.46 | 1.33 | 2.39 |
| $Fe_2O_3$ | 0 | 0.32 | 0.33 | 0 | 0 | 0 | 2.13 | 3.19 | 2.78 |
| $TiO_2$ | 0.23 | 0.76 | 0.32 | 0.23 | 0.18 | 0.36 | 0.31 | 0.33 | 0.48 |
| $Cr_2O_3$ | 0.24 | 0.26 | 0.32 | 0.24 | 0.37 | 0.24 | 0.11 | 0.24 | 0.18 |
| MgO | 16.76 | 14.62 | 16.4 | 16.6 | 16.55 | 15.2 | 14.72 | 15.03 | 14.52 |
| FeO | 4.91 | 5.65 | 5.12 | 5.32 | 4.75 | 6.2 | 6.43 | 4.59 | 6.15 |
| MnO | 0.12 | 0.13 | 0 | 0.17 | 0 | 0 | 0.28 | 0.19 | 0.2 |
| CaO | 22.74 | 22.57 | 23.17 | 22.58 | 22.85 | 22.3 | 20.8 | 21.23 | 20.34 |
| $Na_2O$ | 0 | 0 | 0 | 0 | 0 | 0 | 0.77 | 0.87 | 0.96 |
| Sum | 100.51 | 99.04 | 100.62 | 100.37 | 99.81 | 99.23 | 99.65 | 99.2 | 100.03 |
| | | | | | | | | | |
| T Site Occupancy | | | | | | | | | |
| Si | 1.964 | 1.872 | 1.946 | 1.97 | 1.976 | 1.922 | 1.956 | 1.944 | 1.927 |
| $Al^{IV}$ | 0.036 | 0.128 | 0.054 | 0.03 | 0.024 | 0.078 | 0.044 | 0.056 | 0.073 |
| $Fe^{3+}$ | 0 | 0 | 0 | 0 | 0 | 0 | 0 | 0 | 0 |
| Sum | 2 | 2 | 2 | 2 | 2 | 2 | 2 | 2 | 2 |
| | | | | | | | | | |
| M1 Site Occupancy | | | | | | | | | |
| $Al^{VI}$ | 0.031 | 0.068 | 0.017 | 0.025 | 0.027 | 0.059 | 0.02 | 0.002 | 0.031 |
| $Fe^{3+}$ | 0 | 0.009 | 0.009 | 0 | 0 | 0 | 0.06 | 0.089 | 0.077 |
| $Ti^{4+}$ | 0.006 | 0.021 | 0.009 | 0.006 | 0.005 | 0.01 | 0.009 | 0.009 | 0.013 |
| Cr | 0.007 | 0.008 | 0.009 | 0.007 | 0.011 | 0.007 | 0.003 | 0.007 | 0.005 |
| Mg | 0.909 | 0.812 | 0.893 | 0.904 | 0.904 | 0.841 | 0.815 | 0.834 | 0.801 |
| $Fe^{2+}$ | 0.047 | 0.082 | 0.063 | 0.058 | 0.053 | 0.083 | 0.093 | 0.059 | 0.073 |
| Mn | 0 | 0 | 0 | 0 | 0 | 0 | 0 | 0 | 0 |
| Sum | 1 | 1 | 1 | 1 | 1 | 1 | 1 | 1 | 1 |
| | | | | | | | | | |
| M2 Site Occupancy | | | | | | | | | |
| Mg | 0 | 0 | 0 | 0 | 0 | 0 | 0 | 0 | 0 |
| $Fe^{2+}$ | 0.102 | 0.094 | 0.093 | 0.104 | 0.093 | 0.109 | 0.107 | 0.084 | 0.117 |
| Mn | 0.004 | 0.004 | 0 | 0.005 | 0 | 0 | 0.009 | 0.006 | 0.006 |
| Ca | 0.887 | 0.901 | 0.907 | 0.883 | 0.897 | 0.887 | 0.828 | 0.847 | 0.807 |
| Na | 0 | 0 | 0 | 0 | 0 | 0 | 0.055 | 0.063 | 0.069 |
| Sum | 0.993 | 0.999 | 1 | 0.992 | 0.99 | 0.996 | 0.999 | 1 | 0.999 |
| | | | | | | | | | |
| Mole % Endmembers | | | | | | | | | |
| Wo | 45.51 | 47.37 | 46.16 | 45.19 | 46.07 | 46.2 | 43.31 | 44.14 | 42.9 |
| En | 46.64 | 42.69 | 45.45 | 46.26 | 46.43 | 43.8 | 42.63 | 43.46 | 42.58 |
| Fs | 7.64 | 9.73 | 8.4 | 8.29 | 7.5 | 10 | 13.6 | 12.09 | 14.19 |
| Mn | 0.21 | 0.21 | 0 | 0.26 | 0 | 0 | 0.47 | 0.31 | 0.32 |
| | | | | | | | | | |
| Ratios | | | | | | | | | |
| $Mg\#(Fe^{2+})$ | 0.86 | 0.82 | 0.85 | 0.85 | 0.86 | 0.81 | 0.80 | 0.85 | 0.81 |
| $Mg\#(Fe_{tot})$ | 0.86 | 0.81 | 0.84 | 0.85 | 0.86 | 0.81 | 0.76 | 0.78 | 0.75 |
| $Fe^{3+}/Fe^{2+}$ | 0.00 | 0.05 | 0.06 | 0.00 | 0.00 | 0.00 | 0.30 | 0.62 | 0.41 |
| D.I. | 26.8 | 26.8 | 26.8 | 26.8 | 26.8 | 26.8 | 40.96 | 40.96 | 40.96 |

Clinopyroxene compositions based upon $[M1][M2][T]_2O_6$.

$Mg\#(Fe^{2+}) = Mg/(Fe^{2+}+Mg)$

$Mg\#(Fe_{tot}) = Mg/(Fe^{2+}+Fe^{3+}+Mg)$

Clinopyroxene type classified from Wo - En - Fs quadrilateral.

Proportions $Fe^{3+}$ and $Fe^{2+}$ calculated assuming Cpx stoichiometry and electrostatic neutrality.

** = Rock Type defined in Appendix 1

| Sample (Min.) | px2.1 | px2.2 |
|---|---|---|
| Sample (Rock) | 921012-7 | 921012-7 |
| Rock Type** | Dio | Dio |
| Cpx Type | Diopside | Diopside |
| Oxide % | | |
| $SiO_2$ | 52.87 | 53.24 |
| $Al_2O_3$ | 1.3 | 0.91 |
| $Fe_2O_3$ | 0.86 | 0.43 |
| $TiO_2$ | 0.33 | 0.3 |
| $Cr_2O_3$ | 0.6 | 0.66 |
| MgO | 16.69 | 16.8 |
| FeO | 3.28 | 4.25 |
| MnO | 0.07 | 0.09 |
| CaO | 22.31 | 22.31 |
| $Na_2O$ | 0.39 | 0.24 |
| Sum | 98.7 | 99.23 |
| | | |
| T Site Occupancy | | |
| Si | 1.956 | 1.964 |
| $Al^{IV}$ | 0.044 | 0.036 |
| $Fe^{3+}$ | 0 | 0 |
| Sum | 2 | 2 |
| | | |
| M1 Site Occupancy | | |
| $Al^{VI}$ | 0.013 | 0.004 |
| $Fe^{3+}$ | 0.024 | 0.012 |
| $Ti^{4+}$ | 0.009 | 0.008 |
| Cr | 0.018 | 0.019 |
| Mg | 0.92 | 0.924 |
| $Fe^{2+}$ | 0.016 | 0.033 |
| Mn | 0 | 0 |
| Sum | 1 | 1 |
| | | |
| M2 Site Occupancy | | |
| Mg | 0 | 0 |
| $Fe^{2+}$ | 0.085 | 0.098 |
| Mn | 0.002 | 0.003 |
| Ca | 0.884 | 0.882 |
| Na | 0.028 | 0.017 |
| Sum | 0.999 | 1 |
| | | |
| Mole % Endmembers | | |
| Wo | 45.78 | 45.18 |
| En | 47.64 | 47.34 |
| Fs | 6.47 | 7.33 |
| Mn | 0.1 | 0.15 |
| | | |
| Ratios | | |
| $Mg\#(Fe^{2+})$ | 0.90 | 0.88 |
| $Mg\#(Fe_{tot})$ | 0.88 | 0.87 |
| $Fe^{3+}/Fe^{2+}$ | 0.24 | 0.09 |
| D.I. | 40.96 | 40.96 |

Clinopyroxene compositions based upon $[M1][M2][T]_2O_6$.

$Mg\#(Fe^{2+}) = Mg/(Fe^{2+}+Mg)$

$Mg\#(Fe_{tot}) = Mg/(Fe^{2+}+Fe^{3+}+Mg)$

Clinopyroxene type classified from Wo - En - Fs quadrilateral.

Proportions $Fe^{3+}$ and $Fe^{2+}$ calculated assuming Cpx stoichiometry and electrostatic neutrality.

** = Rock Type defined in Appendix 1

# Magnetite Compositions

| Sample (Min.) | m13.1 | m12.1 | tm1.1 | m7.1 | m1.1 | m3.1 | m2.2 |
|---|---|---|---|---|---|---|---|
| Sample (Rock) | 921018-7 | 921018-7 | 921017-5 | 921011-8 | 921013-8 | 921013-8 | 921013-8 |
| Rock Type** | QMD† | QMD† | Gabbro• | Sy£ | MD† | MD† | MD† |
| Oxide % | | | | | | | |
| $Al_2O_3$ | 0.22 | 0.00 | 0.19 | 0.00 | 0.22 | 0.17 | 0.00 |
| $Cr_2O_3$ | 0.72 | 0.87 | 0.00 | 0.20 | 0.36 | 0.65 | 0.47 |
| $Fe_2O_3$ | 67.17 | 67.00 | 47.32 | 68.31 | 66.94 | 66.66 | 67.54 |
| $V_2O_3$ | 0.27 | 0.38 | 0.34 | 0.15 | 0.25 | 0.44 | 0.31 |
| $TiO_2$ | 0.00 | 0.00 | 11.18 | 0.00 | 0.19 | 0.00 | 0.00 |
| FeO | 30.85 | 30.73 | 41.70 | 30.71 | 30.90 | 30.62 | 30.75 |
| MgO | 0.00 | 0.00 | 0.00 | 0.00 | 0.00 | 0.00 | 0.00 |
| MnO | 0.00 | 0.00 | 0.00 | 0.18 | 0.00 | 0.00 | 0.00 |
| ZnO | 0.00 | 0.00 | 0.00 | 0.00 | 0.00 | 0.00 | 0.00 |
| NiO | 0.00 | 0.00 | 0.00 | 0.00 | 0.00 | 0.00 | 0.00 |
| Sum | 99.23 | 98.98 | 100.73 | 99.55 | 98.86 | 98.54 | 99.07 |
| | | | | | | | |
| Site Allocations | | | | | | | |
| Al | 0.080 | 0.000 | 0.068 | 0.000 | 0.081 | 0.063 | 0.000 |
| Cr | 0.177 | 0.214 | 0.000 | 0.049 | 0.089 | 0.161 | 0.116 |
| $Fe^{+3}$ | 15.675 | 15.692 | 10.765 | 15.914 | 15.680 | 15.668 | 15.807 |
| V | 0.067 | 0.095 | 0.082 | 0.037 | 0.062 | 0.110 | 0.077 |
| Ti | 0.000 | 0.000 | 2.542 | 0.000 | 0.044 | 0.000 | 0.000 |
| Sum | 15.999 | 16.001 | 13.457 | 16.000 | 15.956 | 16.002 | 16.000 |
| | | | | | | | |
| $Fe^{+2}$ | 8.001 | 7.999 | 10.544 | 7.952 | 8.044 | 7.998 | 8.000 |
| Mg | 0.000 | 0.000 | 0.000 | 0.000 | 0.000 | 0.000 | 0.000 |
| Mn | 0.000 | 0.000 | 0.000 | 0.047 | 0.000 | 0.000 | 0.000 |
| Zn | 0.000 | 0.000 | 0.000 | 0.000 | 0.000 | 0.000 | 0.000 |
| Ni | 0.000 | 0.000 | 0.000 | 0.000 | 0.000 | 0.000 | 0.000 |
| Sum | 8.001 | 7.999 | 10.544 | 7.999 | 8.044 | 7.998 | 8.000 |
| | | | | | | | |
| Mole% End Members | | | | | | | |
| Spinl. | 0.00 | 0.00 | 0.00 | 0.00 | 0.00 | 0.00 | 0.00 |
| Hercy. | 0.50 | 0.00 | 0.43 | 0.00 | 0.51 | 0.39 | 0.00 |
| Gahnt. | 0.00 | 0.00 | 0.00 | 0.00 | 0.00 | 0.00 | 0.00 |
| Galax. | 0.00 | 0.00 | 0.00 | 0.00 | 0.00 | 0.00 | 0.00 |
| Mgnsf. | 0.00 | 0.00 | 0.00 | 0.00 | 0.00 | 0.00 | 0.00 |
| Mgnet. | 98.97 | 98.07 | 67.29 | 98.88 | 98.00 | 97.91 | 98.79 |
| Frnkl. | 0.00 | 0.00 | 0.00 | 0.00 | 0.00 | 0.00 | 0.00 |
| Jacob. | 0.00 | 0.00 | 0.00 | 0.59 | 0.00 | 0.00 | 0.00 |
| V Mgt. | 0.42 | 0.59 | 0.51 | 0.23 | 0.39 | 0.69 | 0.48 |
| Mgchr. | 0.00 | 0.00 | 0.00 | 0.00 | 0.00 | 0.00 | 0.00 |
| Chrom. | 1.11 | 1.34 | 0.00 | 0.31 | 0.56 | 1.01 | 0.72 |
| Ulvsp. | 0.00 | 0.00 | 31.78 | 0.00 | 0.55 | 0.00 | 0.00 |
| Trevr. | 0.00 | 0.00 | 0.00 | 0.00 | 0.00 | 0.00 | 0.00 |

** Rock type as defined in Appendix 1
Magnetite formula calculated to 32 oxygens

| Sample (Min.) | m4.1 | m7.2 | m8.1 | m9.1 | m10.1 | m11.1 | m2.1 |
|---|---|---|---|---|---|---|---|
| Sample (Rock) | 921013-8 | 921011-8 | 921011-8 | 921017-5 | 921017-5 | 921018-7 | 921013-8 |
| Rock Type** | MD† | Sy£ | Sy£ | Gabbro• | Gabbro• | QMD† | MD† |
| Oxide % | | | | | | | |
| $Al_2O_3$ | 0.00 | 0.28 | 0.59 | 0.00 | 0.00 | 0.00 | 0.00 |
| $Cr_2O_3$ | 0.51 | 0.12 | 0.00 | 0.10 | 0.00 | 0.74 | 0.39 |
| $Fe_2O_3$ | 67.23 | 67.47 | 66.49 | 66.85 | 67.51 | 66.50 | 67.59 |
| $V_2O_3$ | 0.29 | 0.11 | 0.36 | 0.31 | 0.37 | 0.27 | 0.32 |
| $TiO_2$ | 0.00 | 0.00 | 0.00 | 0.00 | 0.00 | 0.00 | 0.00 |
| FeO | 30.63 | 30.66 | 30.50 | 30.29 | 30.54 | 30.41 | 30.75 |
| MgO | 0.00 | 0.00 | 0.00 | 0.00 | 0.00 | 0.00 | 0.00 |
| MnO | 0.00 | 0.00 | 0.00 | 0.00 | 0.00 | 0.00 | 0.00 |
| ZnO | 0.00 | 0.00 | 0.00 | 0.00 | 0.00 | 0.00 | 0.00 |
| NiO | 0.00 | 0.00 | 0.00 | 0.00 | 0.00 | 0.00 | 0.00 |
| Sum | 98.66 | 98.64 | 97.94 | 97.55 | 98.42 | 97.92 | 99.05 |
| | | | | | | | |
| Site Allocations | | | | | | | |
| Al | 0.000 | 0.103 | 0.218 | 0.000 | 0.000 | 0.000 | 0.000 |
| Cr | 0.126 | 0.030 | 0.000 | 0.025 | 0.000 | 0.184 | 0.096 |
| $Fe^{+3}$ | 15.801 | 15.840 | 15.692 | 15.895 | 15.908 | 15.747 | 15.824 |
| V | 0.073 | 0.028 | 0.091 | 0.079 | 0.093 | 0.068 | 0.080 |
| Ti | 0.000 | 0.000 | 0.000 | 0.000 | 0.000 | 0.000 | 0.000 |
| Sum | 16.000 | 16.001 | 16.001 | 15.999 | 16.001 | 15.999 | 16.000 |
| | | | | | | | |
| $Fe^{+2}$ | 8.000 | 7.999 | 7.999 | 8.003 | 7.998 | 8.002 | 8.001 |
| Mg | 0.000 | 0.000 | 0.000 | 0.000 | 0.000 | 0.000 | 0.000 |
| Mn | 0.000 | 0.000 | 0.000 | 0.000 | 0.000 | 0.000 | 0.000 |
| Zn | 0.000 | 0.000 | 0.000 | 0.000 | 0.000 | 0.000 | 0.000 |
| Ni | 0.000 | 0.000 | 0.000 | 0.000 | 0.000 | 0.000 | 0.000 |
| Sum | 8.000 | 7.999 | 7.999 | 8.003 | 7.998 | 8.002 | 8.001 |
| | | | | | | | |
| Mole% End Members | | | | | | | |
| Spinl. | 0.00 | 0.00 | 0.00 | 0.00 | 0.00 | 0.00 | 0.00 |
| Hercy. | 0.00 | 0.64 | 1.36 | 0.00 | 0.00 | 0.00 | 0.00 |
| Gahnt. | 0.00 | 0.00 | 0.00 | 0.00 | 0.00 | 0.00 | 0.00 |
| Galax. | 0.00 | 0.00 | 0.00 | 0.00 | 0.00 | 0.00 | 0.00 |
| Mgnsf. | 0.00 | 0.00 | 0.00 | 0.00 | 0.00 | 0.00 | 0.00 |
| Mgnet. | 98.76 | 98.99 | 98.07 | 99.35 | 99.42 | 98.42 | 98.90 |
| Frnkl. | 0.00 | 0.00 | 0.00 | 0.00 | 0.00 | 0.00 | 0.00 |
| Jacob. | 0.00 | 0.00 | 0.00 | 0.00 | 0.00 | 0.00 | 0.00 |
| V Mgt. | 0.46 | 0.17 | 0.57 | 0.49 | 0.58 | 0.43 | 0.50 |
| Mgchr. | 0.00 | 0.00 | 0.00 | 0.00 | 0.00 | 0.00 | 0.00 |
| Chrom. | 0.79 | 0.19 | 0.00 | 0.16 | 0.00 | 1.15 | 0.60 |
| Ulvsp. | 0.00 | 0.00 | 0.00 | 0.00 | 0.00 | 0.00 | 0.00 |
| Trevr. | 0.00 | 0.00 | 0.00 | 0.00 | 0.00 | 0.00 | 0.00 |

** Rock type as defined in Appendix 1
Magnetite formula calculated to 32 oxygens

# Titanite Compositions

| Sample (Min.) | s1.1 | s2.1 | s3.1 | s4.1 | s6.1 | s6.2 |
|---|---|---|---|---|---|---|
| Sample (Rock) | 921013-8 | 921013-8 | 921011-8 | 921011-8 | 921011-8 | 921011-8 |
| Rock Type** | MD† | MD† | Sy£ | Sy£ | Sy£ | Sy£ |
| Oxide % | | | | | | |
| $SiO_2$ | 29.72 | 29.86 | 29.26 | 29.12 | 29.25 | 30.35 |
| $Al_2O_3$ | 1.16 | 1.11 | 1.12 | 1.26 | 1.48 | 2.21 |
| $TiO_2$ | 37.22 | 37.45 | 34.40 | 34.28 | 34.92 | 35.32 |
| $V_2O_5$ | 0.37 | 0.40 | 0.00 | 0.00 | 0.00 | 0.38 |
| $Cr_2O_3$ | 0.00 | 0.19 | 0.00 | 0.00 | 0.00 | 0.00 |
| FeO | 1.64 | 1.64 | 2.84 | 3.01 | 2.42 | 1.60 |
| MgO | 0.00 | 0.00 | 0.00 | 0.00 | 0.23 | 0.00 |
| MnO | 0.00 | 0.00 | 0.13 | 0.15 | 0.00 | 0.00 |
| CaO | 27.73 | 27.95 | 26.41 | 26.73 | 26.42 | 27.81 |
| Sum | 97.84 | 98.60 | 94.16 | 94.55 | 94.72 | 97.67 |
| | | | | | | |
| Site Allocations | | | | | | |
| $Si^{4+}$ | 0.996 | 0.994 | 1.023 | 1.016 | 1.013 | 1.015 |
| $Al^{IV}$ | 0.004 | 0.006 | 0 | 0 | 0 | 0 |
| Sum | 1 | 1 | 1.023 | 1.016 | 1.013 | 1.015 |
| | | | | | | |
| $Al^{VI}$ | 0.042 | 0.037 | 0.046 | 0.052 | 0.061 | 0.087 |
| $Ti^{4+}$ | 0.938 | 0.937 | 0.904 | 0.899 | 0.910 | 0.888 |
| $V^{5+}$ | 0.008 | 0.009 | 0.000 | 0.000 | 0.000 | 0.008 |
| $Cr^{3+}$ | 0.000 | 0.005 | 0.000 | 0.000 | 0.000 | 0.000 |
| Sum | 0.988 | 0.988 | 0.950 | 0.951 | 0.971 | 0.983 |
| | | | | | | |
| $Fe^{2+}$ | 0.046 | 0.046 | 0.083 | 0.088 | 0.070 | 0.045 |
| $Mg^{2+}$ | 0.000 | 0.000 | 0.000 | 0.000 | 0.012 | 0.000 |
| $Mn^{2+}$ | 0.000 | 0.000 | 0.004 | 0.004 | 0.000 | 0.000 |
| $Ca^{2+}$ | 0.996 | 0.997 | 0.989 | 0.999 | 0.981 | 0.997 |
| Sum | 1.042 | 1.043 | 1.076 | 1.091 | 1.063 | 1.042 |

** Rock type as defined in Appendix 1
Titanite formula calulated to five oxygens.

| Sample (Min.) | s7.1 | s7.2 | s8.1 | s9.1 | s10.1 |
|---|---|---|---|---|---|
| Sample (Rock) | 921011-8 | 921011-8 | 921017-5 | 921017-5 | 921018-7 |
| Rock Type** | Sy[£] | Sy[£] | Gabbro[¶] | Gabbro[¶] | QMD[†] |
| Oxide % | | | | | |
| $SiO_2$ | 29.30 | 29.84 | 30.56 | 29.76 | 29.53 |
| $Al_2O_3$ | 1.38 | 1.68 | 1.17 | 0.96 | 0.96 |
| $TiO_2$ | 34.13 | 35.11 | 38.59 | 38.58 | 37.28 |
| $V_2O_5$ | 0.00 | 0.32 | 0.00 | 0.00 | 0.00 |
| $Cr_2O_3$ | 0.00 | 0.00 | 0.00 | 0.00 | 0.00 |
| FeO | 2.79 | 2.05 | 1.33 | 0.73 | 1.55 |
| MgO | 0.00 | 0.00 | 0.00 | 0.00 | 0.00 |
| MnO | 0.00 | 0.00 | 0.00 | 0.00 | 0.00 |
| CaO | 26.71 | 27.65 | 28.53 | 27.53 | 27.14 |
| Sum | 94.31 | 96.65 | 100.18 | 97.56 | 96.46 |
| | | | | | |
| Site Allocations | | | | | |
| $Si^{4+}$ | 1.022 | 1.013 | 0.999 | 0.996 | 1.003 |
| $Al^{IV}$ | 0 | 0 | 0.001 | 0.004 | 0 |
| Sum | 1.022 | 1.013 | 1 | 1 | 1.003 |
| | | | | | |
| $Al^{VI}$ | 0.057 | 0.067 | 0.044 | 0.034 | 0.038 |
| $Ti^{4+}$ | 0.895 | 0.896 | 0.949 | 0.971 | 0.952 |
| $V^{5+}$ | 0.000 | 0.007 | 0.000 | 0.000 | 0.000 |
| $Cr^{3+}$ | 0.000 | 0.000 | 0.000 | 0.000 | 0.000 |
| Sum | 0.952 | 0.970 | 0.993 | 1.005 | 0.990 |
| | | | | | |
| $Fe^{2+}$ | 0.081 | 0.058 | 0.036 | 0.021 | 0.044 |
| $Mg^{2+}$ | 0.000 | 0.000 | 0.000 | 0.000 | 0.000 |
| $Mn^{2+}$ | 0.000 | 0.000 | 0.000 | 0.000 | 0.000 |
| $Ca^{2+}$ | 0.998 | 1.005 | 0.999 | 0.987 | 0.988 |
| Sum | 1.079 | 1.063 | 1.035 | 1.008 | 1.032 |

** Rock type as defined in Appendix 1
Titanite formula calulated to five oxygens.

# Barite Composition

| | |
|---|---|
| Sample (Min.) | #14 |
| Sample (Rock) | 921018-6 |
| Rock Type** | QMD |
| Oxide % | |
| BaO | 64.65 |
| CaO | 0.23 |
| FeO | 0.00 |
| MnO | 0.00 |
| MgO | 0.00 |
| SrO | 0.54 |
| $SO_3$ | 32.88 |
| Sum | 98.30 |
| | |
| Site Allocations | |
| Ba | 1.014 |
| Ca | 0.010 |
| Fe | 0.000 |
| Mn | 0.000 |
| Mg | 0.000 |
| Sr | 0.012 |
| Sum | 1.036 |
| | |
| S | 0.988 |
| Sum | 0.988 |
| | |
| Wt.% End Members | |
| Ba | 98.40 |
| Ca | 0.57 |
| Sum | 98.97 |
| | |
| Mole % End Members | |
| Ba | 99.02 |
| Ca | 0.98 |

** Rock type as defined in Appendix 1
Barite formula calculated to four oxygens

# Epidote Compositions

| Sample (Min.) | #2 | #8 |
|---|---|---|
| Sample (Rock) | 930620-3 | 930620-3 |
| Rock Type** | Mo†£ | Mo†£ |
| Oxide % | | |
| $SiO_2$ | 36.64 | 37.37 |
| $Al_2O_3$ | 19.57 | 21.18 |
| $TiO_2$ | 0.00 | 0.00 |
| $Fe_2O_3$ | 15.34 | 15.58 |
| MgO | 0.00 | 0.00 |
| FeO | 1.60 | 0.78 |
| MnO | 0.20 | 0.24 |
| CaO | 21.59 | 22.52 |
| Sum | 94.94 | 97.67 |
| | | |
| Site Allocations | | |
| Si | 6.113 | 6.037 |
| $Al^{IV}$ | 0.000 | 0.000 |
| Sum | 6.113 | 6.037 |
| | | |
| $Al^{VI}$ | 3.849 | 4.033 |
| Ti | 0.000 | 0.000 |
| $Fe^{+3}$ | 1.926 | 1.894 |
| Sum | 5.775 | 5.927 |
| | | |
| Mg | 0.000 | 0.000 |
| $Fe^{+2}$ | 0.223 | 0.106 |
| Mn | 0.029 | 0.033 |
| Ca | 3.860 | 3.898 |
| Sum | 4.112 | 4.037 |

** Rock type as defined in Appendix 1
Epidote formula calculated to twenty-five oxygens.

# Mica Compositions

| Sample (Min.) | bio1.1 | bio1.2 | bio2.2 | bio3.1 | bio4.1 | bio5.1 | bio10.3 | bio-42 |
|---|---|---|---|---|---|---|---|---|
| Sample (Rock) | 921014-9 | 921014-9 | 921014-9 | 921014-9 | 921014-9 | 921014-9 | 921014-9 | 930823-5 |
| Rock Type** | Hbldt | Hbldt | Hbldt | Hbldt | Hbldt | Hbldt | Hbldt | Dio |
| Bio-Type | Biotite | Biotite | Phlogopite | Biotite | Biotite | Biotite | Biotite | Biotite |
| Oxide% | | | | | | | | |
| $SiO_2$ | 37.14 | 37.41 | 37.55 | 37.54 | 37.34 | 37.64 | 37.21 | 37.83 |
| $Al_2O_3$ | 15.8 | 15.59 | 16.13 | 15.52 | 15.97 | 15.53 | 15.59 | 14.93 |
| $Fe_2O_3$ | 8.44 | 6.96 | 10.24 | 7.04 | 8.59 | 6.98 | 7.63 | 5.94 |
| $Cr_2O_3$ | 0.1 | 0.12 | 0.02 | 0.02 | 0.3 | 0.09 | 0.14 | 0.27 |
| $TiO_2$ | 1.71 | 1.75 | 1.18 | 1.87 | 1.37 | 2.42 | 2.58 | 1.41 |
| FeO | 6.66 | 8.13 | 4.65 | 8.56 | 6.55 | 8.62 | 7.42 | 9.34 |
| MnO | 0.1 | 0.19 | 0.12 | 0.1 | 0.17 | 0.15 | 0.06 | 0.16 |
| MgO | 15.91 | 15.73 | 16.8 | 15.68 | 15.99 | 15.58 | 15.39 | 15.78 |
| CaO | 0.04 | 0.05 | 0 | 0.09 | 0.13 | 0.05 | 0.06 | 0 |
| $Na_2O$ | 0.66 | 0.68 | 0.64 | 0.76 | 0.8 | 0.79 | 0.04 | 0 |
| $K_2O$ | 9.97 | 9.95 | 9.87 | 9.82 | 9.72 | 9.91 | 9.73 | 10.01 |
| Cl | 0.05 | 0.07 | 0 | 0.05 | 0.02 | 0.08 | 0.05 | n.d. |
| Sum | 96.53 | 96.56 | 97.2 | 97 | 96.93 | 97.76 | 95.87 | 95.67 |
| | | | | | | | | |
| Z Site Occupancy | | | | | | | | |
| Si | 5.417 | 5.469 | 5.402 | 5.469 | 5.419 | 5.446 | 5.451 | 5.583 |
| $Al^{IV}$ | 2.583 | 2.531 | 2.598 | 2.531 | 2.581 | 2.554 | 2.549 | 2.417 |
| $Fe^{3+}$ | 0 | 0 | 0 | 0 | 0 | 0 | 0 | 0 |
| Sum | 8 | 8 | 8 | 8 | 8 | 8 | 8 | 8 |
| | | | | | | | | |
| Y Site Occupancy | | | | | | | | |
| $Al^{VI}$ | 0.716 | 0.686 | 0.735 | 0.665 | 0.732 | 0.648 | 0.892 | 0.597 |
| $Fe^{3+}$ | 0.926 | 0.766 | 1.109 | 0.772 | 0.938 | 0.76 | 0.842 | 0.659 |
| Cr | 0.012 | 0.014 | 0.002 | 0.002 | 0.034 | 0.01 | 0.016 | 0.032 |
| Ti | 0.188 | 0.192 | 0.128 | 0.205 | 0.15 | 0.263 | 0.284 | 0.157 |
| $Fe^{2+}$ | 0.812 | 0.994 | 0.56 | 1.043 | 0.795 | 1.043 | 0.909 | 1.153 |
| Mn | 0.012 | 0.024 | 0.015 | 0.012 | 0.021 | 0.018 | 0.01 | 0.02 |
| Mg | 3.459 | 3.428 | 3.603 | 3.405 | 3.459 | 3.36 | 3.361 | 3.472 |
| Sum | 6.125 | 6.104 | 6.152 | 6.104 | 6.129 | 6.102 | 6.114 | 6.09 |
| | | | | | | | | |
| X Site Occupancy | | | | | | | | |
| Ca | 0.006 | 0.008 | 0 | 0.014 | 0.02 | 0.008 | 0.009 | 0 |
| Na | 0.187 | 0.193 | 0.179 | 0.215 | 0.225 | 0.222 | 0.011 | 0 |
| K | 1.855 | 1.856 | 1.811 | 1.825 | 1.8 | 1.829 | 1.819 | 1.885 |
| Sum | 2.048 | 2.057 | 1.99 | 2.054 | 2.045 | 2.059 | 1.839 | 1.885 |
| | | | | | | | | |
| Site Occupancy | | | | | | | | |
| Cl | 0.012 | 0.018 | 0 | 0.012 | 0.005 | 0.019 | 0.013 | n.d. |
| Sum | 0.012 | 0.018 | 0 | 0.012 | 0.005 | 0.019 | 0.013 | |
| | | | | | | | | |
| Ratios | | | | | | | | |
| $Fe\#_{tot}$ | 0.334 | 0.339 | 0.317 | 0.348 | 0.334 | 0.349 | 0.349 | 0.349 |
| $Al_{tot}$ | 3.299 | 3.217 | 3.333 | 3.196 | 3.313 | 3.202 | 3.241 | 3.014 |
| T (°C)♦ | 772 | 724 | 768 | 728 | 719 | 799 | 889 | 861 |

Biotite compositions based upon $[X]_2[Y]_6[Z]_8O_{20}[OH+F+Cl]_2$

n.d. = Not determined

$Fe\#_{tot} = (Fe^{2+}+Fe^{3+})/(Fe^{2+}+Fe^{3+}+Mg)$ on a per formula unit basis.

Proportions $Fe^{3+}$ and $Fe^{2+}$ calculated assuming biotite stoichiometry and electrostatic neutrality.

♦ Temperature calculated from the Ti in biotite temperature dependency of Luhr (1984) defined as $(838/(1.0337-(Ti/Fe^{2+})))-273$

** = Rock type defined in Appendix 1

| Sample (Min.) | bio5.2 | bio6.1 | bio6.2 | bio6.3 | bio7.1 | bio7.2 | bio8.1 | bio9.1 |
|---|---|---|---|---|---|---|---|---|
| Sample (Rock) | 921014-9 | 921014-9 | 921014-9 | 921014-9 | 921014-9 | 921014-9 | 921014-9 | 921014-9 |
| Rock Type** | Hbldt | Hbldt | Hbldt | Hbldt | Hbldt | Hbldt | Hbldt | Hbldt |
| Bio-Type | Biotite | Biotite | Biotite | Biotite | Biotite | Biotite | Biotite | Biotite |
| Oxide% | | | | | | | | |
| $SiO_2$ | 37.12 | 37.07 | 37.13 | 37.56 | 37.06 | 37.69 | 37.79 | 37.74 |
| $Al_2O_3$ | 15.28 | 15.22 | 15.25 | 15.45 | 15.89 | 15.49 | 15.71 | 15.83 |
| $Fe_2O_3$ | 9.21 | 6.32 | 6.62 | 7.15 | 9.6 | 7.41 | 6.84 | 7.54 |
| $Cr_2O_3$ | 0.09 | 0.1 | 0.13 | 0.13 | 0.07 | 0.09 | 0.32 | 0.14 |
| $TiO_2$ | 2.17 | 2.61 | 2.61 | 1.97 | 2.14 | 2.61 | 1.85 | 2.36 |
| FeO | 6.41 | 9.54 | 8.68 | 8.29 | 6.48 | 8.12 | 8.4 | 7.83 |
| MnO | 0.15 | 0.19 | 0.17 | 0.12 | 0.16 | 0.18 | 0.18 | 0.19 |
| MgO | 15.88 | 14.88 | 15.34 | 15.73 | 15.37 | 15.54 | 15.78 | 15.69 |
| CaO | 0.01 | 0.11 | 0.2 | 0.03 | 0.03 | 0.04 | 0.01 | 0.07 |
| $Na_2O$ | 0.51 | 0.72 | 0.72 | 0.69 | 0.49 | 0.44 | 0.71 | 0.57 |
| $K_2O$ | 9.69 | 9.84 | 9.73 | 9.81 | 9.71 | 9.59 | 10.12 | 9.9 |
| Cl | 0 | 0.03 | 0.03 | 0.04 | 0.01 | 0.02 | 0.02 | 0.04 |
| Sum | 96.52 | 96.6 | 96.58 | 96.93 | 97 | 97.2 | 97.71 | 97.86 |
| | | | | | | | | |
| Z Site Occupancy | | | | | | | | |
| Si | 5.413 | 5.45 | 5.44 | 5.47 | 5.381 | 5.46 | 5.466 | 5.436 |
| $Al^{IV}$ | 2.587 | 2.55 | 2.56 | 2.53 | 2.619 | 2.54 | 2.534 | 2.564 |
| $Fe^{3+}$ | 0 | 0 | 0 | 0 | 0 | 0 | 0 | 0 |
| Sum | 8 | 8 | 8 | 8 | 8 | 8 | 8 | 8 |
| | | | | | | | | |
| Y Site Occupancy | | | | | | | | |
| $Al^{VI}$ | 0.626 | 0.637 | 0.634 | 0.652 | 0.719 | 0.645 | 0.678 | 0.688 |
| $Fe^{3+}$ | 1.01 | 0.699 | 0.729 | 0.784 | 1.049 | 0.808 | 0.745 | 0.817 |
| Cr | 0.01 | 0.012 | 0.015 | 0.015 | 0.008 | 0.01 | 0.037 | 0.016 |
| Ti | 0.238 | 0.289 | 0.288 | 0.216 | 0.234 | 0.284 | 0.201 | 0.256 |
| $Fe^{2+}$ | 0.781 | 1.174 | 1.063 | 1.01 | 0.787 | 0.984 | 1.017 | 0.944 |
| Mn | 0.019 | 0.024 | 0.021 | 0.015 | 0.02 | 0.022 | 0.022 | 0.023 |
| Mg | 3.452 | 3.261 | 3.35 | 3.415 | 3.327 | 3.356 | 3.402 | 3.369 |
| Sum | 6.136 | 6.096 | 6.1 | 6.107 | 6.144 | 6.109 | 6.102 | 6.113 |
| | | | | | | | | |
| X Site Occupancy | | | | | | | | |
| Ca | 0.002 | 0.017 | 0.031 | 0.005 | 0.005 | 0.006 | 0.002 | 0.011 |
| Na | 0.144 | 0.205 | 0.205 | 0.195 | 0.138 | 0.124 | 0.199 | 0.159 |
| K | 1.803 | 1.846 | 1.819 | 1.823 | 1.799 | 1.772 | 1.867 | 1.819 |
| Sum | 1.949 | 2.068 | 2.055 | 2.023 | 1.942 | 1.902 | 2.068 | 1.989 |
| | | | | | | | | |
| Site Occupancy | | | | | | | | |
| Cl | 0 | 0.008 | 0.007 | 0.009 | 0.001 | 0.006 | 0.004 | 0.009 |
| Sum | 0 | 0.008 | 0.007 | 0.009 | 0.001 | 0.006 | 0.004 | 0.009 |
| | | | | | | | | |
| Ratios | | | | | | | | |
| $Fe\#_{tot}$ | 0.342 | 0.365 | 0.349 | 0.344 | 0.356 | 0.348 | 0.341 | 0.343 |
| $Al_{tot}$ | 3.213 | 3.187 | 3.194 | 3.182 | 3.338 | 3.185 | 3.212 | 3.252 |
| T (°C)♦ | 877 | 791 | 826 | 749 | 885 | 852 | 729 | 826 |

Biotite compositions based upon $[X]_2[Y]_6[Z]_8O_{20}[OH+F+Cl]_2$

n.d. = Not determined

$Fe\#_{tot} = (Fe^{2+}+Fe^{3+})/(Fe^{2+}+Fe^{3+}+Mg)$ on a per formula unit basis.

Proportions $Fe^{3+}$ and $Fe^{2+}$ calculated assuming biotite stoichiometry and electrostatic neutrality.

♦ Temperature calculated from the Ti in biotite temperature dependency of Luhr (1984) defined as (838/(1.0337-(Ti/$Fe^{2+}$)))-273

** = Rock type defined in Appendix 1

| Sample (Min.) | bio6.2 | bio6.3 | bio7.1 | bio7.2 | bio8.1 | bio9.1 | bio10.1 | bio10.2 |
|---|---|---|---|---|---|---|---|---|
| Sample (Rock) | 921014-9 | 921014-9 | 921014-9 | 921014-9 | 921014-9 | 921014-9 | 921014-9 | 921014-9 |
| Rock Type** | Hbldt | Hbldt | Hbldt | Hbldt | Hbldt | Hbldt | Hbldt | Hbldt |
| Bio-Type | Biotite | Biotite | Biotite | Biotite | Biotite | Biotite | Biotite | Biotite |
| Oxide% | | | | | | | | |
| $SiO_2$ | 37.13 | 37.56 | 37.06 | 37.69 | 37.79 | 37.74 | 37.86 | 37.6 |
| $Al_2O_3$ | 15.25 | 15.45 | 15.89 | 15.49 | 15.71 | 15.83 | 15.48 | 16.04 |
| $Fe_2O_3$ | 6.62 | 7.15 | 9.6 | 7.41 | 6.84 | 7.54 | 6.35 | 8.46 |
| $Cr_2O_3$ | 0.13 | 0.13 | 0.07 | 0.09 | 0.32 | 0.14 | 0.07 | 0.01 |
| $TiO_2$ | 2.61 | 1.97 | 2.14 | 2.61 | 1.85 | 2.36 | 2.22 | 1.93 |
| FeO | 8.68 | 8.29 | 6.48 | 8.12 | 8.4 | 7.83 | 8.91 | 7.1 |
| MnO | 0.17 | 0.12 | 0.16 | 0.18 | 0.18 | 0.19 | 0.09 | 0.13 |
| MgO | 15.34 | 15.73 | 15.37 | 15.54 | 15.78 | 15.69 | 15.79 | 15.73 |
| CaO | 0.2 | 0.03 | 0.03 | 0.04 | 0.01 | 0.07 | 0.18 | 0.09 |
| $Na_2O$ | 0.72 | 0.69 | 0.49 | 0.44 | 0.71 | 0.57 | 0.55 | 0.51 |
| $K_2O$ | 9.73 | 9.81 | 9.71 | 9.59 | 10.12 | 9.9 | 9.76 | 9.57 |
| Cl | 0.03 | 0.04 | 0.01 | 0.02 | 0.02 | 0.04 | 0.03 | 0 |
| Sum | 96.58 | 96.93 | 97 | 97.2 | 97.71 | 97.86 | 97.26 | 97.17 |
| | | | | | | | | |
| Z Site Occupancy | | | | | | | | |
| Si | 5.44 | 5.47 | 5.381 | 5.46 | 5.466 | 5.436 | 5.491 | 5.434 |
| $Al^{IV}$ | 2.56 | 2.53 | 2.619 | 2.54 | 2.534 | 2.564 | 2.509 | 2.566 |
| $Fe^{3+}$ | 0 | 0 | 0 | 0 | 0 | 0 | 0 | 0 |
| Sum | 8 | 8 | 8 | 8 | 8 | 8 | 8 | 8 |
| | | | | | | | | |
| Y Site Occupancy | | | | | | | | |
| $Al^{VI}$ | 0.634 | 0.652 | 0.719 | 0.645 | 0.678 | 0.688 | 0.646 | 0.733 |
| $Fe^{3+}$ | 0.729 | 0.784 | 1.049 | 0.808 | 0.745 | 0.817 | 0.693 | 0.92 |
| Cr | 0.015 | 0.015 | 0.008 | 0.01 | 0.037 | 0.016 | 0.008 | 0.001 |
| Ti | 0.288 | 0.216 | 0.234 | 0.284 | 0.201 | 0.256 | 0.242 | 0.21 |
| $Fe^{2+}$ | 1.063 | 1.01 | 0.787 | 0.984 | 1.017 | 0.944 | 1.08 | 0.858 |
| Mn | 0.021 | 0.015 | 0.02 | 0.022 | 0.022 | 0.023 | 0.011 | 0.016 |
| Mg | 3.35 | 3.415 | 3.327 | 3.356 | 3.402 | 3.369 | 3.414 | 3.389 |
| Sum | 6.1 | 6.107 | 6.144 | 6.109 | 6.102 | 6.113 | 6.094 | 6.127 |
| | | | | | | | | |
| X Site Occupancy | | | | | | | | |
| Ca | 0.031 | 0.005 | 0.005 | 0.006 | 0.002 | 0.011 | 0.028 | 0.014 |
| Na | 0.205 | 0.195 | 0.138 | 0.124 | 0.199 | 0.159 | 0.155 | 0.143 |
| K | 1.819 | 1.823 | 1.799 | 1.772 | 1.867 | 1.819 | 1.806 | 1.765 |
| Sum | 2.055 | 2.023 | 1.942 | 1.902 | 2.068 | 1.989 | 1.989 | 1.922 |
| | | | | | | | | |
| Site Occupancy | | | | | | | | |
| Cl | 0.007 | 0.009 | 0.001 | 0.006 | 0.004 | 0.009 | 0.006 | 0 |
| Sum | 0.007 | 0.009 | 0.001 | 0.006 | 0.004 | 0.009 | 0.006 | 0 |
| | | | | | | | | |
| Ratios | | | | | | | | |
| $Fe\#_{tot}$ | 0.349 | 0.344 | 0.356 | 0.348 | 0.341 | 0.343 | 0.342 | 0.344 |
| $Al_{tot}$ | 3.194 | 3.182 | 3.338 | 3.185 | 3.212 | 3.252 | 3.155 | 3.299 |
| T (°C)♦ | 826 | 749 | 865 | 852 | 729 | 826 | 762 | 789 |

Biotite compositions based upon $[X]_2[Y]_6[Z]_8O_{20}[OH+F+Cl]_2$

n.d. = Not determined

$Fe\#_{tot} = (Fe^{2+}+Fe^{3+})/(Fe^{2+}+Fe^{3+}+Mg)$ on a per formula unit basis.

Proportions $Fe^{3+}$ and $Fe^{2+}$ calculated assuming biotite stoichiometry and electrostatic neutrality.

♦ Temperature calculated from the Ti in biotite temperature dependency of Luhr (1984) defined as $(838/(1.0337-(Ti/Fe^{2+})))-273$

** = Rock type defined in Appendix 1

# Appendix 5
# Isotopic Analysis Procedure

## Sm-Nd and Rb-Sr Isotopic Analysis

Thin sections were examined to find primary minerals of large enough size, and exhibiting negligible alteration effects, for isotopic analysis. Selected grab samples were cut to remove surface alteration and crushed in a jaw crusher. The granular material produced was mechanically sieved using screens of mesh sizes 20, 30, 60, and 80, to obtain a sample of the same size range as the minerals observed in thin section. Pre-concentration of desired phases was facilitated by the removal of magnetite by hand magnet, and the use of a Franz L-1 isodynamic separator. High purity mineral separates of titanite, apatite, allanite, epidote, actinolite, and hornblende were obtained by handpicking under a binocular microscope and placed in a ultrasonic cleaner for 2 minutes in 0.8 wt.% HF to dislodge any foreign minerals. The separate was then washed in acetone, dried, and further hand-picked to produce pure (>99 %) mineral concentrates for dissolution.

Mineral separates were dissolved in HF-$HNO_3$ at 180 °C in Savillex Ltd. Teflon screw-top vials and taken to dryness at 200 °C, then subjected to a second dissolution in 6.2N HCl at 150 °C. Double-distilled HF and $HNO_3$, produced by sub-boiling, were purchased from Seastar Chemicals Ltd., British Columbia. Sub-boiling single distilled HCl was produced from reagent grade stock at the University of Ottawa in a quartz still. Total blanks are less than <0.25 ng for Nd and <0.1 ng for Sr, negligible in comparison to the amounts of Sr and Nd in the samples. The concentrations of Rb, Sr, Nd, and Sm were determined by isotopic dilution using $^{87}$Rb-, $^{84}$Sr-, $^{148}$Nd- and $^{149}$Sm- enriched spikes.

Rubidium, Sr and rare-earth elements (REE) were separated using Bio Rad AG 50 W-X8 (200-400 mesh) resin. The elution procedure for Rb-Sr and REE collection is as

follows. Following dissolution and desiccation, samples were re-dissolved and brought up to 2ml. in 2.5N HCl. Sample aliquots were then loaded in 2.5N HCl pre-equilibrated columns and Rb and Sr were eluted with 2.5N HCl. The REE were collected with a 6.2N HCl elution. Separation columns were then flushed with 6.2N HCl and re-equilibrated with 2.5N HCl in preparation for the next sample aliquot.

Neodymium and Sm were separated from the REE collection with the aid of a di-ethylhexyl orthophosphoric acid coated Teflon resin. Samarium and Nd were separated from the REE collection as follows. A 0.2 ml aliquot of REE separate was eluted with 0.25 N HCl to collect Nd. Samarium was collected from a 0.6 N HCl elution.

Isotopic measurements were made at Carleton University by Kéiko Hattori in static mode on a Finnigan MAT 261 multi-collector mass spectrometer, and the ratios for Sr and Nd isotopes were normalized to $^{86}Sr/^{88}Sr$ of 0.1194 and $^{146}Nd/^{144}Nd$ of 0.7219. Ratio measurements were carried out until the counting statistic errors ($2\bar{\sigma}$) reach <0.004 %. During the course of isotopic analysis, NBS-987 and the La Jolla Wa standard yielded $^{87}Sr/^{86}Sr$ ratios of 0.710246 ± 6 (N=15) and $^{143}Nd/^{144}Nd$ ratios of 0.511864 ± 8 (N=16), respectively.